

Cover Page



Universiteit Leiden



The handle <http://hdl.handle.net/1887/30141> holds various files of this Leiden University dissertation

Author: Zheng, Tingting
Title: Zipping into fusion
Issue Date: 2014-12-17

Zippping into Fusion

Proefschrift

ter verkrijging van
de graad van Doctor aan de Universiteit Leiden,
op gezag van de Rector Magnificus Prof.mr. C.J.J.M. Stolker,
Volgens besluit van het College voor Promoties
Te verdedigen op woensdag 17 december 2014
Klokke 12.30 uur

door

Tingting Zheng

Geboren te China

In 1982

Promotiecommissie

Promotor: Prof. Dr. Ir. J. G. E. M. Fraaije

Co-promotor: Dr. A. Kros

Overige leden: Prof. Dr. M. C. Van Hemert
Prof. Dr. J. Lugtenburg
Dr. J. A. A. W. Elemans

Contents

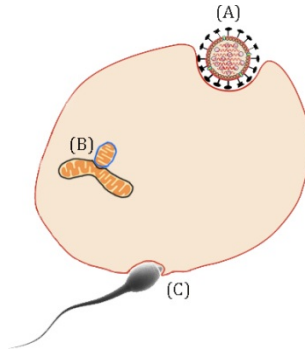
1. Introduction	1
2. Probing coiled-coil assembly by paramagnetic NMR spectroscopy	9
3. An antiparallel tetrameric coiled-coil	45
4. Controlled liposome fusion mediated by SNARE protein mimics	83
5. Controlling the rate of coiled coil driven membrane fusion	115
6. Increasing the membrane fusion efficiency by reducing undesired peptide-peptide interactions	143
Summary	175
Samenvatting	181
Abbreviations	187
Curriculum vitae	191
List of publications	193
Acknowledgements	195

Chapter 1

Introduction

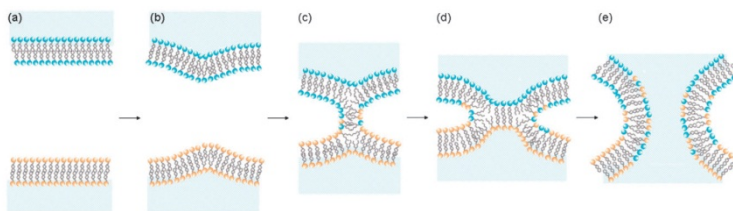


Membrane fusion is one of the most fundamental processes in living organisms.¹ Main performances of natural membrane fusion are for example virus-host cell fusion, intracellular fusion (e.g. mitochondria fusion) and extracellular membrane fusion (e.g. sperm-egg fusion) (Scheme 1).²⁻⁴



Scheme 1. Diagrammatic sketch of different kinds of natural membrane fusion. (A) indicates pathogen with host cell fusion. (B) indicates mitochondria fusion as an example of intracellular organelles fusion. (C) indicates sperm oocytes fusion as an example of extracellular fusion of eukaryotic cells.

In order to achieve fusion, the two opposing membranes are first brought into close proximity, following by surface docking, and the formation of a stalk intermediate connecting the membranes. Before cargo transfer can occur, the stalk intermediate further develops in a hemifusion state, which is followed by a pore formation and expansion. (Scheme 2).^{5, 6} However, all these processes are energy driven. Studies show that membrane fusion proteins are in charge of the energy supply in whole process of membrane fusion.⁷



Scheme 2. (A) Two opposing membranes in the pre-fusion state. (B) A point-like membrane protrusion minimizes the energy of the hydration repulsion between the proximal leaflets of the membranes coming into immediate contact. (C) A hemifusion stalk with proximal leaflets fused and distal leaflets unfused. (D) Stalk expansion yields the hemifusion diaphragm. (E) A fusion pore forms either in the hemifusion diaphragm bilayer or directly from the stalk.⁵

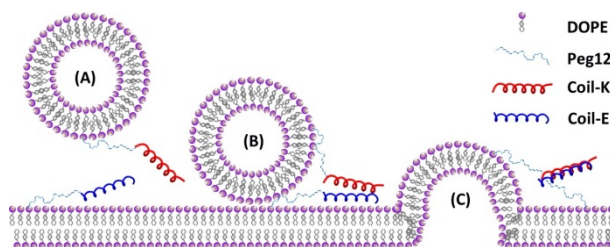
The SNARE (soluble N-ethyl maleimide sensitive factor attachment protein receptors) protein complex family is known to play a vital role in facilitating most intracellular and

Introduction

exocytic membrane fusion.⁸⁻¹⁰ However, understanding of membrane fusion at the molecular level is at a rather primitive stage due to the complexity of native fusogenic systems. According to Nobel prize laureate Südhof, how SNARE proteins promote fusion remains a major question in cell biology.¹¹ Do SNAREs only bring the opposing membranes together, or is there another function to promote membrane fusion?

Therefore, a bottom-up approach is proposed by several groups using synthetic analogues inspired by the natural fusion machinery in order to gain insight in coiled coil mediated membrane fusion. In this approach the chemical structure and composition of synthetic analogues can be systematically varied in order to study the influence of each segment on the fusion process. Thus, studying membrane fusion of this biomimetic model system will yield valuable information on the mechanism on a molecular level resulting in a better general understanding of coiled coil mediated membrane fusion. Inspired by this this fascinating process, our group mimicked the intricate natural SNARE proteins mediated membrane fusion into a simple coiled coil peptide complex mediated liposome fusion model.¹²

The beauty of the reduced membrane fusion system is that all the fusion parts are artificial. In our model system, the natural membrane bilayer is replaced by a liposomal bilayer, and the SNARE protein coiled coil tetramer is replaced by heterodimeric coiled coil. Previous work has shown that this model system can achieve a high efficiency in targeted content mixing, which is the hallmark of natural fusion.¹²⁻¹⁹ Thus our model is a highly controllable supramolecular membrane fusion system. The study not only simplifies the membrane fusion study, but also opens new possibilities for membrane fusion applications, for example it may use as a drug delivery system or nanoreactors.



Scheme 1. Schematic diagram of peptide coiled coil induced membrane fusion. (A) liposome membrane is drawn in close proximity to lipid bilayer by peptide Coil-K (red) and Coil-E (blue) electrostatic attraction. (B) Liposome is docking on surface of lipid bilayer by forming of CC-K/E coiled coil. (C) Accomplishment of membrane fusion between liposome and lipid bilayer. DOPE=1,2-dioleoyl-sn-glycero-3-phosphoethanolamine; Peg12=12-polyethylene glycol. Coil-K= Ac-(KIAALKE)₃-CONH₂; Coil-E= Ac-(EIAALEK)₃-CONH₂.

The aim of this thesis was to optimize the reduced membrane fusion model system resulting in more efficient content mixing in liposomal membrane fusion studies. One of the most essential parts to trigger our fusion model is peptide coiled coil complex. Therefore, this thesis starts with coiled coil zipping peptides studies, and following by the coiled coil mediated membrane fusion studies, in title of ‘zipping into fusion’.

Chapter 2 investigates the coiled coil peptide quaternary structure by paramagnetic NMR spectroscopy. In this chapter, a new approach of investigating coiled coil self-assembly has been described. The innovation of the method is based on a combination of site-directed spin labeling and fluorescent aromatic amino acid labeling on peptides. Using this approach, coiled coil interactions can be studied by paramagnetic $^1\text{H-NMR}$ and compared with steady state fluorescence measurements.

Chapter 3 describes the design and characterization of an antiparallel tetrameric coiled coil complex. The coiled coil quaternary structure was determined using the approach described in Chapter 2 and confirmed with from experimental and theoretical modeling. Finally, the fusogenicity of the antiparallel tetrameric coiled coil was studied and compared with the original liposome fusion model.

In Chapter 4, we tried to manipulate membrane fusion rate and efficiency by tuning either fusogen or lipid concentration. DLS and optical microscopy revealed that there are two fusion regimes – the fusion of thousands of liposomes through multiple fusion rounds into giant liposomes up to $10\ \mu\text{m}$ in diameter, and the fusion of two liposomes. This mapping of the rate and route of liposome fusion under different conditions gives a detailed understanding of the capacity of the reduced SNARE model to fuse liposome membranes. This understanding paves the way for future applications of the minimal model such as controlled nanoreactor mixing and the directed delivery of drugs to cells.

Chapter 5 describes attempts to control the rate of coiled coil driven membrane fusion. In this chapter, the thermal stability of the coiled coil motif was varied by changing the length of the peptides by using either two, three or four heptad repeat units. This study shows that the rate of liposome fusion can be manipulated by tuning coiled coil binding energy.

In Chapter 6 the liposome fusion efficiency was increased by decreasing the tendency of the peptides to aggregate in the prefusion state. In this chapter, the charges of the peptides was varied by single amino acid mutations at specific positions. The binding energies of these new coiled coil peptides were determined and the fusogenicity was determined

Introduction

revealing that amino acid mutations at positions not critical for coiled coil formation can influence the tendency to aggregate in the pre-fusion stage. Further, the membrane fusion efficiency was investigated.

Chapter 7 summarizes the findings of this work and gives and a general discussion is given.

Reference

1. R. Jahn, T. Lang and T. C. Sudhof, *Cell*, 2003, **112**, 519-533.
2. B. Westermann, *Journal of Biological Chemistry*, 2008, **283**, 13501-13505.
3. D. W. Wilson, S. W. Whiteheart and J. E. Rothman, *Trends in Biochemical Sciences*, 1991, **16**, 334-337.
4. B. Westermann, *Nature Reviews Molecular Cell Biology*, 2010, **11**, 872-884.
5. H. R. Marsden, I. Tomatsu and A. Kros, *Chem. Soc. Rev.*, 2011, **40**, 1572-1585.
6. B. R. Lentz, *Biophysical Journal*, 2006, **91**, 2747-2748.
7. S. M. Dennison, M. E. Bowen, A. T. Brunger and B. R. Lentz, *Biophysical Journal*, 2006, **90**, 1661-1675.
8. G. Nordlund, P. Brzezinski and C. von Ballmoos, *Nature Communications*, 2014, **5**.
9. W. Antonin, D. Fasshauer, S. Becker, R. Jahn and T. R. Schneider, *Nature Structural Biology*, 2002, **9**, 107-111.
10. J. M. Hernandez, A. J. B. Kreutzberger, V. Kiessling, L. K. Tamm and R. Jahn, *Proceedings of the National Academy of Sciences of the United States of America*, 2014, **111**, 12037-12042.
11. P. Zhou, T. Bacaj, X. F. Yang, Z. P. P. Pang and T. C. Sudhof, *Neuron*, 2013, **80**, 470-483.
12. H. R. Marsden, N. A. Elbers, P. H. H. Bomans, N. Sommerdijk and A. Kros, *Angewandte Chemie-International Edition*, 2009, **48**, 2330-2333.
13. F. Versluis, J. Voskuhl, J. Vos, H. Friedrich, B. J. Ravoo, P. H. H. Bomans, M. C. A. Stuart, N. A. J. M. Sommerdijk and A. Kros, *Soft Matter*, 2014.
14. I. Tomatsu, H. R. Marsden, M. Rabe, F. Versluis, T. T. Zheng, H. Zope and A. Kros, *Journal of Materials Chemistry*, 2011, **21**, 18927-18933.
15. H. R. Marsden, T. T. Zheng and A. Kros, *Abstracts of Papers of the American Chemical Society*, 2013, **245**.
16. T. T. Zheng, J. Voskuhl, F. Versluis, H. R. Zope, I. Tomatsu, H. R. Marsden and A. Kros, *Chemical Communications*, 2013, **49**, 3649-3651.
17. F. Versluis, J. Dominguez, J. Voskuhl and A. Kros, *Faraday Discussions*, 2013, **166**, 349-359.
18. F. Versluis, J. Voskuhl, B. van Kolck, H. Zope, M. Bremmer, T. Albrechtse and A. Kros, *Journal of the American Chemical Society*, 2013, **135**, 8057-8062.
19. H. R. Zope, F. Versluis, A. Ordas, J. Voskuhl, H. P. Spaink and A. Kros, *Angewandte Chemie-International Edition*, 2013, **52**, 14247-14251.

Chapter 2

Probing coiled-coil assembly by paramagnetic NMR spectroscopy



Zheng, T. T.; Boyle A.; Marsden, H. R.; Raap, J.; Valdink, D.; Martelli, G.; Kros, A., Probing coiled-coil assembly by paramagnetic NMR spectroscopy. *Organic & biomolecular chemistry*. 2014, Accepted.

Abstract

Here a new method to monitor the aggregation process and orientation of coiled coil peptide motifs is described. Peptides Coil-K and Coil-E which are designed to form a heterodimeric complex were labeled with aromatic FRET pair tryptophan (W) and tyrosine (Y) on the C-terminus respectively as a 'fingerprint' residue. One of the peptides was also labeled with the paramagnetic probe MTSL. Circular dichroism spectroscopy confirmed that the introduction of the MTSL label did not change the peptide secondary structure. One dimensional (1D)-proton NMR spectroscopy was used to study the peptide quaternary structure by monitoring the fluorophore aromatic NMR signal suppression due to proximity of the nitroxyl radical MTSL. 1D-NMR confirmed that peptide Coil-K and Coil-E form a heterodimer coiled coil with a parallel orientation. In addition, fluorescence emission quenching of the aromatic residue due to electron exchange with a nitroxyl radical confirmed the parallel coiled coil orientation. Thus, paramagnetic nitroxide and aromatic fluorophore labeling of peptides yield valuable information on the quaternary structure from 1D-NMR and steady-state fluorescence measurements. This convenient method is useful not only to investigate coiled coil assembly, but can also be applied to other supramolecular assemblies or biomacromolecules with a defined structure.

Introduction

Coiled coils are a structural motif comprised of two to seven α -helices folding around each other in a superhelical fashion and are one of the important subunit motifs found in proteins.¹⁻⁸ In nature, this versatile protein folding motif assembles in a wide range of structures with a variety of functions.⁹ One of the well-known coiled coil motifs are the so-called SNARE proteins, which is at center of the highly controlled intracellular membrane fusion mechanism enabling cell-to-cell communication in the nervous system.^{10, 11} Recently, a model system for in vitro membrane fusion, mimicking the SNARE protein complex has been designed.¹²⁻¹⁵ Here, membrane fusion was achieved by a pair of complementary lipidated peptides comprised of the heterodimeric coiled coil pair CC-K/E.¹⁶ However, the details of the fusion mechanism are still unclear. To obtain a better view on the membrane fusion mechanism, the coiled coil peptide CC-K/E quaternary structure has been studied. Typically X-ray diffraction, disulfide exchange, electron paramagnetic resonance (EPR),

Probing coiled-coil assembly by paramagnetic NMR spectroscopy

two-dimensional nuclear magnetic resonance (2D-NMR), 3D-NMR and even 4D-NMR techniques are employed to study the architecture of coiled coil peptide quaternary structures, for example the number of peptides in an assembly, the stoichiometry and their relative orientation.¹⁷⁻²⁸ However most of these techniques require expensive and complex equipment, which is not always readily available. Therefore, it is valuable to develop simple method that only requires standard laboratory equipment.

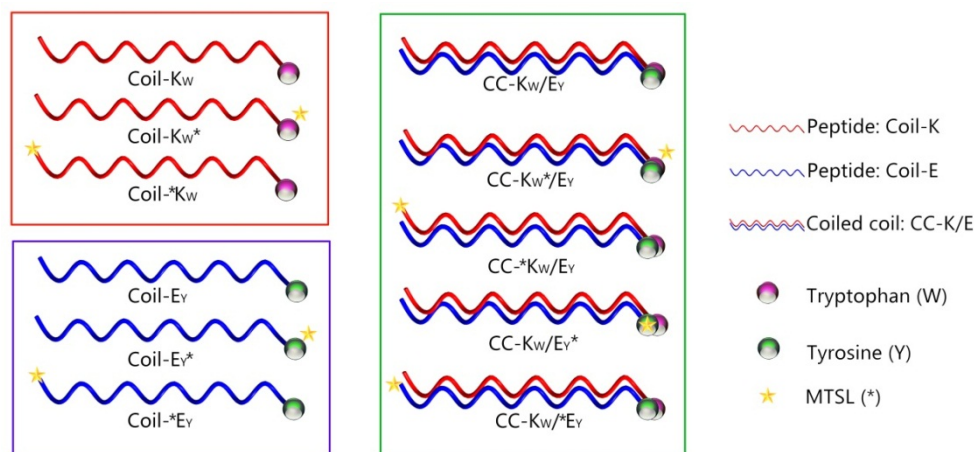
Here, a simple and easy method to investigate the coiled coil peptide assembly and orientation with a simple one-dimensional proton nuclear magnetic resonance (¹H-NMR) and steady state fluorescence measurements is reported.

To demonstrate our approach, the well-known E/K motif developed by Litowsky and Hodges was used as a model system. In recent years this coiled coil has been used by several groups in the field of supramolecular chemistry, polymers and membrane fusion.²⁹⁻³⁵ The coiled coil peptides Coil-K (Ac-(KIAALKE)₃-CONH₂) and Coil-E (Ac-(EIAALEK)₃-CONH₂) were labeled with tryptophan (W) and tyrosine (Y) at the C-terminus as a fluorophore FRET (fluorescence resonance energy transfer) pair respectively. Furthermore, the aromatic signals in 1D-proton NMR spectra are well-separated from all other proton signals. This allows for easy paramagnetic NMR spectroscopy analysis to determine the peptide orientation within the coiled coil motif. According to their characteristics in ¹H-NMR and fluorescence measurements, W and Y are defined as the 'fingerprint' functional group of peptide Coil-K and Coil-E respectively.

In this study, the paramagnetic nitroxyl radical MTSL (S-(2,2,5,5-tetramethyl-2,5-dihydro-1H-pyrrol-3-yl)methyl methanesulfonothioate) (see Appendix Part 6 for its chemical structure) was introduced at specific positions in the peptide to investigate the coiled coil assembly and peptide orientation.^{36, 37} In ¹H-NMR, there are magnetic dipolar interactions if the distance between a nucleus and an unpaired electron of a paramagnetic center is within 13.0 Å radius, leading to paramagnetic relaxation enhancement (PRE).³⁸⁻⁴³ This increases the relaxation rate of the nuclear magnetization, and results in the suppression of the nucleus NMR signal.^{40, 44} As a result, the neighboring signal will be drastically suppressed when it is located within 10.5 Å of the spin label. For example, in a 1D-proton NMR experiment, the proton signals of W or Y will be significantly suppressed when they are in proximity of the paramagnetic MTSL probe. In addition, the fluorescence will also be quenched by the intermolecular electron-exchange interaction between the ground-state stable nitroxide (MTSL) radical and the excited singlet state aromatic fluorophore (W and

Y) when the distance is less than 12 \AA .⁴⁵⁻⁴⁹ Thus in both NMR and fluorescence measurements, the proximity of a MTSL probe leads to signal suppression (See Appendix Figure A11 for the summary of the signal response regions from various measurements).

An equimolar mixture of Coil-K and Coil-E peptide results in the formation of a heterodimeric coiled coil motif CC-K/E. Both C-termini will be in close proximity when a parallel orientation is adopted; but will be on opposite sides of the coiled coil when an antiparallel orientation is adopted (Scheme 1.).



Scheme 1. Schematic illustration of designed peptides and coiled coil motifs. Coil-K peptides are labeled with a tryptophan(W) residue while Coil-E peptide are decorated with a tyrosine(Y) residue. A red helix represents peptide Coil-K, while a blue helix represents peptide Coil-E. Purple ball stands for tryptophan (W) labeled while green ball stands for tyrosine (Y) labeled. In this paper W and Y are always decorated on the C-terminus of all the peptides. A yellow star represents the MTSL- (*) nitroxyl radical spin label, which labeled either on C- or on N- terminus for investigating the possibility of CC-K/E parallel and antiparallel orientation respectively. Coiled coils formed by equimolar mixing of various Coil-K and Coil-E peptides are defined as CC-K/E. (See Table 1. for primary sequences of all peptides.)

The paramagnetic 1D-proton NMR and steady state fluorescence study demonstrates that the peptide Coil-K and Coil-E are forming a parallel heterodimeric coiled coil CC-K/E in neutral PBS buffer (Phosphate Buffer Saline). This is the first time that a paramagnetic nitroxide moiety is used to determine unequivocally the orientation and assembly of peptide strands in a coiled coil motif. Furthermore the peptide assembly ratio can be determined within a hetero-coiled coil complex. This method does not disturb self-

assembly and can be used to more complicate coiled coil motifs and allows broader applications in biomaterials field.

Experimental Section

Materials.

Fmoc-protected amino acids and Rink Amide resin (0.53 mmol g^{-1}) were purchased from NovaBiochem. HCTU (O-(1H-6-Chlorobenzotriazole-1-yl)-1,1,2,2-tetramethyluronium hexafluorophosphate), HOBT (1-Hydroxybenzotriazole) and DIPEA (N,N-Diisopropylethylamine) were from IRIS Biotech GmbH. NMP (N-methyl-2-pyrrolidone) and DMF (N,N-dimethylformamide) were from Biosolve. DCM (dichloromethane), TFE (2,2,2-Trifluoroethanol), TFE-D₃ (2,2,2-Trifluoroethanol-d₃), and deuterium oxide were obtained from Sigma-Aldrich. Acetic anhydride, piperidine, MeCN (acetonitrile), TFA (trifluoroacetic acid), and TIS (triisopropylsilane) were obtained from Fluka Chemie GmbH. MTSL ((S-(2,2,5,5-tetramethyl-2,5-dihydro-1H-pyrrol-3-yl)methyl methanesulfonothioate) was obtained from Toronto Research Chemicals Inc. PBS buffer contains: 30 mM K₂HPO₄, 19 mM KH₂PO₄, 150 mM NaCl, pH=7.4. The pH value was adjusted with either 0.1 M HCl or 0.1 M NaOH. Tris buffer contains 1M tris (2-Amino-2-hydroxymethyl-propane-1,3-diol), pH=7.0.

Peptide Synthesis.

Solid-phase peptide synthesis.

Peptides were synthesized on a CEM-Liberty 1 Single Channel Microwave Peptide Synthesizer using standard Fmoc chemistry.⁵⁰ Fmoc-protected Rink amide resin (0.53 mmol g^{-1}) was used to synthesize the peptides on a 0.25 mmol scale. The resin was swollen in DMF for 30 mins before use. Fmoc deprotection was performed using 20% (v/v) piperidine in DMF for 3 mins at 50 W with a maximum temperature of 80 °C. Four equivalents of a Fmoc-amino acid, four equivalents of HCTU and five equivalents of DIPEA in DMF were used for amino acid coupling for 5 mins at 40 W with a maximum temperature of 80 °C. For each amino acid coupling cycle, a deprotection and coupling time of 5 and 30 mins were used respectively. For cysteine coupling a cycle comprising 2

mins at 0 W followed by 4 mins at 40 W with a maximum temperature of 50 °C was used. Two wash steps (1.5 mL DMF) were performed between every amino acid coupling cycle. All peptides were acetylated manually at the N-terminus after completion of the synthesis using 20% (v/v) acetic anhydride in DMF for 1.5 hour. Peptides without a cysteine residue, were cleaved from the resin and side-chain deprotected using a mixture of TFA/water/TIS=95:2.5:2.5 (v/v) for 1 hour.⁵¹ Peptides with a Trt (trityl-) protected cysteine residue were cleaved from the resin with simultaneous side-chain deprotection using TFA/thioanisole/ethandithiol/phenol/H₂O=8.4:0.7:0.5:0.2:0.2 (v/v) for 3 hours at room temperature.⁵² The resulting solution was added drop-wise into an excess of 50ml cold diethyl ether to precipitate the deprotected peptide, followed by centrifugation and the liquid supernatant was removed. This procedure was repeated 3 times with the addition of fresh cold diethyl ether. All the peptides were dried under vacuum, dissolved in MilliQ water and lyophilized yielding a white powder.

MTSL nitroxyl radical label.

MTSL was conjugated to the peptide via a disulfide bond with the cysteine residue. One equivalent peptide (1 mM) was dissolved in 1 M tris buffer (pH=7.0) and five equivalents of MTSL in DMF (50 mM) were added slowly under an argon atmosphere and the final mixture was stirred for 3 hours at room temperature.⁵³ Next, the samples were lyophilized and stored at -20 °C before purification.

Peptide Purification.

The crude peptides were purified by RP-HPLC, using a Shimadzu HPLC system with two LC-8A pumps, and an SPD-10A VP UV-VIS detector. Samples elution was monitored by UV detection at 214 nm and 254 nm. Purification of peptides was performed on a Vydac C18 reversed phase preparative column with a flow rate 15 mL min⁻¹. Peptides were dissolved at a concentration of 5 mg ml⁻¹ in a mixture of Acetonitrile/H₂O/tert-butanol=1:1:1 (v/v) and eluted with a linear gradient from B to A. Solvent A=acetonitrile, while solvent B=0.1% TFA in H₂O. Acetylated peptides were purified using a 20 min gradient from 90% to 10% B, with a yield of 30%. MTSL labeled peptides were purified using a 25 min gradient elution from 80% to 20% B, with a typical yield of 20%. Purified

peptides were lyophilized and characterized by LC-MS using a Vydac C18 analytical column with a 1 mL min⁻¹ flow rate.

Circular Dichroism Spectroscopy.

CD (circular Dichroism Spectroscopy) spectra were obtained using a Jasco J-815 spectropolarimeter equipped with a peltier controlled thermostatic cell. The ellipticity is given as mean residue molar ellipticity, $[\theta]$ (10³ deg cm² dmol⁻¹), calculated by Eqn (1).¹¹
54

$$[\theta] = (\theta_{\text{obs}} \times \text{MRW}) / (10 \times lc) \quad (1)$$

Where θ_{obs} is the ellipticity in millidegrees, MRW is the mean residue molecular weight, l is the path length of the cuvette in cm and c is the peptide concentration in mg/mL.

A 1.0 mm quartz cuvette and a final concentration of 200 μ M peptide in PBS (pH=7.4). Spectra were recorded from 250 nm to 200 nm at 25 °C. Unless stated otherwise data points were collected with a 0.5 nm interval with a 1 nm bandwidth and scan speed of 1 nm per second. Each spectrum was an average of 5 scans. For analysis each spectrum had the appropriate background spectrum (buffer or 50% TFE) subtracted.

For determination of the coiled coil thermal dissociation constant, temperature dependent CD spectra were obtained using an external temperature sensor immersed in the sample.⁵⁵
⁵⁶ The temperature was controlled with the internal sensor and measured with the external sensor. A 10 mm quartz cuvette was used, and the solutions were stirred at 900 rpm. Spectra were recorded from 250 nm to 200 nm, with data collected at 0.5 nm intervals with a 1 nm bandwidth and a scan speed of 1 nm per second. The temperature range was 6 °C to 96 °C with a temperature gradient of 2.0 °C/minute and a 60 s delay after reaching the set temperature. The spectrum of PBS at 6 °C (average of 5 scans) was subtracted from each spectrum. All the thermal unfolding curves were analyzed using a two-state conformation transition model.^{57, 58}

The data was analyzed using a two-state unfolding model to determine the fraction folded using Eqn. (2),

$$F_f = ([\theta] - [\theta]_U) / ([\theta]_F - [\theta]_U) \quad (2)$$

Where $[\theta]$ is the observed molar ellipticity, $[\theta]_U$ is the ellipticity at 222 nm of the denatured state, as determined from the plateau of the ellipticity vs. temperature curve, and $[\theta]_F$ is the

ellipticity at 222 nm of the folded state at that temperature as determined from a linear fit of the initial stages of the ellipticity vs. temperature curve.

The fraction unfolded, F_U , was calculated by Eqn. (3),

$$F_U = 1 - F_f \quad (3)$$

The dimer dissociation constant in the transition zone was calculated using Eqn. (4),

$$K_U = 2P_t F_U^2 / F_f \quad (4)$$

P_t is the total peptide concentration. By taking the derivative of the $\ln(K_U)$ vs. Temperature and using this in the van't Hoff equation, Eqn. (5), the change in enthalpy associated with unfolding with temperature can be plotted:

$$\Delta H_U = RT^2 \times \frac{d\ln(K_U)}{dT} \quad (5)$$

The gradient of enthalpy vs. Temperature plot ΔC_p , is the difference in heat capacity between the folded and unfolded forms, and can be used in the Gibbs-Helmholtz equation adapted to monomer-dimer equilibrium, Eqn. (6), to obtain the Gibbs free energy of unfolding as a function of temperature by least-squares fitting,

$$\Delta G_U = \Delta H_m(1 - T/T_m) + \Delta C_p[T - T_m - T\ln(T/T_m)] - RT\ln[P_t] \quad (6)$$

T_m and H_m is the temperature and enthalpy at the midpoint of the transition at which the fraction of monomeric peptide is 0.5.¹²

¹H-magnetic resonance spectroscopy.

To monitor the aromatic region ¹H-NMR signals in the range from 8 ppm to 6 ppm of the amino acid W and Y, the proton signals of the peptide amide bonds were suppressed by proton-deuterium exchange using D₂O. Lyophilized peptide samples were dissolved at a concentration of 0.5 mg ml⁻¹ and incubated in D₂O for one hour, followed by lyophilization. This procedure was repeated three times. PBS (10ml, pH=7.4) was lyophilized and redissolved in D₂O to prepare a PBS/D₂O buffer solution. Peptide samples were prepared with a final concentration of 0.8 mM in PBS/D₂O buffer solution. All ¹H-NMR spectra were recorded at 298 K on a Bruker Avance III 600 MHz spectrometer with 32 scans for each sample.

Fluorescent spectroscopy.

Fluorescent experiments were conducted on a TECAN Infinite M1000 PRO fluorometer using a 96 well plate. The Z-position was 12500 μm , and the gain was optimized according to the amount of fluorophore in the sample. Excitation and emission slits were set at 5 nm. Emission spectra were measured from 290 nm to 450 nm in 1 nm steps at a fixed excitation wavelength of 275 nm. The temperature was set at 25°C. For consistent mixing, the plate was shaken inside the fluorometer for 30 seconds (2 mm linearly, 70 \times per minute). The spectra were corrected by subtraction of PBS or PBS/ TFE=1:1 (v/v) spectra as a background spectrum. The concentration of peptide E or K was 20 μM in each measurement, with 250 μL volume of peptide solution in each well.

Results and discussion

Peptide design and synthesis.

In this study the feasibility to use paramagnetic NMR and fluorescence spectroscopy to investigate the orientation of the complementary peptides in a coiled coil motif was explored. For this, the well-known shortest pair of heterodimeric coiled coil scaffold Coil-K and Coil-E was used as a model system. These sequences were modified with an aromatic amino acid, either a tryptophan (W) or tyrosine (Y) at the C-terminus and the paramagnetic nitroxyl radical MTSL at selected position as the sensitive 'signal suppression' functional group (Table 1.).^{16, 18, 54} A Glycine residue was added between the aromatic fluorophore and the original peptide sequence to minimize any potential influence on the coiled coil assembly. Furthermore, a cysteine residue was introduced at either the C- or N-terminus in order to label the peptide with the paramagnetic nitroxide radical via a sited-directed spin labeling (SDSL) method. MTSL was introduced via a disulfide bond to a cysteine residue as 'signal suppression' functional group.⁵⁹ The distance between the aromatic fluorophore and the nitroxide determines whether the signal is suppressed or not. Initially, MTSL was conjugated to the C-terminus of the peptide to probe the parallel assembly orientation in the coiled coil heterodimer. For comparison, the MTSL probe was placed at the N-terminus of the peptide to probe whether the antiparallel orientation would (co)exist as well (Table 1.).

All peptides which are synthesis by standard Fmoc solid phase synthesis on Rink Amide resin, and further purified by C18 RP-HPLC are characterized by both MALDI-TOF MS and LC-MS mass spectrometry. Analytical HPLC confirmed the purity of the peptide to be 99%, while UV measurements showed a purity of at least 95% (see Appendix).

Table 1. Peptide primary structure and molecular characterization.

Peptide Name	Sequence (from N to C terminus)	Molecular weight (g mol ⁻¹)	¹ H-NMR signal ^a	Fluorescence signal ^b
Coil-K _W	Ac ⁻ (KIAALKE) ₃ GW ⁻ CONH ₂	2564	✓	✓
Coil-K _W *	Ac ⁻ (KIAALKE) ₃ GW ⁻ CONH ₂ MTSL	2854	×	×
Coil-*K _W	Ac ⁻ C(KIAALKE) ₃ GW ⁻ CONH ₂ MTSL	2854	✓	✓
Coil-E _Y	Ac ⁻ (EIAALEK) ₃ GY ⁻ CONH ₂	2544	✓	✓
Coil-E _Y *	Ac ⁻ (EIAALEK) ₃ GY ⁻ CONH ₂ MTSL	2833	×	×
Coil-*E _Y	Ac ⁻ C(EIAALEK) ₃ GY ⁻ CONH ₂ MTSL	2833	✓	✓

^a. Refers to 1D-proton NMR chemical signal for aromatic protons of tryptophan (W) and tyrosine (Y) in the range of 6-8 ppm. ^b. Refers to fluorescence emission spectra wavelength from 285-445 nm with excitation at 275 nm. Both ¹H-NMR and fluorescence measurements were performed in presence of pH=7.4 PBS buffer. '✓' indicates there is signal observed while '×' indicates there is no signal observed.

Circular Dichroism Spectroscopy.

As single mutations in an amino acid sequence might alter the propensity to form coiled coils, the secondary structures and binding properties of all the Coil-K and Coil-E peptides including their derivatives were studied using circular dichroism (CD) spectroscopy (Figure 1 and Table 2). These results showed that in PBS buffer (pH=7.4) there is no significant change in the peptide secondary structure after introduction of the aromatic amino acids and the spin-label MTSL. All single Coil-K and Coil-E peptides retained their α -helical signature with two minimal bimodal at 222 nm and 208 nm (Fig.1A and 1B). The α -helicity and value of $[\theta]_{222}/[\theta]_{208}$ increased when the peptides were measured in 1:1 (v/v)

Probing coiled-coil assembly by paramagnetic NMR spectroscopy

TFE: PBS buffer as compared to the measurements performed in PBS buffer (Table 2). This indicates that all single peptides derivatives either with or without MTSL spin label consistently kept their ability to fold in a α -helix conformation. Thus, introduction of the MTSL label does not significantly alter the secondary structure of the peptides (CD spectra of the original Coil-K ((KIAALKE)₃) and Coil-E ((EIAALEK)₃) are shown in Appendix Figure A4).

Next, coiled coil formation of an equimolar mixture of Coil-K and Coil-E (including their MTSL derivatives) was studied, showing the typical coiled coil interactions with the helix content higher than 90% and the ratio of $[\theta]_{222}/[\theta]_{208}$ close to 1 (Figure 1C).^{60, 61} Trifluoroethanol (TFE) is known to enhance the intramolecular α -helicity while disrupting intermolecular interactions.^{62, 63} Addition of TFE resulted in a lower $[\theta]_{222}/[\theta]_{208}$ ratio and a decreased α -helicity confirming the existence of a coiled coil complex CC-K/E (Figure 1D).¹ CD measurements on an equimolar mixture of peptide Coil-K and peptide Coil-E with or without MTSL label showed that this modification did not significantly alter the coiled coil formation process.

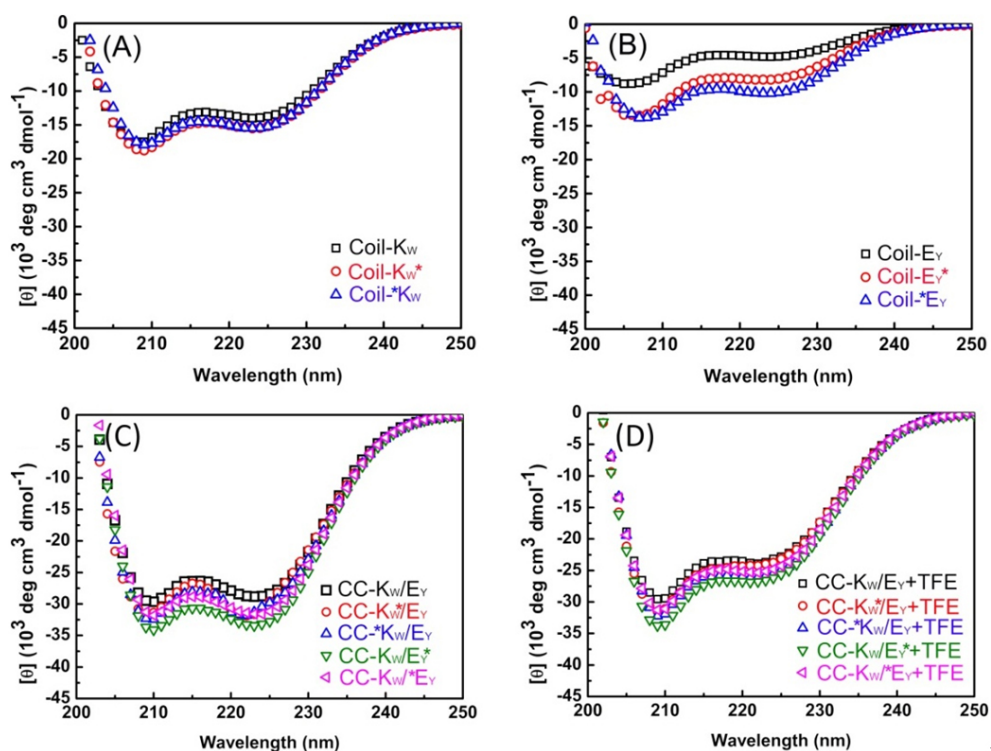


Figure 1. (A) CD spectra of secondary structure comparison of the peptides Coil-K_W, Coil-K_W^{*} and Coil-^{*}K_W were measured. (B) Secondary structure comparison of CD spectra from the peptides Coil-E_Y, Coil-E_Y^{*} and Coil-^{*}E. (C) Comparison of CD spectra of coiled coil motifs CC-K/E (including CC-K_W/E_Y, CC-K_W^{*}/E_Y, CC-^{*}K_W/E_Y, CC-^{*}K_W/E_Y^{*}, CC-K_W^{*}/E_Y) from an equimolar mixture of Coil-K and Coil-E peptides in pH=7.4 PBS saline. (D) Comparison of the CD spectra of the coiled coil motifs CC-K/E (including CC-K_W/E_Y, CC-K_W^{*}/E_Y, CC-^{*}K_W/E_Y, CC-K_W/E_Y^{*}, CC-K_W^{*}/E_Y) from an equimolar mixture of Coil-K and Coil-E peptides in 1:1 (v/v) PBS: TFE. [Total peptide]= 200 μM, PBS, pH=7.4, 25 °C.

Table 2. Secondary and quaternary CD spectroscopic data of synthetic peptides used in this study.

peptide ^a	[θ] ₂₂₂		% α-helix ^b		[θ] ₂₂₂ /[θ] ₂₀₈		Coiled-coil ^c
	50% TFE		50% TFE		50% TFE		
	PBS	In PBS	Benign	In PBS	Benign	In PBS	
Coil-K _W	-13925	-19699	43	60	0.70	0.81	-
Coil-K _W [*]	-15337	-19805	46	61	0.80	0.82	-
Coil- [*] K _W	-15411	-20057	47	61	0.81	0.82	-
Coil-E _Y	-4748	-16080	14	50	0.53	0.78	-
Coil-E _Y [*]	-8180	-17727	25	54	0.61	0.78	-
Coil- [*] E _Y	-10119	-18886	31	58	0.70	0.80	-
CC-K _W /E _Y	-28747	-23909	90	74	1.02	0.83	+
CC-K _W [*] /E _Y	-31892	-24251	99	75	1.04	0.78	+
CC- [*] K _W /E _Y	-31818	-260565	99	80	1.02	0.84	+
CC-K _W /E _Y [*]	-33297	-267780	100	82	1.04	0.81	+
CC-K _W [*] /E _Y	-31395	-25326	98	78	1.07	0.84	+

^a CC-K/E refers to equimolar concentration mixtures of the Coil-K and Coil-E peptides. ^b The percentage of α-helicity is calculated from 100 times the ratio between observed [θ]₂₂₂ to the predicted [θ]₂₂₂ for an α-helical peptide of n residues. The predicted α-helicity is reckoned from formula: [θ]₂₂₂ = -40000 × (1 - 4.6/n). ^{64, 65} ^c The signal + signifies a significant decrease in the [θ]₂₂₂/[θ]₂₀₈ ratio from benign to 50% TFE in PBS, indicative of the folded coiled-coil structure and vice versa. [Total Peptide]=200μM, PBS, pH=7.4, 25 °C.

Probing coiled-coil assembly by paramagnetic NMR spectroscopy

Next, the stoichiometry and binding energy of all coiled coil forming peptide pairs were determined. The binding stoichiometry of Coil-K and Coil-E mixtures was measured at a total peptide concentration of 200 μM with variable mol fractions of peptide Coil-K and Coil-E. A job-plot of $[\theta]_{222}$ as a function of the mol fraction of Coil-E peptide yields the binding stoichiometry.^{66, 67} For all CC-K/E (including their MTSL derivants) coiled coil complexes studied, a minimum of $[\theta]_{222}$ was always observed at an equimolar ratio of peptide Coil-K and Coil-E, indicating that peptide Coil-K (including MTSL derivants) and peptide Coil-E (including MTSL derivants) bind in a 1:1 stoichiometry (Figure 2A). This again proves that introduction of MTSL does not interfere with the classical 1 to 1 Coil-K and Coil-E heterodimerization (Original K/E stoichiometry see Appendix, Figure A5).

The molar ellipticity at 222 nm is directly proportional to the amount of helical structure and therefore thermal denaturation curves provide information of their folding stabilities.^{64, 68} Thus the thermodynamic stability of the CC-K/E pairs was determined by measuring the molar ellipticity at 222 nm wavelength as a function of temperature.¹¹ All peptide pairs showed a smooth cooperative transition from an α -helical coiled-coil structure to a random coil conformation (Figure 2B). All transitions showed to be fully reversible by lowering the temperature (See Appendix Figure A6).

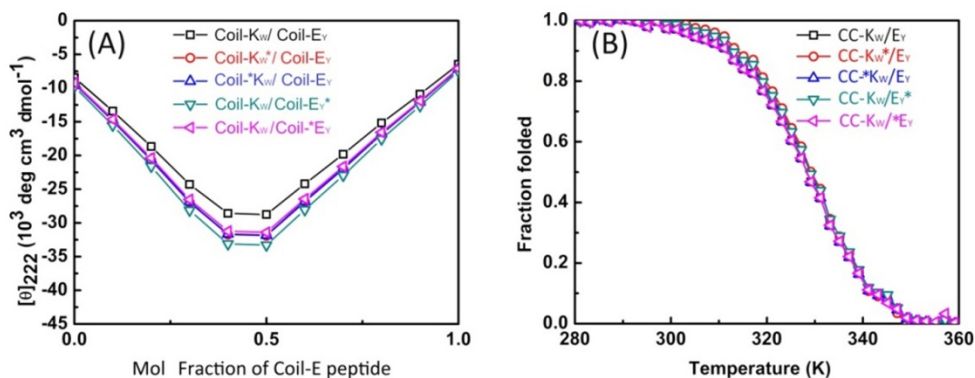


Figure 2. (A) Mean residue molar ellipticities at 222 nm wavelength for mixtures of the Coil-K and Coil-E peptides as a function of the mol fraction of the Coil-E peptide. All the measurements were carried out at a total peptide concentration of 200 μM on 25°C, in 1 mm quartz cuvette. (B) Thermal unfolding curves based on $[\theta]_{222}$ as a function of temperature. 1 cm quartz cuvette with stirring at 900 rpm was used. [Total peptide] = 40 μM , PBS, pH=7.4.

Temperature-dependent CD measurements showed that all the peptide complexes used in this study have an identical two-state transition denaturation process, dissociating from coiled coil to random coil. The binding parameters are summarized in Table 2. The dissociation constants for all coiled coils are in the same order of magnitude (10^{-8} M), showing that introduction of the MTSL residue does not influence the secondary structure, coiled coil formation and stability.

Table 3. Dissociation constants of E and K coiled coil complex from CD spectroscopy

Coiled-coil Complex	T_m (°C) ^b	ΔG_u (kcal mol ⁻¹) ^c	K_d (M) ^d
CC-K/E ^a	58	9.6	7×10^{-8}
CC-K _W /E _Y	57	10.8	7.7×10^{-8}
CC-K _W [*] /E _Y	56	11.6	6.4×10^{-8}
CC- [*] K _W /E _Y	57	11.0	7.5×10^{-8}
CC-K _W /E _Y [*]	56	11.8	6.5×10^{-8}
CC-K _W [*] /E _Y [*]	57	10.7	7.6×10^{-8}

^a data taken from literature.^{11, 16} ^b T_m = melting temperature, at which half of the peptide is in the unfolded form. ^c Gibbs free energy of unfolding at 25°C. ^d K_d = the dissociation constant.

¹H-NMR spectroscopy.

600 MHz ¹H-nuclear magnetic resonance spectroscopy was used to study the peptide coiled coil complex formation of peptide Coil-K and Coil-E including orientation and binding stoichiometry. Tryptophan (W) and Tyrosine (Y) residues show characteristic aromatic signals with a chemical shift in the range of 6 to 8 ppm, which in this study were used as a ‘fingerprint’ region in peptide Coil-K and Coil-E respectively. To avoid overlap, the N-H signals were suppressed by ‘H-D exchange’. Typical NMR signals of tryptophan (W) and tyrosine (Y) in the 6-8 ppm range of peptide Coil-K and Coil-E separately are shown in (Figure 3 A/C, blue line). When a MTSL label is located close to the aromatic functional group in the same peptide, the aromatic signals are fully suppressed (Figure 3 A/C, red line), due to paramagnetic relaxation enhancement (PRE).^{36, 41, 69-72} The linewidth of a proton signal will get significantly perturbed when the proton is within 13.0 Å from

Probing coiled-coil assembly by paramagnetic NMR spectroscopy

the paramagnetic MTSL probe, and fully suppressed if the distance is less than 10.5 Å due to its fast transverse relaxation rate.^{19,43} Theoretical calculation using Hyperchem software showed that the average distance between the MTSL nitroxide radical and the aromatic protons of the Tryptophan (W) group is 6.6 Å in Coil-K_W^{*} while in peptide Coil-E_Y^{*} the distance between MTSL and the aromatic Tyrosine (Y) group is 13.0 Å. Therefore a significant suppression of the NMR signals is observed (Figure 3 A/C, red line). In contrast, when the MTSL label is positioned on the N-terminus of the peptides, the distance between the nitroxyl radical and the tyrosine or tryptophan residues is too large in order to observe the PRE effect (Figure 3 A/C, black line). In peptide Coil-K_W^{*}, the average distance between radical and W is 36.7 Å while in peptide Coil-E_Y^{*} the distance between radical and Y is 40.1 Å. Next, ¹H-NMR spectra of the individual peptides were measured in 1:1 (v/v) TFE: PBS solution to eliminate any line broadening caused by peptide aggregation and to induce maximum α -helicity.⁷³ In NMR experiments, peptides aggregation results in the severe NMR signals decrease and line-broadening.^{18, 74-76} Even in TFE/PBS=1:1 (v/v) solution, a complete suppression of the aromatic proton was observed in Coil-K_W^{*} and Coil-E_Y^{*} confirming that the NMR signal suppression is only due to intramolecular paramagnetic relaxation enhancement (PRE) (Figure 3 B/D).

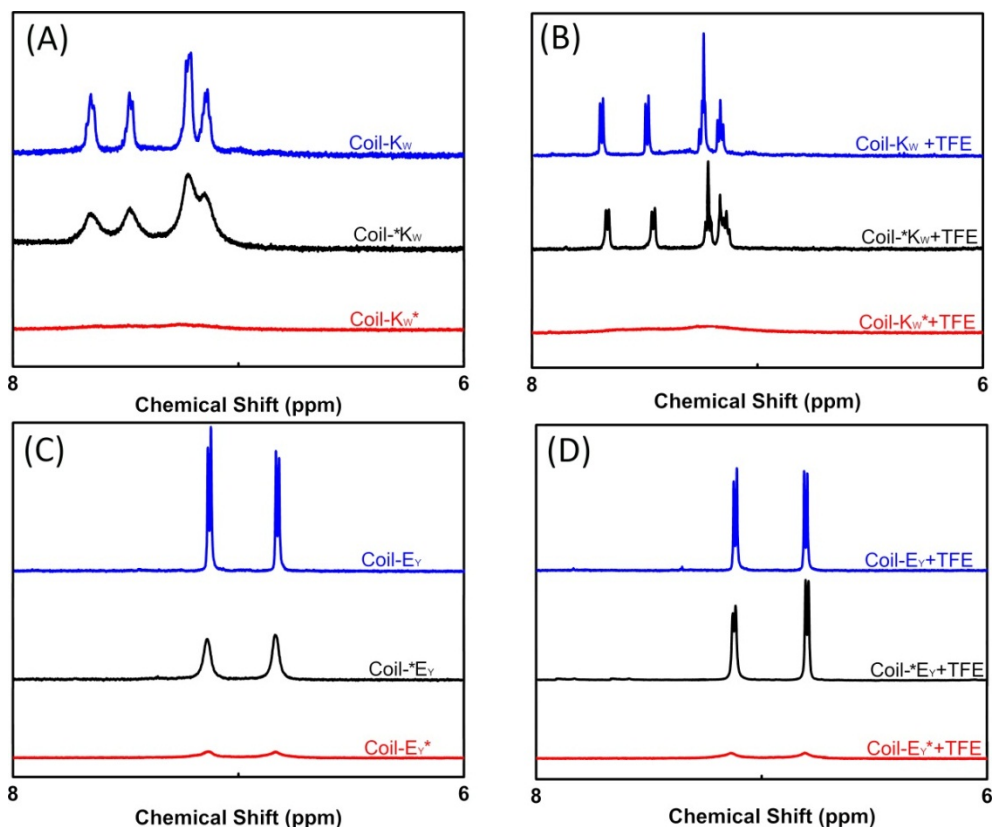


Figure 3. Aromatic region (6-8 ppm) of 600 MHz ^1H -nuclear magnetic resonance spectra showing tryptophan indole and tyrosine hydroxyphenyl functional groups of Coil-K and Coil-E derivatives respectively. (A) From top to bottom are the aromatic signals of Coil- K_W , Coil- $^*\text{K}_\text{W}$ and Coil- K_W^* in PBS. (B) From top to bottom are the aromatic signals of Coil- K_W , Coil- $^*\text{K}_\text{W}$ and Coil- K_W^* in 1:1 (v/v) PBS: TFE solution. (C) From top to bottom are the aromatic signals of Coil- E_Y , Coil- $^*\text{E}_\text{Y}$ and Coil- E_Y^* in PBS. (D) From top to bottom are the aromatic signals of Coil- E_Y , Coil- $^*\text{E}_\text{Y}$ and Coil- E_Y^* in 1:1 (v/v) PBS: TFE solution. [Total peptide]=0.8 mM.

Next, the coiled coil assembly of all the peptide pairs has been investigated (CC-K/E, Scheme 1). In coiled coils, complementary peptides zip together into close proximity resulting in a tight peptide complex. Therefore the PRE effect can be utilized to probe coiled coil formation and the relative orientation of the peptides within the complex.

When the MTS� label was positioned at the C-terminus of either Coil-K or Coil-E, it effectively gave suppression for both of their complementary peptides aromatic signals (Figure 4 A/C, compare blue and red trace). This indicates that peptide Coil-K and Coil-E assemble into a parallel coiled coil complex CC-K/E. In contrast, when the MTS� label

Probing coiled-coil assembly by paramagnetic NMR spectroscopy

was positioned at the N- terminus, no PRE effect was observed, confirming the peptides parallel orientation (Figure 4 A/C, compare blue and black trace).

Measuring the same peptide mixtures CC-K/E in 1:1 (v/v) TFE: PBS revealed the dissociation of the coiled coil complex as observed by the reappearance of the aromatic protons of the non-MTSL labeled peptide (Figure 4 B/D).

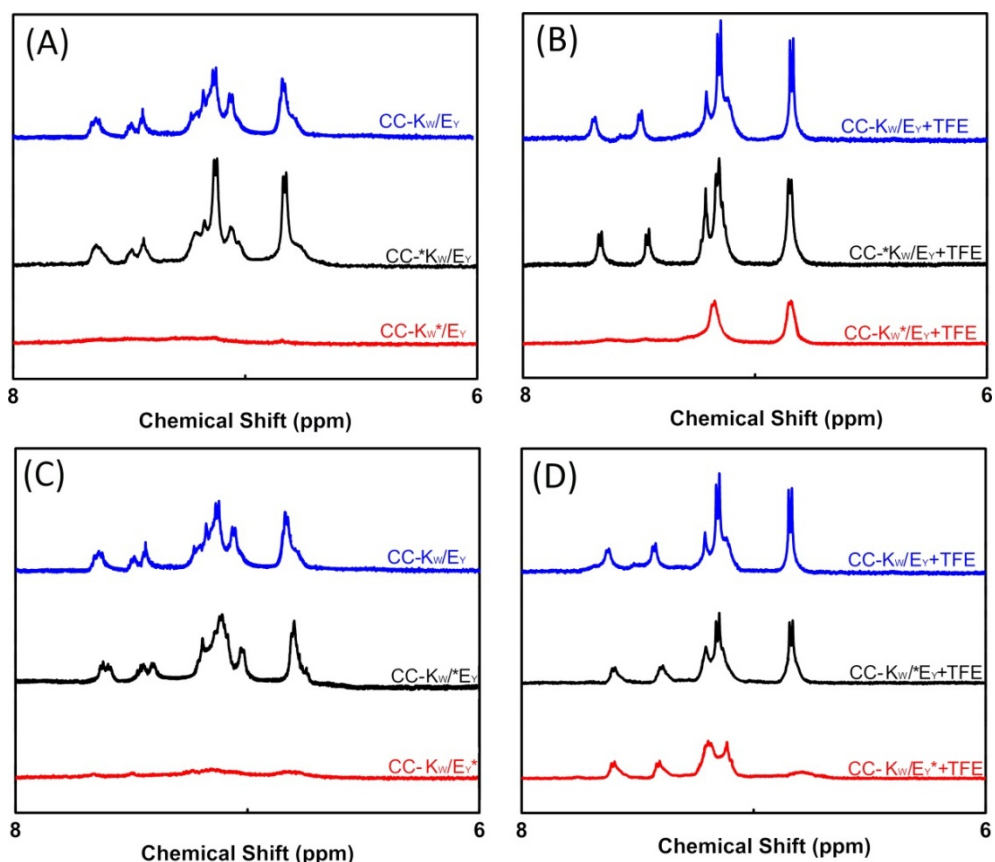


Figure 4. Aromatic Region (6-8 ppm) of 600 MHz ^1H -nuclear magnetic resonance spectra showing tryptophan indole and tyrosine hydroxyphenyl functional groups of equimolar mixtures of Coil-K and Coil-E (short name CC-K/E). (A) Aromatic signals of peptide CC-K/E complex in PBS. Blue line indicates CC-K_W/E_Y, black line indicates CC-^{*}K_W/E_Y and red line indicates CC-K_W^{*}/E_Y. (B) Aromatic signals of CC-K/E in 1:1 (v/v) TFE: PBS. Blue line indicate CC-K_W/E_Y, black line indicates CC-^{*}K_W/E_Y and red line indicates CC-K_W^{*}/E_Y. (C) Aromatic signals of CC-K/E in PBS. Blue line indicates CC-K_W/E_Y, black line indicates CC-K_W^{*}/E_Y and red line indicates CC-K_W/E_Y^{*}. (D) Aromatic signals of CC-K/E in 1:1 (v/v) TFE: PBS. Blue line indicates Coil-K_W/E_Y, black line indicates Coil-K_W^{*}/E_Y and red line indicates Coil-K_W/E_Y^{*}. [Total peptide]= 0.8 mM, PBS, pH=7.4.

Next, $^1\text{H-NMR}$ measurements were used to study the coiled coil binding stoichiometry. The molar ratio of Coil-K and Coil-E was varied from 2:1, 1:1 and 1:2 using peptides Coil- K_W^* and Coil- E_Y (Figure 5 A). Parallel coiled coil formation results in PRE suppression of the tyrosine residue NMR signal at the Coil- E_Y peptide as well as the tryptophan residue NMR signal at peptide Coil- K_W^* , due to their close proximity with MTSL. The measurements show that at a 2:1 and 1:1 ratio, the aromatic NMR region is silent. However, at a 1:2 ratio of peptide Coil- K_W^* and Coil- E_Y , the tyrosine signals were visible. This shows that peptides Coil-K and Coil-E indeed form a 1:1 coiled coil complex as the excess of peptide Coil- E_Y is not bound to Coil- K_W^* and thus no longer suppressed. Measuring the $^1\text{H-NMR}$ spectrum of MTSL labeled peptide Coil-E and non-labeled peptide Coil-K mixtures confirmed this finding (Figure 5B).

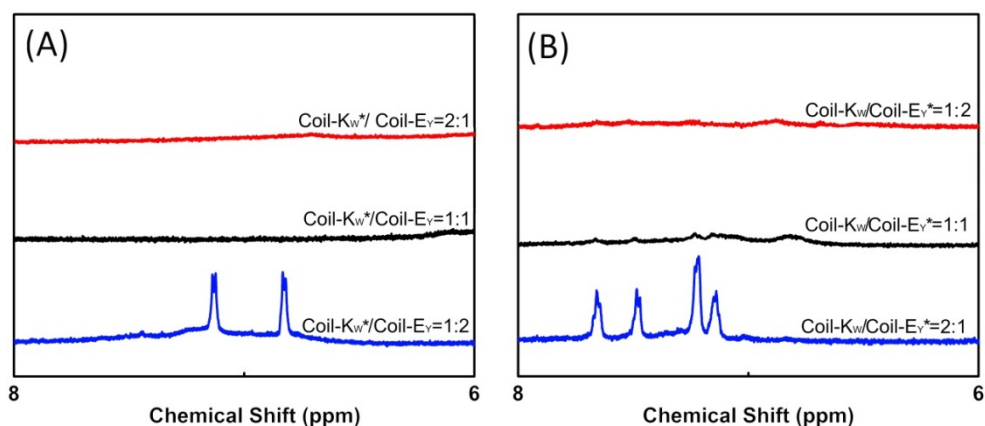


Figure 5. Aromatic region (6-8 ppm) of 600 MHz ^1H -nuclear magnetic resonance spectra showing tryptophan indole and tyrosine hydroxyphenyl functional groups of different molar ratio mixtures of Coil-K and Coil-E. (A) Aromatic signals of peptide Coil- K_W^* and Coil- E_Y mixtures. From top to bottom, the molar ratio between Coil- K_W^* and Coil- E_Y is 2:1, 1:1 and 1:2 respectively. (B) Aromatic signals of peptide Coil- K_W and Coil- E_Y^* mixtures. From top to bottom, the molar ratio between Coil- K_W and Coil- E_Y^* is 1:2, 1:1 and 2:1. [Total peptide]=0.8 mM

Thus nitroxyl radical PRE ‘signal suppression’ in $^1\text{H-NMR}$ experiments is a fast and reliable method to determine the peptide folding in a coiled coil motif, showing not only the peptide orientation but also the stoichiometry.

Fluorescence spectroscopy

To support $^1\text{H-NMR}$ measurements, steady-state fluorescence spectroscopy was used to probe the orientation of peptide E and K in the coiled coils by monitoring fluorophore electron excited singlet state quenching.⁴⁸ Within a 12 Å radius, fluorescence emission quenching occurs due to electron exchange interaction between the MTSL nitroxyl radical and a tryptophan (W) or a tyrosine (Y) fluorophore.^{46, 77-82} The degree of quenching is proportional to the electron exchange interaction, which is inverse proportional to the distance.^{83, 84}

Excitation at a wavelength of 275 nm results in fluorescence of both tryptophan and tyrosine residues. When a MTSL group is present at the C-terminus, significant fluorescence quenching was observed for Coil-KW* and Coil-EY* (Figure 6, blue line). However, when the MTSL label is positioned at the N-terminus, the quenching is almost absent (Figure 6, red line).

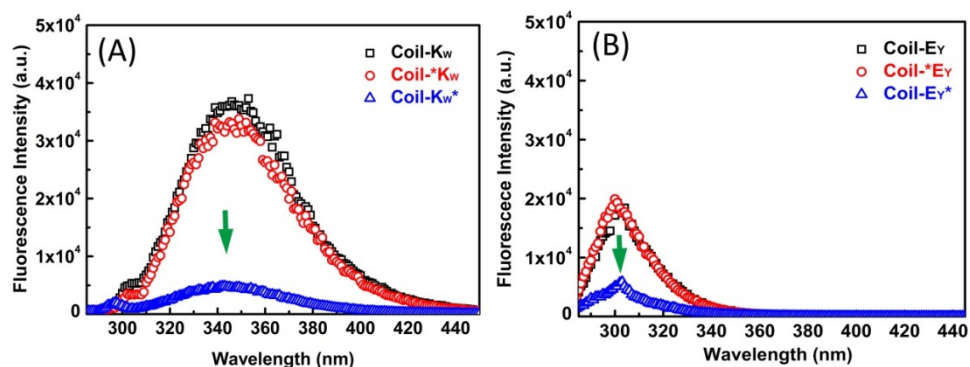


Figure 6. Fluorescence emission spectra (extension at 275 nm) of fluorescently labeled peptides Coil-K and Coil-E 50 μM in pH=7.4 PBS buffer solution at 25 $^\circ\text{C}$. (A) Presents peptide Coil-K_W (\square) in black, Coil-K_W* (\circ) in red and Coil-K_W* (Δ) in blue. (B) Presents peptide Coil-E_Y (\square) in black, Coil-E_Y* (\circ) in red and Coil-E_Y* (Δ) in blue. Green arrows indicate the fluorescence quenching position.

In the CC-K/E coiled coils both the donor fluorophore tyrosine (Y) and the acceptor fluorophore tryptophan (W) are located at the C-terminus. If peptide Coil-K_W and Coil-E_Y are adopting a parallel coiled coil orientation, the distance between W and Y is within the Förster distance ($R_0 \approx 1$ nm) resulting in fluorescence resonance energy transfer (FRET).

When the peptides assemble in an antiparallel fashion, no FRET will be observed.⁸⁵ Indeed, an equimolar mixture of peptide Coil-KW and Coil-EY results in an increased fluorescence signal of acceptor tryptophan (W) and a decreased fluorescence signal of donor tyrosine (Y) due to FRET, thus indicating a parallel coiled coil orientation of peptide E and K. In the presence of TFE, the energy transfer is lost due to the dissociation of coiled coil complex (Figure 7A).

When the MTSL nitroxyl radical is close to the fluorophore on the C- terminus, the fluorophore signal will be quenched due to the electron exchange interaction (Figure 6). If the complementary peptide is close to the MTSL labeled peptide due to coiled coil formation with a parallel orientation, the signal of the complementary peptide fluorophore is also quenched (Figure 7 B/C). For example, in peptide Coil-KW*, the MTSL quenches the tryptophan signal. In an equimolar mixture of Coil-KW* and Coil-EY, the tyrosine (Y) is also quenched, indicating that the tyrosine is in the vicinity of MTSL due to coiled coil formation. This can only occur when peptide Coil-K and Coil-E assemble into a parallel heterodimer. Addition of TFE results in separation of the peptides and the tyrosine signal reappears (Figure 7B). This indicates that peptide Coil-K is close to peptide Coil-E with a parallel orientation in the coiled coil motif.

The fluorescence quenching on the other peptide pair, Coil-EY* and Coil-KW has also been studied. In this complementary coiled coil forming peptide pair, peptide Coil-EY* was labeled with both the MTSL and Tyrosine (Y) at the C- terminus. As a result, the Tyrosine emission signal was quenched. In an equimolar mixture of Coil-EY* and Coil-KW, the signal of Tryptophan (W) was significantly quenched but was recovered upon TFE addition due to the coiled coil dissociation (Figure 7C). This again proves the parallel orientation in a CC-K/E coiled coil, supporting the findings of the paramagnetic NMR studies.

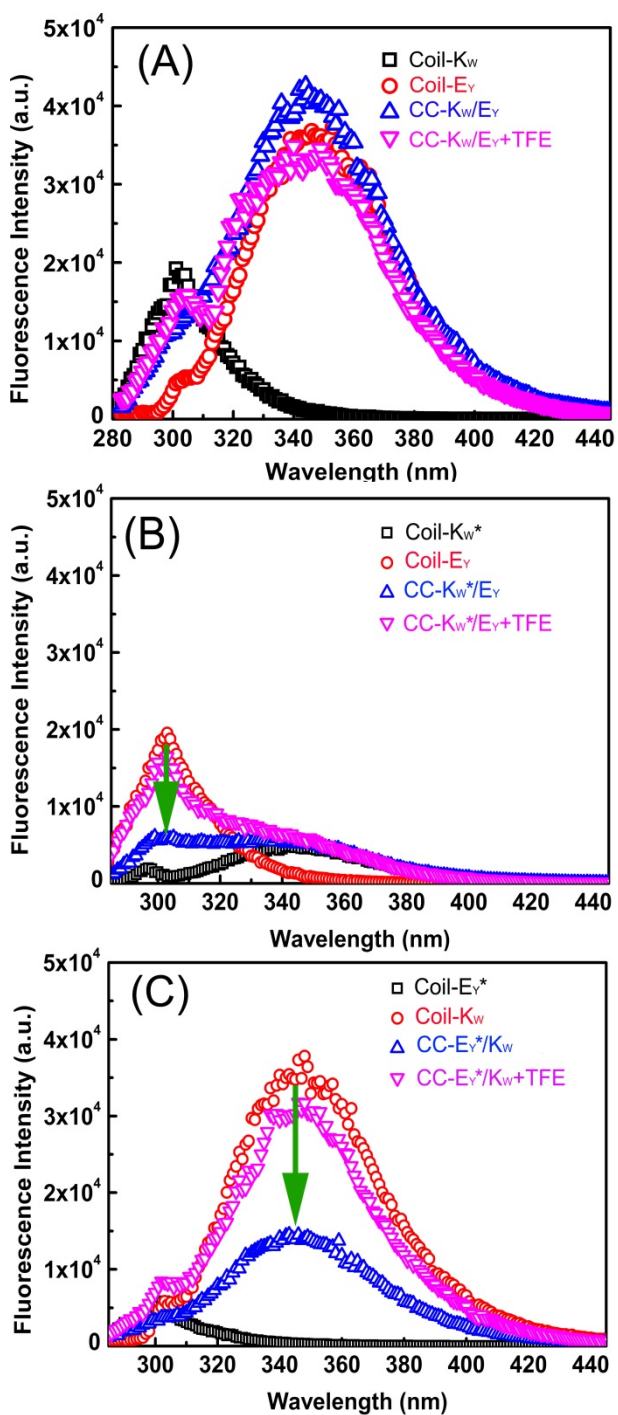


Figure 7. Fluorescence emission spectra of fluorescence labeled peptides Coil-K, Coil-E and CC-K/E (an equimolar mixture of Coil-K and Coil-E) in pH=7.4 PBS buffer solution and in 1:1 (v/v) PBS: TFE on 25 °C. [Total peptide]=50 μM. (A) Presents peptide Coil-K_W (□) in black, Coil-E_Y (○) in red, CC-K_W/E_Y (Δ) in blue and CC-K_W/E_Y+TFE (▽) in pink. (B) Presents peptide Coil-K_W^{*} (□) in black, Coil-E_Y (○) in red, Coil-K_W^{*}/E_Y (Δ) in blue and Coil-K_W^{*}/E_Y+TFE (▽) in rosy. (C) Presents peptide Coil-E_Y^{*} (□) in black, Coil-K_W (○) in red, Coil-E_Y^{*}/K_W (Δ) in blue and Coil-E_Y^{*}/K_W+TFE (▽) in pink. Green arrow signs the fluorescence quenching position.

Conclusions

Here a new approach to investigate the supramolecular assembly of a well-known coiled coil pair, using a combination of ¹H-NMR and fluorescence measurements has been shown. Labeling of the peptides with Tryptophan, Tyrosine and MTSL did not influence the secondary structure of the peptides. MTSL induced suppression of specific NMR signals enables the determination of the orientation and the stoichiometry in coiled coil motifs. Fluorescence quenching by MTSL using the same peptides confirmed the finding of the NMR studies. In this study aromatic fluorophore were used as the proton signals are well-separated from the other peptide signals. In principle however, every proton signal could be used for this purpose, for example the amide signal.⁴¹

Comparing with the existing methods to study coiled coil assembly, this method does not require changing of the environment (e.g. Crystallization necessary for X-ray diffraction) and avoid intermolecular interaction competition between chemical bond and hydrophobic core (e.g. disulfide exchange). The field of paramagnetic NMR spectroscopy is rapidly developing, and in this contribution the use in coiled coil assembly is shown. In addition, it is compatible with two- or multi-dimensional NMR, and the same peptides can be used for EPR measurements as well for further studies.⁸⁶

All the required manipulations are easily performed and with high efficiency. The careful choice in labeling combined with fast ¹H-NMR, fluorescence measurement significantly simplifies they study of non-covalent interactions in coiled coil s or other supramolecular assemblies. Further development of this approach will extensively spread on investigation of not only the peptide quaternary structure, but also most self-assembly systems.

Appendix

Part 1. Mass spectra for all the purified peptides

LC-MS spectra of all the purified peptides are shown in Figure A1.

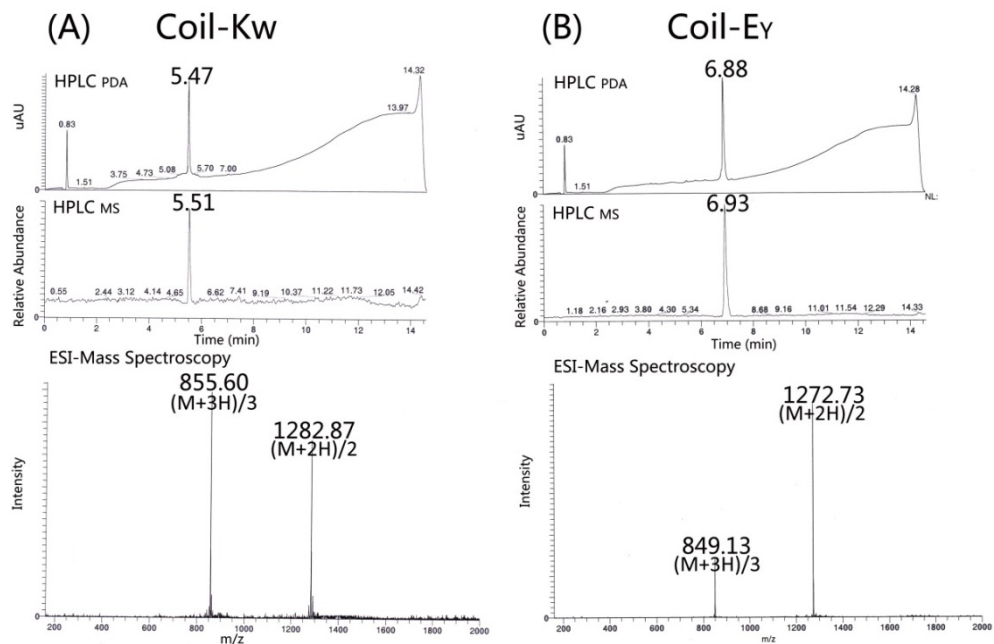


Figure A1. (A) LC-MS spectra of purified Coil-K_w, (B) LC-MS spectra of purified Coil-E_y. From top to bottom: UV (ultraviolet-visible) spectrum, ESI (electrospray ionization) spectrum, and mass spectrum.

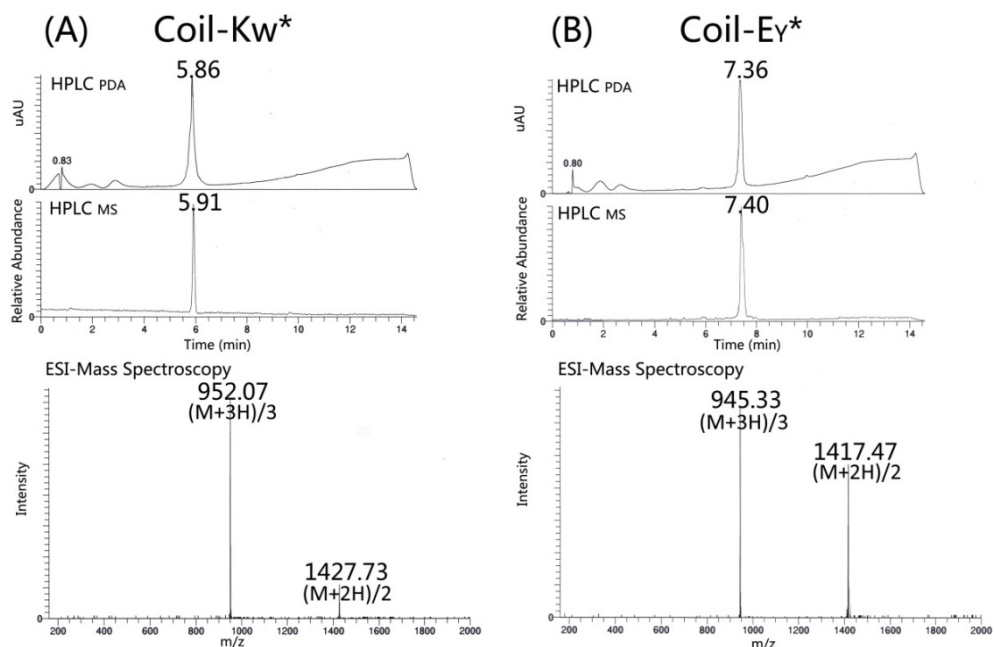


Figure A2. (A) LC-MS spectra of purified Coil-K_w* , (B) LC-MS spectra of purified Coil-E_γ* . From top to bottom: UV (ultraviolet-visible) spectrum, ESI (electrospray ionization) spectrum, and mass spectrum.

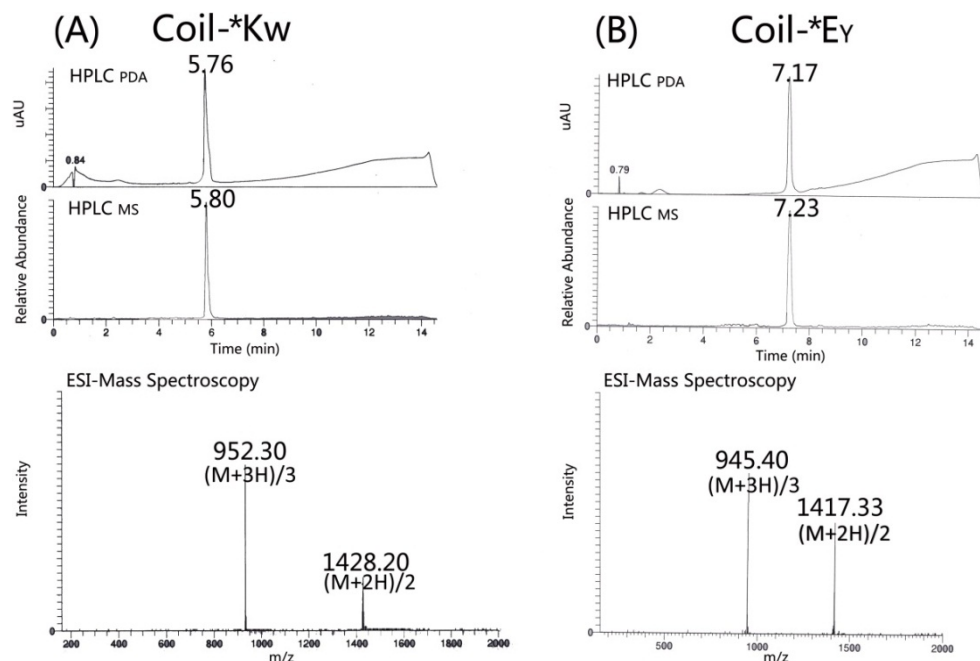


Figure A3. (A) LC-MS spectra of purified Coil-K*, (B) LC-MS spectra of purified Coil-E*. From top to bottom: UV (ultraviolet-visible) spectrum, ESI (electrospray ionization) spectrum, and mass spectrum.

Part 2. CD analysis for the Hodges Coil-K and Coil-E binding.

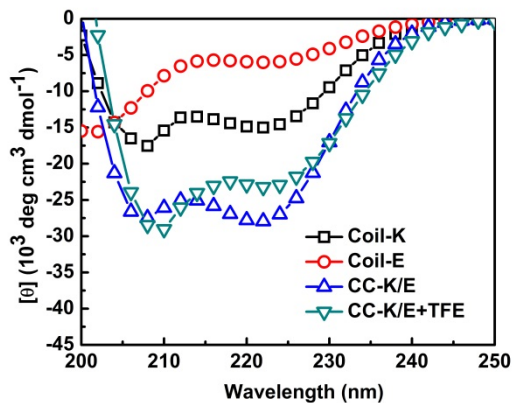


Figure A4. CD-spectra of peptide Coil-K (Ac-(KIAALKE)₃-CONH₂), Coil-E (Ac-(EIAALEK)₃-CONH₂), 1:1 mixture of Coil-K and Coil-E (CC-K/E) [total peptide]=200 μM in PBS (pH=7.4), 25 oC or TFE/PBS=1:1 (v/v).

Table A1. CD spectroscopic data of Coil-K, Coil-E and equimolar mixtures thereof.

Peptide ^a	θ_{222}		% α -helix ^b		$\theta_{222}/\theta_{208}$		Coiled-coil ^c
	Benign	50 % TFE	Benign	50 % TFE	Benign	50 % TFE	
Coil-K	-15010	-19788	48	63	0.86	0.92	-
Coil-E	-6016	-17067	19	55	0.6	0.78	-
CC-K/E	-27923	-23234	90	74	1.01	0.82	+

^a CC-K/E refers to an equimolar mixture of Coil-K and Coil-E. ^b The percentage α -helicity is calculated from 100 times the ratio between observed $[\theta]_{222}$ to the predicted $[\theta]_{222}$ for an α -helical peptide of n residues. The predicted α -helicity is calculated using the formula: $[\theta]_{222} = -40000 \times (1 - 4.6/n)$.^{64, 65} ^c The + sign signifies a significant decrease in the $[\theta]_{222}/[\theta]_{208}$ ratio from PBS to 50% TFE in PBS, indicative of the folded coiled-coil structure and vice versa. [Total Peptide]= 200 μ M in pH=7.4 PBS at 25 °C.

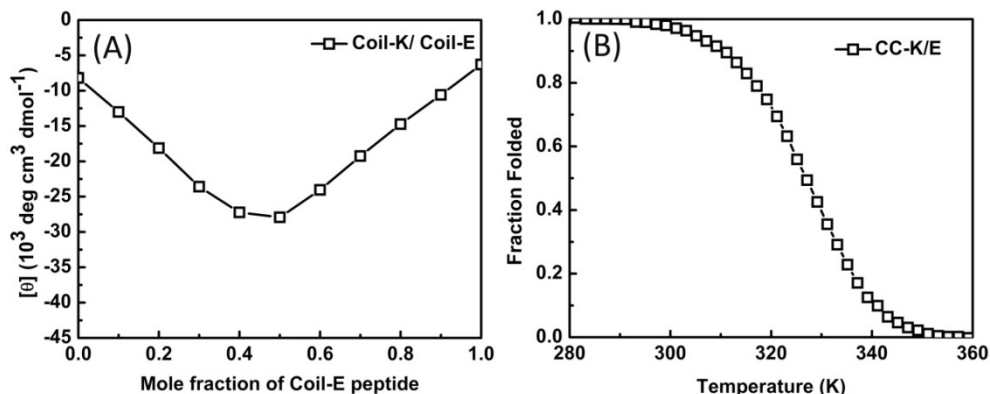


Figure A5. (A) Job plot of the mean residue molar ellipticity (222 nm) for mixtures of Coil-K and Coil-E as a function of the mole fraction of the Coil-E peptide. All the measurements were carried out at a total peptide concentration of 200 μ M in pH=7.4 PBS saline buffer on 25 °C, in a 1 mm quartz cuvette. (B) Thermal unfolding curve based on changes in $[\theta]_{222}$ due to dissociation of coiled coil CC-K/E. [Total peptide]=40 μ M, PBS, pH=7.4, 1 cm quartz cuvette.

Part 3. CD association fraction folded transitions of all coiled coils.

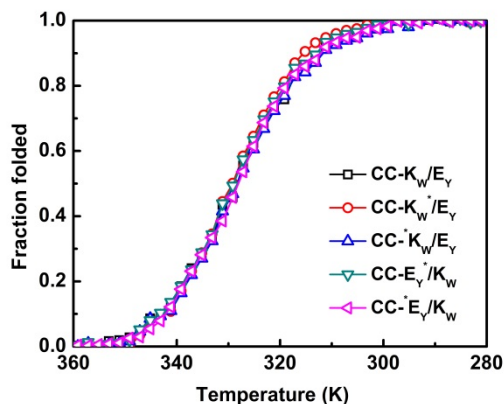


Figure A6. Thermal folding curve based on changes in $[\theta]_{222}$ as followed by CD by decreasing the temperature from 360 to 280 K. [Total peptide]=40 μ M, PBS, pH 7.4, 1 cm quartz cuvette.

Part 4. Hyperchem simulations⁸⁷

Hyperchem release 8.0 package has been used to simulate the peptide conformation and to determine the distance between MTSL and the aromatic amino acids in Coil-E and Coil-K. For this, Coil-K, Coil-E or their 1:1 complex were placed in a periodic box containing water molecules and the system was equilibrated at 300 K. The peptide can move in a constant-density environment which is similar to being in a liquid. The size of the box was set as a cube with $W=H=D= 56.104 \text{ \AA}$, and the minimum distance between solvent and solute atoms (atoms from peptides) is 2.3 \AA .⁸⁸

Molecular Mechanics simulation was based on a classical Newtonian calculation. Here, atoms were treated as Newtonian particles interacting through a potential energy function, which depend on bond lengths, bond angles, torsion angles, and nonbonded interactions (including van der Waals forces, electrostatic interactions, and hydrogen bonds). In these calculations, the forces on atoms are functions of the atomic position.

Furthermore, the AMBER force field which is typically used for developing proteins and nucleic acids was used to develop an all-atom model. The simulations were performed in standard way, with temperature at 300 K and 30 ps run time.

Figures beneath shows the details of the peptide conformation zoom in to atom level after simulation. In general, Coil-K peptide secondary structure is shown in red color, Coil-E peptide secondary structure in blue color and coiled coil motif either CC-K/E or CC-E/K in

brown color. From Hyperchem simulation, information of the different distances between MTSL nitroxide radical with either proton on W or on Y have been gained as support information to the paramagnetic 1D-proton NMR spectra results (Figure A7-10).

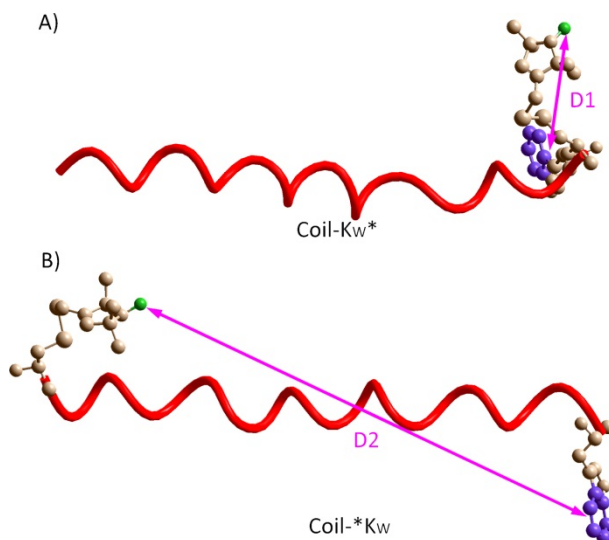


Figure A7. Structure tertiary structures of peptide Coil-KW* (A) and Coil- *KW (B). In A) D1 indicates the distance between nitroxyl group and the W in peptide Coil-KW*. The average distance D1 is 6.617 Å. In B) the average distance D2 between MTSL and W is 36.701 Å.

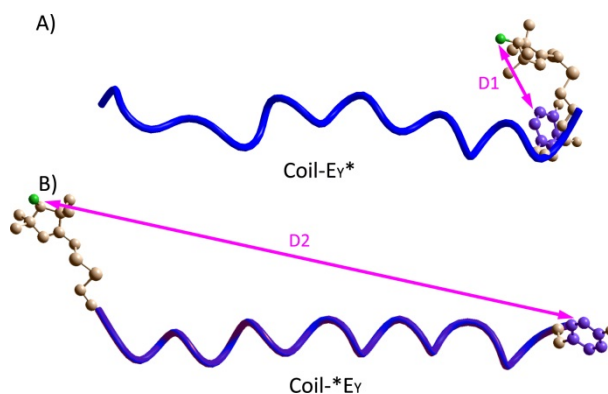


Figure A8. Structure of peptide Coil-EY* (A) and Coil- *EY (B). (A) the average distance D1= 13.0357 Å. (B) The average distance D2 = 40.0889 Å.

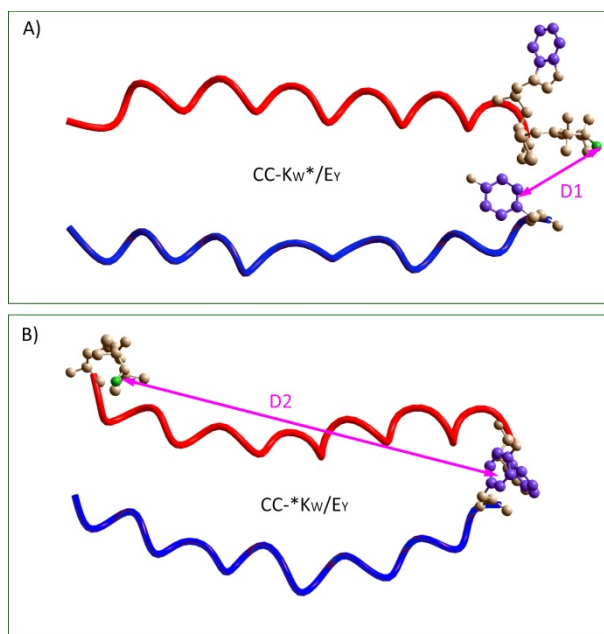


Figure A9. Coiled coil CC-K/E quaternary structure between subunits Coil-K (red) and Coil-E (blue). (A) Quaternary structure of peptide coiled coil complex CC-KW*/EY, the average distance $D1=8.9315 \text{ \AA}$. (B) Quaternary structure of CC-*KW/EY, the average distance $D2=37.2628 \text{ \AA}$.

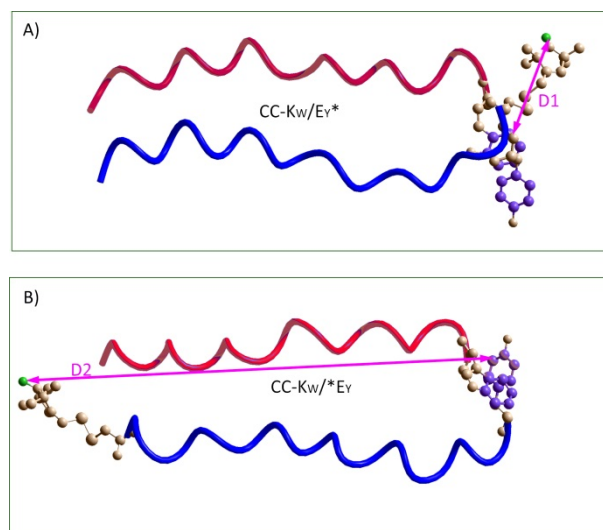


Figure A10. Coiled coil CC-K/E quaternary structure between subunits Coil-K (red) and Coil-E (blue). (A) Quaternary structure of peptide coiled coil complex CC- KW/EY*, the average distance $D1=8.9315 \text{ \AA}$. (B) Quaternary structure of CC-KW/*EY, the average

distance $D_2=38.7715 \text{ \AA}$.

Part 5. The summary of the signal intensity associated with distance.

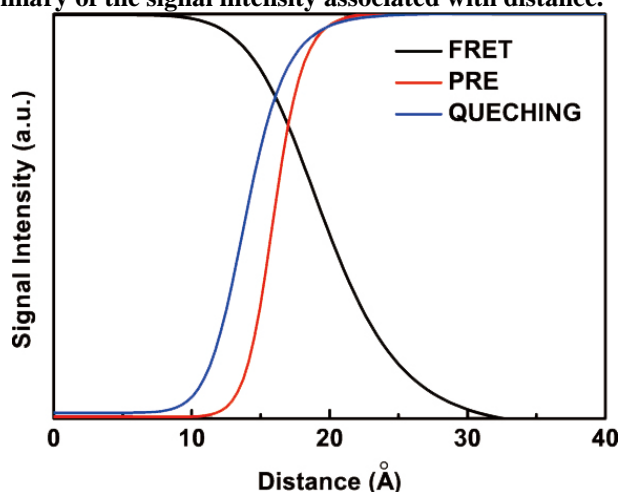
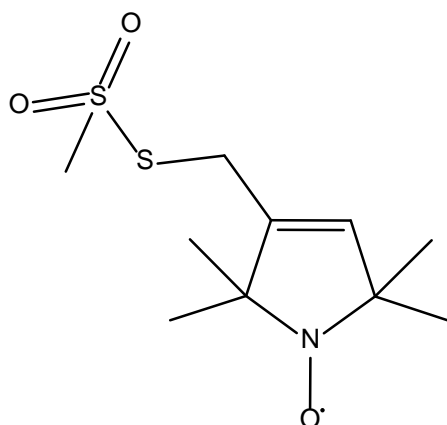


Figure A11. The distance depended signal intensity of FRET, PRE or fluorescence quenching method. The black line indicates the response distance between the FRET pair (donor and acceptor) in fluorescence resonance energy transfer (FRET) measurement; the red line indicates the response distance between the aromatic fluorophore and the MTSL nitroxyl radical in paramagnetic $^1\text{H-NMR}$ measurement; the blue line indicates the response distance between the fluorophore and the MTSL nitroxyl radical in fluorescence quenching measurement.

Part 6. Chemical Structure of MTSL



Reference

1. B. Apostolovic and H. A. Klok, *Biomacromolecules*, 2008, **9**, 3173-3180.
2. P. Burkhard, J. Stetefeld and S. V. Strelkov, *Trends in Cell Biology*, 2001, **11**, 82-88.
3. J. M. Mason and K. M. Arndt, *ChemBiochem*, 2004, **5**, 170-176.
4. A. M. Slovic, J. D. Lear and W. F. DeGrado, *Journal of Peptide Research*, 2005, **65**, 312-321.
5. A. L. Boyle and D. N. Woolfson, *Chemical Society Reviews*, 2011, **40**, 4295-4306.
6. M. Spinola-Amilibia, J. Rivera, M. Ortiz-Lombardia, A. Romero, J. L. Neira and J. Bravo, *Journal of Molecular Biology*, 2011, **411**, 1114-1127.
7. J. Liu, Q. Zheng, Y. Q. Deng, C. S. Cheng, N. R. Kallenbach and M. Lu, *Proceedings of the National Academy of Sciences of the United States of America*, 2006, **103**, 15457-15462.
8. G. Grigoryan and A. E. Keating, *Current Opinion in Structural Biology*, 2008, **18**, 477-483.
9. A. Lupas, *Trends in Biochemical Sciences*, 1996, **21**, 375-382.
10. S. Takamori, M. Holt, K. Stenius, E. A. Lemke, M. Gronborg, D. Riedel, H. Urlaub, S. Schenck, B. Brugger, P. Ringler, S. A. Muller, B. Rammner, F. Grater, J. S. Hub, B. L. De Groot, G. Mieskes, Y. Moriyama, J. Klingauf, H. Grubmuller, J. Heuser, F. Wieland and R. Jahn, *Cell*, 2006, **127**, 831-846.
11. H. Robson Marsden, A. V. Korobko, T. Zheng, J. Voskuhl and A. Kros, *Biomaterials Science*, 2013.
12. T. Zheng, J. Voskuhl, F. Versluis, H. R. Zope, I. Tomatsu, H. R. Marsden and A. Kros, *Chemical Communications*, 2013, **49**, 3649-3651.
13. H. R. Marsden, N. A. Elbers, P. H. H. Bomans, N. Sommerdijk and A. Kros, *Angewandte Chemie-International Edition*, 2009, **48**, 2330-2333.
14. F. Versluis, J. Dominguez, J. Voskuhl and A. Kros, *Faraday Discussions*, 2013.
15. F. Versluis, J. Voskuhl, B. van Kolck, H. Zope, M. Bremmer, T. Albregtse and A. Kros, *Journal of the American Chemical Society*, 2013, **135**, 8057-8062.
16. J. R. Litowski and R. S. Hodges, *Journal of Biological Chemistry*, 2002, **277**, 37272-37279.
17. M. N. Oda, T. M. Forte, R. O. Ryan and J. C. Voss, *Nature Structural Biology*, 2003, **10**, 455-460.
18. D. A. Lindhout, J. R. Litowski, P. Mercier, R. S. Hodges and B. D. Sykes, *Biopolymers*, 2004, **75**, 367-375.
19. C. Landon, F. Barbault, M. Legrain, L. Menin, M. Guenneugues, V. Schott, F. Vovelle and J. L. Dimarcq, *Protein Science*, 2004, **13**, 703-713.
20. M. Huber, S. Hiller, P. Schanda, M. Ernst, A. Bockmann, R. Verel and B. H. Meier, *Chemphyschem*, 2011, **12**, 915-918.
21. D. Sheppard, C. Y. Guo and V. Tugarinov, *Journal of the American Chemical Society*, 2009, **131**, 1364-+.
22. R. P. Meadows, D. Nettesheim, R. X. Xu, E. T. Olejniczak, A. M. Petros, T. F. Holzman, J. Severin, E. Gubbins, H. Smith and S. W. Fesik, *Journal of Cellular Biochemistry*, 1993, 279-279.

- 23.M. Huber, A. Bockmann, S. Hiller and B. H. Meier, *Physical Chemistry Chemical Physics*, 2012, **14**, 5239-5246.
- 24.D. M. Engelman and P. B. Moore, *Proceedings of the National Academy of Sciences of the United States of America*, 1972, **69**, 1997-&.
- 25.E. K. Oshea, J. D. Klemm, P. S. Kim and T. Alber, *Science*, 1991, **254**, 539-544.
- 26.K. Nagai and H. Hori, *Febs Letters*, 1978, **93**, 275-277.
- 27.M. G. Oakley and P. S. Kim, *Biochemistry*, 1998, **37**, 12603-12610.
- 28.U. I. M. Gerling, E. Brandenburg, H. von Berlepsch, K. Pagel and B. Koksch, *Biomacromolecules*, 2011, **12**, 2988-2996.
- 29.B. Apostolovic and H. A. Klok, *Biomacromolecules*, 2010, **11**, 1891-1895.
- 30.B. Apostolovic, M. Danial and H. A. Klok, *Chemical Society Reviews*, 2010, **39**, 3541-3575.
- 31.J. Voskuhl, C. Wendeln, F. Versluis, E. C. Fritz, O. Roling, H. Zope, C. Schulz, S. Rinnen, H. F. Arlinghaus, B. J. Ravoo and A. Kros, *Angewandte Chemie-International Edition*, 2012, **51**, 12616-12620.
- 32.F. Versluis, J. Dominguez, J. Voskuhl and A. Kros, *Faraday Discussions*, 2013.
- 33.A. S. Lygina, K. Meyenberg, R. Jahn and U. Diederichsen, *Angewandte Chemie-International Edition*, 2011, **50**, 8597-8601.
- 34.G. Martelli, H. R. Zope, M. Brovia Capell and A. Kros, *Chemical Communications*, 2013.
- 35.H. Zope, C. B. Quer, P. H. H. Bomans, N. A. J. M. Sommerdijk, A. Kros and W. Jiskoot, *Advanced Healthcare Materials*, 2013, n/a-n/a.
- 36.L. J. Berliner, J. Grunwald, H. O. Hankovszky and K. Hideg, *Analytical Biochemistry*, 1982, **119**, 450-455.
- 37.G. L. Kenyon and T. W. Bruice, in *Methods in Enzymology*, eds. C. H. W. Hirs and N. T. Serge, Academic Press, 1977, vol. Volume 47, pp. 407-430.
- 38.I. Solomon, *Physical Review*, 1955, **99**, 559-565.
- 39.N. Bloembergen and L. O. Morgan, *Journal of Chemical Physics*, 1961, **34**, 842-&.
- 40.J. Iwahara and G. M. Clore, *Nature*, 2006, **440**, 1227-1230.
- 41.C. Peggion, M. Jost, W. M. De Borggraeve, M. Crisma, F. Formaggio and C. Toniolo, *Chemistry & Biodiversity*, 2007, **4**, 1256-1268.
- 42.K. A. Bolin, P. Hanson, S. J. Wright and G. L. Millhauser, *Journal of Magnetic Resonance*, 1998, **131**, 248-253.
- 43.Z. O. Shenkarev, A. S. Paramonov, T. A. Balashova, Z. A. Yakimenko, M. B. Baru, L. G. Mustaeva, J. Raap, T. V. Ovchinnikova and A. S. Arseniev, *Biochemical and Biophysical Research Communications*, 2004, **325**, 1099-1105.
- 44.H. E. Lindfors, P. E. de Koning, J. W. Drijfhout, B. Venezia and M. Ubbink, *Journal of Biomolecular Nmr*, 2008, **41**, 157-167.
- 45.S. A. Green, D. J. Simpson, G. Zhou, P. S. Ho and N. V. Blough, *Journal of the American Chemical Society*, 1990, **112**, 7337-7346.
- 46.N. V. Blough and D. J. Simpson, *Journal of the American Chemical Society*, 1988, **110**, 1915-1917.
- 47.P. L. Privalov, E. I. Tiktopulo and V. M. Tischenko, *Journal of Molecular Biology*, 1979, **127**, 203-216.

- 48.S. E. Herbelin and N. V. Blough, *Journal of Physical Chemistry B*, 1998, **102**, 8170-8176.
- 49.B. Pispisa, A. Palleschi, L. Stella, M. Venanzi and C. Toniolo, *Journal of Physical Chemistry B*, 1998, **102**, 7890-7898.
- 50.S. A. Palasek, Z. J. Cox and J. M. Collins, *Journal of Peptide Science*, 2007, **13**, 143-148.
- 51.H. Robson Marsden and A. Kros, *Angewandte Chemie (International ed. in English)*, 2010, **49**, 2988-3005.
- 52.T. Kaiser, G. J. Nicholson, H. J. Kohlbau and W. Voelter, *Tetrahedron Letters*, 1996, **37**, 1187-1190.
- 53.A. Y. Kornilova, J. F. Wishart, W. Z. Xiao, R. C. Lasey, A. Fedorova, Y. K. Shin and M. Y. Ogawa, *Journal of the American Chemical Society*, 2000, **122**, 7999-8006.
- 54.J. R. Litowski and R. S. Hodges, *Journal of Peptide Research*, 2001, **58**, 477-492.
- 55.S. M. Kelly and N. C. Price, *Biochimica Et Biophysica Acta-Protein Structure and Molecular Enzymology*, 1997, **1338**, 161-185.
- 56.S. M. Kelly, T. J. Jess and N. C. Price, *Biochimica Et Biophysica Acta-Proteins and Proteomics*, 2005, **1751**, 119-139.
- 57.P. Lavigne, M. P. Crump, S. M. Gagne, R. S. Hodges, C. M. Kay and B. D. Sykes, *Journal of Molecular Biology*, 1998, **281**, 165-181.
- 58.P. Lavigne, L. H. Kondejewski, M. E. Houston, F. D. Sonnichsen, B. Lix, B. D. Sykes, R. S. Hodges and C. M. Kay, *Journal of Molecular Biology*, 1995, **254**, 505-520.
- 59.E. J. Hustedt and A. H. Beth, *Annual Review of Biophysics and Biomolecular Structure*, 1999, **28**, 129-153.
- 60.N. E. Zhou, C. M. Kay and R. S. Hodges, *Biochemistry*, 1992, **31**, 5739-5746.
- 61.N. E. Zhou, C. M. Kay and R. S. Hodges, *Journal of Biological Chemistry*, 1992, **267**, 2664-2670.
- 62.N. J. Greenfield, *Nature Protocols*, 2006, **1**, 2527-2535.
- 63.N. J. Greenfield, *Nature Protocols*, 2006, **1**, 2876-2890.
- 64.Y. H. Chen, J. T. Yang and K. H. Chau, *Biochemistry*, 1974, **13**, 3350-3359.
- 65.N. J. Greenfield, *Nature Protocols*, 2006, **1**, 2733-2741.
- 66.C. Y. Huang, *Methods in Enzymology*, 1982, **87**, 509-525.
- 67.Z. D. Hill and P. Maccarthy, *Journal of Chemical Education*, 1986, **63**, 162-167.
- 68.J. A. Boice, G. R. Dieckmann, W. F. DeGrado and R. Fairman, *Biochemistry*, 1996, **35**, 14480-14485.
- 69.T. Gruene, M. K. Cho, I. Karyagina, H. Y. Kim, C. Grosse, K. Giller, M. Zweckstetter and S. Becker, *Journal of Biomolecular Nmr*, 2011, **49**, 111-119.
- 70.J. Y. Guan, P. H. J. Keizers, W. M. Liu, F. Lohr, S. P. Skinner, E. A. Heeneman, H. Schwalbe, M. Ubbink and G. Siegal, *Journal of the American Chemical Society*, 2013, **135**, 5859-5868.
- 71.S. Scanu, J. M. Foerster, G. M. Ullmann and M. Ubbink, *Journal of the American Chemical Society*, 2013, **135**, 7681-7692.
- 72.S. P. Skinner, M. Moshev, M. A. S. Hass and M. Ubbink, *Journal of Biomolecular Nmr*, 2013, **55**, 379-389.

- 73.J. Davies and L. Riechmann, *Febs Letters*, 1994, **339**, 285-290.
- 74.T. Sugiki, C. Yoshiura, Y. Kofuku, T. Ueda, I. Shimada and H. Takahashi, *Protein Science*, 2009, **18**, 1115-1120.
- 75.R. Page, W. Peti, I. A. Wilson, R. C. Stevens and K. Wuthrich, *Proceedings of the National Academy of Sciences of the United States of America*, 2005, **102**, 1901-1905.
- 76.S. Y. M. Lau, A. K. Taneja and R. S. Hodges, *Journal of Biological Chemistry*, 1984, **259**, 3253-3261.
- 77.F. Mito, T. Yamasaki, Y. Ito, M. Yamato, H. Mino, H. Sadasue, C. Shirahama, K. Sakai, H. Utsumi and K. Yamada, *Chemical Communications*, 2011, **47**, 5070-5072.
- 78.G. I. Likhtenstein, K. Ishii and S. Nakatsuji, *Photochemistry and Photobiology*, 2007, **83**, 871-881.
- 79.E. Gatto, G. Bocchinfuso, A. Palleschi, S. Oncea, M. De Zotti, F. Formaggio, C. Toniolo and M. Venanzi, *Chemistry & Biodiversity*, 2013, **10**, 887-903.
- 80.S. K. Chattopadhyay, P. K. Das and G. L. Hug, *Journal of the American Chemical Society*, 1983, **105**, 6205-6210.
- 81.C. V. Kumar, S. K. Chattopadhyay and P. K. Das, *Journal of the American Chemical Society*, 1983, **105**, 5143-5144.
- 82.W. A. Yee, V. A. Kuzmin, D. S. Kliger, G. S. Hammond and A. J. Twarowski, *Journal of the American Chemical Society*, 1979, **101**, 5104-5106.
- 83.J. Karpiuk and Z. R. Grabowski, *Chemical Physics Letters*, 1989, **160**, 451-456.
- 84.S. Atik and L. A. Singer, *Journal of the American Chemical Society*, 1978, **100**, 3234-3235.
- 85.J. Eisinger, *Biochemistry*, 1969, **8**, 3902-&.
- 86.X. Han, J. H. Bushweller, D. S. Cafiso and L. K. Tamm, *Nature Structural Biology*, 2001, **8**, 715-720.
- 87.I. Hypercube, 2002, 2220.

Chapter 3

An antiparallel tetrameric coiled coil



Zheng, T. T.; Bulacu, M.; Boyle, A.; Versluis, F.; Marsden, H. R.; Valdink, D.; Martelli, G.; Raap, J.; Sevink, A.; Kros, A., An antiparallel tetrameric coiled coil. Manuscript in preparation.

Abstract

The complementary peptides Coil-K and Coil-E were designed to assemble into a heterodimeric coiled coil. In this chapter the effect of reversing the amino acid sequence of peptide Coil-E on complex formation with peptide Coil-K was investigated. Coiled coil assembly was studied using multiple techniques including circular dichroism, paramagnetic proton NMR, steady state fluorescence spectroscopy measurements, sedimentation equilibrium analytical ultracentrifugation and computational simulations. All results show that the reversed peptide Coil-E_r folds with Coil-K to form a stable antiparallel coiled coil tetramer and not an antiparallel heterodimer as previously reported. Thus, this study shows that reversing the amino acid sequence of coiled coil peptides can strongly affect the self-assembly process. Cholesterol modified peptide Coil-K and Coil-E_r were tested as a model system for membrane fusion and its fusogenicity was compared to the original model system. Lipid and content mixing assays showed no significant difference between the heterodimeric and the tetramer coiled coil mediated fusion. This indicates that peptide orientation and oligomerization state does not influence this model system for membrane fusion.

Introduction

One of the most important vital vesicle trafficking processes is SNARE-dependent (SNARE: soluble N-ethylmaleimide-sensitive factor attachment protein receptor) membrane fusion.¹⁻³ There are three key steps in this process: membrane surface conjugated SNARE proteins self-assemble as SNAREpins (a four-helix SNARE proteins coiled coil bundle), followed by docking of the two opposing lipid membrane resulting in full fusion and content transfer.⁴

One of the reduced SNARE membrane fusion models is based on the complementary peptide pair Coil-K ([KIAALKE]₃) and Coil-E ([EIAALEK]₃).⁵ These two peptides were designed to assemble into a parallel heterodimeric coiled coil. In this reduced peptide-induced membrane fusion model, the SNARE proteins are mimicked by lipidated conjugates of Coil-K and Coil-E.⁶⁻⁹ Upon mixing equimolar amounts of Coil-E modified liposomes with Coil-K liposomes, parallel coiled coil formation (CC-K/E) forces the two opposing membrane into close proximity resulting in full fusion of the liposomes.^{10, 11}

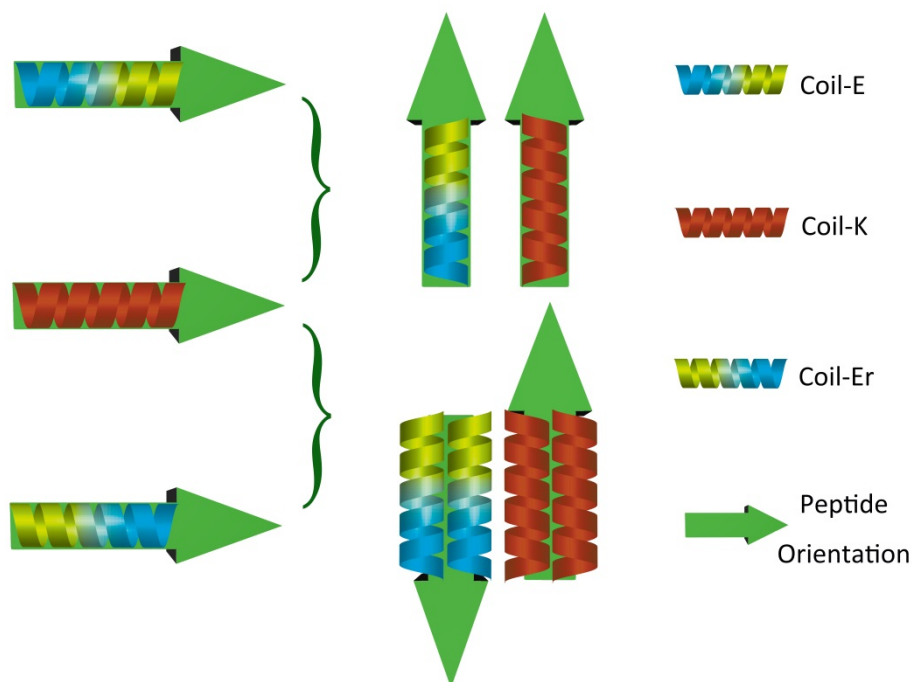
An antiparallel tetrameric coiled coil

Recently, there were two contradictory studies with the point of contention that whether the parallel zipper-like coiled coil motif orientation is required for membrane fusion. Two different approaches were used to design a non-zipper-like coiled coil motif orientation: the Diederichsen group designed an anti-parallel coiled coil motif in which the membrane anchor is located at both peptides C-terminus; while Kros designed parallel coiled coil forming peptides in which the membrane anchor is located at opposite peptide termini (See Appendix Figure A1).^{12, 13} In the first approach it was shown that a non-zipper-like coiled coil assembly inhibits membrane fusion, indicating the necessity of a zipper-like coiled coil orientation in the fusion process similar to the SNARE protein mediated fusion; In contrast, Kros showed that a non-zipper-like coiled coil motif also induces membrane fusion, indicating that the coiled coil orientation (i.e. parallel vs antiparallel) does not affect the rate of fusion with these short peptides. It is important to note that while the Kros group used the original Coil-K/Coil-E (CC-K/E) peptides; the Diederichsen group used Coil-E with a reversed amino acid sequence (i.e. Coil-E_r). It was hypothesized that Coil-K with Coil-E_r ([KELAAIE]₃) would form an antiparallel dimeric coiled coil. However no experimental data supporting this assumption was given.

The effect of reversing the amino acid primary sequence on self-assembly behavior has been studied before.¹⁴⁻¹⁶ However most of these studies on inverted protein/peptide focused on single protein/peptide intramolecular interactions and not on heterodimeric coiled coil motifs.¹⁷ Therefore we set out to study the assembly of Coil-K and Coil-E_r and to find out whether an antiparallel heterodimer is formed (Scheme 1).

For this, a variety of spectroscopic techniques were used to study the coiled coil assembly of Coil-E and Coil-E_r with Coil-K. Circular Dichroism (CD) showed that the peptides Coil-E and Coil-E_r have a similar α -helical secondary structure. However, when mixed with an equimolar amount of Coil-K, different coiled coil assemblies were observed. While Coil-K and Coil-E form a parallel dimer, Coil-K and Coil-E_r assemble into an antiparallel tetramer. Paramagnetic NMR and fluorescence studies revealed the antiparallel orientation.

Furthermore, computer simulations and sedimentation equilibrium ultracentrifugation experiments confirmed the formation of a stable tetrameric species. This study thus showed that reversing the amino acid sequence of a hetero coiled coil motif can significantly alter its self-assembly behavior.^{5, 14, 18-20} Finally the fusogenicity of cholesterol anchored Coil-K and Coil-E_r was compared to our Coil-K/Coil-E_r model system for membrane fusion.



Scheme 1. Schematic representation of Coil-E, Coil-Er and their assembly with Coil-K. The green arrow indicates the orientation of peptide from N terminus to C terminus. An equimolar mixture of Coil-E with Coil-K yields a parallel dimer. An equimolar mixture of peptide Coil-Er with Coil-K yields an antiparallel tetramer.

Experimental Section

Materials.

Fmoc-protected amino acids and Rink Amide resin (0.53 mmol g^{-1}) were purchased from NovaBiochem. HCTU (O-(1H-6-Chlorobenzotriazole-1-yl)-1,1,2,2-tetramethyluronium hexafluorophosphate), HOBT (1-Hydroxybenzotriazole) and DIPEA (N,N-Diisopropylethylamine) were from IRIS Biotech GmbH. NMP (N-methyl-2-pyrrolidone) and DMF (N,N-dimethylformamide) were from Biosolve. DCM (dichloromethane), TFE (2,2,2-Trifluoroethanol), TFE- D_3 (2,2,2-Trifluoroethanol- d_3), and deuterium oxide were obtained from Sigma-Aldrich. Acetic anhydride, piperidine, MeCN (acetonitrile), TFA (trifluoroacetic acid), and TIS (triisopropylsilane) were obtained from Fluka Chemie GmbH. MTSL ((S-(2,2,5,5-tetramethyl-2,5-dihydro-1H-pyrrol-3-yl)methyl methanesulfonothioate) was obtained from Toronto Research Chemicals Inc. PBS buffer

An antiparallel tetrameric coiled coil

contains: 30 mM K₂HPO₄, 19 mM KH₂PO₄, 150 mM NaCl, pH=7.4. The pH value was adjusted with either 0.1 M HCl or 0.1 M NaOH. Tris buffer contains 1M tris (2-Amino-2-hydroxymethyl-propane-1,3-diol), pH=7.0.

Peptide Synthesis.

Solid-phase peptide synthesis.

Peptides were synthesized on a CEM-Liberty 1 Single Channel Microwave Peptide Synthesizer using standard Fmoc chemistry.²¹ Fmoc-protected Rink amide resin (0.53 mmol g⁻¹) was used to synthesize the peptides on a 0.25 mmol scale. The resin was swollen in DMF for 30 mins before use. Fmoc deprotection was performed using 20% (v/v) piperidine in DMF for 3 mins at 50 W with a maximum temperature of 80 °C. Four equivalents of a Fmoc-amino acid, four equivalents of HCTU and five equivalents of DIPEA in DMF were used for amino acid coupling for 5 mins at 40 W with a maximum temperature of 80 °C. For each amino acid coupling cycle, a deprotection and coupling time of 5 and 30 mins were used respectively. For cysteine coupling a cycle comprising 2 mins at 0 W followed by 4 mins at 40 W with a maximum temperature of 50 °C was used. Two wash steps (1.5 mL DMF) were performed between every amino acid coupling cycle. All peptides were acetylated manually at the N-terminus after completion of the synthesis using 20% (v/v) acetic anhydride in DMF for 1.5 hour. Peptides without a cysteine residue, were cleaved from the resin and side-chain deprotected using a mixture of TFA/water/TIS=95:2.5:2.5 (v/v) for 1 hour.²² Peptides with a Trt (trityl-) protected cysteine residue were cleaved from the resin with simultaneous side-chain deprotection using TFA/thioanisole/ethanedithiol/phenol/H₂O=8.4:0.7:0.5:0.2:0.2 (v/v) for 3 hours at room temperature.²³ The resulting solution was added drop-wise into an excess of 50 ml cold diethyl ether to precipitate the deprotected peptide, followed by centrifugation and the liquid supernatant was removed. This procedure was repeated 3 times with the addition of fresh cold diethyl ether. All the peptides were dried under vacuum, dissolved in MilliQ water and lyophilized yielding a white powder.

MTSL nitroxyl radical label.

MTSL was conjugated to the peptide via a disulfide bond with the cysteine residue. One equivalent peptide (1 mM) was dissolved in 1 M tris buffer (pH=7.0) and five equivalents of MTSL in DMF (50 mM) were added slowly under an argon atmosphere and the final mixture was stirred for 3 hours at room temperature.²⁴ Next, the samples were lyophilized and stored at -20 °C before purification.

Peptide Purification.

The crude peptides were purified by RP-HPLC, using a Shimadzu HPLC system with two LC-8A pumps, and an SPD-10A VP UV-VIS detector. Samples elution was monitored by UV detection at 214 nm and 254 nm. Purification of peptides was performed on a Vydac C18 reversed phase preparative column with a flow rate 15 mL min⁻¹. Peptides were dissolved at a concentration of 5 mg ml⁻¹ in a mixture of Acetonitrile/H₂O/tert-butanol=1:1:1 (v/v) and eluted with a linear gradient from B to A. Solvent A=acetonitrile, while solvent B=0.1% TFA in H₂O. Acetylated peptides were purified using a 20 min gradient from 90% to 10% B, with a yield of 30%. MTSL labeled peptides were purified using a 25 min gradient elution from 80% to 20% B, with a typical yield of 20%. Purified peptides were lyophilized and characterized by LC-MS using a Vydac C18 analytical column with a 1 mL min⁻¹ flow rate.

Circular Dichroism Spectroscopy.

CD (circular dichroism spectroscopy) spectra were obtained using a Jasco J-815 spectropolarimeter equipped with a peltier controlled thermostatic cell. The ellipticity is given as mean residue molar ellipticity, $[\theta]$ (10³deg cm² dmol⁻¹), calculated by Eqn (1).^{6, 25}

$$[\theta] = (\theta_{\text{obs}} \times \text{MRW}) / (10 \times lc) \quad (1)$$

Where θ_{obs} is the ellipticity in millidegrees, MRW is the mean residue molecular weight, l is the path length of the cuvette in cm and c is the peptide concentration in mg/mL.

A 1.0 mm quartz cuvette and a final concentration of 200 μ M peptide in PBS (pH=7.4) were used. Spectra were recorded from 250 nm to 200 nm at 25 °C. Unless stated otherwise data points were collected with a 0.5 nm interval with a 1 nm bandwidth and

An antiparallel tetrameric coiled coil

scan speed of 1 nm per second. Each spectrum was an average of 5 scans. For analysis each spectrum had the appropriate background spectrum (buffer or 50% TFE) subtracted.

For determination of the coiled coil thermal dissociation constant, temperature dependent CD spectra were obtained using an external temperature sensor immersed in the sample.^{26,}

²⁷ The temperature was controlled with the internal sensor and measured with the external sensor. A 10 mm quartz cuvette was used, and the solutions were stirred at 900 rpm. Spectra were recorded from 250 nm to 200 nm, with data collected at 0.5 nm intervals with a 1 nm bandwidth and a scan speed of 1 nm per second. The temperature range was 6 °C to 96 °C with a temperature gradient of 2.0 °C minute⁻¹ and a 60 s delay after reaching the set temperature. The spectrum of PBS at 6 °C (average of 5 scans) was subtracted from each spectrum. All the thermal unfolding curves were analyzed using a two-state conformation transition model.^{28, 29}

The data was analyzed using a two-state unfolding model to determine the fraction folded using Eqn. (2),

$$F_f = ([\theta] - [\theta]_U)/([\theta]_F - [\theta]_U) \quad (2)$$

Where $[\theta]$ is the observed molar ellipticity, $[\theta]_U$ is the ellipticity at 222 nm of the denatured state, as determined from the plateau of the ellipticity vs. temperature curve, and $[\theta]_F$ is the ellipticity at 222 nm of the folded state at that temperature as determined from a linear fit of the initial stages of the ellipticity vs. temperature curve.

The fraction unfolded, F_U , was calculated by Eqn. (3),

$$F_U = 1 - F_f \quad (3)$$

The dimer dissociation constant in the transition zone was calculated using Eqn. (4),

$$K_U = 2P_t F_U^2 / F_f \quad (4)$$

P_t is the total peptide concentration. By taking the derivative of the $\ln(K_U)$ vs. temperature curve and using this in the van't Hoff equation, Eqn. (5), the change in enthalpy associated with unfolding with temperature can be plotted:

$$\Delta H_U = RT^2 \times \frac{d\ln(K_U)}{dT} \quad (5)$$

The gradient of the enthalpy vs. temperature plot ΔC_p , is the difference in heat capacity between the folded and unfolded forms, and can be used in the Gibbs-Helmholtz equation adapted to monomer-dimer equilibrium, Eqn. (6), to obtain the Gibbs free energy of unfolding as a function of temperature by least-squares fitting,

$$\Delta G_U = \Delta H_m(1 - T/T_m) + \Delta C_p[T - T_m - T\ln(T/T_m)] - RT\ln[P_t] \quad (6)$$

T_m and H_m are the temperature and enthalpy at the midpoint of the transition at which the fraction of monomeric peptide is 0.5.⁹

¹H-magnetic resonance spectroscopy.

To monitor the aromatic region ¹H-NMR signals in the range from 6 ppm to 8 ppm of the amino acids W and Y, the peptide amide proton signals were suppressed by proton-deuterium exchange using D₂O. Lyophilized peptide samples were dissolved at a concentration of 0.5 mg ml⁻¹ and incubated in D₂O for one hour, followed by lyophilization. This procedure was repeated three times. PBS (10 ml, pH=7.4) was lyophilized and redissolved in D₂O to prepare a PBS/D₂O buffer solution. Peptide samples were prepared with a final concentration of 0.8 mM in PBS/D₂O buffer solution. All ¹H-NMR spectra were recorded at 298 K on a Bruker Avance III 600 MHz spectrometer with 32 scans for each sample.

Fluorescence spectroscopy.

Fluorescence experiments were conducted on a TECAN Infinite M1000 PRO fluorometer using a 96 well plate. The Z-position was 12500 μm, and the gain was optimized according to the amount of fluorophore in the sample. Excitation and emission slits were set at 5 nm. Emission spectra were measured from 290 nm to 450 nm in 1 nm steps at a fixed excitation wavelength of 275 nm. The temperature was set at 25°C. For consistent mixing, the plate was shaken inside the fluorometer for 30 seconds (2 mm linearly, 70 × per minute). The spectra were corrected by subtraction of PBS or PBS/ TFE=1:1 (v/v) spectra as a background spectrum. The concentration of peptide E or K was 20 μM in each measurement, with 250 μL volume of peptide solution in each well.

Sedimentation Equilibrium Analytical Ultracentrifugation

Sedimentation equilibrium analytical ultracentrifugation measurements were conducted using a Beckman-Optima XL-I analytical ultracentrifuge fitted with an An-60 Ti rotor. Peptide solutions were prepared in PBS buffer, pH 7.4, at peptide concentrations which gave an initial absorbance in the range 0.2-0.6 A.U. The samples were spun at three speeds

An antiparallel tetrameric coiled coil

(between 34,000-50,000 rpm) at 20 °C. The data was then fitted to a single-ideal species model using Ultrascan.³⁰

Molecular simulation

All simulations were carried out with the GROMACS molecular dynamics package using the version 2.1 of the MARTINI coarse-grained force field and its extension to proteins.³¹⁻³³ Using this model, the association behavior of several proteins in model membranes has been already simulated and the computational results show good agreement with previous atomistic simulations or experiment.³⁴⁻³⁶ To characterize the self-assembly process of Coil-E_r and Coil-K peptides, we have performed 20 independent simulations of four peptides (two Coil-E_r and two Coil-K) randomly distributed in solvent (water with Na⁺ and Cl⁻ ions). The starting coarse-gained structures for the Coil-K have been mapped from the 20 atomistic models of the exactly same peptide reported by Hodges group using NMR.³⁷ The structures for the Coil-E_r were mapped from 20 coordinates frames obtained during atomistic simulation of a generated α -helical peptide in solution. Before carrying out the MD (molecular dynamics) simulations, a steepest descent minimization was performed, followed by relaxation of the solvent (position restraints on the whole peptide) and of the side chain beads (position restraints on the peptide backbone). After this, the system was further simulated without any restraints to allow self-assembly and equilibration of the formed supramolecular structures for at least 40 microseconds. The detailed description of the model and the simulation conditions are given in the appendix.

Results and discussion

Peptide design and Synthesis.

In this study, Coil-K retains its original sequence whilst Coil-E_r was designed with the reversed amino acid sequence from Coil-E (Table 1). Tryptophan (W) and Tyrosine (Y) were attached to the C- terminus of peptide Coil-K and the N- terminus of peptide Coil-E_r respectively to allow for quantification and analytical studies. A glycine was introduced in order to act as a spacer. This results in derivatives Coil-K_W and Coil-_YE_r. To study the orientation of the peptides in coiled coils, the paramagnetic nitroxyl radical was conjugated

to the C-terminus of Coil-K_W by introduction of the MTSL to a cysteine. When MTSL is conjugated to the C-terminus, it yields peptide Coil-K_W^{*}; whereas on the N-terminus, peptide Coil-K_W will be generated. This approach offers the opportunity to investigate the intermolecular self-assembly stoichiometry and the relative peptide orientation by paramagnetic proton NMR and steady state fluorescence measurements.

Table 1. Peptide primary structure and molecular characterization

Peptide Name	Sequence (from N to C terminus)	Molecular weight (g mol ⁻¹)	D(*, w) ^a	¹ H-NMR signal _b	Fluorescence signal ^c
Coil-K	Ac ⁻ (KIAALKE) ₃ -CONH ₂	2321	N/A	N/A	N/A
Coil-K _W	Ac ⁻ (KIAALKE) ₃ GW ⁻ CONH ₂	2564	N/A	✓	✓
Coil-K _W [*]	Ac ⁻ (KIAALKE) ₃ GW ⁻ CONH ₂ MTSL	2854	6.6	×	×
Coil-K _W [*]	Ac ⁻ C(KIAALKE) ₃ GW ⁻ CONH ₂ MTSL	2854	36.7	✓	✓
Coil-E	Ac ⁻ (EIAALEK) ₃ -CONH ₂	2324	N/A	N/A	N/A
Coil-E _r	Ac ⁻ (KELAAIE) ₃ -CONH ₂	2324	N/A	N/A	N/A
Coil-γE _r	Ac ⁻ YG(KELAAIE) ₃ -CONH ₂	2544	N/A	✓	✓

^a. ‘D’ short for distance, ‘*’ denotes the position of the ‘MTSL’ spin label and ‘w’ denote for the tryptophan residue, indicating the distance between the MTSL and the tryptophan functional group. Distances between the ‘*’ paramagnetic nitroxide and the tryptophan play a decisive role in both the NMR and fluorescence signal of ‘w’. Within 10.5 Å, the NMR signal of W will get totally suppressed while its fluorescence signal gets quenched.³⁸⁻⁴⁸ ^b Refers to 1D-proton NMR chemical shifts from 6-8 ppm. ^c Refers to fluorescence emission spectra from 285-445 nm with excitation at 275 nm. Both NMR and fluorescence measurements were performed in presence of pH=7.4 PBS buffer. ‘✓’ indicates there is signal observed while ‘×’ indicates there is no signal observed.

All peptides were synthesized by standard Fmoc solid phase synthesis on Rink Amide resin and further purified by C18 RP-HPLC. Peptides were identified using LC-MS mass spectrometry and analytical HPLC results confirm that the purity of the peptides is higher than 99% (See Appendix Figure A2-A4).

Circular Dichroism spectroscopy

Circular dichroism spectroscopy was used to study the secondary structure of the peptides. Both Coil-K and Coil-Er show α -helical structures with two minima at 222 nm and 208 nm wavelength in phosphate buffered saline (PBS, pH=7.4) at room temperature. The equimolar mixture shows typical coiled-coil characteristics with the $[\theta]_{222}/[\theta]_{208}$ ellipticity ratio > 1 (Figure 1A).⁴⁹ To further investigate the peptide secondary structure, TFE was added. TFE is known to enhance intramolecular α -helicity while disrupting any intermolecular interactions (i.e. coiled coil assemblies).⁵⁰ Comparison of the $[\theta]_{222}/[\theta]_{208}$ ellipticity ratio and α -helix values before and after TFE addition showed that in both peptides Coil-K and Coil-Er, the $[\theta]_{222}/[\theta]_{208}$ ellipticity ratio and α -helix values increases, indicative of monomeric α -helices. In contrast, for the equimolar peptide complex CC-K/Er, both the ellipticity ratio and helicity decreased, indicating the disturbance of intermolecular coiling, affirming the existence of coiled coils (Table 2).⁵¹

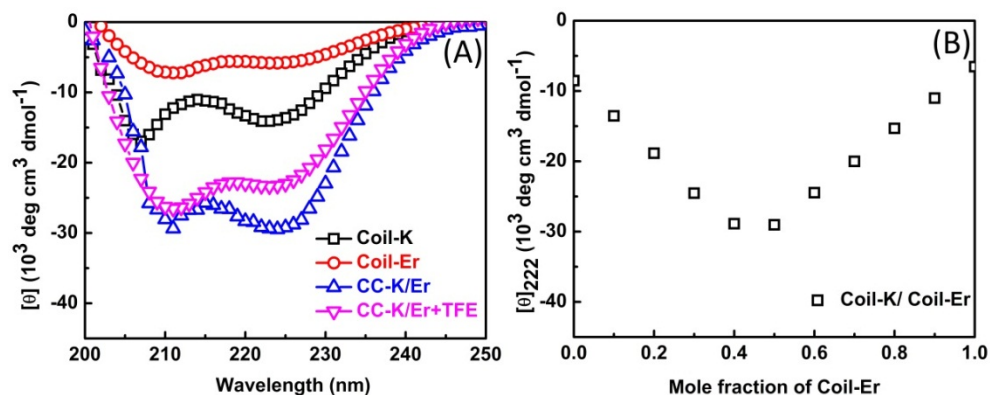


Figure 1. Circular dichroism spectra of peptide Coil-K, Coil-Er and their 1:1 mixture. (A) Secondary structures of peptide Coil-K, Coil-Er and their equimolar mixture CC-K/Er in pH=7.4 PBS buffer, as well as CC-K/Er in TFE/PBS=1:1 (v/v) solution. (B) Binding stoichiometry of the peptide Coil-K and Coil-Er. Mean residue molar ellipticities at 222 nm wavelength for mixtures of the Coil-K and Coil-E peptides as a function of the mol fraction of the Coil-E peptide. [Total peptide]= 200 μ M, PBS, pH=7.4, 25 $^{\circ}$ C.

Furthermore, CD spectra were also used to determine the coiled coil binding properties. First the Coil-K and Coil-E_r binding stoichiometry was measured using a Job-plot by changing the ratio of the mole fraction between Coil-K and Coil-Er, while keeping the total

peptide concentration constant at 200 μM (i.e. Plotting $[\theta]_{222}$ as a function of the mole fraction of Coil- E_r). A minimum molar ellipticity at $[\theta]_{222}$ was observed when Coil-K and Coil- E_r were mixed with equimolar amounts, indicative of a 1:1 stoichiometry (Figure 1B).

Table 2. Secondary and quaternary CD spectroscopic data of CC-K/ E_r .

Peptide ^a	$[\theta]_{222}$		% α -helix ^b		$[\theta]_{222}/[\theta]_{208}$		Coiled-Coil ^c
	Benign	50% TFE	Benign	50% TFE	Benign	50% TFE	
Coil-K	-14105	-19965	45	64	0.82	0.85	-
Coil- E_r	-5758	-16476	18	53	0.83	0.85	-
CC-K/ E_r	-29163	-23280	93	75	1.13	0.87	+

^a CC-K/ E_r refers to an equimolar concentration of Coil-K and Coil- E_r . ^b The percentage of α -helicity is calculated from 100 times the ratio between observed $[\theta]_{222}$ and predicted $[\theta]_{222}$ for an α -helical peptide of n residues. The predicted α -helicity is determined from the formula: $[\theta]_{222} = -40000 \times (1 - 4.6/n)$. ^{52, 53c} The signal + signifies a significant decrease in the $[\theta]_{222}/[\theta]_{208}$ ratio from PBS to 50% TFE in PBS, indicative of the folded coiled-coil structure and vice versa. [Total Peptide]=200 μM , PBS, pH=7.4, 25 $^{\circ}\text{C}$.

Next, the thermal stability of CC-K/ E_r was determined by plotting the molar ellipticity at 222 nm as a function of temperature. ^{6, 52} The transition showed to be reversible (Figure 2).

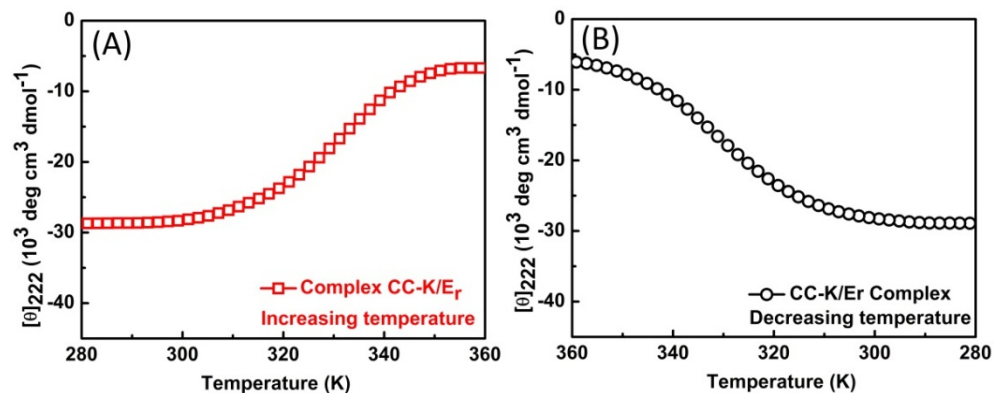


Figure 2. The thermal dissociation and association curves of CC-K/ E_r , indicated by the temperature dependent value of $[\theta]_{222}$. (A) Reveals decreasing absolute values of $[\theta]_{222}$ due to the disassembly of the CC-K/ E_r complex by temperature increase. (B) Reveals increasing absolute values of $[\theta]_{222}$ due to the assembly of the CC-K/ E_r complex by temperature decrease. [Total peptide]= 40 μM , PBS, pH=7.4.

An antiparallel tetrameric coiled coil

CC-K/E_r showed to have a two-state transition from 100% folded to 0% folded. The T_m was determined from the unfolding curve to be 58 °C (Figure 3A). The enthalpy of the temperature dependent unfolding curve was calculated from the Van't Hoff plot (Figure 3B). For the CC-K/E_r complex, the enthalpy value increases linearly with rising temperature, which is the expected behavior for a two-state transition (Figure 3C).⁴⁰ The gradient of the enthalpy-temperature curve is the heat capacity between the folded complex state and the unfolded monomer state.⁵⁴ The positive value (0.26 kcal mol⁻¹ K⁻¹) of the heat capacity indicates that nonpolar surfaces are exposed to water during dissociation of the coiled coil complex.⁵⁵ Using the heat capacity value, the change in free energy of unfolding at different temperatures was calculated to be 9.6 kcal mol⁻¹ (Figure 3D). This is similar to the original CC-K/E (See Appendix Figure A5). The dissociation constant at 25 °C associated with this $\Delta G^{\text{H}_2\text{O}}$ value is 6.4×10^{-8} M. This value is close to the reported 7.0×10^{-8} M for CC-K/E (Table 3).²⁵

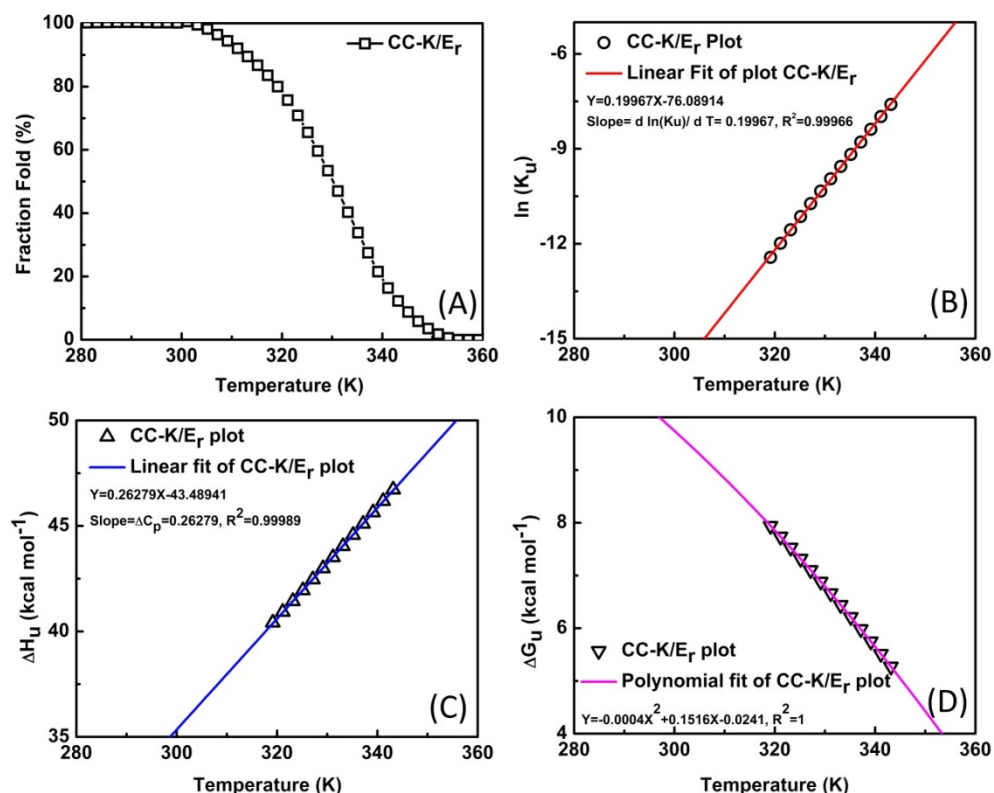


Figure 3. Thermal unfolding properties of CC-K/E_r. (A) Thermal dissociation curve of coiled coil complex CC-K/E_r. Melting temperature is 331 K (58 °C). (B) Van't Hoff plot of

the thermal denaturation of CC-K/E_r. The dissociation constant at 25 °C is $K_u = 6.4 \times 10^{-8}$ M. (C) Shows the linear dependence of the enthalpy of unfolding of CC-K/E_r on temperature. (D) Describes the free energy associated with the unfolding of CC-K/E_r as a function of temperature. The least-squares fit gives a $\Delta G^{\text{H}_2\text{O}}$ value at 25 °C of 9.6 kcal/mol. [Total peptide]= 40 μ M, PBS, pH=7.4.

Table 3. Coiled coil dissociation constant measured from CD spectroscopy.

Coiled-coil Complex	T_m (°C) ^b	ΔG_u (kcal mol ⁻¹) ^c	K_d (M) ^d
CC-K/E ^a	58	9.6	7×10^{-8}
CC-K/E _r	58	9.6	6.4×10^{-8}

^a data taken from literature and we further confirmed by repeating the measurements (See Appendix).^{5,6} ^b T_m = melting temperature, at which 50% of the coiled coil complex was dissociated. ^c Gibbs free energy of unfolding at 25 °C. ^d K_d = the dissociation constant.

Comparison of the CD spectra of CC-K/E and CC-K/E_r did not show any significant differences. Remarkably, the binding energy was almost identical. To this point, CC-K/E and CC-K/E_r showed to behave similarly.

¹H-proton NMR spectroscopy

600 MHz ¹H-nuclear magnetic resonance spectroscopy was used to study the orientation and assembly stoichiometry of the coiled coil scaffold CC-K/E_r. Paramagnetic NMR spectroscopy was used to investigate the peptide quaternary structure. With this method, one can easily recognize the complementary coiled coil peptide orientation and assembly stoichiometry of the complex by determining whether suppression of the peptide specific proton signals due to the paramagnetic relaxation enhancement (PRE) effect.⁵⁶

For this, the peptides need to have a functional group with a characteristic NMR signal and one of the peptides is modified with a signal suppressing paramagnetic spin label. In this study, Tryptophan (W) and Tyrosine (Y) were used to label the C- terminus of Coil-K and the N- terminus of Coil-E_r respectively, as the characteristic aromatic signals are well separated from the other signals (i.e. Coil-K_W and Coil-Y_r). In addition, the paramagnetic spin label MTSL was introduced onto either the N- or the C-terminus of Coil-K_W, yielding Coil-*K_W or Coil-K_W*. To avoid spectral overlap of the aromatic protons with N-H amide protons, the latter were suppressed by ‘H-D exchange’ before each NMR experiment.

The aromatic region of tryptophan (W) has four multiplets while tyrosine (Y) shows two doublets within the 6 to 8 ppm range. Peptide Coil-K_W* shows full suppression of the

An antiparallel tetrameric coiled coil

tryptophan signals (Figure 4). This is due to the MTSL nitroxide PRE effect. PRE suppression only occurs when a nucleus is in close proximity with the paramagnetic center ($< 13 \text{ \AA}$), and full suppression occurs within a 10.5 \AA radius.⁴⁶ In peptide Coil-K_W^{*}, the average distance between the tryptophan aromatic protons and the nitroxyl radical is 6.6 \AA , resulting in suppression of the aromatic protons. In contrast, in peptide Coil-^{*}K_W the average distance between the aromatic protons and the nitroxyl radical is 36.7 \AA and therefore no PRE effect is observed (Figure 4) (All the distances were calculated using Hyperchem).

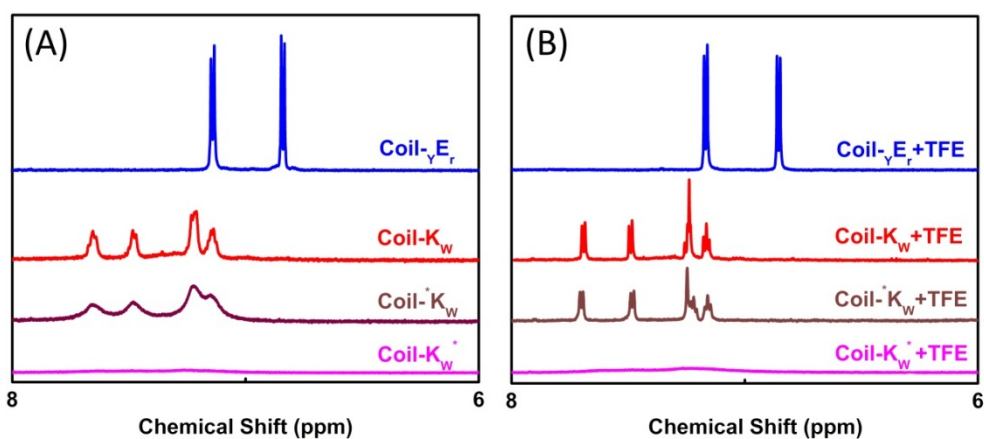


Figure 4. Aromatic region (6-8 ppm) of 600 MHz ¹H-nuclear magnetic resonance spectra showing tryptophan indole and tyrosine hydroxyphenyl functional groups of Coil-K and Coil-E derivatives respectively. (A) The aromatic signal of Coil- γ E_r, Coil-K_W, Coil-^{*}K_W and Coil-K_W^{*} in PBS buffer. (B) The aromatic signal of single peptides in the presence of 50% TFE in PBS buffer. [Total peptide]= 0.8 mM, 25 °C.

An equimolar mixture of peptide Coil-K_W and Coil- γ E_r and their MTSL labeled variants were studied in PBS at room temperature to obtain information regarding the relative peptide orientation (Figure 5). When the peptides are assembled into coiled coils, the characteristic knobs-into-holes packing leads to the close distance of the peptides identical termini, but the distance of the opposite termini is too large for the PRE effect (length of Coil-K = 37.1 \AA).³⁷ Thus the PRE effect can be used to determine the peptide orientation during self-assembly of the coiled coil. It is obvious that the tyrosine aromatic signals in Coil- γ E_r, only gets suppressed when an antiparallel orientation is adopted in coiled coil formation with Coil-K_W^{*}. This was indeed observed (Figure 5). Recovery of the tyrosine signal was obtained upon the addition of 50% TFE due to disassembly of the coiled coil.

This strongly suggests that peptide Coil-K_W and Coil-_YE_r form an antiparallel coiled coil motif. An equimolar mixture of Coil-^{*}K_W and Coil-_YE_r did not show suppression of the tyrosine signal, thereby supporting the antiparallel orientation (Figure 5).

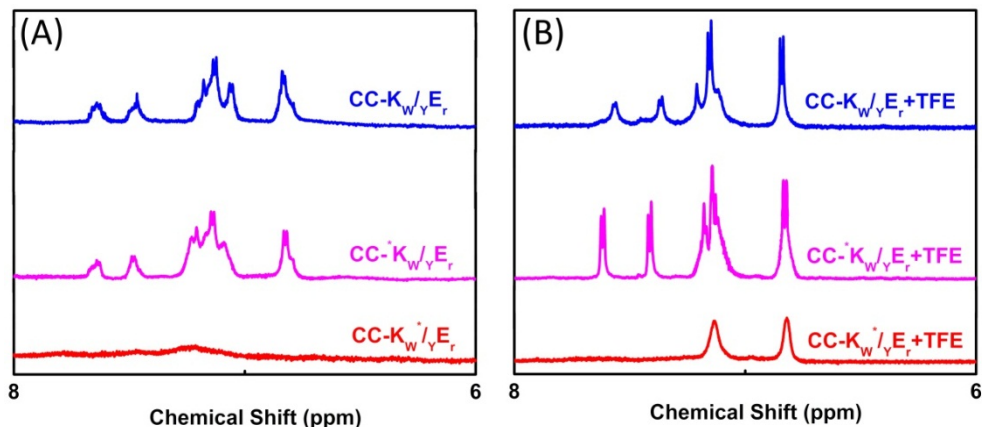


Figure 5. Aromatic Region (6-8 ppm) of 600 MHz ¹H-nuclear magnetic resonance spectra showing tryptophan indole and tyrosine hydroxyphenyl functional groups of equimolar mixtures of Coil-K and Coil-E (short name CC-K/E). (A) Aromatic signals of peptide CC-K/E complex in PBS. Blue line indicates CC-K_W/_YE_r, pink line indicates CC-^{*}K_W/_YE_r and red line indicates CC-K_W^{*}/_YE_r. (B) Aromatic signals of CC-K/E in 1:1 (v/v) TFE: PBS. Blue line indicates CC-K_W/_YE_r, pink line indicates CC-^{*}K_W/_YE_r and red line indicates CC-K_W^{*}/_YE_r. [Total peptide]= 0.8 mM, PBS, pH=7.4, 25 °C.

Next, the stoichiometry of Coil-K and Coil-_YE coiled coil formation was investigated by paramagnetic NMR. First, Coil-K_W^{*} and Coil-_YE_r were mixed in a 2:1 molar ratio (Figure 6). Here the tyrosine aromatic proton signals are fully suppressed. This was also observed for the equimolar mixture. However, when Coil-K_W^{*} and Coil-_YE_r were mixed in 1:2 molar ratio, tyrosine aromatic protons were observed. This is indicative that there is an excess of Coil-_YE_r which is not suppressed. This shows that Coil-K and the reverse sequence Coil-E_r bind approximately in a 1:1 stoichiometry.

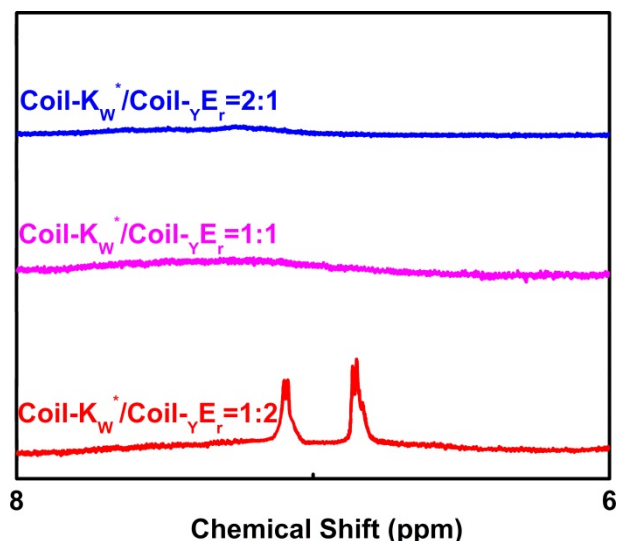


Figure 6. Aromatic region (6-8 ppm) of 600 MHz ^1H -nuclear magnetic resonance spectra showing tyrosine hydroxyphenyl functional groups of different molar ratio mixtures of Coil- K_W^* and Coil- γE_r . (A) From top to bottom, the molar ratio between Coil- K_W^* and Coil- γE_r is 2:1, 1:1 and 1:2 respectively. [Total peptide]=0.8 mM, PBS, pH=7.4, 25 °C.

Steady state fluorescence spectroscopy

To confirm the relative peptide orientation in the coiled coil, steady state fluorescence spectroscopy studies were performed using FRET (fluorescence resonance energy transfer) or fluorescence quenching assays. The fluorescence emission spectra of the individual peptides are shown in Figure 7. Typical spectra were obtained except for Coil- K_W^* , due to the presence of spin label in the vicinity of the tryptophan (vide infra).

FRET only occurs when the donor and acceptor are within the Förster Distance (≈ 1 nm).⁵⁷ When a mixture of Coil- γE_r and Coil- K_W forms coiled coils with an antiparallel orientation, FRET between the donor tyrosine and the acceptor tryptophan is expected. Indeed, FRET was observed using an excitation wavelength of 275 nm. From the emission spectra in Figure 8A, it is noticeable that when an equimolar mixture of Coil- K_W and Coil- γE_r is used, the Coil- K_W fluorescence intensity increases while the Coil- γE_r fluorescence intensity decreases due to the FRET phenomenon leading to the energy transfer from the donor Y to the acceptor W. This confirms the small distance between the N-terminus of peptide Coil- γE_r and the C-terminus of peptide Coil- K_W , implying an antiparallel orientation of CC- $\text{K}_\text{W}/\gamma\text{E}_\text{r}$. Upon the addition of 50% TFE, the coiled coil dissociates, which led to an

increase of tyrosine fluorescence, and a decrease of tryptophan fluorescence. Thus addition of TFE leads to a loss of FRET due to disassembly of the antiparallel coiled coil of Coil-K and Coil-E_r.

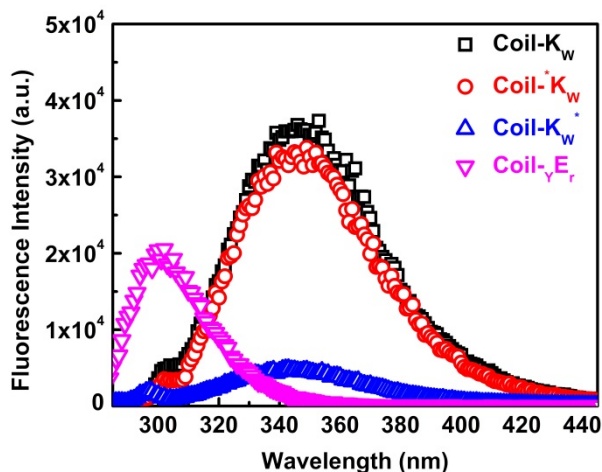


Figure 7. Fluorescence emission spectra of W and Y on peptide Coil-K_W and Coil-_YE_r and their derivatives are shown with excitation at 275 nm. [Total peptide]= 50 μM, PBS, pH=7.4, 25 °C.

This FRET assay strongly suggests an antiparallel orientation of the peptides in the coiled coil, but it might not be accurate enough to distinguish between dimeric or multimeric assemblies.

Therefore a fluorescence quenching assay was performed. In fluorescence spectroscopy measurements, the fluorophore electron excited singlet state will be quenched when a stable nitroxyl radical is within a distance of 12 Å due to an electron exchange interaction.^{39, 41, 58-63} For example, tryptophan fluorescence is quenched in peptide Coil-K_W^{*}, as the distance to the nitroxyl radical of the MTSL label is shorter than 12 Å; while in peptide Coil-K_W^{*} no quenching is observed as the distance between the nitroxyl radical and tryptophan is longer than 12 Å (Figure 7).

Here, peptide Coil-K_W^{*} and peptide Coil-_YE_r were utilized to confirm the antiparallel orientation of the peptides in CC-K/E_r. In an equimolar mixture of these two peptides, the fluorescence signal of Coil-_YE_r is quenched (Figure 8B). Addition of 50% TFE resulted in the dissociation of the coiled coil. As a result, the distance between Coil-K_W^{*} and Coil-_YE_r increases, and the tryptophan fluorescence was observed. These findings further proof that the CC-K/E_r coiled coil motif has indeed an antiparallel orientation.

An antiparallel tetrameric coiled coil

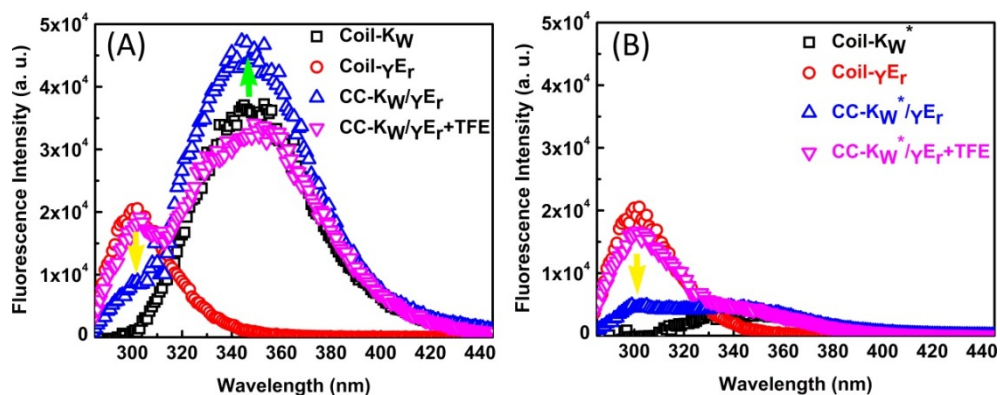


Figure 8. Fluorescence emission spectra of W and Y on single peptides and in the coiled coil complex are shown with excitation at 275 nm. (A) presents the fluorescence spectra of Coil- K_W and Coil- γE_r , and their equimolar mixture emission FRET spectra in PBS buffer as well as emission spectra in TFE/ PBS=1:1 (v/v). The green arrow indicates the signal increase of W and the yellow arrow indicates the signal decrease of Y. (B) presents the single peptide fluorescence spectra of Coil- K_W^* and Coil- γE_r , and their equimolar mixture emission quenching spectra in PBS buffer as well as emission spectra in TFE/ PBS=1:1 (v/v). The yellow arrow indicates the signal decrease of Y. [Total peptide]=50 μ M, 25 $^{\circ}$ C.

In summary, FRET and fluorescence quenching experiments show strong evidence for the antiparallel peptide orientation in the CC-K/ E_r coiled coil motif. This result further supports the finding of the paramagnetic NMR study.

Sedimentation Equilibrium

To determine the oligomer state of the CC-K/ E_r species in solution, sedimentation equilibrium measurements were performed using ultracentrifugation (AUC). Datasets were fitted to a single-ideal species model using Ultrascan and the average mass of the species was determined to be 10,620 Da, with 95% confidence limits (determined by Monte Carlo analysis) to be +57 Da, -64 Da. There are no systematic residuals for the fitting. Hence, weight-averaged molecular weights typical of a tetramer for CC-K/ E_r were observed.

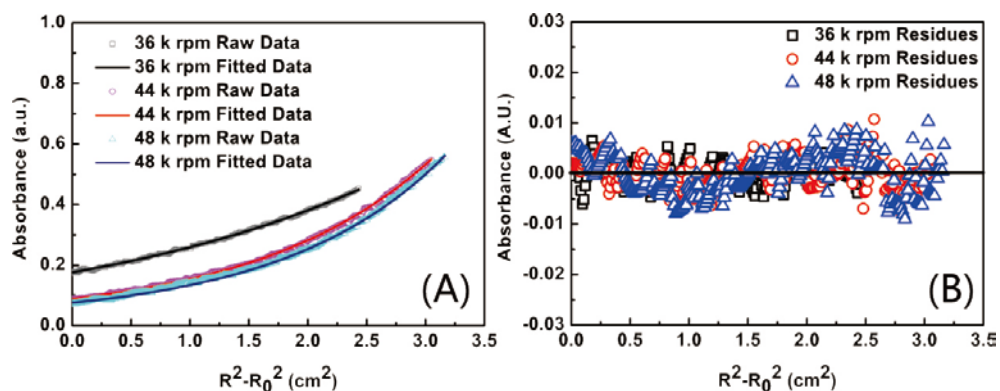


Figure 9. AUC (analytical ultracentrifugation) data for the CC-K/Er species (A) and residuals (B).

Molecular simulation

All the experimental data has shown so far that in an equimolar mixture of Coil-K and Coil-E_r, coiled coils are only formed with an antiparallel orientation of the peptides. However, the exact arrangement of the peptides within this tetramer is still unknown. To have further information about the peptide orientation of the peptides within the tetramer, molecular simulations were performed. In all the simulations, the randomly distributed peptides (two Coil-K and two Coil-E_r) spontaneously aggregated into supra-molecular structures. The four peptides first came into contact, and then orientate parallel to each other forming a 4-helix-bundle with a hydrophobic core. The aggregation process itself is relatively fast, approximately 0.5 microseconds, while 20 to 40 microseconds are needed for equilibration (each peptide rotation around its own axis or flipping to optimize the core). After equilibration, each peptide makes two longitudinal interfaces with two neighboring peptides, and the final cylinder is ~2.5 nm in diameter and the height.

All the possible tetramer configurations can be classified in two major classes: (1) having four K-E_r interfaces or (2) having two K-E_r interfaces, together with one K-K and one E_r-E_r interface. Likewise all the formed interfaces may be in parallel or in antiparallel orientation. This gives eleven distinct possible conformations for the obtained tetramers.

Our self-assembly simulations show two possible tetramer structures with high forming probability and stability: one with two K-E_r interfaces and the other with four K-E_r

An antiparallel tetrameric coiled coil

interfaces. Both of these complexes have antiparallel orientations between Coil-K and Coil-E_r helices, but the two copies of both Coil-K and Coil-E_r are taking parallel orientations (Figure 10).

These simulations compliment the experimental techniques by providing information about binding motifs or conformations in the tetramers. As these binding conformations in solution are currently inaccessible for experimental imaging techniques, this is an important result. To decisively determine the most stable conformations by CGMD (coarse grained molecular dynamics), the systems should be equilibrated for considerably increased timescales and/or free energies should be extracted for all eleven possible conformations. Before such an effort is undertaken, one should judge whether the additional insight gained by such a study outweighs the huge computational investment required for such an analysis. Supported by our well-chosen computational setup, i.e. avoiding a bias in the starting conditions, and the observation of a complete reorientation event within simulation time for the heterodimer case, we are confident to conclude that the most probable binding conformations are indeed sampled by our CGMD simulations. Thus, this simulation showed unequivocally that Coil-K and Coil-E_r assemble in a tetramer only, which is in line with the sedimentation equilibrium study.

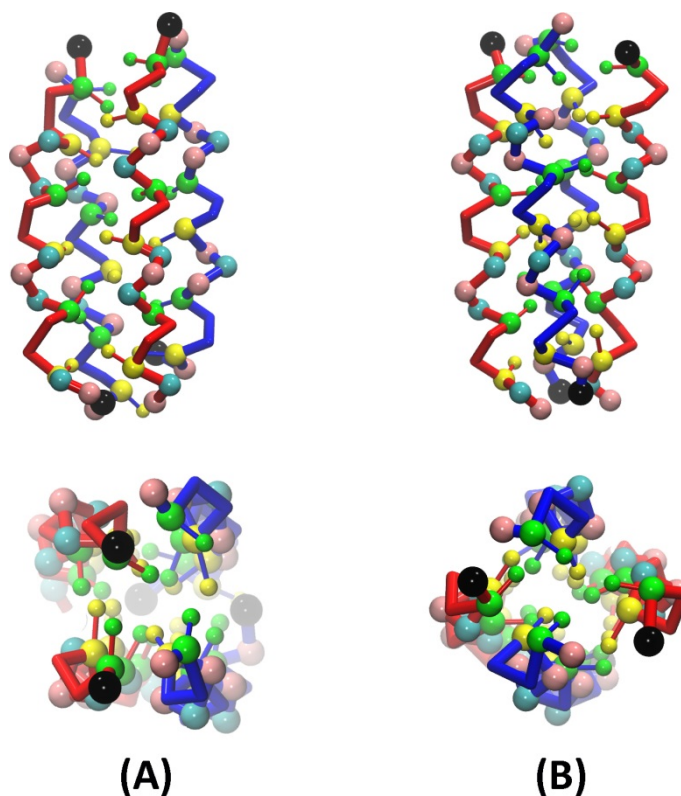


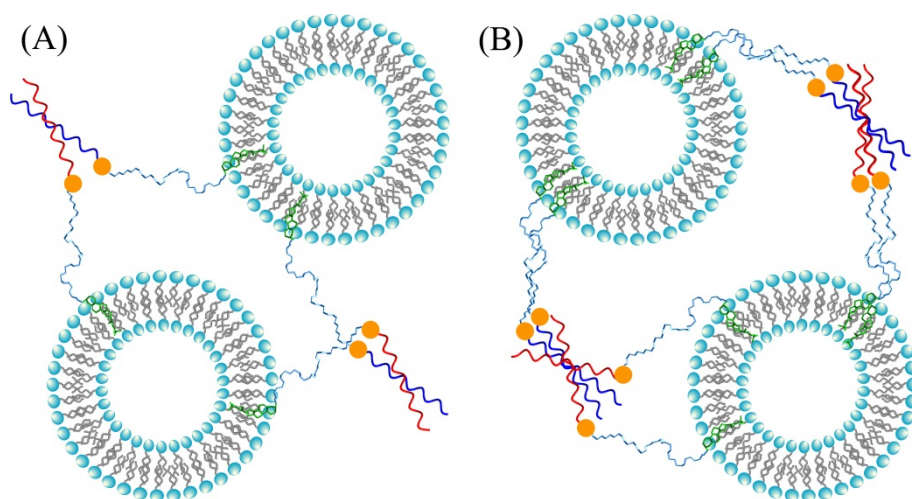
Figure 10. Two possible CC-K/Er tetramer configurations resulting from molecular dynamics simulations. Up is the lateral view and down is the top view. (A) shows CC-K/Er antiparallel tetramer with two K-Er interfaces. (B) shows CC-K/Er antiparallel tetramer with four K-Er interfaces.

Liposome fusion study

By using various analytical techniques it has been demonstrated that combining peptides Coil-K and Coil-E_r leads to the formation of anti-parallel tetrameric coiled coils, whereas peptides Coil-K and Coil-E form parallel dimeric coiled coils. Remarkably, these two peptide pairs have a similar binding energy. Once incorporated into liposomal membranes, peptides Coil-K and Coil-E have shown to induce efficient and targeted membrane fusion.⁶ Here the contest of the aggregation state and orientation vs. binding energy of the coiled coil complexes on the ability to induce membrane fusion was investigated (Scheme 2). For this reason, fusogenic peptides were synthesized which consist of three distinct segments: 1)

An antiparallel tetrameric coiled coil

the peptide segment, which serves as the recognition unit, 2) a hydrophobic anchor, which enables the stable anchoring of the peptides into liposomal membranes and 3) a hydrophilic spacer, which supplies the peptides with the ability to reorient in order to form coiled coil motifs efficiently.¹³ The peptide segment consisted of Coil-K, Coil-E or Coil-E_r, whereas the anchor was constituted by cholesterol and the spacer by 12-polyethylene glycol (PEG₁₂). The resulting lipidated peptides are denoted CPK, CPE and CPE_r. Peptide decorated liposomes were prepared (lipid composition: DOPC/DOPE/CH, 2/1/1 molar ratio and 1 mol% lipidated peptide) by mixing appropriate amounts of lipid and lipidated peptide stock solutions (in CHCl₃ and CHCl₃/MeOH 1/1 respectively), evaporating the solvent, addition of PBS buffer (yielding a total lipid concentration of 0.1 mM) and sonication for 1 minute at 50°C. A typical fusion experiment was performed by combining equimolar amounts of Coil-K decorated liposomes with Coil-E or Coil-E_r decorated liposomes. The characterization of the fusion events was performed by optical density measurements and DLS, as well as lipid and content mixing assays.



Scheme 2. Schematic diagram of liposome fusion. (A) zipper like fusion model: parallel dimeric coiled coil induced liposome fusion, the blue helix indicates the Coil-E peptide. (B) Non-zipper like fusion model: antiparallel tetrameric coiled coil induced liposome fusion, the blue helix indicates the Coil-E_r peptide. Common symbols: light blue bilayer vesicle=liposome; red helix=Coil-K; green anchor=Cholesterol; light blue linker=PEG12; orange dot=peptide N-terminus.

Upon combining Coil-K decorated liposomes with Coil-E (or Coil-E_r) decorated liposomes, an increase in particle size is expected due to coiled coil formation. The particle size increase can reflect fusion events and/or aggregation and was determined by measuring the optical density of the mixed liposomes at $\lambda=400$ nm. A rapid increase in size was observed for both vesicle combinations (equimolar amount of CPK-liposome with CPE-liposome or with CPE_r-liposome), which indicates that both coiled coil motifs are formed efficiently (Figure 11A).

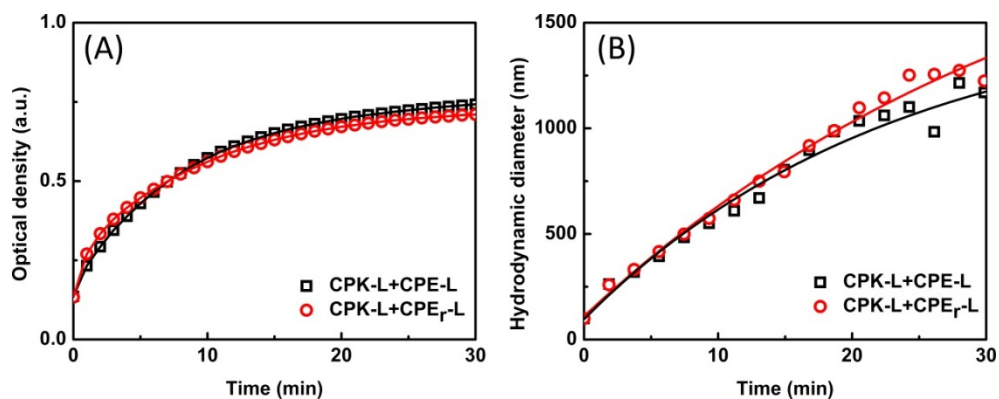


Figure 11. (A) Optical density measurements at $\lambda=400$ nm. (B) Dynamic light scattering of liposome fusion size increasing. Black line shows plots of equimolar mixture of Coil-K decorated liposome with Coil-E decorated liposome, while red line shows plots of equimolar mixture of Coil-K decorated liposome with Coil-E_r decorated liposome. Liposome concentration is 0.25mM with 1% peptide decoration. All the measurements were done in PBS, pH 7.4, at 25 °C.

DLS measurements confirmed these results and indicated that aggregates of particles >1 μm were formed (Figure 11B). Next, lipid mixing experiments were performed to investigate the extent to which both coiled coil motifs were able to induce lipid mixing. For this assay, a FRET pair was incorporated in the membrane of the Coil-K decorated liposomes (donor: DOPE-NBD and acceptor: DOPE-LR). Upon lipid mixing of these Coil-K liposomes (CPK-L) with Coil-E liposomes (CPE-L) or Coil-E_r liposomes (CPE_r-L), the average distance between donor and acceptor increases, giving rise to an increase in donor emission. The donor emissions were continuously measured for 30 minutes and the results show no notable differences between parallel and anti-parallel coiled coil formation, both coiled coil orientations are able to induce fusion between liposomes in an efficient manner (Figure 12A).

An antiparallel tetrameric coiled coil

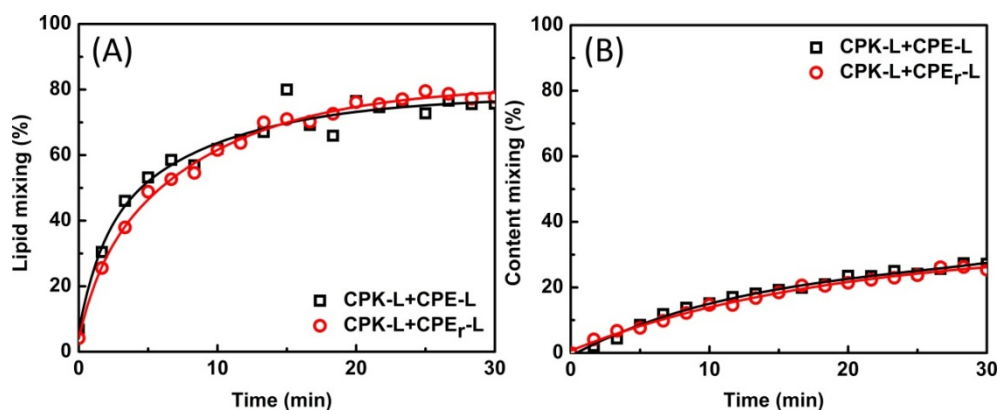


Figure 12. (A) Fluorescence traces showing lipid mixing between fluorescence (NBD/LR) labeled CPK liposomes with non-fluorescence labeled CPE or CPE_r liposomes. (B) Content mixing between non-fluorescent CPK liposomes with sulforhodamine labeled (20mM) CPE or CPE_r liposomes. Black line shows plots of equimolar mixture of CPK liposomes with CPE liposomes, while red line shows plots of equimolar mixture of CPK liposomes with CPE_r liposomes. Liposome concentration is 0.1 mM with 1% peptide. All the measurements were performed in PBS, pH 7.4, at 25 °C.

However, full fusion is defined as lipid and content mixing and therefore we proceeded by performing a content mixing assay. Here, Coil-E or Coil-E_r decorated liposomes were loaded with sulforhodamine B at a self-quenching concentration of 20 mM. Content mixing of these Coil-E or Coil-E_r decorated liposomes with the non-fluorescent Coil-K liposomes decreases the concentration of sulforhodamine B, which results in relief of self-quenching and an increase in fluorescence intensity (Figure 12B). Consistent with the lipid mixing experiments, no significant difference in content mixing was observed between both coiled coil motifs, both orientations and oligomer states induce efficient content mixing. This indicates that for this peptide mediated fusion system, the coiled coil binding energy plays an important role and not its aggregation state or the relative peptide orientation.

Conclusion

Reversing the peptide sequence of Coil-E yields Coil-E_r which in the presence of equimolar amounts of Coil-K, results in the formation of an antiparallel tetrameric coiled coil and not an antiparallel heterodimeric coiled coil. This shows that reversing the peptide

sequence significantly alters the assembly behavior, which is in line with previous studies on proteins.^{5, 6, 37, 51}

Remarkably, the binding energy is similar but the oligomer state and relative peptide orientation are different. This study shows that reversing the amino acid sequence in a heterodimeric parallel coiled coil motif significantly alters its self-assembly property and one cannot assume that it yields an antiparallel heterodimer, as previously reported.^{12, 64} This study demonstrates that a coiled coil assembly is sensitive to small changes and care should be taken when redesigning the amino acid sequence of known coiled coil structures. In addition, this study offers a new coiled coil candidate for the reduced SNARE induced membrane fusion model study. Cholesterol modified peptide Coil-K and Coil-E_r induced liposome fusion comparable to the Coil-K and Coil-E induced liposome fusion. This suggests that in this peptide mediated membrane fusion system, the coiled coil binding energy is a more decisive factor while the peptide orientation and oligomer state is not.

Appendix

Part 1. Non-zipper like liposome fusion model.

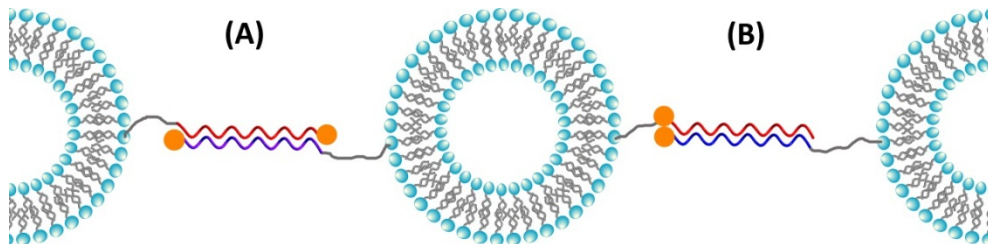


Figure A1. Schematic diagram of (A) Diederichsen and (B) Kros non-zipper like liposome fusion model. Red helix indicates peptide Coil-K ([KIAALKE]₃), purple helix indicates peptide Coil-E_r ([KELAAIE]₃), blue helix indicates peptide Coil-E ([EIAALEK]₃). The orange ball indicates the peptide N-terminus.

Part 2. Mass spectra of the peptides

LC-MS spectra of all the purified peptides are shown below (Figure A 2-4).

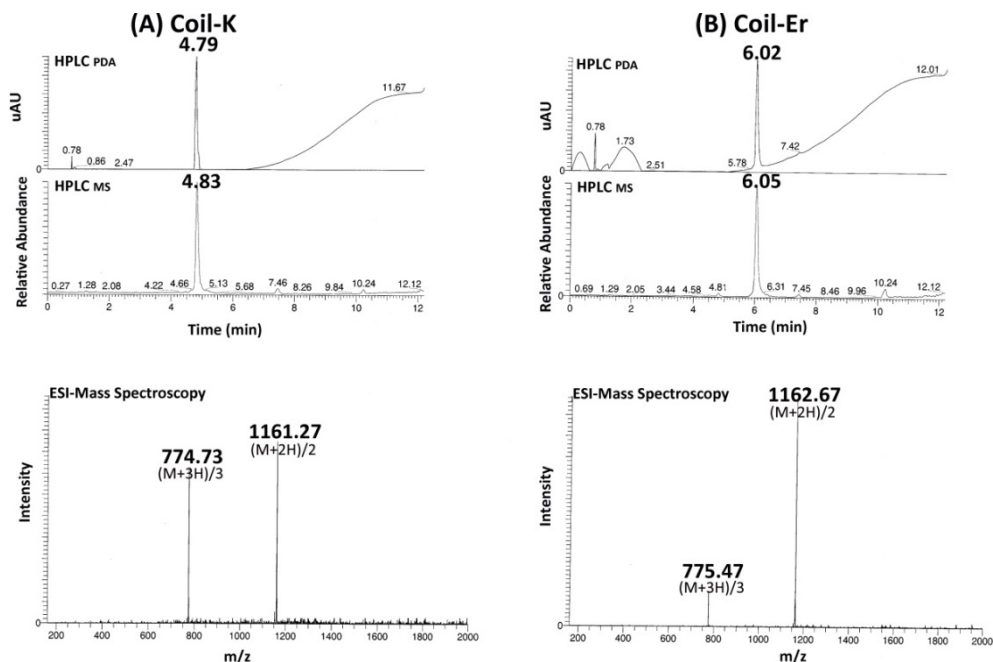


Figure A2. (A) LC-MS spectra of purified Coil-K, (B) LC-MS spectra of purified Coil-E_r. From top to bottom: UV (ultraviolet-visible) spectrum, ESI (electrospray ionization) spectrum, and mass spectrum.

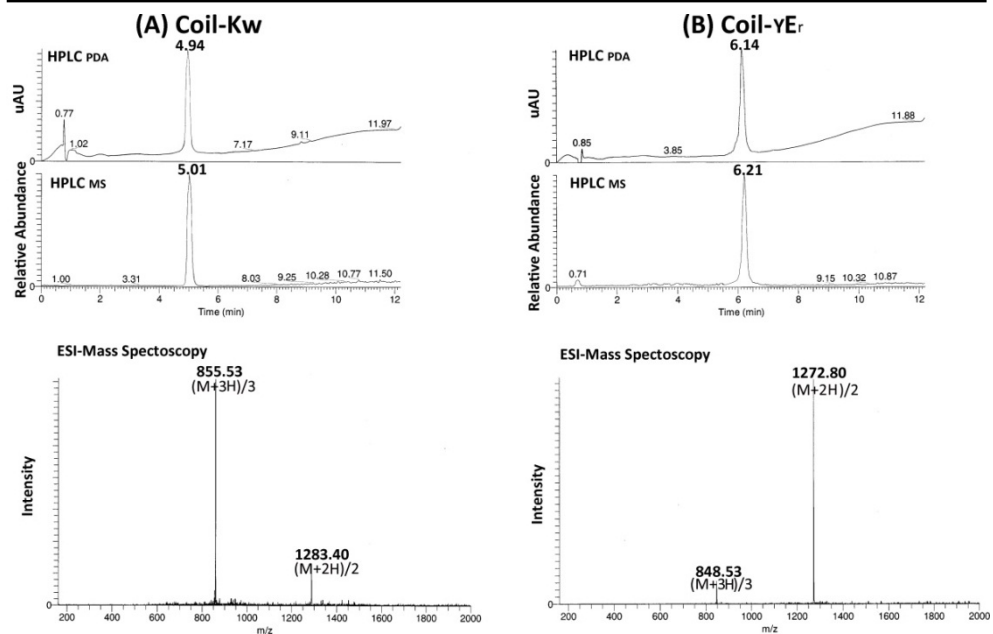


Figure A3. (A) LC-MS spectra of purified Coil-K_w, (B) LC-MS spectra of purified Coil- γ E_r. From top to bottom: UV (ultraviolet-visible) spectrum, ESI (electrospray ionization) spectrum, and mass spectrum.

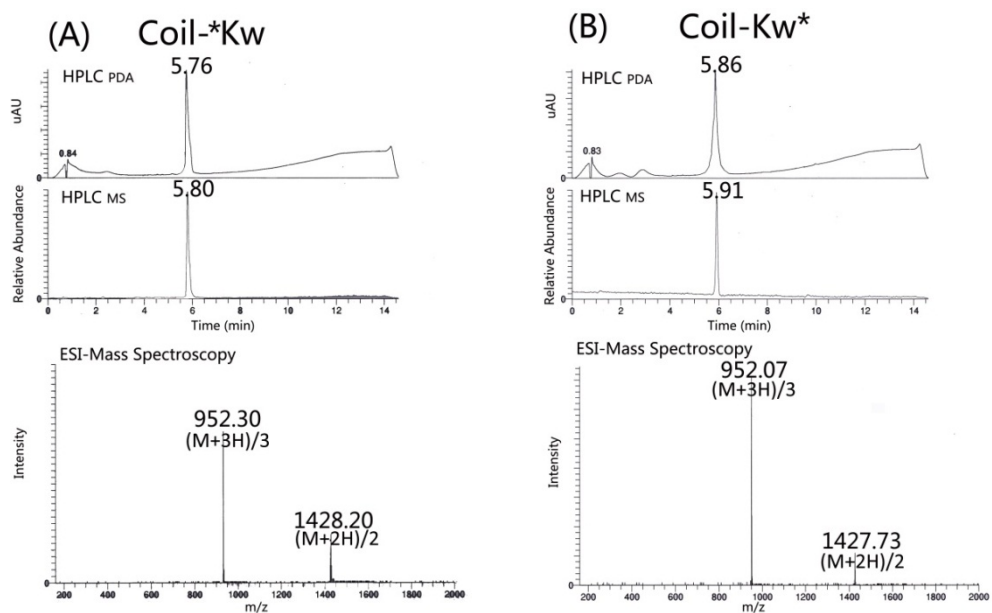


Figure A4. (A) LC-MS spectra of purified Coil-K_W^{*}, (B) LC-MS spectra of purified Coil-K_W^{*}. From top to bottom: UV (ultraviolet-visible) spectrum, ESI (electrospray ionization) spectrum, and mass spectrum.

Part 3. UV measurement for peptide concentration calculation

Lyophilized peptides may contain anywhere 10%~70% bound water and salts by weight. Therefore, it is better to ascertain the actual peptide concentration by UV spectroscopy.

The W and Y chromophore labeled peptide Coil-K and Coil-E concentration can be conveniently determined as follows:

1. Molar extinction coefficients (ϵ) of chromophoric residues at neutral pH using a 1 cm cell:^{65, 66}

Tryptophan (W) 5690 AU/mmol/ml, peak at 280.8 nm wavelength.

Tyrosine (Y) 1490 AU/mmol/ml, peak at 275.5 nm wavelength.

2. Calculations: peptide concentration (mol/L) = $(A_{\text{peak}} \times \text{DF}) / \epsilon$, where A_{peak} is the actual absorbance of the solution at peak value in a 1 cm cuvette, DF is dilution factor, MW is the molecular weight of the peptide and ϵ is the molar extinction coefficient of each chromophore.

Part 4. CC-K/E CD thermal denaturation dissociation constant calculation

Summary of the original CC-K/E temperature denaturation parameters.

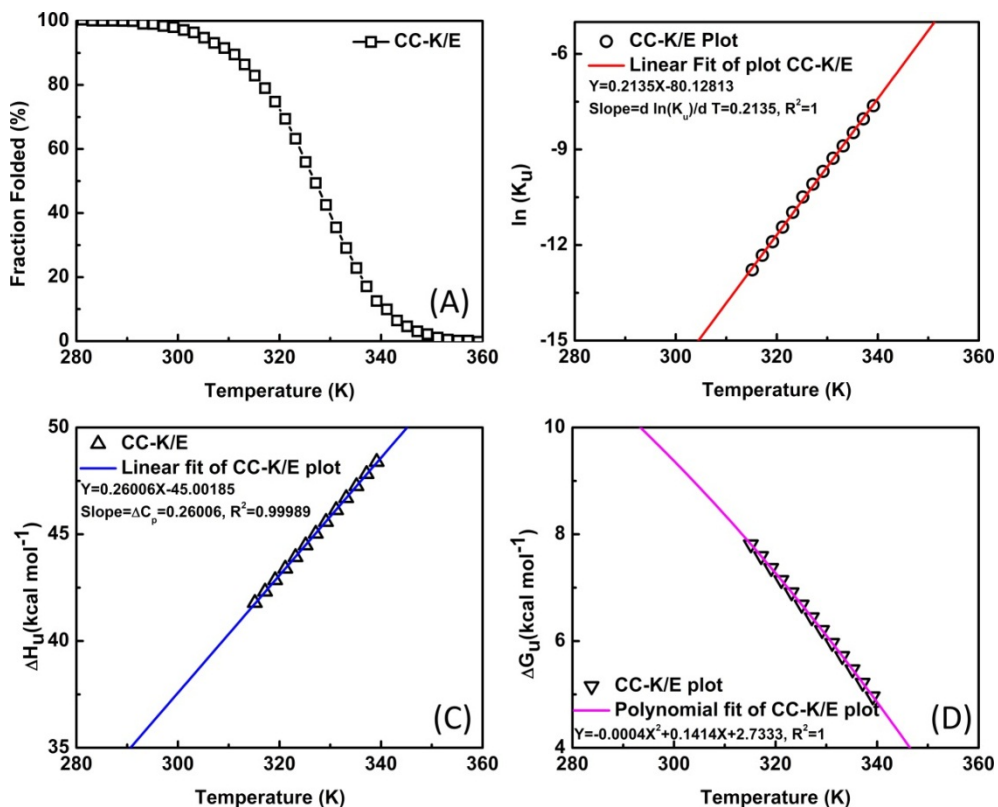


Figure A5. Thermal unfolding properties of CC-K/E. (A) Describes thermal dissociation curve of coiled coil complex CC-K/E, disassembling from 100% folding to 0% folding. Melting temperature is 331.15 K. (B) Describes the Van't Hoff plot of the thermal denaturation of CC-K/E. The dissociation constant at 25 °C is $K_u = 7.0 \times 10^{-8}$ M. (C) Describes the dependence of the enthalpy of unfolding of CC-K/E on temperature. (D) Describes free energy associated with the unfolding of CC-K/E as a function of temperature. The least-squares fit gives a ΔG^{H_2O} value at 25 °C of 9.33 kcal/mol. [Total peptide]= 40 μ M, PBS pH 7.4.

Part 5. Hyperchem simulation of peptide structure⁶⁷

Hyperchem release 8.0 package was used to simulate the peptide conformation and to determine the average distance between the spin label and the W (Tryptophan) aromatic amino acids in both peptide Coil- K_W^* and Coil- *K_W .

For this, both Coil-K peptides were placed in a periodic box containing water molecules and the system was equilibrated at 300 K. The peptide can move in a constant-density environment which is similar to being in a liquid. The size of the box was set as a cube with $W=H=D= 56.104 \text{ \AA}$, and the minimum distance between solvent and solute atoms (atoms from peptides) is 2.3 \AA .⁸⁸

Molecular Mechanics simulation was based on a classical Newtonian calculation. Here, atoms were treated as Newtonian particles interacting through a potential energy function, which depend on bond lengths, bond angles, torsion angles, and non-bonded interactions (including van der Waals forces, electrostatic interactions, and hydrogen bonds). In these calculations, the forces on atoms are functions of the atomic position.

Furthermore, the AMBER force field which is typically used for developing proteins and nucleic acids was used to develop an all-atom model. The simulations were performed at 300 K with a 30 ps run time. Figures A6 shows the peptide conformation after simulation.

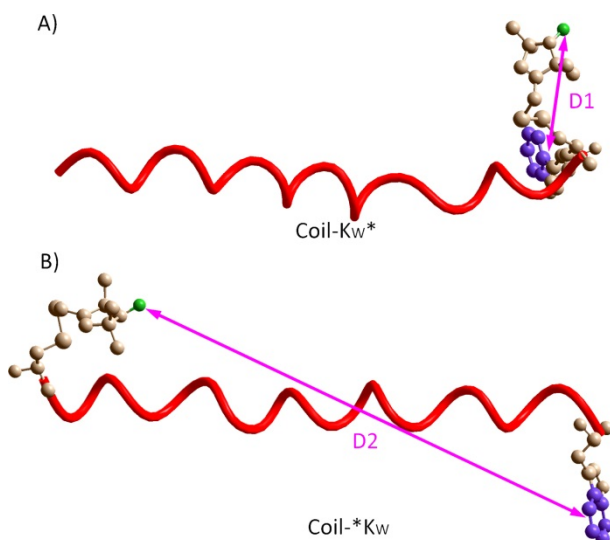


Figure A6. Structure of peptide Coil- K_W^* (A) and Coil- *K_W (B). In A) D1 indicates the distance between nitroxyl group and the W in peptide Coil- K_W^* . The average distance D1 is 6.6 \AA . In B) the average distance D2 between the spin label and W is 36.7 \AA .

Part 6. Molecular simulation

In the Martini model, groups of atoms (typically four) are united into specific interaction centers that absorb all the molecular detail of the replaced atoms. The coarse-grained particles interact via Lennard-Jones potential (with different well depth parameters depending on the specific pair type), screened electrostatic Coulomb potential, while the connectivity of the molecules is modeled by elastic bonds and angle potentials. By reducing the number of particles and the complexity of the interactions between them, longer simulation times can be achieved. Each of the five types of amino acids: E, A, I, L and K, constituting either Coil-K or Coil-E_r, is described at the coarse-grained level by an apolar interaction site representing the backbone and one or more interaction sites representing the side chains. The superposition of the atomistic and the coarse-grained representations of the CC-K/E coiled-coil structure is shown in Figure A7. The interaction parameters (hydrophobicity and polarity) for the coarse-grained particles have been set to closely reproduce the difference between particle's solvation free energy in polar and in apolar media. The α -helicity of the peptides is imposed through dihedral potentials along the backbone beads during the simulations.

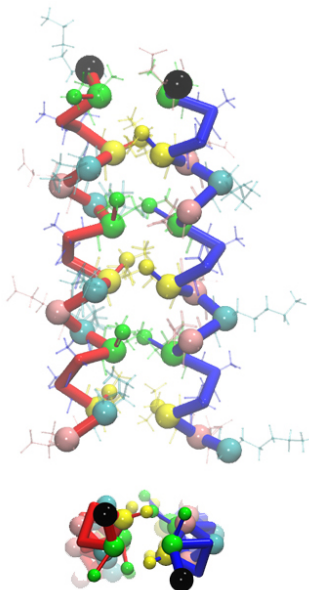


Figure A7. Lateral and top views of the parallel CC-K/E, as reported by Hodges group by NMR measurements. Red backbone stands for the secondary structure of peptide Coil-K; while blue backbone stands for the secondary structure of either peptide Coil-E. Green bead is Glutamic acid (E); cyan bead is Lysine (K); green bead is Isoleucine (I); yellow

An antiparallel tetrameric coiled coil

bead is Leucine (K) amino acid. Alanine (A) amino acid is omitted here. For each peptide, the starting amino acid on N-terminus is colored in black. In the lateral view, the atomistic structure is overlaid, in transparent licorice representation.

In a typical simulation for this study, two Coil-K and two Coil-E_r peptides are randomly distributed (position and rotation randomness) in an 11 nm × 11 nm × 11 nm simulation box and solvated by water and ions, mimicking the buffer solution. At completion, the system consists of ~10000 coarse-grained particles: four peptides (21 amino acids for each), water particles (one coarse-grained water particle representing four real water molecules) and ions (Na⁺ and Cl⁻). Periodic boundary conditions in all directions were employed. Standard MARTINI simulations were used.³² The Berendsen thermostat and barostat kept the temperature (t=300 K) and pressure (P=1 atm, isotropically) constant; the integration time step was t=20 fs.

Reference

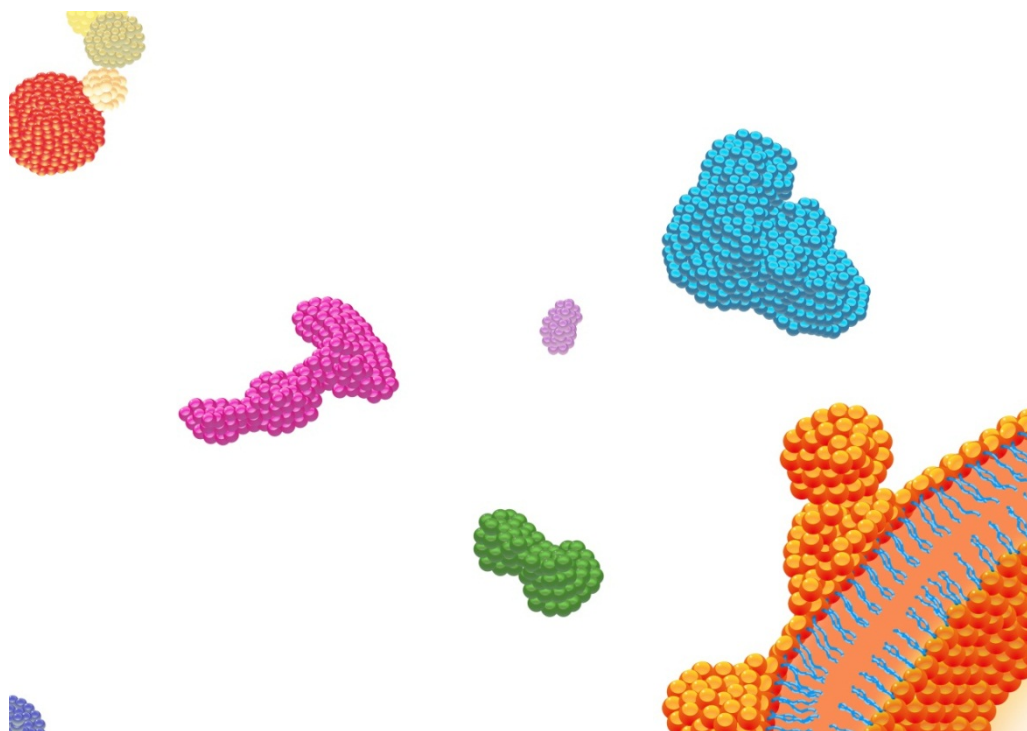
1. A. Maximov, J. Tang, X. F. Yang, Z. P. P. Pang and T. C. Sudhof, *Science*, 2009, **323**, 516-521.
2. T. C. Sudhof and J. E. Rothman, *Science*, 2009, **323**, 474-477.
3. C. Hu, M. Ahmed, T. J. Melia, T. H. Sollner, T. Mayer and J. E. Rothman, *Science*, 2003, **300**, 1745-1749.
4. T. Weber, B. V. Zemelman, J. A. McNew, B. Westermann, M. Gmachl, F. Parlati, T. H. Sollner and J. E. Rothman, *Cell*, 1998, **92**, 759-772.
5. J. R. Litowski and R. S. Hodges, *Journal of Biological Chemistry*, 2002, **277**, 37272-37279.
6. H. Robson Marsden, A. V. Korobko, T. Zheng, J. Voskuhl and A. Kros, *Biomaterials Science*, 2013.
7. H. R. Marsden, N. A. Elbers, P. H. H. Bomans, N. Sommerdijk and A. Kros, *Angewandte Chemie-International Edition*, 2009, **48**, 2330-2333.
8. F. Versluis, J. Voskuhl, B. van Kolck, H. Zope, M. Bremmer, T. Albregtse and A. Kros, *Journal of the American Chemical Society*, 2013, **135**, 8057-8062.
9. T. Zheng, J. Voskuhl, F. Versluis, H. R. Zope, I. Tomatsu, H. R. Marsden and A. Kros, *Chemical Communications*, 2013, **49**, 3649-3651.
10. H. R. Marsden, I. Tomatsu and A. Kros, *Chemical Society Reviews*, 2011, **40**, 1572-1585.
11. T. T. Zheng, J. Voskuhl, F. Versluis, H. R. Zope, I. Tomatsu, H. R. Marsden and A. Kros, *Chemical Communications*, 2013, **49**, 3649-3651.
12. G. Pahler, C. Panse, U. Diederichsen and A. Janshoff, *Biophysical Journal*, 2012, **103**, 2295-2303.
13. F. Versluis, J. Dominguez, J. Voskuhl and A. Kros, *Faraday Discussions*, 2013.
14. P. R. E. Mittl, C. Deillon, D. Sargent, N. K. Liu, S. Klauser, R. M. Thomas, B. Gutte and M. G. Grutter, *Proceedings of the National Academy of Sciences of the United States of America*, 2000, **97**, 2562-2566.
15. M. E. Holtzer, E. Braswell, R. H. Angeletti, L. Mints, D. Zhu and A. Holtzer, *Biophysical Journal*, 2000, **78**, 2037-2048.
16. M. Goodman and M. Chorev, *Accounts of Chemical Research*, 1979, **12**, 1-7.
17. S. Lorenzen, C. Gille, R. Preissner and C. Frommel, *Febs Letters*, 2003, **545**, 105-109.
18. Y. Q. Deng, J. Liu, Q. Zheng, D. Eliezer, N. R. Kallenbach and M. Lu, *Structure*, 2006, **14**, 247-255.
19. S. R. Whitson, W. M. LeSturgeon and A. M. Krezel, *Journal of Molecular Biology*, 2005, **350**, 319-337.
20. A. Lombardi, C. M. Summa, S. Geremia, L. Randaccio, V. Pavone and W. F. DeGrado, *Proceedings of the National Academy of Sciences of the United States of America*, 2000, **97**, 6298-6305.
21. S. A. Palasek, Z. J. Cox and J. M. Collins, *Journal of Peptide Science*, 2007, **13**, 143-148.
22. H. Robson Marsden and A. Kros, *Angewandte Chemie (International ed. in English)*, 2010, **49**, 2988-3005.

23. T. Kaiser, G. J. Nicholson, H. J. Kohlbau and W. Voelter, *Tetrahedron Letters*, 1996, **37**, 1187-1190.
24. A. Y. Kornilova, J. F. Wishart, W. Z. Xiao, R. C. Lasey, A. Fedorova, Y. K. Shin and M. Y. Ogawa, *Journal of the American Chemical Society*, 2000, **122**, 7999-8006.
25. J. R. Litowski and R. S. Hodges, *Journal of Peptide Research*, 2001, **58**, 477-492.
26. S. M. Kelly and N. C. Price, *Biochimica Et Biophysica Acta-Protein Structure and Molecular Enzymology*, 1997, **1338**, 161-185.
27. S. M. Kelly, T. J. Jess and N. C. Price, *Biochimica Et Biophysica Acta-Proteins and Proteomics*, 2005, **1751**, 119-139.
28. P. Lavigne, M. P. Crump, S. M. Gagne, R. S. Hodges, C. M. Kay and B. D. Sykes, *Journal of Molecular Biology*, 1998, **281**, 165-181.
29. P. Lavigne, L. H. Kondejewski, M. E. Houston, F. D. Sonnichsen, B. Lix, B. D. Sykes, R. S. Hodges and C. M. Kay, *Journal of Molecular Biology*, 1995, **254**, 505-520.
30. A. L. Boyle, E. H. C. Bromley, G. J. Bartlett, R. B. Sessions, T. H. Sharp, C. L. Williams, P. M. G. Curmi, N. R. Forde, H. Linke and D. N. Woolfson, *Journal of the American Chemical Society*, 2012, **134**, 15457-15467.
31. B. Hess, C. Kutzner, D. van der Spoel and E. Lindahl, *Journal of Chemical Theory and Computation*, 2008, **4**, 435-447.
32. S. J. Marrink, H. J. Risselada, S. Yefimov, D. P. Tieleman and A. H. de Vries, *Journal of Physical Chemistry B*, 2007, **111**, 7812-7824.
33. L. Monticelli, S. K. Kandasamy, X. Periole, R. G. Larson, D. P. Tieleman and S. J. Marrink, *Journal of Chemical Theory and Computation*, 2008, **4**, 819-834.
34. D. Sengupta and S. J. Marrink, *Physical Chemistry Chemical Physics*, 2010, **12**, 12987-12996.
35. L. V. Schafer, D. H. de Jong, A. Holt, A. J. Rzepiela, A. H. de Vries, B. Poolman, J. A. Killian and S. J. Marrink, *Proceedings of the National Academy of Sciences of the United States of America*, 2011, **108**, 1343-1348.
36. X. Periole, A. M. Knepp, T. P. Sakmar, S. J. Marrink and T. Huber, *Journal of the American Chemical Society*, 2012, **134**, 10959-10965.
37. D. A. Lindhout, J. R. Litowski, P. Mercier, R. S. Hodges and B. D. Sykes, *Biopolymers*, 2004, **75**, 367-375.
38. S. A. Green, D. J. Simpson, G. Zhou, P. S. Ho and N. V. Blough, *Journal of the American Chemical Society*, 1990, **112**, 7337-7346.
39. N. V. Blough and D. J. Simpson, *Journal of the American Chemical Society*, 1988, **110**, 1915-1917.
40. P. L. Privalov, E. I. Tiktopulo and V. M. Tischenko, *Journal of Molecular Biology*, 1979, **127**, 203-216.
41. S. E. Herbelin and N. V. Blough, *Journal of Physical Chemistry B*, 1998, **102**, 8170-8176.
42. B. Pispisa, A. Palleschi, L. Stella, M. Venanzi and C. Toniolo, *Journal of Physical Chemistry B*, 1998, **102**, 7890-7898.
43. I. Solomon, *Physical Review*, 1955, **99**, 559-565.
44. N. Bloembergen and L. O. Morgan, *Journal of Chemical Physics*, 1961, **34**, 842-&.

45. J. Iwahara and G. M. Clore, *Nature*, 2006, **440**, 1227-1230.
46. C. Peggion, M. Jost, W. M. De Borggraeve, M. Crisma, F. Formaggio and C. Toniolo, *Chemistry & Biodiversity*, 2007, **4**, 1256-1268.
47. K. A. Bolin, P. Hanson, S. J. Wright and G. L. Millhauser, *Journal of Magnetic Resonance*, 1998, **131**, 248-253.
48. Z. O. Shenkarev, A. S. Paramonov, T. A. Balashova, Z. A. Yakimenko, M. B. Baru, L. G. Mustaeva, J. Raap, T. V. Ovchinnikova and A. S. Arseniev, *Biochemical and Biophysical Research Communications*, 2004, **325**, 1099-1105.
49. N. E. Zhou, C. M. Kay and R. S. Hodges, *Journal of Biological Chemistry*, 1992, **267**, 2664-2670.
50. S. Y. M. Lau, A. K. Taneja and R. S. Hodges, *Journal of Biological Chemistry*, 1984, **259**, 3253-3261.
51. B. Apostolovic and H. A. Klok, *Biomacromolecules*, 2008, **9**, 3173-3180.
52. Y. H. Chen, J. T. Yang and K. H. Chau, *Biochemistry*, 1974, **13**, 3350-3359.
53. N. J. Greenfield, *Nature Protocols*, 2006, **1**, 2733-2741.
54. R. Defrancesco, A. Pastore, G. Vecchio and R. Cortese, *Biochemistry*, 1991, **30**, 143-147.
55. J. M. Sturtevant, *Proceedings of the National Academy of Sciences of the United States of America*, 1977, **74**, 2236-2240.
56. T. Gruene, M. K. Cho, I. Karyagina, H. Y. Kim, C. Grosse, K. Giller, M. Zweckstetter and S. Becker, *Journal of Biomolecular Nmr*, 2011, **49**, 111-119.
57. J. Eisinger, B. Feuer and A. A. Lamola, *Biochemistry*, 1969, **8**, 3908-&.
58. F. Mito, T. Yamasaki, Y. Ito, M. Yamato, H. Mino, H. Sadasue, C. Shirahama, K. Sakai, H. Utsumi and K. Yamada, *Chemical Communications*, 2011, **47**, 5070-5072.
59. G. I. Likhtenstein, K. Ishii and S. Nakatsuji, *Photochemistry and Photobiology*, 2007, **83**, 871-881.
60. E. Gatto, G. Bocchinfuso, A. Palleschi, S. Oncea, M. De Zotti, F. Formaggio, C. Toniolo and M. Venanzi, *Chemistry & Biodiversity*, 2013, **10**, 887-903.
61. S. K. Chattopadhyay, P. K. Das and G. L. Hug, *Journal of the American Chemical Society*, 1983, **105**, 6205-6210.
62. C. V. Kumar, S. K. Chattopadhyay and P. K. Das, *Journal of the American Chemical Society*, 1983, **105**, 5143-5144.
63. W. A. Yee, V. A. Kuzmin, D. S. Kliger, G. S. Hammond and A. J. Twarowski, *Journal of the American Chemical Society*, 1979, **101**, 5104-5106.
64. F. Versluis, J. Dominguez, J. Voskuhl and A. Kros, *Faraday Discussions*, 2013.
65. H. Edelhoch, *Biochemistry*, 1967, **6**, 1948-&.
66. C. N. Pace, F. Vajdos, L. Fee, G. Grimsley and T. Gray, *Protein Science*, 1995, **4**, 2411-2423.
67. I. Hypercube, 2002, 2220.

Chapter 4

Controlled liposome fusion mediated by SNARE protein mimics



Marsden, H. R.; Zheng, T. T.; Voskuhl, J.; Kros, A., Controlled liposome fusion mediated by SNARE protein mimics. *Biomaterials Science* 2013, 1 (10), 1046-1054.

Abstract

The fusion of lipid membranes is essential for the delivery of chemicals across biological barriers to specific cellular locations. Intracellular membrane fusion is particularly precise, and is critically mediated by SNARE proteins. To allow membrane fusion to be better understood and harnessed, a simple bottom-up model in which synthetic fusogens replicate the essential features of SNARE proteins has been used to mimic this important process. In our fusogens, the coiled-coil molecular recognition motif of SNARE proteins is replaced by the coiled-coil E/K peptide complex, which is one ninth the size. The peptides are anchored in liposome membranes via pegylated lipids. Here, how the liposome fusion process is controlled by different parameters within the minimal model has been discussed. The lipopeptide fusogens form specific coiled coils that dock liposomes together, resulting in the merging of membranes via the stalk intermediate. Unusually for model systems, the lipopeptides can rapidly lead to fusion of entire liposome populations and the liposomes can undergo many rounds of fusion. The rate and extent of fusion and the number of fusion rounds can be manipulated by adjusting the fusogen and liposome concentrations. For example, these parameters can be tuned such that tens of thousands of ~100 nm liposomes fuse into a single giant liposome ~10 μm in diameter, alternatively, conditions can be selected such that only two liposomes fuse. The improved understanding of membrane fusion shows how application-specific fusion attributes can be achieved, and paves the way for controlled nanoreactor mixing and the controlled delivery of cargo to cells.

Introduction

The fusion of biological membranes is a very significant process as it allows the delivery of molecules across lipid bilayers, barriers that are usually impervious to the molecules. Intracellular membrane fusion, which is mediated by SNARE-proteins, is of particular interest as it is highly controlled in terms of which membranes will fuse and the location of fusion. The mechanism relies on the specific coiled-coil interaction between complementary proteins that are spatially organized.¹ The most widely studied SNARE-proteins are involved with cell-to-cell communication in the nervous system. Within neurons there are small liposomes called synaptic vesicles that are packed with neurotransmitters and whose outer lipid surface is extensively covered by proteins.² SNARE-proteins make up ~0.35 mol% of the molecules of the synaptic vesicle.² The

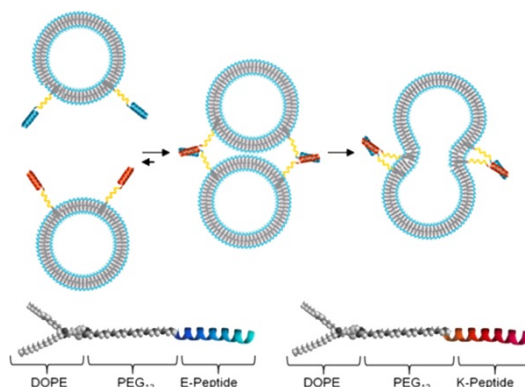
Controlled liposome fusion mediated by SNARE protein mimics

fusion process can be dissected into three stages: collision, docking, fusion. Firstly synaptic vesicles approach the neuronal membrane, they then dock to the target membrane by way of a coiled-coil bundle, which forms between the SNARE protein on the vesicle and two other complementary SNARE proteins, one anchored in the neuronal membrane, and one in the cytoplasm. Finally, lipid mixing results in the transfer of the neurotransmitters out of the neuron. In vitro experiments using reconstituted SNARE proteins have shown that the formation of the coiled-coil bundle docking the vesicles to the target membrane is sufficient to locally disrupt the lipids and cause the membranes to merge.³⁻⁵

The ability to controllably fuse specific lipid membranes has much potential, and an improved understanding of membrane fusion will allow the development of more sophisticated applications. The most highly anticipated application of controlled membrane fusion is the targeted transport of cargo such as drugs or gene therapies into cells. This would reduce side effects for patients and increase the efficacy of treatments.

For the application of controlled membrane fusion it is advantageous to use small synthetic fusogens rather than the groups of large proteins that have evolved in competitive cellular environments, which are cumbersome to manage. For the same reasons of ease of use and interpretation it is preferable to use liposomes or supported lipid bilayers as model membranes rather than whole cells. There have been previous membrane fusion models proposed using metal ions^{6,7} or synthetic fusogens, most of which are based on the concept of the fusion of viruses with cells, in which case a conformational change in a peptide causes it to bury a hydrophobic domain into the 'target' membrane.⁸⁻¹³ In this case the binding is non-specific, with binding occurring randomly on the surface, and it is often a leaky process.¹¹ In other models the fusion is more SNARE-like in that it relies on the specific interaction between molecules.¹⁴⁻²⁰ In a previous contribution, our group presented the first model system in which the fusogens are simplified versions of SNARE proteins.²¹ As with native SNARE-based fusion, the mechanism is based on the formation of coiled-coil complexes which dock and fuse the target membranes (Scheme 1). Two coiled-coil forming peptides, denoted E and K, were lipidated via a short PEG spacer, and are denoted LPE and LPK.²² The lipid tail (DOPE) anchors the peptides into lipid membranes. One set of liposomes is decorated with LPE and another with LPK. It was shown that when the liposome populations are mixed, the interaction between the coiled-coil forming peptides E and K leads to mixing of the liposome membranes and contents mixing without leakage, ie. clean liposome fusion.²¹ The model displays the same key characteristics as native

membrane fusion and the reduced SNARE proteins are also simple enough to enable ready synthesis and use in a range of settings.



Scheme. 1. Schematic illustration of liposome fusion mediated by simple SNARE protein mimics. Liposomes are modified with the lipopeptides LPE or LPK and upon mixing the peptide interactions trigger liposome fusion. E-peptide is (EIAALEK)₃ and K-peptide is (KIAALKE)₃ from N- to C- terminus.

Having established a model that achieves membrane fusion showing the desired characteristics, the boundaries within which it functions and it how the fusion process differs within this scope need to be thoroughly investigated to maximize its future use. Here the determinants for liposome fusion using this minimal model has been assessed. The influence of lipopeptide concentration, lipid concentration, and lipids of positive curvature on liposome fusion have been characterized. This chapter describes how the juxtaposition of liposome collision, docking and lipid mixing rates shapes the varied outcomes of liposome fusion within the reduced SNARE model.

Results and Discussion

1. Targeted fusion

When anchored in liposome membranes the fusogens LPK and LPE can cause rapid and complete fusion of all initial liposomes, as determined by a fluorescence-based lipid mixing assay (Figure 2).²³ Control experiments did not result in significant lipid mixing, confirming that the specific molecular recognition between peptides E and K is necessary for fusion, and that this is the only route to fusion in this model (Figure 2).

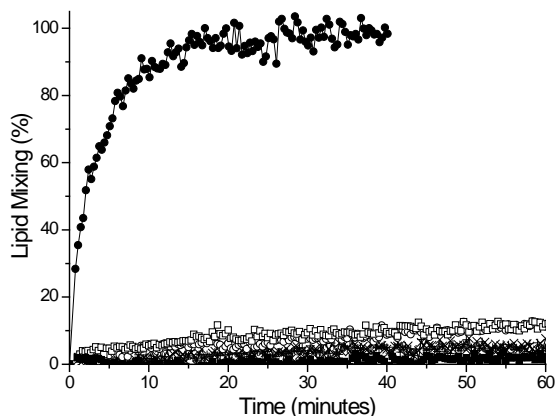


Figure 2. Lipid mixing as monitored by fluorescence spectroscopy between LPK-modified and LPE-modified liposomes (●), LPK-modified and plain liposomes (×), LPE-modified and plain liposomes (+), LPK-modified liposomes (○), LPE-modified liposomes (□), and plain liposomes (■). Fusogen proportion 1 mol%, [lipids] = 0.25 mM.

Models for membrane fusion can be divided into two classes: non-targeted, in which the fusion is caused by interactions between the fusogen and lipid bilayers, and targeted, i.e. in which the fusion is caused by molecular recognition between membrane-bound fusogens.²⁴ Many peptide fusogens, both synthetic and native (i.e. those involved with virus-cell membrane fusion), are non-targeted. They adopt an amphipathic helical conformation in the presence of lipid bilayers and penetrate into the membranes, destabilizing them and causing membrane fusion,²⁴ which is often accompanied by leakage.¹¹ When anchored in liposomes, the peptide components of LPE and LPK are in the α -helical conformation, with isoleucine and leucine residues making up a hydrophobic face running the length of the α -helix. However, when either LPK- or LPE-modified liposomes are added to non-modified liposomes there is no significant lipid mixing observed by fluorescence spectroscopy (Figure 2). These results demonstrate that the penetration of E or K peptides into the membrane of an opposing liposome does not cause membrane fusion, i.e. the fusion mechanism is not ‘virus-like’, but rather is ‘SNARE-like’, with membrane fusion triggered by molecular recognition between fusogens. As with SNARE-mediated fusion, this molecular recognition is specific to the hetero coiled-coil complex formation, with no significant lipid mixing occurring between LPK-modified liposomes or between LPE-modified liposomes due to homocoiling (Figure 2). The possibility of the electrostatically neutral E/K peptide complex inserting into the bilayer was investigated with tryptophan fluorescence, which is highly sensitive to the polarity of its local environment (see

Appendix). For liposomes decorated with tryptophan-labeled LPK the tryptophan fluorescence indicates that the C-terminus of LPK is in close proximity to the liposome membrane. Upon mixing LPK- and LPE-modified liposomes the tryptophan emission maximum becomes typical of a completely water-exposed environment.²⁵ These results indicate that after the molecular recognition between E and K the peptide complex remains outside the liposomes rather than penetrating into the liposome membrane.

2. Effect of fusogen concentration on liposome fusion

The specific molecular recognition between the peptides E and K can rapidly lead to complete membrane fusion of all liposomes (Figure 2). This efficiency is important for potential applications. To evaluate the effect of fusogen concentration on the fusion process, the lipid mixing assay was conducted with samples containing a fixed concentration of total lipids (1 mM), but with decreasing proportions of the lipopeptide fusogens (Figure 3A).²⁶ Incorporating as little as 0.5 mol% lipopeptide results in all of the initial liposomes going through at least one round of fusion (which is the limit of lipid mixing that can be monitored with this assay) within 30 minutes. Upon the incorporation of lower proportions of fusogen the rate of lipid mixing decreases, with the lower limit under these conditions being ~0.05 mol% lipopeptides, corresponding to an average of only 40 lipopeptides decorating the outer surface of a 120 nm liposome. In comparison, synaptic vesicles are ~40 nm in diameter and are decorated with ~70 copies of the SNARE proteins that dock to the target area of the neuronal membrane.²

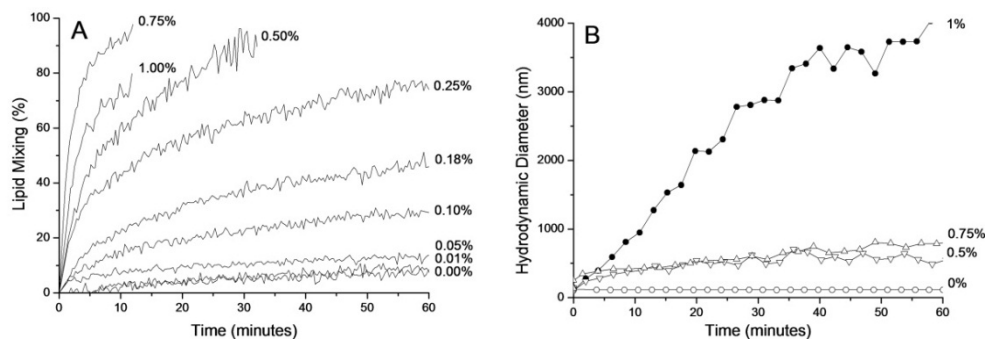


Figure 3. A) Total lipid mixing recorded by fluorescence spectroscopy for liposomes modified with between 0 and 1 mol% LPE and LPK. B) Average particle sizes determined by DLS for liposomes modified with between 0 and 1 mol% LPE and LPK. [Lipids] = 1 mM.

The general trend of increasing membrane fusion rates with increasing proportions of fusogens arises because two liposomes that diffuse into close proximity are more likely to be displaying complementary peptides in the correct orientation for binding in the approaching area, and hence are more likely to dock and undergo fusion. However, the most rapid lipid mixing occurs for liposomes with a surface modification of 0.75 mol% lipopeptides. Circular dichroism (CD) data demonstrates that when 0.75 mol% LPE or LPK are incorporated into the liposome membranes the peptides E and K have typical α -helical conformations, with minima at 208 and 222 nm and an ellipticity ratio $\ll 1$ (Figure 4A), implying that the lipopeptides are molecularly dispersed across the surface.^{27,28} Upon mixing, E and K bind together forming coiled coils (ellipticity ratio > 1 , Figure 4A), which dock liposomes together and lead to their fusion. However, when the amount of fusogen decorating the liposomes is increased to 1 mol%, peptide K is more constrained on the surface of the decorated liposomes, with CD spectra indicative of LPK homo-coiled coils (Figure 4B). No change in liposome size, lipid mixing, or peptide structure is detected with time for LPK-modified liposomes, thus peptide K forms homo-coiled coils on the surface of individual liposomes rather than between liposomes. Upon mixing LPE and LPK liposomes with 1 mol% surface modification E/K coiled coils still form (Figure 4B), docking liposomes together, however the rate of lipid mixing is decreased in comparison to 0.75 mol% fusogen due to the reduced accessibility of peptide K and the reduced energy gain of E/K binding.

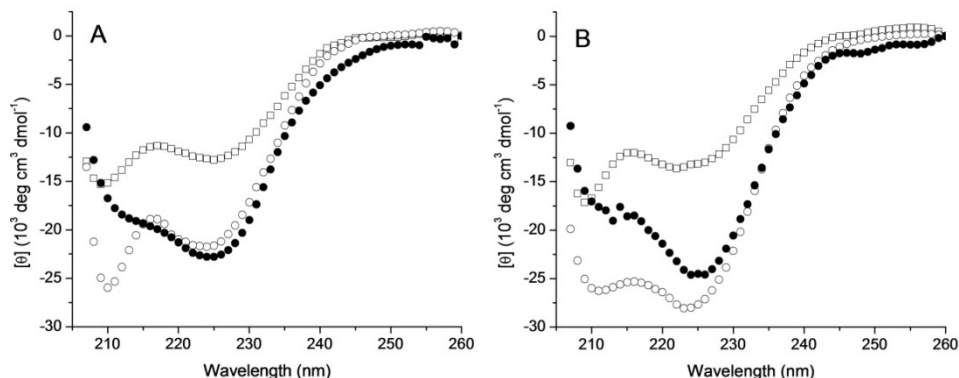


Figure 4. Circular dichroism data of A) liposomes modified with 0.75 mol% LPE (\square), LPK (\circ) and an equimolar mixture thereof (\bullet). B) liposomes modified with 1 mol% LPE (\square), LPK (\circ) and an equimolar mixture thereof (\bullet). [Lipids] = 0.5 mM.

2.1 Rapid Fusion of multiple liposomes

At lipopeptide proportions above ~ 0.5 mol%, when complete lipid mixing is rapidly achieved (Figure 3A), the particle sizes increased upon mixing LPE- and LPK-modified liposomes, as monitored by DLS (Figure 3B) and the liposomes sedimented to the bottom of the flask within hours (note that this size increase is the reason for the truncated fluorescence data in Figure 3A).²⁹ While the initial liposomes have an average diameter of ~ 120 nm, upon mixing the LPE- and LPK-modified liposomes particles with a larger hydrodynamic diameter are formed which increase in diameter and intensity with time, while the distribution containing the original LPE and LPK modified liposomes decreases in intensity.

Optical microscopy revealed that the macroscopic particles detected by DLS are clusters of docked and fused liposomes. An example of the morphological development is shown in Figure 5 for liposomes bearing 0.75 mol% fusogens. Initially the LPK- and LPE-modified liposomes are ~ 120 nm in diameter and are not visible by optical microscopy (Figure 5A). One hour after mixing the liposomes, particles ~ 1 μm in diameter are visible (Figure 5B), consistent with the sizes measured by DLS. Five hours after mixing, the liposomes are predominantly docked into large clusters and giant liposomes 5 μm in diameter can be discerned within the clusters (Figure 5C). These clusters of giant liposomes sediment out of solution. The liposomes continue to increase in size, with images taken three days after mixing showing the membranes of giant liposomes up to 10 μm in diameter (Figure 5D). These giant liposomes sometimes displayed elongated morphologies (Figure 5E), which may be a mechanism to conserve membrane area and internal volume.

Controlled liposome fusion mediated by SNARE protein mimics

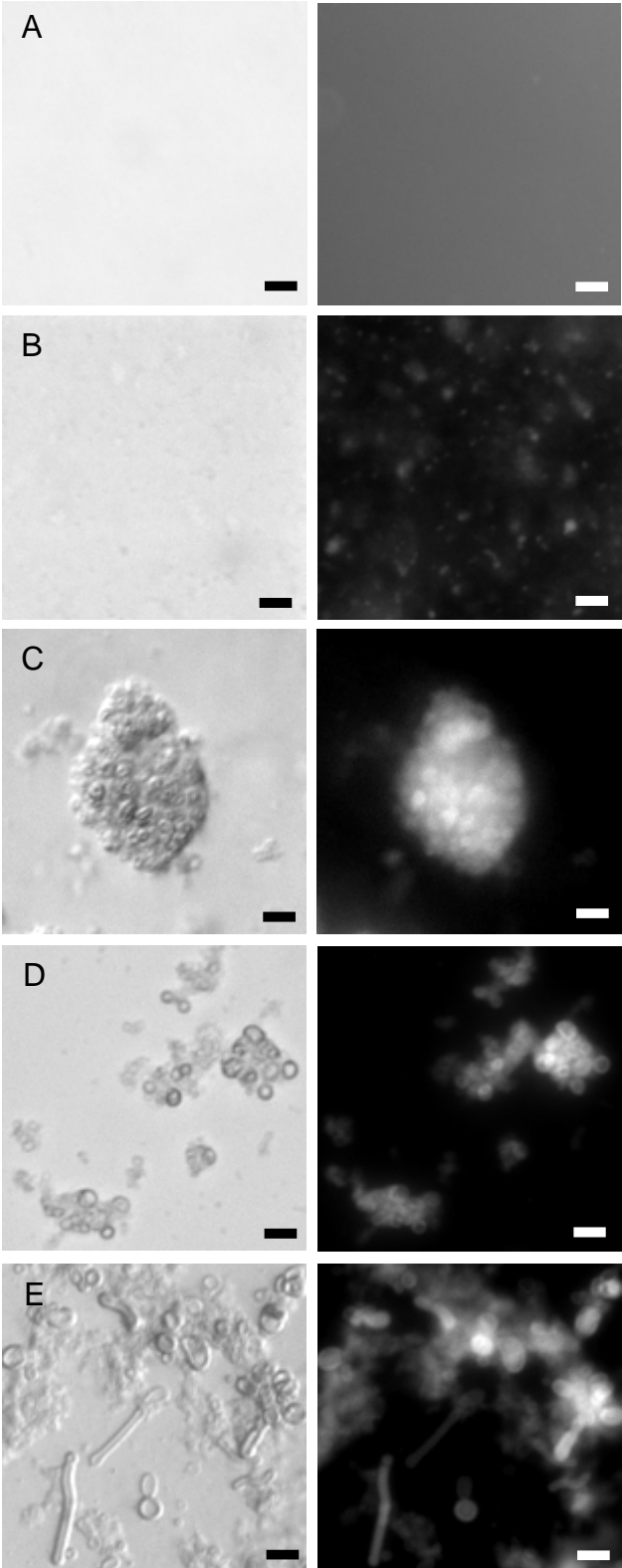


Figure 5. Optical and fluorescent microscopy images (left and right columns respectively) showing docking and fusion of liposomes modified with 0.75 mol% LPE and LPK. A) 5 minutes after mixing. B) 1 hour after mixing. C) 5 hours after mixing. D, E) 3 days after mixing. [Lipids] = 1mM lipids. Scale bars 10 μm .

For conditions under which liposome clustering occurs, the complete lipid mixing coupled with the large liposome size increases have molecular scale implications. The observation of liposome clusters means that a single liposome can be docked to multiple other liposomes, with the inference that not all of the lipopeptides that decorate a liposome are involved in a single fusion event. The accumulation of docked liposomes rather than their immediate transition through the fusion process is in line with expectations because each stage of liposome fusion – docking, hemifusion, complete fusion – requires further energy input.³⁰ It is presumed that after docking the energy input required to complete the fusion process arises from the more gradual attainment of a critical number and/or arrangement of lipopeptides. This finding is in line with the enhancement of membrane fusion through the physical arrangement of multiple complexes as observed for SNARE-protein mediated membrane fusion by experimental and computational studies.²⁹⁻³³⁵

The increase in liposome diameter over two orders of magnitude, from ~ 100 nm to ~ 10 μm (meaning that over 5×10^5 of the original liposomes have fused to grow into a single giant liposome), demonstrates that the liposomes can go through many rounds of fusion. This means that some fusogens on liposomes that have already fused are able to participate in subsequent fusion events. It is presumed that unless physically or kinetically impeded, the lipopeptides are able to laterally diffuse through the lipid leaflet in which they are anchored, such that following a fusion event the peptides E and K that were not involved with the fusion event would diffuse into close proximity with one another and form a coiled coil on the surface of the liposome. Due to the low dissociation constant for an unmodified and isolated E/K coiled coil complex in solution ($\sim 3.3 \times 10^{-8}$ M at 25 $^{\circ}\text{C}$, see Appendix), lipopeptides that have formed a complex on the surface of a single liposome are presumed to be effectively blocked from further fusion events. It is therefore assumed that some of the lipopeptides are physically prevented from forming a complex on the surface of a pre-fused liposome, most likely because the rate of docking is higher than the rate of lateral diffusion of the lipopeptides. Further study is required to elucidate how lipopeptides on pre-fused liposomes are available for subsequent fusion rounds.

2.2 Fusion of two liposomes

When the total lipid concentration is maintained at 1 mM but the liposomes are decorated with lower proportions of lipopeptide, the fusion process results in distinctly different physical changes to the liposome populations. For mixtures of liposomes modified with 0.25 mol% of each lipopeptide or less, the lipid mixing (e.g. Figure 6A) is accompanied by an initial small size increase of the particles as detected by DLS followed by a gradual decrease (e.g. Figure 6B). After mixing LPE- and LPK-modified liposomes the hydrodynamic diameter of the particles increases close to that expected if two liposomes have docked. The hydrodynamic diameter then decreases with time, reaching a plateau at the size corresponding to the fusion of two liposomes in which the volume is conserved rather than the outer surface area. These results are in accordance with our previous experiments in which no leakage was detected during fusion, and cryo-TEM images, in which internalized bilayers were observed.²¹

The two liposome fusion regimes, i.e., the fusion of tens of thousands of liposomes and the fusion of two liposomes, have the same total lipid concentration, therefore the liposome collision rate is the same. The dramatically different outcome arises because with fewer fusogens decorating the surface of the liposomes there is a lower probability that colliding liposomes are properly oriented to allow docking. The observation that with 0.25 mol% fusogen or less present an average of two liposomes fuse is presumably because after the first fusion event the lipopeptides that were not involved in the fusion event diffuse on the surface and form non-active E/K complexes before there is another opportunity for docking.

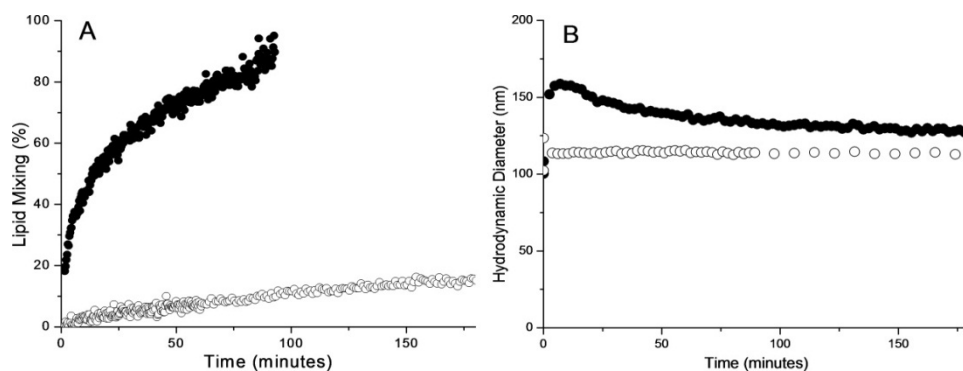


Figure 6. A) Total lipid mixing recorded by fluorescence spectroscopy for liposomes modified with 0.25 mol% (●) and 0 mol% (○) LPE and LPK. B) Average particle sizes determined by DLS for liposomes modified with 0.25 mol% (●) and 0 mol% (○) LPE and LPK. [Lipids] = 1 mM.

3. Effect of lipid concentration on membrane fusion

The fusion process is less sensitive to dilution of the liposomes, i.e. changing the liposome collision rate, than it is to the lipopeptide concentration, i.e. changing the probability that peptides are at the correct position and orientation for docking. Fluorescence time series were recorded to follow the total lipid mixing of mixtures containing 1 mol% fusogen and different concentrations of lipid (Figure 7A). Complete lipid mixing is observed within 30 minutes for lipid concentrations from 1 mM to 0.25 mM. In more dilute samples the rate of lipid mixing decreases, but remains significant at 0.01mM lipids. The lipid mixing is more efficient if there are more fusogens on fewer liposomes rather than fewer fusogens on more liposomes (Figure 7A vs. Figure 3A). DLS time series (Figure 7B) showed large particle size increases for lipid concentrations down to 0.1mM, while at 0.025 mM lipids (i.e. 0.25 μ M lipopeptide) and lower there is no sustained size increase with time, rather a slight increase is followed by a decrease to the hydrodynamic diameter expected for volume-conserved two-liposome fusion. For mixtures with 1 mM lipids and different lipopeptide concentrations this transition between the multiple liposome fusion regime and the two liposome fusion regime occurred at 0.25 mol% fusogen (i.e. 2.5 μ M lipopeptide). This means that the multiple liposome fusion regime is maintained with \sim 10x less fusogen if the liposomes are diluted in buffer rather than the number of fusogens modifying the surface of the liposomes is reduced. The docking efficiency is determined more by the number of fusogens (so that two approaching liposomes are more likely to be in the correct orientation

Controlled liposome fusion mediated by SNARE protein mimics

for the complementary lipopeptides to form a coiled-coil complex bridging the liposomes), than by the number of liposomes (the time between liposomes diffusing into close proximity).

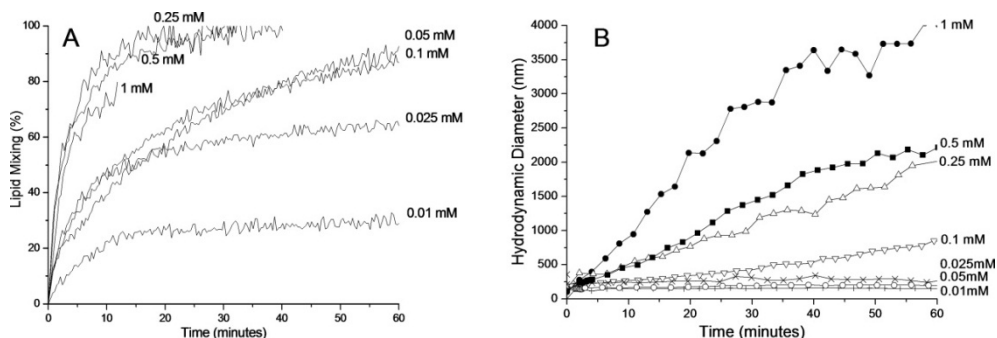


Figure 7. A) Total lipid mixing recorded by fluorescence spectroscopy for liposomes modified with 1 mol% LPE and LPK. Total [lipid] is varied between 0.01 and 1 mM. B) Average particle sizes determined by DLS for liposomes modified with 1 mol% LPE and LPK. Total [lipid] is varied between 0.01 and 1 mM.

4. Effect of positive curvature lipids on fusion process

In a previous contribution introducing this minimal model it was shown that the fusion mechanism proceeds through the stalk intermediate that is thought to be part of native fusion.²¹ In the stalk intermediate the outer leaflets of two approaching liposomes have merged at the contact point, forming a ‘stalk’ that connects the liposomes. The stalk intermediate requires a negative curvature, and while lipids of positive curvature are able to form part of a bilayer they are physically unsuited to the structure of the stalk intermediate, therefore their incorporation into liposomes reduces lipid mixing. The role of the positive curvature lipid lysophosphatidylcholine (LPC) in preventing fusion was further investigated.

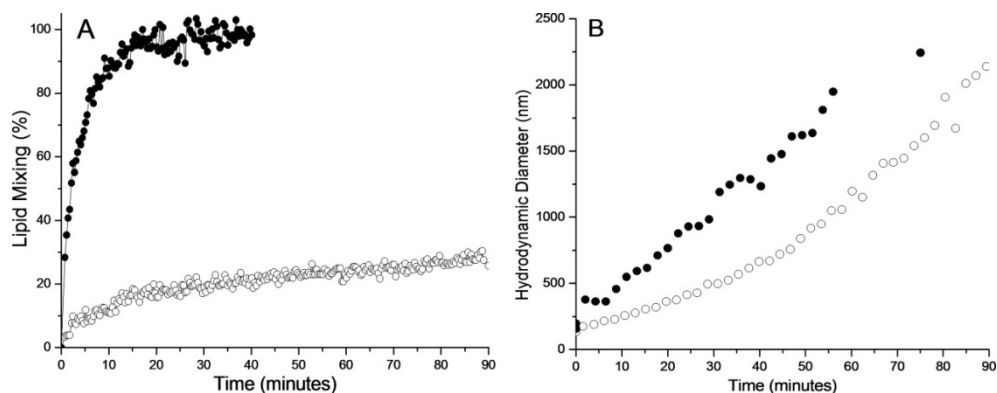


Figure 8. A) Total lipid mixing recorded by fluorescence spectroscopy for liposomes with the standard composition (●) and with 15 mol% LPC (○). B) Average particle sizes determined by DLS for liposomes with the standard composition (●) and with 15 mol% LPC (○). 1 mol% lipopeptides, [lipid] = 0.25 mM.

As expected, the inclusion of 15 mol% LPC to liposomes dramatically decreases lipid mixing (Figure 8A). However, a large size increase was observed with DLS for liposomes with and without LPC (Figure 8B). With optical microscopy the cause of this size increase is apparent (Figure 9). It can be seen that for liposomes of the standard composition there are many giant liposomes $\sim 5 \mu\text{m}$ in diameter one day after mixing, with ~ 10 giant liposomes docked together in clusters. In contrast, for liposomes containing 15 mol% LPC there are hundreds of liposomes of less than $1 \mu\text{m}$ docked into clusters. These results show that LPC does not prevent the first step of fusion, docking, which is insensitive to the liposome composition, but it does inhibit the following two stages, hemifusion and full fusion.

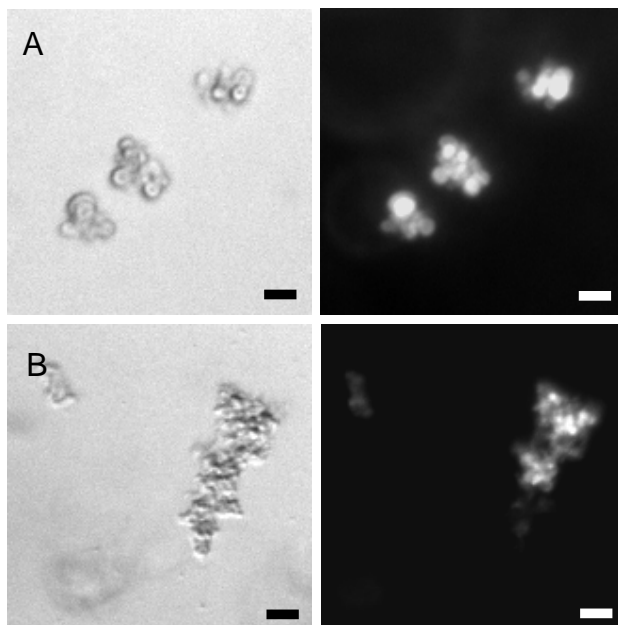


Figure 9. Optical and fluorescent microscopy images (left and right columns respectively) showing docking and fusion of liposomes one day after mixing. A) Standard liposome composition, i.e. DOPE/DOPC/CH 50/25/25 mol%. B) With 15 mol% LPC, i.e. DOPC/DOPE/CH/LPC 43/21/21/15 mol%. 1 mol% lipopeptide, [lipid] = 0.25 mM. Scale bars 10 μ m.

Conclusions

The functional determinants of a reduced SNARE model for membrane fusion were investigated. Complementary lipopeptides are incorporated into liposomes and lead to their docking, then via the stalk intermediate to complete membrane fusion. As with SNARE protein mediated fusion, molecular recognition occurs through coiled-coil binding, without fusion caused by viral-like aspecific peptide-lipid interactions. The coiled-coil formation can lead to the rapid membrane mixing of all initial liposomes, and the effects of lipopeptide and lipid concentrations on this process were studied. The optimal surface modification for rapid lipid mixing occurs when 0.75 mol% lipopeptide is incorporated into the liposome membrane, while complete lipid mixing still occurs with lower proportions of fusogens than there are SNARE proteins in synaptic vesicles. DLS and optical microscopy revealed that there are two fusion regimes – the fusion of thousands of

liposomes through multiple fusion rounds into giant liposomes up to 10 μm in diameter, and the fusion of two liposomes. This mapping of the rate and route of liposome fusion under different conditions gives a detailed understanding of the capacity of the reduced SNARE model to fuse liposome membranes. This understanding paves the way for future applications of the minimal model such as controlled nanoreactor mixing and the directed delivery of drugs to cells.

Experimental section

Materials

Lipopeptides were synthesized and purified as described previously.²¹ The amino acid sequence of peptide K was (KIAALKE)₃-NH₂, and that of peptide E was (EIAALEK)₃-NH₂. The molecular weights of LPK and LPE were 3703.7 g mol⁻¹ and 3706.6 g mol⁻¹ respectively. DOPE was purchased from Lipoid AG, and cholesterol was obtained from Fluka. DOPE-NBD and DOPE-LR were obtained from Avanti Polar Lipids. All other reagents and solvents were obtained at the highest purity available from Sigma-Aldrich or BioSolve Ltd. and used without further purification. Milli-Q water with a resistance of more than 18.2 MΩ/cm was provided by a Millipore Milli-Q filtering system with filtration through a 0.22 μm Millipak filter.

Liposome Preparation

Liposomes were composed of DOPC/DOPE/CH (50:25:25 mol%). Fluorescently labeled liposomes also contained 0.5 mol% LR-DOPE and NBD-DOPE. Lipid stock solutions (1 mM) were prepared in chloroform. Lipopeptide stock solutions (10 μM) were prepared in 1:1 (v/v) chloroform:methanol. Liposomes were prepared by drying appropriate volumes of the lipid and lipopeptide stock solutions in a 20 mL bottle under reduced pressure, addition of TES buffer (*N*-Tris(hydroxymethyl)methyl-2-aminoethanesulfonic acid sodium salt 10 mM, NaCl 100 mM, adjusted to pH 7.4) and sonication for ~5 minutes in a bath sonicator with the water bath at ~60°C.

Experimental Methods

Differential interference contrast (DIC) optical micrographs were recorded with a Zeiss axiovert-200 inverted microscope equipped with a 63 x objective long-range working lens. The images were recorded with a black and white CCD camera (AxioCam MRm) connected to an image-recording and -processing system (Axiovision 4.4).

Experimental diffusion coefficients, *D*, were measured at 25 °C by dynamic light scattering using a Malvern Zetasizer Nano ZS ZEN3500 equipped with a peltier-controlled thermostatic cell holder. The laser wavelength was 633 nm and the scattering angle was 173°. The Stokes-Einstein relationship $D = k_B T / 3\pi\eta D_h$ was used to estimate the hydrodynamic radius, *D_h*. Here *k_B* is the Boltzman constant, and η is the solvent viscosity.

The results are expressed as the hydrodynamic diameter with units of nm. For individual liposome batches the sample was allowed to equilibrate for 2 minutes. For DLS time series the solutions were mixed in the cuvette (1000 rpm for 30 seconds). Measurements were started immediately after mixing.

FRET-based lipid mixing experiments were conducted on a Tecan X fluorometer using a 96 well plate. The z-position was 12500 μm , and the gain was optimized according to the amount of fluorophore in the sample. Excitation and emission slits were set at 10 nm. The excitation wavelength was 460 nm, and NBD emission was monitored 535 nm. The temperature was set at 24 $^{\circ}\text{C}$ and the measured temperature was 28 – 29 $^{\circ}\text{C}$. 100 μL of fluorescent and non-fluorescent liposomes were combined, and for consistent mixing the plate was shaken inside the fluorometer for 30 seconds (2mm linearly, 70 x per minute). Data was collected every 20 seconds for at least 1 hour. Using 0.5 mol% of each fluorophore in the fluorescent liposomes and mixing fluorescent and non-fluorescent liposomes in a 1:1 molar ratio the increase in NBD fluorescence is proportional to lipid mixing (see Appendix). The data was calibrated to show the percentage of liposomes that have undergone lipid mixing by $\text{LM} (\%) = (I_t - I_0)/(I_{100} - I_0) \times 100$, where I_0 is the NBD intensity of 1:1 (v/v) fluorescent liposomes:TES, and I_{100} is the NBD intensity of liposomes of the same concentration prepared using an equimolar mixture of fluorescent and non-fluorescent stock solutions. I_0 and I_{100} were monitored with time as they are temperature sensitive. This assay only detects fusion between the original liposomes. e.g. if two pre-fused liposomes fuse the distance between the fluorophores does not change so the event is not detected.

Circular dichroism spectra were obtained using a Jasco J-815 spectropolarimeter equipped with a peltier-controlled thermostatic cell holder (Jasco PTC-423S). Spectra were recorded from 260 nm to 200 nm in a quartz cuvette with 5.0 mm pathlength at 25 $^{\circ}\text{C}$. Data were collected at 1.0 nm intervals with a 1 nm bandwidth and 1 s readings. Each spectrum was the average of 5 scans. The spectra had a baseline of plain liposomes in TES buffer subtracted. The ellipticity is given as the mean residue molar ellipticity, $[\theta]$ ($10^3 \text{ deg cm}^2 \text{ dmol}^{-1}$), calculated from $[\theta] = (\theta_{\text{obs}} \times \text{MRW}) / (10 \times l \times c)$, where θ_{obs} is the observed ellipticity in millidegrees, MRW is the mean residue molecular weight (i.e. the molecular weight of the peptide divided by the number of amino acid residues), l is the path length of the cuvette in cm and c is the peptide concentration in mg mL^{-1} . The mean residue molecular weights are 107.8 g mol^{-1} and 107.7 g mol^{-1} , and the peptide concentrations of 1

Controlled liposome fusion mediated by SNARE protein mimics

mol% in 0.5 mM lipid suspensions correspond to 11.3 mg L^{-1} and 11.3 mg L^{-1} for peptides LPE and LPK, respectively.

Appendix

Part 1. CD of acetylated peptides in TES

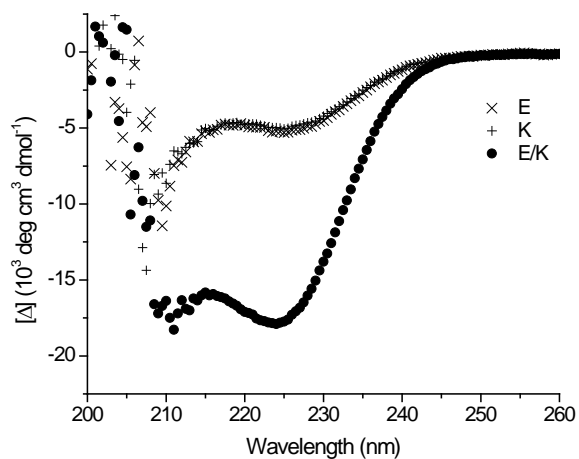


Figure A1. CD Spectroscopic Data of E (Δ), K (+), and an equimolar mixture of E and K (\bullet) in TES, pH 7.4, 25 °C. [Total Peptide] = 40 μ M.

Part 2. Temperature dependent CD data and analysis

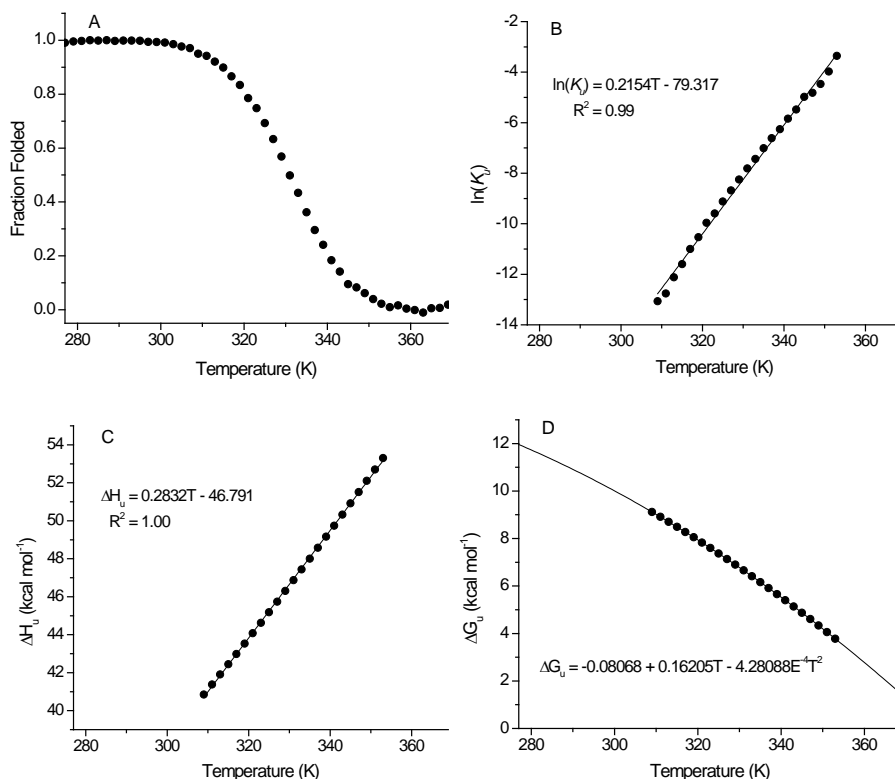


Figure A2. A) Thermal unfolding curve of unmodified E/K in TES buffer, pH 7.4, as followed by CD. [Total Peptide] = 40 μ M. B) Van't Hoff plot of the thermal denaturation of E/K. C) Dependence of the enthalpy of unfolding of E/K on temperature. ΔH_u values were obtained from the derivative of the van't Hoff plot. D) Free energy associated with the unfolding of E/K as a function of temperature. The least-squares fit gives a ΔG_u value at 25 °C of 10.2 kcal mol⁻¹.

Temperature dependent CD spectra were obtained using an external temperature sensor immersed in the sample. The temperature was controlled with the internal sensor and measured with the external sensor. A 10 mm quartz cuvette was used, and the solutions were stirred at 900 rpm. Spectra were recorded from 260 nm to 200 nm, with data collected at 0.5 nm intervals with a 1 nm bandwidth and 1 s readings. Each spectrum was one scan. The temperature range was 4 °C to 96 °C with a temperature gradient of 2.0 °C/minute and a 60 s delay after reaching the set temperature. The spectrum of TES at 4 °C (average of 5 scans) was subtracted from each spectrum.

The data was analyzed using a two-state unfolding model to determine the fraction folded using Eqn. (1),

$$F_f = (\theta - \theta_u) / (\theta_f - \theta_u) \quad (1)$$

Where θ is the observed ellipticity at 222 nm, θ_u is the ellipticity at 222 nm of the denatured state, as determined from the plateau of the ellipticity vs. temperature curve, and θ_f is the ellipticity at 222 nm of the folded state at that temperature as determined from a linear fit of the initial stages of the ellipticity vs. temperature curve.

The fraction unfolded, F_u , was calculated by Eqn. (2),

$$F_u = 1 - F_f \quad (2)$$

The dimer dissociation constant in the transition zone was calculated using Eqn. (3),

$$K_u = 2 P_t F_u^2 / F_f \quad (3)$$

where P_t is the total peptide concentration. By taking the derivative of the $\ln(K_u)$ vs. temperature and using this in the van't Hoff equation, Eqn. (4), the change in enthalpy associated with unfolding with temperature can be plotted:

$$d\ln(K_u) / dT = \Delta H_u / RT^2 \quad (4)$$

The gradient of this plot, ΔC_p , is the difference in heat capacity between the folded and unfolded forms, and can be used in the Gibbs-Helmholtz equation adapted to monomer-dimer equilibrium, Eqn. (5), to obtain the Gibbs free energy of unfolding as a function of temperature:

$$\Delta G_u = \Delta H_m (1 - T / T_m) + \Delta C_p [T - T_m - T \ln(T/T_m)] - RT \ln[P_d] \quad (5)$$

where T_m and H_m are the temperature and enthalpy at the midpoint of the transition, as determined by the maximum of the derivative of the ellipticity vs. temperature graph.

Part 3. Calibration of fluorescence based lipid mixing assay

The lipid mixing assay monitors NBD fluorescence, which depends on the distance between the FRET pair NBD and LR. One liposome population contains 0.5 mol% of DOPE-NBD and DOPE-LR (headgroup labeled), while the other population is non-fluorescent. As non-fluorescent and fluorescent liposomes fuse the distance between the fluorophores increases, resulting in decreased FRET efficiency and an increase in NBD fluorescence. Using 0.5 mol% of each fluorophore the increase in NBD fluorescence is proportional to lipid mixing (Figure A3).

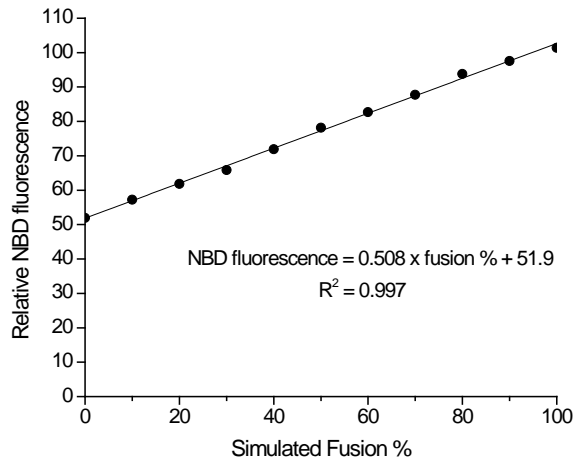


Figure A3. Samples which simulated 0-100% lipid mixing were prepared by combining the appropriate ratios of fluorescent and plain lipid stock solutions. The NBD fluorescence of these samples was monitored for 1 hr. The relative NBD fluorescence increases linearly with increasing fusion percent.

For the lipid mixing experiments each sample was calibrated by monitoring its fluorescence over time relative to an I0 sample (the fluorescent liposomes were diluted 1:1 with TES) and an I100 sample (liposomes prepared from an equimolar mixture of fluorescent and plain lipid stock solutions). The NBD fluorescence of mixed liposomes is not affected by the lipopeptide, thus the I100 samples did not contain lipopeptide.

Using this assay the lipid mixing is calibrated using an “I100” sample that simulates the distance between the fluorophores (and hence NBD intensity) if all of the original liposomes have fused. The most commonly used method for calibrating the fluorescence data is to add Triton-X to the sample after monitoring. This method results in a very large distance between the fluorophores, much larger than is possible using 1:1 fluorescent and non-fluorescent liposomes. In that case the monitored fluorescence increase is not proportional to lipid mixing. Using Triton-X 100% lipid mixing corresponds to ~20-30% fluorescence increase.

Part 4. Tryptophan fluorescence

The manner in which the coiled-coil formation between SNARE proteins leads to membrane distortion and fusion is unknown. A possible mechanism for both SNARE-mediated and LPK/LPE-mediated membrane fusion is molecular recognition followed by ‘virus-like’ membrane penetration and destabilization. This is of particular consideration for the minimal model as the E/K coiled-coil dimer is electrostatically neutral and hence may have a greater propensity for membrane insertion. In order to probe this possibility a tryptophan residue was included in the first generation LPK. Tryptophan fluorescence is highly sensitive to the polarity of its local environment, and to monitor environmental changes during the fusion process the LPK fusogen was synthesized containing tryptophan at the C-terminus (with the PEG spacer and lipid anchor at the N-terminus). Before fusion the C-terminus of LPK is in a relatively polar environment (the tryptophan emission maximum of LPK-decorated liposomes is at 342.5 nm, Figure A4).²⁵ Within one minute of mixing LPK- and LPE-modified liposomes the tryptophan emission maximum had red-shifted to 350 nm, indicating that upon E/K complex formation the C-terminus of the peptide moves from a relatively polar to a completely water-exposed environment.^{25, 34} These results indicate that after the molecular recognition between E and K initiates membrane fusion the peptide complex is situated outside the liposomes, rather than buried in the liposome membrane. Thus, the membrane distortion required for membrane fusion does not appear to arise via penetration of the peptide complex into the bilayer. Having established that the E/K peptide complex is unlikely to cause liposome fusion by ‘viral-like’ membrane burial, the second generation LPK, as employed for all other experiments in this paper, does not contain the tryptophan residue.

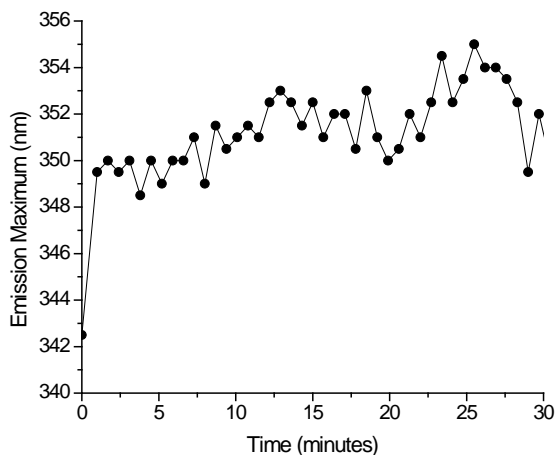


Figure A4. The wavelength of the tryptophan fluorescence maximum before ($t = 0$ minutes) and during lipopeptide induced fusion of liposomes. Lipid concentration 1mM, fusogen proportion 3%.

Tryptophan emission spectra were measured with a FS920 fluorometer from Edinburgh Instruments with a DTMS-300X excitation monochromator and a peltier-controlled thermostatic cell. Spectra were obtained at 25 °C using a quartz cuvette with a 1 cm path length. The step size was 0.5 nm, with a sampling time of 0.5 s at each wavelength, and 1 scan was measured for each spectrum. The excitation and emission slits were 5 nm. Emission spectra were measured from 330 nm to 360 nm at a fixed excitation wavelength of 280 nm. Measurements were started immediately after mixing the solutions in the cuvette (30 seconds stirring at 1000 rpm).

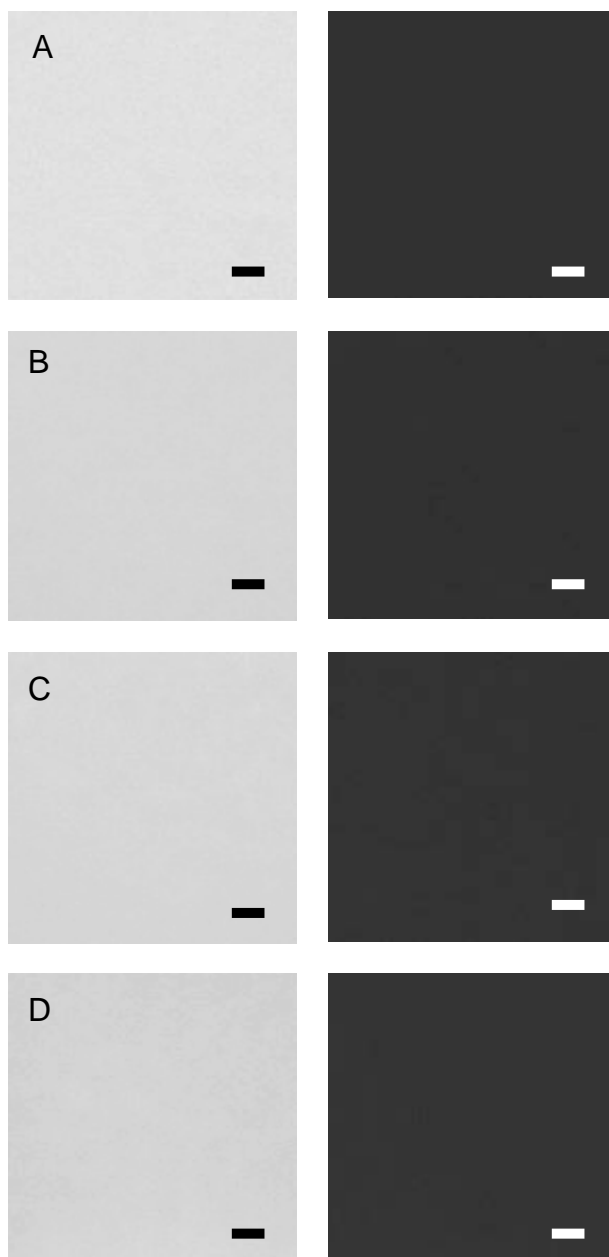
Part 5. Optical microscopy control experiment

Figure A5. Optical and fluorescent microscopy images (left and right columns respectively) of liposomes without lipopeptide modification. A) 5 minutes after mixing plain and fluorescently labeled liposomes. B) 1 hour after mixing. C) 5 hours after mixing. D) 3 days after mixing. [Lipids] = 1mM lipids. Scale bars 10 μm.

Part 6. Content mixing

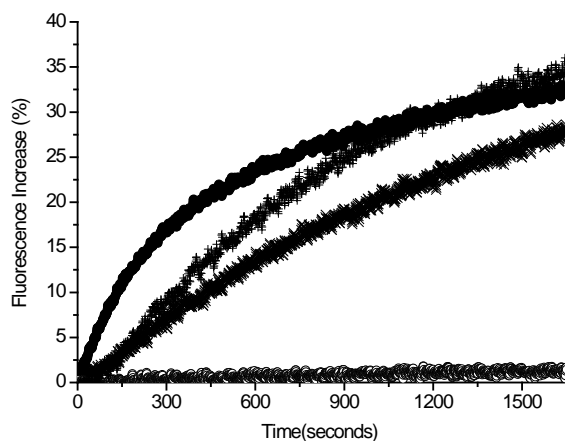


Figure A6. Content mixing recorded by fluorescence spectroscopy for liposomes modified with 1 mol% LPE and LPK. [lipid] 0.25 mM (●), 0.1 mM (+), 0.025 mM (×). Control with liposomes modified with 1 mol% LPE and 0 mol% LPK, [lipid] 0.1 mM (○).

To measure content mixing, LPE-modified liposomes containing sulforhodamine B at a self-quenching concentration were added to LPK-modified liposomes. Upon fusion the contents of the liposomes mix, resulting in an increased sulforhodamine B fluorescence signal due to the relief of self-quenching.^{3,4} The fluorescence signal is calibrated by adding Triton-X to lyse the liposomes and reach the maximum dilution. The sulforhodamine B dilution is much greater than the two-fold dilution expected if all LPE- and LPK-modified liposomes fuse, therefore the extent of the content mixing cannot be compared with the extent of the lipid mixing. In previous experiments (3 mol% fusogen, [lipid] 0.4 mM, PBS buffer), it was observed that content mixing proceeded without leakage.⁵

For content mixing experiments a dried film containing DOPC/DOPE/CH 50:25:25 mol% and 1 mol % LPE was hydrated and sonicated (5 min at 50 °C) in TES buffer solution (N-Tris(hydroxymethyl)methyl-2-aminoethanesulfonic acid sodium salt 10 mM, NaCl 100 mM, adjusted to pH 7.4) containing sulforhodamine B (20 mM). The final lipid concentration was 1 mM. To remove the non-encapsulated dye, the liposome suspension was subjected to Sephadex (G50, Superfine) using TES buffer as the eluent. The fraction containing liposomes was collected and diluted to the final lipid concentration. Sulforhodamine fluorescence was measured with a Perkin Elmer Luminescence

Spectrometer LS 50B at room temperature. The excitation and emission slits were 2.5 nm. The excitation wavelength was 520 nm and the emission wavelength was 580 nm. 800 μL of the LPE-decorated liposomes with encapsulated sulforhodamine B were added to a small volume disposable cuvette. The fluorescence signal of the sulforhodamine was detected and 800 μL of unmodified or LPK-modified liposomes (1:1 molar ratio with the LPE-modified liposomes) were added and the increase of sulforhodamine B fluorescence was detected due to a relief of self quenching. After 30 minutes 160 μL of 10% (v/v) solution of Triton X was added. To calculate the percentage of fluorescence increase the following equation was used:

$$F\% = (F_{(t)} - F_{(0)}) / (F_{(\text{max})} - F_{(0)}) \times 100$$

where $F_{(t)}$ is the fluorescence at a certain time, $F_{(\text{max})}$ is the fluorescence after lyses of the liposomes with Triton X and $F_{(0)}$ is the starting fluorescence after addition of the LPK-modified liposomes.

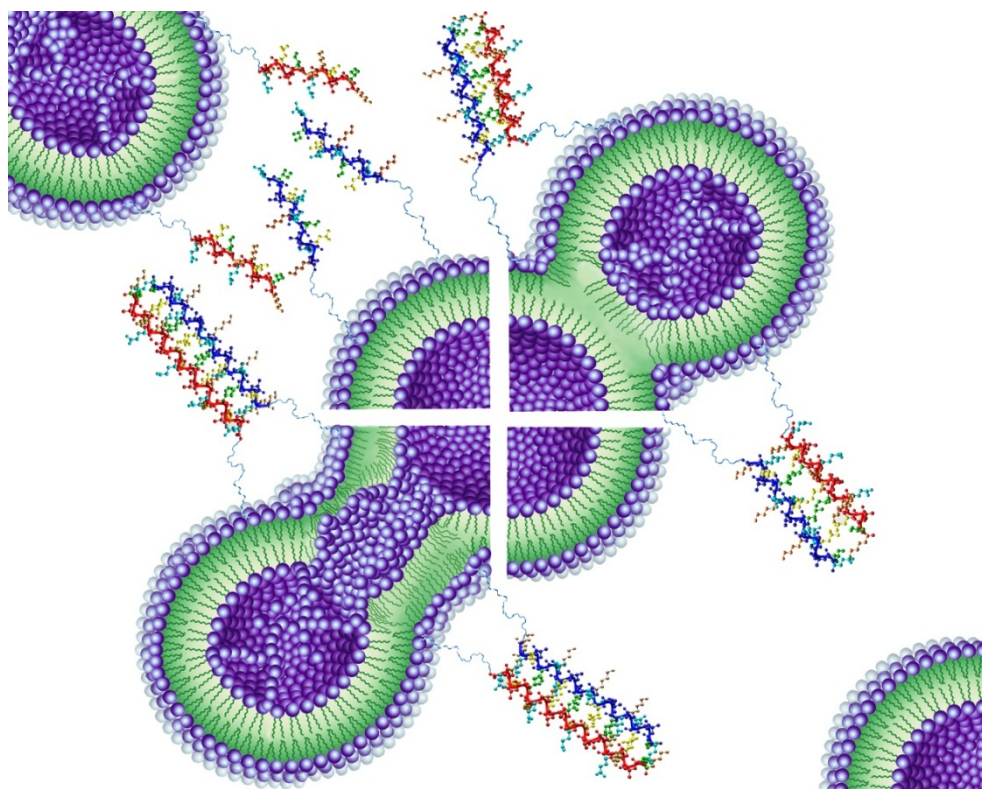
Reference

1. R. Jahn and R. H. Scheller, *Nat Rev Mol Cell Biol*, 2006, **7**, 631-643.
2. S. Takamori, M. Holt, K. Stenius, E. A. Lemke, M. Grønberg, D. Riedel, H. Urlaub, S. Schenck, B. Brügger, P. Ringler, S. A. Müller, B. Rammner, F. Gräter, J. S. Hub, B. L. De Groot, G. Mieskes, Y. Moriyama, J. Klingauf, H. Grubmüller, J. Heuser, F. Wieland and R. Jahn, *Cell*, 2006, **127**, 831-846.
3. T. Weber, B. V. Zemelman, J. A. McNew, B. Westermann, M. Gmachl, F. Parlati, T. H. Söllner and J. E. Rothman, *Cell*, 1998, **92**, 759-772.
4. C. G. Schuette, K. Hatsuzawa, M. Margittai, A. Stein, D. Riedel, P. KÅ¼ster, M. KÅ¼nig, C. Seidel and R. Jahn, *Proceedings of the National Academy of Sciences of the United States of America*, 2004, **101**, 2858-2863.
5. J. M. Hernandez, A. Stein, E. Behrmann, D. Riedel, A. Cypionka, Z. Farsi, P. J. Walla, S. Raunser and R. Jahn, *Science*, **336**, 1581-1584.
6. B. J. Ravoo and J. B. F. N. Engberts, *Journal of the Chemical Society, Perkin Transactions 2*, 2001, 1869-1886.
7. A. Richard, V. r. Marchi-Artzner, M.-N. l. Laloz, M.-J. p. Brienne, F. Artzner, T. e. Gulik-Krzywicki, M.-A. Guedeau-Boudeville and J.-M. Lehn, *Proceedings of the National Academy of Sciences of the United States of America*, 2004, **101**, 15279-15284.
8. R. A. Parente, S. Nir and F. C. Szoka, *Journal of Biological Chemistry*, 1988, **263**, 4724-4730.
9. F. Nomura, T. Inaba, S. Ishikawa, M. Nagata, S. Takahashi, H. Hotani and K. Takiguchi, *Proceedings of the National Academy of Sciences of the United States of America*, 2004, **101**, 3420-3425.
10. M. W. Hofmann, K. Weise, J. Ollesch, P. Agrawal, H. Stalz, W. Stelzer, F. Hulsbergen, H. de Groot, K. Gerwert, J. Reed and D. Langosch, *Proceedings of the National Academy of Sciences of the United States of America*, 2004, **101**, 14776-14781.
11. A. l. Lorin, B. Charloteaux, Y. Fridmann-Sirkis, A. Thomas, Y. Shai and R. Bressan, *Journal of Biological Chemistry*, 2007, **282**, 18388-18396.
12. T. P. Etzerodt, S. Trier, J. R. Henriksen and T. L. Andresen, *Soft Matter*, 2012, **8**, 5933-5939.
13. J. P. M. Motion, J. Nguyen and F. C. Szoka, *Angewandte Chemie International Edition*, 2012, **51**, 9047-9051.
14. A. Kashiwada, M. Tsuboi, N. Takamura, E. Brandenburg, K. Matsuda and B. Kokschi, *Chemistry – A European Journal*, 2011, n/a-n/a.
15. L. Simonsson, P. Jönsson, G. Stengel and F. Höök, *ChemPhysChem*, 2011, **11**, 1011-1017.
16. Y.-H. M. Chan, B. van Lengerich and S. G. Boxer, *Proceedings of the National Academy of Sciences*, 2009, **106**, 979-984.
17. M. Ma, Y. Gong and D. Bong, *Journal of the American Chemical Society*, 2009, **131**, 16919-16926.
18. Y. Gong, M. Ma, Y. Luo and D. Bong, *Journal of the American Chemical Society*, 2008, **130**, 6196-6205.

- 19.K. Meyenberg, A. S. Lygina, G. van den Bogaart, R. Jahn and U. Diederichsen, *Chemical Communications*, 2011, **47**, 9405-9407.
- 20.Robert J. Rawle, B. van Lengerich, M. Chung, Poul M. Bendix and Steven G. Boxer, *Biophysical Journal*, 2011, **101**, L37-L39.
- 21.H. Robson Marsden, N. A. Elbers, P. H. H. Bomans, N. A. J. M. Sommerdijk and A. Kros, *Angewandte Chemie International Edition*, 2009, **48**, 2330-2333.
- 22.See Supporting Information for circular dichroism characterisation, including the binding energy, of E/K coiled coil formation in TES buffer.
- 23.The lipid mixing assay used in this study was calibrated to reflect the extent of membrane mixing on a liposome population level.
- 24.H. R. Marsden, I. Tomatsu and A. Kros, *Chemical Society Reviews*, 2011, **40**, 1572-1585.
- 25.D. Swaving Dijkstra, J. Broos, J. S. Lolkema, H. Enequist, W. Minke and G. T. Robillard, *Biochemistry*, 1996, **35**, 6628-6634.
- 26.In our previous contribution which introduced this minimal model for membrane fusion 3 mol% lipopeptide was incorporated into the liposomes. This value was chosen so that the changes in peptide conformation during the fusion process could be reliably interpreted by circular dichroism. Upon mixing LPE- and LPK-modified liposomes the peptide conformation changed from homo coiled coils to aggregated coiled coils. Note that the first generation lipopeptides had 1-2 terminal amino acids in addition to the current three heptad repeats.
- 27.N. E. Zhou, C. M. Kay and R. S. Hodges, *Journal of Biological Chemistry*, 1992, **267**, 2664-2670.
- 28.J. R. Litowski and R. S. Hodges, *Journal of Biological Chemistry*, 2002, **277**, 37272-37279.
- 29.M. K. Domanska, V. Kiessling, A. Stein, D. Fasshauer and L. K. Tamm, *Journal of Biological Chemistry*, 2009, **284**, 32158-32166.
- 30.X. Lu, Y. Zhang and Y.-K. Shin, *Nat Struct Mol Biol*, 2008, **15**, 700-706.
- 31.R. Mohrmann, H. de Wit, M. Verhage, E. Neher and J. B. Sorensen, *Science*, 2010, **330**, 502-505.
- 32.W. J. Cho, J.-S. Lee, L. Zhang, G. Ren, L. Shin, C. W. Manke, J. Potoff, N. Kotaria, M. G. Zhvania and B. P. Jena, *Journal of Cellular and Molecular Medicine*, 2011, **15**, 31-37.
- 33.H. J. Risselada, C. Kutzner and H. Grubmüller, *ChemBioChem*, 2011, **12**, 1049-1055.
- 34.A. S. Ladokhin, S. Jayasinghe and S. H. White, *Analytical Biochemistry*, 2000, **285**, 235-245.

Chapter 5

Controlling the rate of coiled coil driven membrane fusion



Zheng, T. T.; Voskuhl, J.; Versluis, F.; Zope, H. R.; Tomatsu, I.; Marsden, H. R.; Kros, A., Controlling the rate of coiled coil driven membrane fusion. *Chemical Communications* 2013, 49 (35), 3649-3651.

Abstract

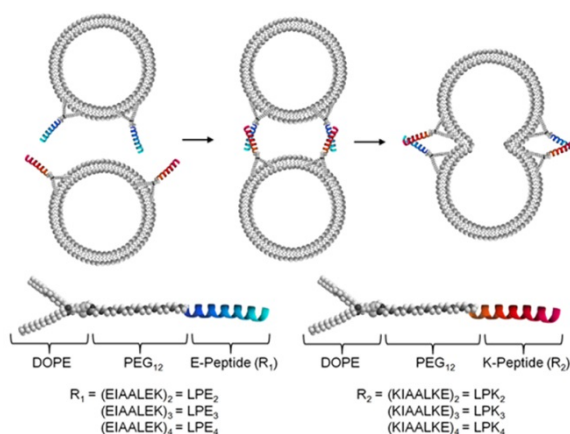
Sets of complementary lipidated coiled-coil forming peptides inducing membrane fusion have been designed. The influence of the coiled-coil motif on the rate of liposome fusion was studied, by varying the number of heptad repeats. It was shown that an increased coiled-coil stability of complementary peptides translates into increased rates of membrane fusion of liposomes.

Introduction

The onset of supramolecular chemistry in recent decades has supplied scientists with a wealth of strategies to design functional materials.¹⁻⁷ The self-assembly of molecular components into well-defined supra structures is governed by non-covalent interactions. The careful orchestration of these weak molecular interactions allows for the rational design of supramolecular complexes with predictable and tunable properties.⁸⁻¹⁴ Often, the inspiration for these assemblies comes from nature. Living systems display a staggering number of simultaneous orthogonal self-assembly processes. In particular, the well-defined secondary, tertiary and quaternary structures present in proteins have served as an invaluable motivation for research. For example, the specific recognition of DNA, RNA and carbohydrates, by proteins is based on the exact spatial placement of amino acid residues in the protein structure. With the rise of solid phase peptide chemistry it has become almost trivially easy to synthesize parts of proteins, i.e. peptides, with a well-defined amino acid structure and controllable self-assembly properties.¹⁵⁻¹⁹ These peptides are therefore often able to mimic protein functions. An important area of research where this principle has been convincingly shown is membrane fusion. Membrane fusion is a vital process for the transport of molecules in all eukaryotic cells.²⁰⁻²³ SNARE proteins are an important family of proteins which induce membrane fusion *in vivo* through the formation of a coiled coil complex and have been studied extensively.^{24, 25} Recently, synthetic systems have been shown to promote membrane fusion based on specific interactions between a variety of fusogenic entities, such as peptides,²⁶⁻³⁰ DNA³¹⁻³³ and other supramolecular recognition motifs.³⁴ Inspired by native SNARE proteins, our group has synthesized simplified SNAREs which are composed of a pair of coiled coil forming lipidated peptides (LPE and LPK). In our model system, molecular recognition between membrane bound peptides E and K leads to coiled coil formation, which drives fusion

Controlling the rate of coiled coil driven membrane fusion

between liposomes.³⁵ The synthetic lipopeptides consist of a hydrophobic tail (DOPE), a flexible linker (PEG₁₂) and coiled coil forming peptides E and K (Scheme 1). Peptides “E₃” (EIAALEK)₃ and “K₃” (KIAALKE)₃ consist of three heptad repeats, which form a heterodimeric coiled-coil motif upon binding.³⁶ The lipid tail ensures the efficient confinement of the peptide at the surface of the liposome. The advantage of our model system is that these peptide amphiphiles can be synthesized in a few days and chemical modifications can be easily introduced. Therefore, they can be tailored according to the needs of the particular application.



Scheme 1: Schematic illustration of liposome fusion mediated by lipopeptides, as well as an overview of the lipopeptides used in this study. Liposomes are decorated with LPK_x (red) or LPE_x (blue) and upon mixing coiled-coil formation brings the opposite liposomes in close proximity, and ultimately leads to fusion.

Results and discussion

In this chapter, the relationship between the stability of the coiled-coil motif formed by the membrane bound peptides and the efficiency of liposome-liposome fusion process was investigated. Therefore three sets of lipidated coiled-coil forming peptides E_x-K_x composed of 2, 3 and 4 heptad repeat units were synthesized. It is envisaged that the peptide length could influence the efficiency of lipopeptide mediated fusion through the stability of the resulting coiled-coil complex. First, the stability of coiled-coils assembled from complementary acetylated peptides was evaluated using circular dichroism (CD) spectroscopy (Fig. 1). Coiled-coil unfolding as a function of temperature was followed by

measuring the ellipticity at 222 nm, which yields insights into the stability of all peptide pairs. First the symmetrical peptide pairs have been evaluated, i.e. peptide pairs with identical numbers of heptad repeats in each peptide. It was observed that the magnitude of the binding affinity was ordered as expected: $K_4-E_4 > K_3-E_3 > K_2-E_2$. The K_3-E_3 pair has a binding affinity of 11 kcal/mol at 25 °C, whereas the values for K_4-E_4 and K_2-E_2 could not be determined as they are either too strong or too weak to be measured, respectively. Thus, increased coiled-coil stability is obtained upon increasing the peptide chain length, due to the increased number of non-covalent interactions between peptides E and K. Next, the ability to induce fusion between liposomes was studied for all symmetrical lipidated peptide pairs. First, a lipid mixing assay³⁷⁻³⁹ was used to compare the extent of mixing of the membrane constituents of the liposomes (Fig. 2). In this assay, LPK_x decorated liposomes (with a hydrodynamic diameter of ~120 nm) contained the FRET pair DOPE-NBD (1,2-dioleoyl-sn-glycero-3-phosphoethanolamine-N-(7-nitro-2-1,3-benzoxadiazol-4-yl) and DOPE-LR (1,2-dioleoyl-sn-glycero-3-phosphatidylethanolamine-lissamine-rhodamine B), while the LPE_x decorated liposomes (~100 nm) did not contain any fluorescent label.

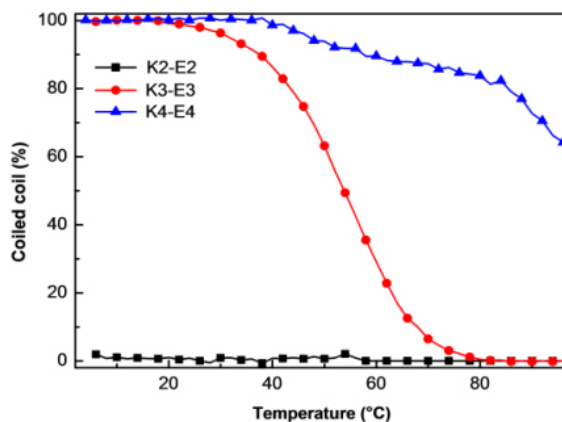


Figure 1: Thermal folding curve of E_x/K_x , as obtained from CD curves. [Total peptide] = 40 μ M in PBS (pH=7.4, 50mM phosphate, 150mM NaCl).

Both sets of liposomes were stable in time and did not show any auto-fusion. However, upon mixing the two batches of liposomes, an increase in the NBD emission was observed due to the increased average distance between the NBD and LR dyes. This is indicative of

Controlling the rate of coiled coil driven membrane fusion

lipid mixing between the liposomes. Interestingly, a correlation between the stability of the coiled-coil motif and the extent of lipid mixing was observed. The largest fluorescence increase was found for liposomes decorated with LPE₄-LPK₄, followed by LPE₃-LPK₃ and finally LPE₂-LPK₂ (Fig. 2). The LPE₂/LPK₂ decorated liposomes show some degree of lipid mixing, even though the acetylated peptides E₂/K₂ are unable to form a coiled-coil complex. However, confinement of peptides at a lipid membrane interface induces α -helicity, even when these peptides adopt a random coil conformation in solution. This induced folding induces the complementary peptides to interact (see Table A2). Control experiments showed that lipid mixing only occurs when both complementary peptides are present and are able to form a coiled-coil motif, when one of the peptides is omitted, no lipid mixing occurs (Fig.2). Additional experiments were performed to investigate the effect of coiled-coil formation on the extent of lipid mixing as a function of temperature. Increasing the temperature from 25 °C to 60 °C led to strongly decreased lipid mixing for LPE₃-LPK₃ modified liposomes and no fusion at all was observed for LPE₂-LPK₂. In contrast, lipid mixing for LPE₄-LPK₄ decorated liposomes was hardly influenced (Fig. 2B). This observation is consistent with the CD measurements of the acetylated peptides, namely that E₃-K₃ show a decreased ability to assemble into coiled-coils upon raising the temperature to 60 °C, while E₄-K₄ remains predominantly in a coiled-coil formation. Several reports have shown that the fusion of liposomes can be halted at the hemifusion state, resulting in lipid mixing only.²¹

To test whether the trend in lipid mixing translated to full fusion events, a content mixing fluorescence assay was performed (Fig. 3). In this experiment, LPE-decorated liposomes were loaded with sulphorhodamine B at a self-quenching concentration (20 mM). Upon the addition of non-fluorescent LPK liposomes, content mixing results in a dilution of the dye, diminishing self-quenching and resulting in an increased fluorescent intensity. Consistent with the lipid mixing data, liposomes decorated with LPE₄ and LPK₄ showed the most efficient content mixing, followed by LPE₃ and LPK₃ and finally LPE₂ and LPK₂ (Fig 4). Again, this data correlates with the trend in the coiled-coil stability.

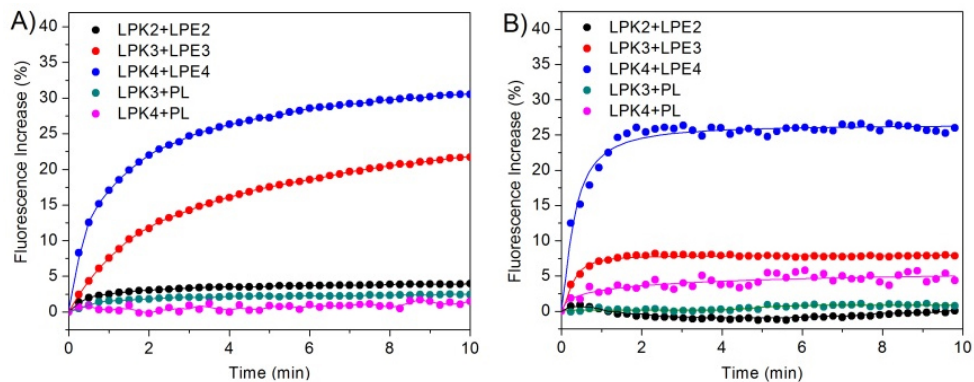


Figure 2. Fluorescence increase at A) 25 °C and B) 60 °C, due to lipid mixing between two batches of liposomes decorated with 1 mol% LPE₂-LPK₂, LPE₃-LPK₃, LPE₄-LPK₄. Two control experiments are shown; lipid mixing between LPK₃ or 4-decorated liposome with plain liposomes (PL). [lipid] = 0.1 mM. LPK_x-decorated liposomes contained 0.5 mol% of DOPE-NBD and 0.5 mol% of DOPE-LR.

In addition, the evolution of particle sizes was measured upon mixing batches of LPE_x- and LPK_x-decorated liposomes using dynamic light scattering (DLS). Again, the strongest effect was observed for LPE₄ and LPK₄ modified liposomes, which is in good agreement with the content and lipid mixing assays. A summary of all fusion experiments, including content mixing (CM), lipid mixing (LM) and size increase (SI) measurements is given in table 1 and Figure 4. Next, the fusogenicity of the various lipopeptide-decorated liposomes as a function of pH was investigated. This parameter strongly influences coiled-coil formation, since the peptides are designed to display opposite charges (Lys vs. Glu) at fixed sites of the assembly, controlling orientation and stability of the coiled-coil motif. The lipopeptide pairs LPE₃/LPK₃ and LPE₄/LPK₄ show significant lipid mixing throughout the studied pH range (pH 5-8, see Figure A16-19). Especially the peptide pair with four repeating heptads showed high lipid mixing values irrespective of pH, indicating that hydrophobic interactions are the driving force for coiled-coil formation, whereas the stabilization of the coiled-coil through opposite charges plays a minor role. These findings reveal that the E₄/K₄ coiled-coil binding motif can be used under a wide range of conditions (pH = 5-8, T = 25-60 °C). Finally, the properties of asymmetric peptide pairs have been evaluated, i.e. peptide pairs with a different number of heptad repeat units.

It was found for the acetylated peptides that both K₂/E₃ and K₃/E₂ showed no significant binding, which translated for the lipopeptides in negligible lipid mixing, content mixing and particle size increase (Table 1 and Figure 4). Large binding energies were found for

Controlling the rate of coiled coil driven membrane fusion

samples containing the acetylated pairs K_4/E_2 and K_2/E_4 , although they were lower than for K_3/E_3 .

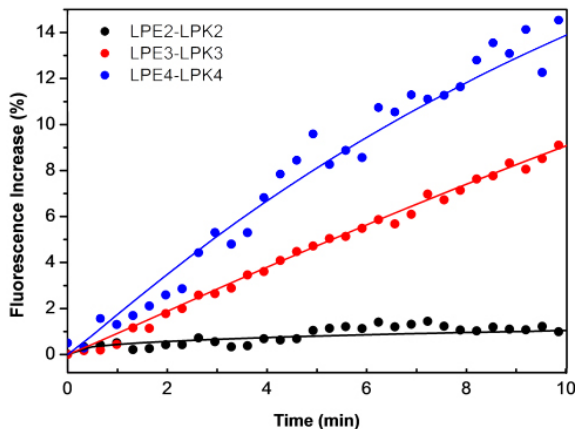


Figure 3: Content mixing assay; LPE_x decorated liposomes were loaded with 20 mM sulphorhodamine B and mixed with LPK_x liposomes. All spectra were obtained after mixing the liposomes. [total lipid] = 0.1 mM and 1% of lipopeptides LPE_4-LPK_4 , LPE_3-LPK_3 or LPE_2-LPK_2 , in HEPES buffer at pH = 7.2.

It is known that K_4 and E_4 form homocoils, complicating interpretation of binding energies. However, control lipid mixing experiments in which one lipopeptide from asymmetric pairs were omitted did not result in any significant lipid mixing (Fig. 2), indicating that asymmetric pairs do contribute to the observed binding energies.

Peptide	C-C ^a	BE ^b	T _m ^c	Lipopeptide	% CM ^d	% LM ^e	% SI ^f	R-LM ^g
Symmetric coiled-coil motifs ^o								
K ₂ -E ₂ ^o	- ^o	- ^o	- ^o	LPK ₂ -LPE ₂ ^o	1 ^o	4 ^o	0 ^o	2 ^o
K ₃ -E ₃ ^o	+ ^o	11 ^o	58 ^o	LPK ₃ -LPE ₃ ^o	9 ^o	21 ^o	148 ^o	8 ^o
K ₄ -E ₄ ^o	+ ^o	n.d. ^o	>96 ^o	LPK ₄ -LPE ₄ ^o	14 ^o	31 ^o	176 ^o	17 ^o
Asymmetric coiled-coil motifs ^o								
K ₂ -E ₃ ^o	- ^o	- ^o	- ^o	LPK ₂ -LPE ₃ ^o	1 ^o	2 ^o	2 ^o	2 ^o
K ₃ -E ₂ ^o	- ^o	- ^o	- ^o	LPK ₃ -LPE ₂ ^o	1 ^o	3 ^o	0 ^o	2 ^o
K ₂ -E ₄ ^o	+ ^o	9 ^o	38 ^o	LPK ₂ -LPE ₄ ^o	5 ^o	16 ^o	68 ^o	7 ^o
K ₄ -E ₂ ^o	+ ^o	10 ^o	58 ^o	LPK ₄ -LPE ₂ ^o	5 ^o	16 ^o	71 ^o	7 ^o
K ₄ -E ₃ ^o	+ ^o	12 ^o	70 ^o	LPK ₄ -LPE ₃ ^o	9 ^o	21 ^o	86 ^o	11 ^o
K ₃ -E ₄ ^o	+ ^o	13 ^o	76 ^o	LPK ₃ -LPE ₄ ^o	9 ^o	21 ^o	100 ^o	12 ^o

Table 1: Summary of coiled-coil formation studies of acetylated peptides and key data of liposome fusion studies using the lipidated peptide pairs LPE_x and LPK_x. ^aC-C = coiled coil; the + sign signifies the formation of a coiled-coil motif. ^bBE = binding energies in kcal/mol, ^cT_m = melting temperature in °C. n.d.= not determined. ^dCM = content mixing after 10 minutes, ^eLM = lipid mixing after 10 minutes, ^fSI = size increase of liposomes after 60 minutes, ^gR-LM=initial lipid mixing rate.

The strong tendency of the 4 heptad repeat peptides to form α -helices ensures the folding of the 2 heptad repeat peptides into α -helices upon binding. When confined to the surface of liposomes, these peptide pairs induced significant lipid and content mixing albeit to a lesser extent than E₃/K₄. Finally, samples containing the pairs K₄/E₃ and K₃/E₄ showed slightly higher binding energies than E₃/K₃ and yielded similar lipid and content mixing efficiencies. These results show that the stability of the coiled-coil pairs is reflected by the rate of fusion as determined by lipid and content mixing assays.

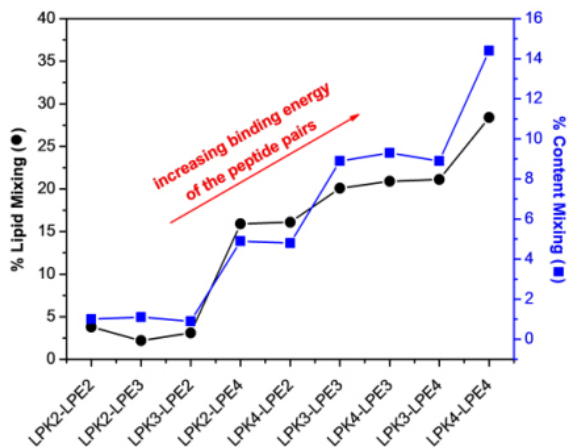


Figure 4: Correlation of lipid and content mixing to the coiled-coil lipidated peptide pairs with increasing stability.

Conclusion

In summary, the increased coiled-coil stability of complementary peptides translates into increased rates of membrane fusion of liposomes modified with the corresponding lipidated peptides, as observed by the different assays (content mixing, lipid mixing and size increase). Liposomes carrying lipidated peptides with 4 repeating units (i.e. E₄ and K₄) were found to be the most fusogenic, and can be used in a wide range of temperature and pH.

This lipopeptide induced fusion system can be applied beyond traditional membrane fusion, enabling the formation of complex supramolecular assemblies composed of nontraditional amphiphiles or to induce live cell fusion resulting in a direct drug delivery system.

Appendix

1. Materials and Methods

1.1 Materials

Fmoc-protected amino acids and Sieber Amide resin were purchased from Novabiochem. Fmoc-NH-PEG₁₂-COOH was purchased from IRIS Biotech. DOPC was purchased from Avanti Polar Lipids, DOPE was purchased from Phospholipid, and cholesterol was obtained from Fluka. DOPE-NBD and DOPE-LR were obtained from Avanti Polar Lipids, All other reagents and solvents were obtained at the highest purity available from Sigma-Aldrich or BioSolve Ltd. And used without further purification. Milli-Q water with a resistance of more than 18.2 MQ cm⁻¹ was provided by a Millipore Milli-Q filtering system with filtration through a 22 um Millipak filter. Phosphate buffered saline, PBS: 5 mM KH₂PO₄, 15mM K₂HPO₄, 150 mM NaCl, pH 7.4.

1.2 General Methods

RP-HPLC was performed with a Shimadzu HPLC system with two LC-8A pumps, and an SPD-10A VP UV-VIS detector, Sample elution was monitored by UV detection at 214nm and 256nm. Sample elution was monitored by UV detection at 214nm and 256 nm. Samples were eluted with a linear gradient from A to B, A being ACN, and B 0.1% (V:V) TFA in H₂O. Purification of the peptides and hybrids was performed on a C18 Vydac Column with a flow rated of 15ml/min. Sample purity was verified by LCMS. MALDI-TOF mass spectra were acquired using an Applied Biosystems Voyager System 6069 MALDI-TOF spectrometer with an ACH matrix. Samples were dissolved in 1:1 (v/v) 0.1% TFA in water:acetonitrile(TA), at concentrations of ~0.3mg/ml for K and E. Solutions for spots consisted of (V/V) 1:10 sample solution: 10 mg/ml ACH in TA. Phosphate buffered saline, PBS: 5 mM KH₂PO₄, 15 mM K₂HPO₄, 150 mM NaCl, pH 7.4.

2. Experimental details

2.1 Peptide Synthesis:

The peptides E_x and K_x were prepared using standard Fmoc-chemistry on a Syro-1 peptide synthesizer (Biotage). The peptides were synthesized on Sieber-Amide resin (0.62 mmol/g of NH₂). HCTU was used to activate the amino acids derivatives. The peptides were acetylated. Cleavage and de-protection was carried out using 95:2.5:2.5 (V/V)

Controlling the rate of coiled coil driven membrane fusion

TFA:H₂O:TIS for 1 hour. The cleavage mixture and three subsequent rinses of the resin with the TFA mixture were added drop-wise to cold diethyl ether. The white precipitate was compacted with centrifugation and the supernatant removed. This was repeated three times with the addition of fresh diethyl ether. The pellets were dried in air or under reduced pressure.

The crude products were purified by RP-HPLC. ACN used as mobile phase A, H₂O with 0.1% TFA as mobile phase B. Samples were eluted with a linear gradient from 90% to 10% B (V/V). After purification all compounds were lyophilized from water to give white material with typically a yield of 40% for all the peptides.

2.2 Lipopeptide synthesis:

The peptide components of LPE and LPK were prepared with standard solid-phase peptide synthesis protocols using Fmoc-chemistry on a Syro-1 automated peptide synthesizer (Biotage), with a PL-sieber Amide resin on a 0.25 mmol scale. The peptide coupling reagent was HCTU. The N-terminal Fmoc was removed with 20% (V/V) piperidine in NMP. After the peptide component was prepared, the resin was removed from the reaction vessel and Fmoc-NH-PEG₁₂-COOH was coupled to the immobilized peptides. The resin was swollen in NMP for 1 hour. 2.5 equivalents of Fmoc-NH-PEG₁₂-COOH and 2.5 equivalents of HCTU were dissolved in NMP(20ml) and mixed with 5 equivalents of DIPEA. After pre-activation for 1 minute the mixture was added to the peptide-resin and shaken for 20 hours. The uncoupled amines were capped with 0.05 M acetic anhydride, 0.125 M DIPEA in NMP. The N-terminal Fmoc was removed with 20% (V/V) piperidine in NMP. The resin was washed thoroughly with 10×10 ml DCM. Next, succinic anhydride was coupled to the immobilized peptide-PEG. The resin was swollen in NMP. 5 equivalents of succinic anhydride were dissolved in NMP (20mL) and mixed with 6 TEA. The mixture was added to the resin and shaken for 15 hours. The resin was washed thoroughly with 10×10mL NMP, and 10×10mL DCM. DOPE was coupled to the immobilized peptide-PEG₁₂-succinic acid in the same way, except that 3 equivalents of DOPE, 3 equivalents of HCTU, and 6 equivalents of DIPEA were used, and 1:1 (V/V) NMP: DCM was used to swell the resin and to couple the DOPE. After the peptide synthesis and after each subsequent coupling step the synthesis was tested by MALDI-TOF mass spectroscopy. Cleavage from the resin and deprotection was carried out by shaking 15 mg resin with 95: 2.5:2.5 (V/V) TFA:H₂O:TIS for one hour. The cleavage mixture and

three subsequent rinses of the resin with the TFA mixture were added drop-wise to cold diethyl ether. The white precipitate was compacted with centrifugation and the supernatant removed. This was repeated three times with the addition of fresh cold diethyl ether. The pellets were dried in air or under reduced pressure. Bulk cleavage of the compounds was performed in the same way except using Bulk cleavage of the compounds was performed in the same way except using 47.5: 47.5: 2.5: 2.5 (V/V) TFA: DCM: H₂O: TIS for one hour. The crude products were purified by RP-HPLC, the yield of LPE₂ and LPK₂ are 40%, LPK₄ 30%, LPE₄ 20%. For each compound the purity was estimated from RP-HPLC to be greater than 95%, with a mobile phase of 0.1% TFA ACN, and H₂O.

2.3 Electrospray ionization (ESI) mass spectrometry and HPLC

Lipopeptide	Molecular weight	HPLC purity
LPE ₂	2952.8	> 95%
LPK ₂	2950.9	> 95%
LPE ₃	3706.2	> 95%
LPK ₃	3703.4	> 95%
LPE ₄	4461.6	> 95%
LPK ₄	4458.3	> 95%

Table A1: Overview about calculated and found masses via MALDI-MS

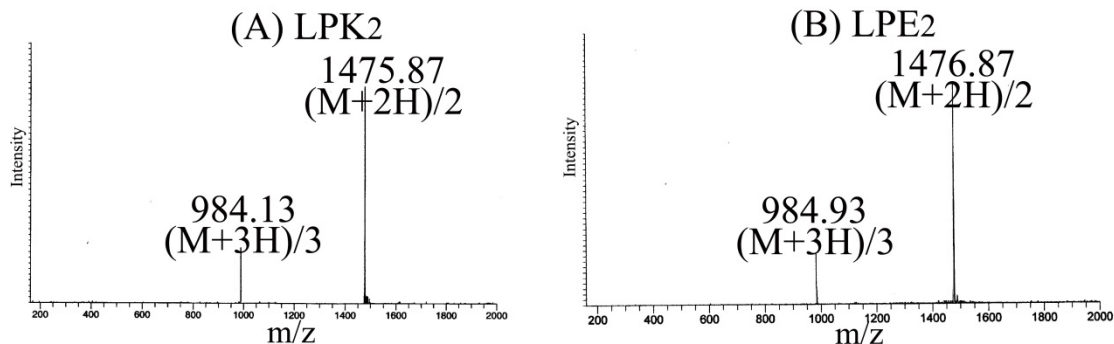


Figure.A1: ESI-mass spectra of (A) LPK₂ and (B) LPE₂.

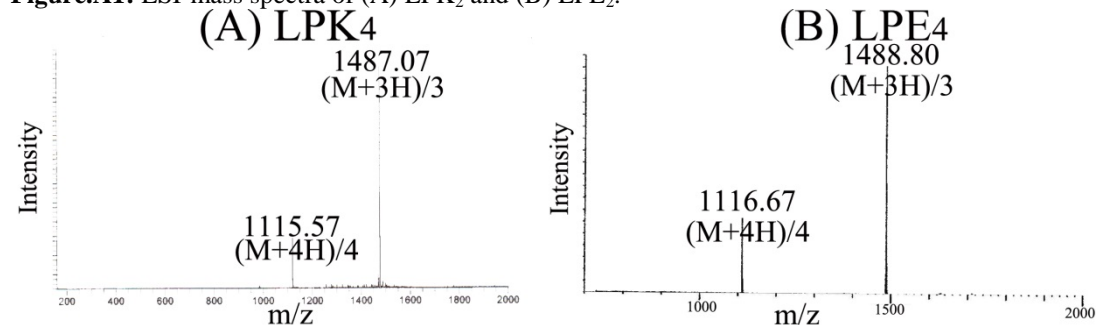


Figure.A2: ESI-mass spectra of (A) LPK₄ and (B) LPE₄

3. Liposomes

3.1 Liposome preparation:

1mM lipid stock solutions were made in chloroform with the composition DOPC/DOPE/CH 50:25:25 mol%. 1mM lipopeptide stock solutions were made in 1:1 (v/v) chloroform: methanol. Unless otherwise stated, liposome solutions are 1 mM in PBS. Three types of liposome solutions were prepared: plain liposomes, liposomes with 1 mol% LPE (99:1 (v/v) lipid stock solution: LPE stock solution), and liposomes with 1 mol% LPK (99:1 (v/v) lipid stock solution: LPK stock solution). To prepare small unilamellar vesicles the solvent was removed from the stock solution (2 mL) using a rotary evaporator to get a lipid film. Following this PBS (2 mL) was added to prepare a 1 mM liposome solution. The sample was vortexed for 1 minute and sonicated at 50 °C to form large unilamellar vesicles (it takes approximately 5 minutes for plain liposomes and 2 minutes for decorated liposomes respectively). The hydrodynamic diameter was approximately 100 nm as determined by DLS.

3.2 Content Mixing

Content mixing experiments were carried out as follows: A dried film containing DOPC/DOPE/CH 50:25:25 mol% and the corresponding E-Peptides (1 % of either LPE₂, LPE₃ or LPE₄) were hydrated and sonicated (5 min at 50°C) with a sulforhodamine B (20 mM) containing HEPES buffer solution (20 mM HEPES, 90 mM NaCl) at pH 7.2. The final lipid concentration was 1 mM. To get rid of non-encapsulated dye the liposomal solution was subjected to Sephadex (G50, Superfine) using HEPES (20 mM Hepes-Na, 90 mM NaCl) buffer as eluent. The fraction containing liposomes was collected and diluted to a final liposome concentration of 0.1 mM. 400 µL of the E-Peptide containing liposomes with encapsulated sulforhodamine B were added to a small volume disposable cuvette. The fluorescence signal of the Sulforhodamine ($\lambda_{em} = 580$ nm) was detected and another 400 µL of the corresponding K-Peptide containing liposomes (0.1 mM) in HEPES-buffer at pH = 7,2 were added and the increase of sulforhodamine B fluorescence, due to a relief of self-quenching, was detected. After a certain time 100 µL of 10% (v/v) solution of Triton X was added to lyse the liposomes and reach the maximum dilution. To calculate the percentage of fusion the following equation was used:

$$F\% = (F_{(t)} - F_{(0)}) / (F_{(max)} - F_{(0)}) \times 100$$

where $F(t)$ is the fluorescence at a certain time, F_{max} is the fluorescence after lyses of the liposomes with Triton X and $F(0)$ is the starting fluorescence after addition of the K-Peptide containing liposomes.

3.3 Lipid Mixing.

All spectra were obtained at room temperature using a quartz cuvette with a 1 cm path length. Liposomes consisting of DOPC/DOPE/CHOL/NBD-DOPE/RHD-DOPE (49.5/24.75/24.75/0.5/0.5 mol %) and 1 % of LPK_x where mixed with liposomes consisting of DOPC/DOPE/CHOL (59/25/25 mol %) and 1% of LPE_x. The NBD fluorescence was used to calculate the lipid mixing percentage with time. Fluorescence time series measurements were started immediately after mixing 750 μ L of the fluorescent-labeled liposome suspension with 750 μ L of unlabeled liposome suspension in the cuvette. The NBD fluorescence intensity at 530 nm was monitored in a continuous fashion for 3000 seconds. After that the liposomes were lysed by the addition of 150 μ L of 10 wt % Triton X-100 in PBS to obtain 100 % increments.

The values measured after lysis were multiplied by 1.82 to take into account the effect of Triton X-100 on the NBD fluorescence and dilution, which was obtained from a separate lysis experiment of a liposome solution that only contained DOPE-NBD. The percentage of fluorescence increase (%) is calculated as:

$$F(\%) = (F(t) - F_0) / (F_{max} \times 1.82 - F_0) \times 100$$

where $F(t)$ is the fluorescence intensity measured at time t , F_0 is the 0% fluorescence and F_{max} is the fluorescence intensity measured after addition of Triton X-100.

3.4 Initial fusion rate

The initial lipid mixing rate as characterization of the initial fusion rate and is calculated as:

$$R = \Delta F / \Delta t$$

ΔF stands for Fluoresce increase, Δt is time increase after 1:1 equimolar mix fluorescent label K liposome with non-fluorescent label E liposome. The increase in lipid mixing during the first minute of fusion is almost linear, therefore the increase in fluorescence in the first minute is used to calculate the rate of fusion.

4. Additional measurements

4.1 Circular Dichroism Spectroscopy

4.1.1 Peptide conformation and binding energy assay:

CD spectra were obtained using a Jasco J-815 spectropolarimeter equipped with a peltier controlled thermostatic cell (Fig. A3,4). The ellipticity is given as mean residue molar ellipticity, $[\theta](10^3 \text{degcm}^2 \text{dmol}^{-1})$, calculated by Eqn. (1),

$$[\theta] = (\theta_{\text{obs}} \times \text{MRW}) / (10 \times l \times c) \quad (1)$$

Where θ_{obs} is the ellipticity in millidegrees, MRW is the mean residue molecular weight, l is the path length of the cuvette in cm and c is the peptide concentration in mg/mL.

A 1.0mm quartz cuvette and 200 μM concentration of peptide in pH=7.4 PBS were used for detection of the peptide secondary structure. Spectra were recorded from 260nm to 200nm at 25°C. Data was collected at 0.5nm intervals with a 1nm bandwidth and 1s readings. Each spectrum was the average of 5 scans. For analysis each spectrum had the appropriate background spectrum subtracted.

Temperature dependent CD spectra (Fig. A3,4) for calculation of the peptide binding energy were obtained using an external temperature sensor immersed in the sample. The temperature was controlled with the internal sensor and measured with the external sensor. A 10 mm quartz cuvette was used, and the solutions were stirred at 900 rpm. Spectra were recorded from 260 nm to 200 nm, with data collected at 0.5 nm intervals with a 1 nm bandwidth and 1 s readings. Each spectrum was one scan. The temperature range was 6 °C to 96 °C with a temperature gradient of 2.0°C/minute and a 60 s delay after reaching the set temperature. The solutions took 5 minutes to return to 6 °C. The spectrum of PBS at 6 °C (average of 5 scans) was subtracted from each spectrum.

The data was analyzed using a two-state unfolding model to determine the fraction folded using Eqn. (2),

$$F_f = ([\theta] - [\theta]_U) / ([\theta]_F - [\theta]_U) \quad (2)$$

Where $[\theta]$ is the observed molar ellipticity, $[\theta]_U$ is the ellipticity of the denatured state, as determined from the plateau of the ellipticity vs. temperature curve, and $[\theta]_F$ is the ellipticity of the folded state at that temperature as determined from a linear fit of the initial stages of the ellipticity vs. temperature curve.

The fraction unfolded, F_U , was calculated by Eqn. (3),

$$F_U = 1 - F_f \quad (3)$$

The dimer dissociation constant in the transition zone was calculated using Eqn. (4),

$$K_U = 2P_t F_U^2 / F_f \quad (4)$$

P_t is the total peptide concentration. By taking the derivative of the $\ln(K_U)$ vs. Temperature and using this in the van't Hoff equation, Eqn. (5), the change in enthalpy associated with unfolding with temperature can be plotted:

$$d\ln(K_U)/dT = \Delta H_U / RT^2 \quad (5)$$

The gradient of this plot ΔC_p , is the difference in heat capacity between the folded and unfolded forms, and can be used in the Gibbs-Helmholtz equation adapted to monomer-dimer equilibrium, Eqn. (6), to obtain the Gibbs free energy of unfolding as a function of temperature

$$\Delta G_U = \Delta H_m(1 - T/T_m) + \Delta C_p[T - T_m - T \ln(T/T_m)] - RT \ln[P] \quad (6)$$

T_m and H_m , the temperature and enthalpy at the midpoint of the transition, is determined by the maximum of derivative of the ellipticity vs. temperature graph.

All binding energy calculations were based on the assumption that the peptide pairs form a 1:1 heterodimer complex (1:1 complex of E_x and K_x).

With the formula above, the binding energy of E/K complex from the graphs below has been calculated (Fig. A3,4):

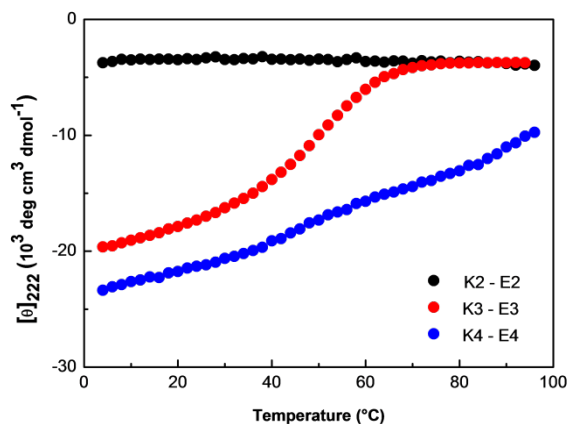


Figure.A3: Temperature dependent CD spectra monitored molar ellipticity changing at 222nm. K_n/E_n pairs in 20mM phosphate, 150mM NaCl, pH 7.4, [Total peptide] = 40 μ M.

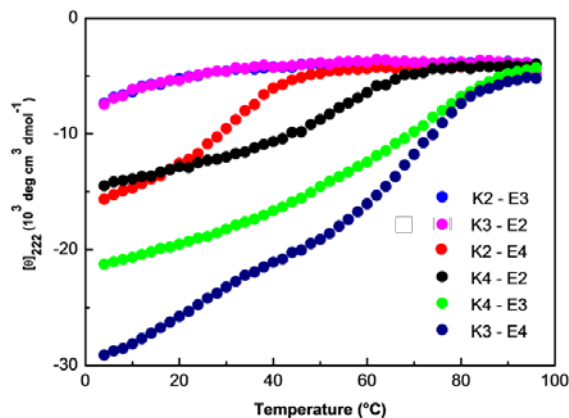


Figure A4: Temperature dependent CD spectra monitored molar ellipticity changing on wavelength 222nm. K_m/E_n pairs in 20mM phosphate, 150mM NaCl, pH 7.4, [Total peptide] = 40 μ M.

Figure A5 and A6 show the temperature dependent CD-spectra for E_3 - K_3 and with E_4 - K_4 . With increasing temperature the E_3 - K_3 coiled coil dissociates, but the E_4 - K_4 coiled coil still exists even when the temperature reaches 96 °C.

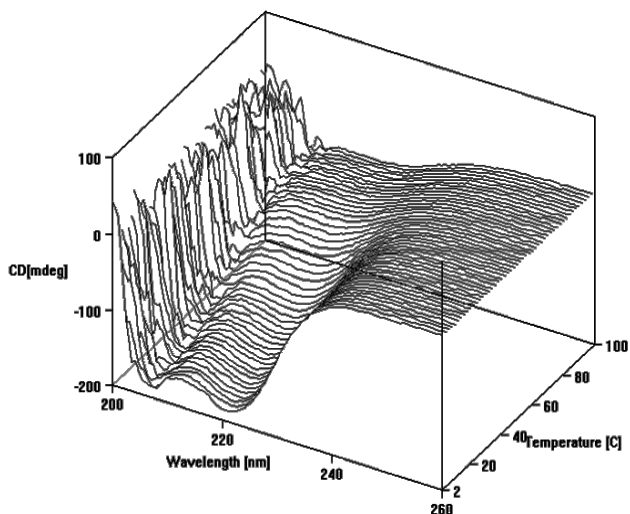


Figure.A5: 3D spectrum of the E_3/K_3 coiled-coil complex ellipticity upon increasing the temperature from 2-96°C.

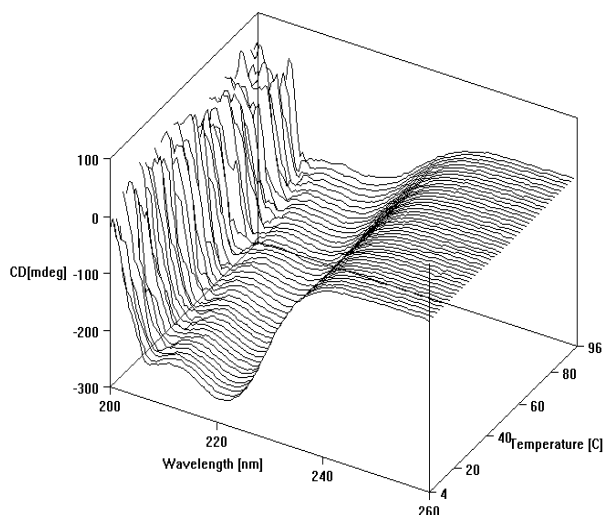


Figure A6: 3D spectrum of E4/K4 coiled coil complex ellipticity following by the temperature increasing from 2-96°C.³⁶

4.1.2 Determination of the percentage α -helix and the confirmation coiled-coils

The percentage α -helicity is the ratio of the observed $[\theta]_{222}$ to the predicted $[\theta]_{222}$ for an α -helical peptide of n residues $\times 100$. The predicted $[\theta]_{222} = -40000 \times (1 - 4.6/n)$.⁴⁰ Peptide interactions were further confirmed by TFE-CD measurements. TFE is known to enhance intramolecular α -helicity but decrease intermolecular interactions.⁴¹ Equimolar E and K mixture has been measured first in PBS, then TFE: PBS 1:1 (v/v). If there is a significant decrease in the in the $[\theta]_{222}/[\theta]_{208}$ ratio from PBS to 50% TFE in PBS, one can assume, that there is a destruction of the coiled-coil binding motif. Here total peptide concentration is 1 mg /mL in 50 mM phosphate, 150 mM NaCl, pH 7.4, 25°C.

Controlling the rate of coiled coil driven membrane fusion

Peptide	θ_{222}		% α -helix		$\theta_{222}/\theta_{208}$		Coiled-coil
	PBS	50%TFE	PBS	50%TF	PBS	50%TFE	
E2	-2490	-17718	9	66	0.50	0.73	-
K2	-1876	-14142	7	53	0.32	0.73	-
E2+K2	-3561	-17786	13	66	0.37	0.73	-
E3	-5819	-22465	19	72	0.59	0.84	-
K3	-6638	-23139	21	74	0.73	0.84	-
E3+K3	-24705	-23277	79	75	1.10	0.90	+
E4	-22173	-23176	66	69	1.43	0.86	+
K4	-24714	-25812	74	77	1.25	0.86	+
E4+K4	-31066	-31341	93	94	1.11	0.90	+

Table A1. Concentrations of the peptides: 1mg/ml, Buffer 50mM phosphate, 150mM NaCl, pH 7.4, 25°C.

4.1.3 Comparison of secondary structure of E₂, K₂ and liposomes modified with LPE₂ and LPK₂.

Peptide	% α -helicity	Peptide	% α -helicity
Ac-E2	9	LPE2	20
Ac-K2	7	LPK2	19
Ac-E2+Ac-K2	13	LPE2+LPK2	40

Table A2. Comparison of acetylated E₂,K₂, E₂+K₂ percentage of alpha-helix changed from uniform disperse in buffer with fixed on surface of liposome. Acetylated peptide were measured in pH=7.4 PBS buffer (PBS buffer as baseline), 25°C. LPE₂, LPK₂ and LPE₂+LPK₂ were decorated on surface of liposome to make them water-soluble (plain liposome in same buffer as baseline). All the acetylated peptide were measured in 1mg/ml concentration, 1 mm cuvette was used, 4 scans for each peptide, while all the lipopeptide were decorated 1% on liposome surface which compose of 0.5mM lipid in pH=7.4 PBS in 5mm cuvette on 25°C, 6 scans for each lipopeptide.

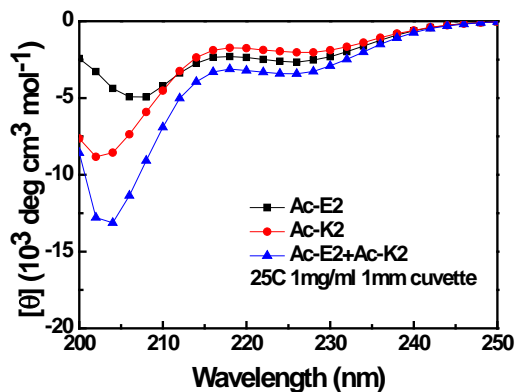


Figure A7: CD spectroscopic data of acetylated E2, K2 and E2-K2 complex. 1mg/ml peptides in pH=7.4 PBS (50mM phosphate, 150mM NaCl) were measured with 1mm cuvette on 25°C.

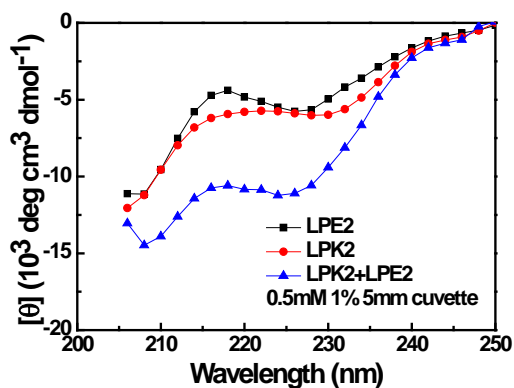


Figure A8: CD spectroscopic data of LPE2, LPK2, LPE2+LPK2 complex. All lipopeptide were decorated on surface of liposome, to make them water soluble, meanwhile use plain liposome as baseline during all the lipopeptide-liposome measurements. All the samples content 0.5mM lipid and 1% lipopeptide, and measured by 5mm cuvette was used on 25°C.

4.2 Lipid Mixing (Cross combinations)

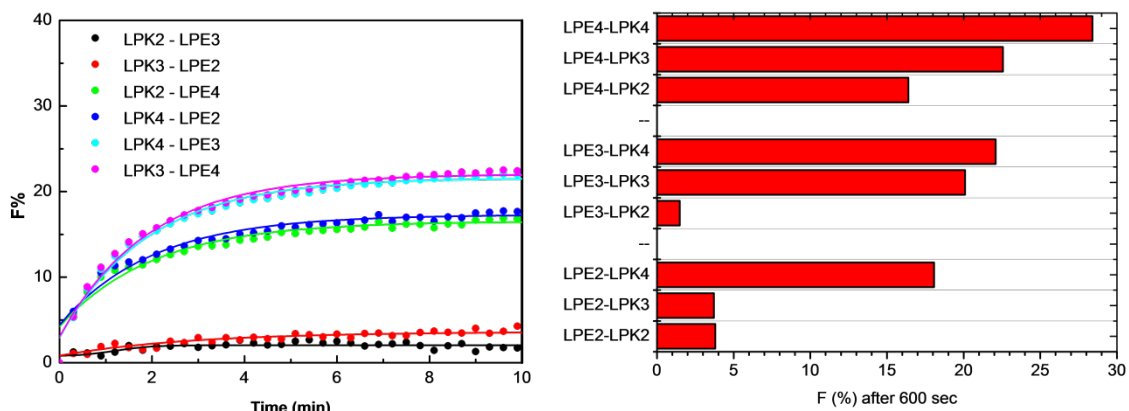


Figure A9: Lipid mixing based on the fluorescence increase upon mixing LPK_x decorated fluorescent liposomes and LPE_x decorated liposomes.

4.3 Content mixing (cross combinations)

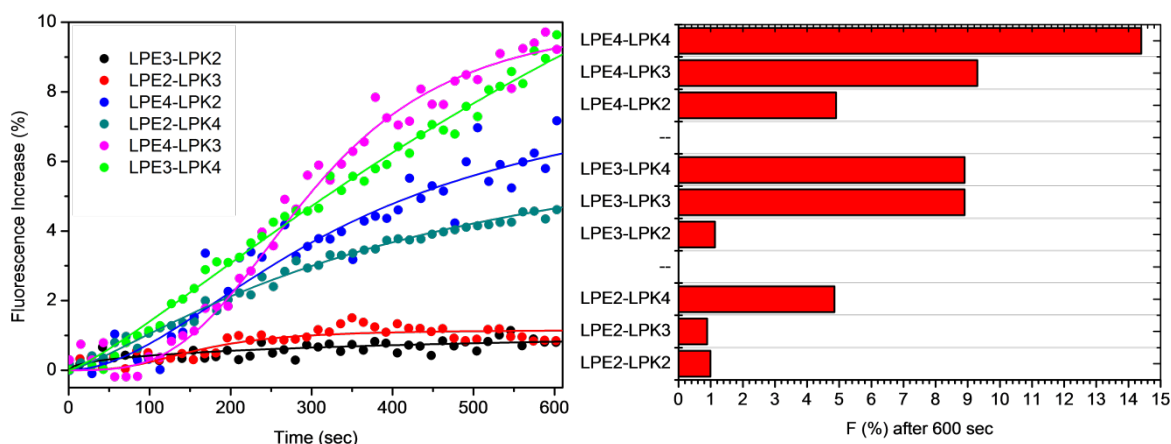


Figure A10: Lipid mixing based on the fluorescence increase upon mixing LPK_x decorated liposomes and LPE_x decorated liposomes with encapsulated sulphorhodamine (20 mM).

4.4 Dynamic light scattering (cross combinations)

Hydrodynamic diameters were estimated at 25 °C by dynamic light scattering using a Malvern Zetasizer Nano ZS ZEN3500 equipped with a peltier-controlled thermostatic cell holder. The laser wavelength was 633 nm and the scattering angle was 173°. For individual liposome batches the samples were allowed to equilibrate for 2 minutes. For DLS time series the solutions were mixed in the cuvette for 30 second. Measurements were started immediately after mixing without 2 minutes of

sample equilibration, and continued for 1h:

$$\text{Size increase \%} = 100 \cdot (S_{1h} - S_0) / S_0$$

(S_{1h} : Zeta average diameter after 1 hour mixing, S_0 : Zeta average diameter immediately after mixing).

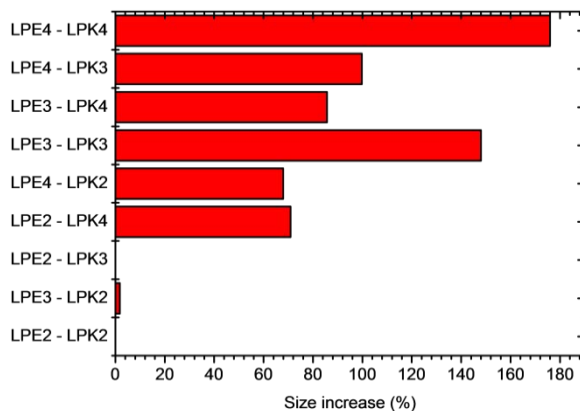


Figure A11: Size increase in percentage of all cross combination.

4.5 Comparison of different conditions

4.5.1 Rate of fusion as a function of temperature:

The same method that mentioned in main text for the lipid mixing has been applied, except, that a controllable water bath was used to determine the lipid mixing at different temperature.

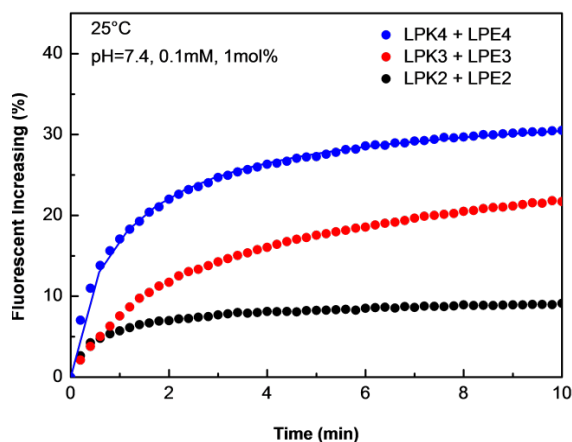


Figure A12 : Lipid mixing at, pH=7.4.

Controlling the rate of coiled coil driven membrane fusion

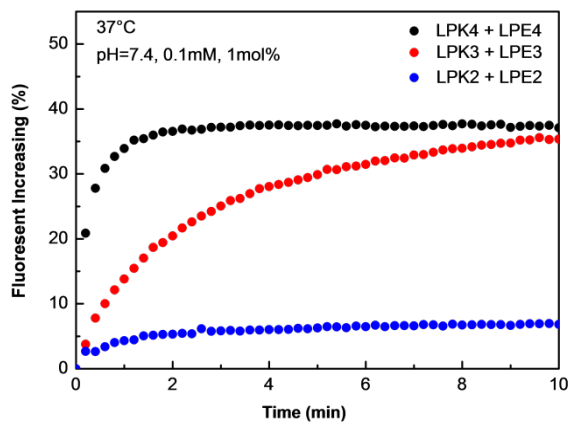


Figure A13 Lipid mixing at 37°C, pH=7.4.

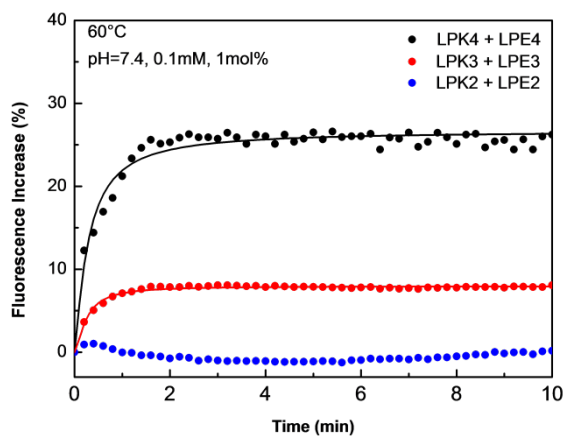


Figure A14: Lipid mixing at 60 °C, pH=7.4.

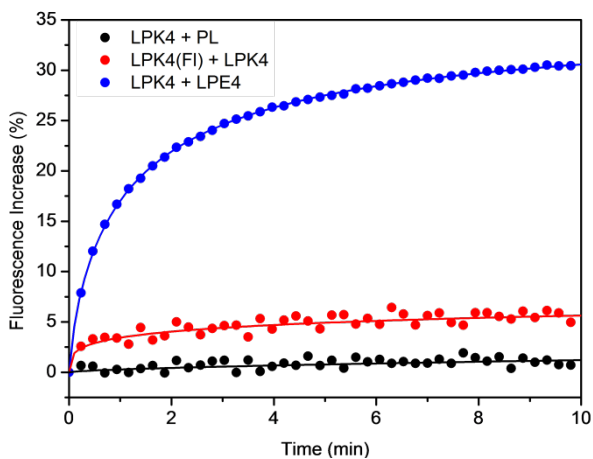


Figure A15: Lipid Mixing at 25°C, Control experiments, pH = 7.4.

4.5.2 Rate of fusion as a function of pH:

The same lipid mixing method as mentioned before has been performed, except, that the pH was varied.

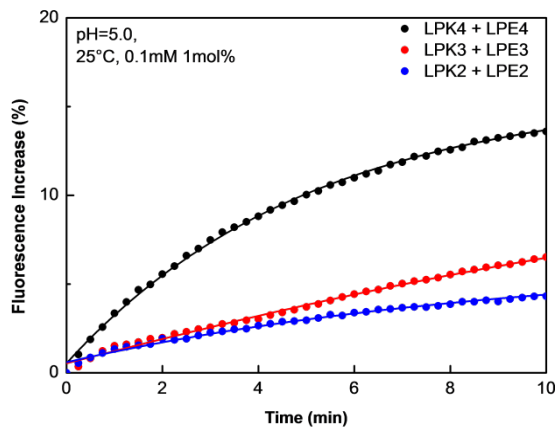


Figure A16: Liposome fusion at 25°C, pH=5.0.

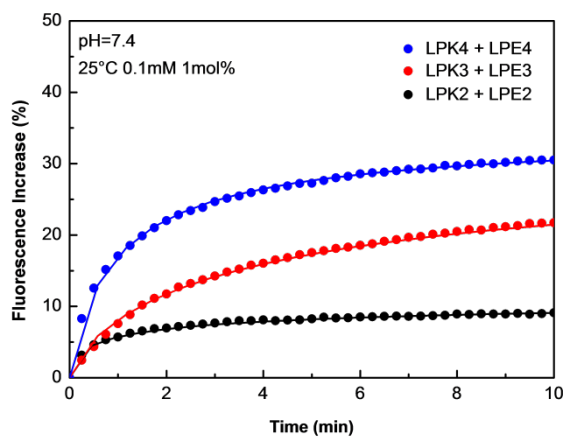


Figure A17: Liposome fusion at 25 °C pH=7.4.

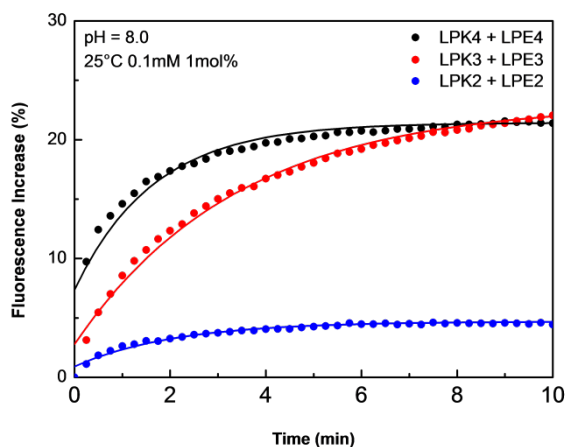


Figure A18: Liposome fusion at 25°C, pH=8.0.

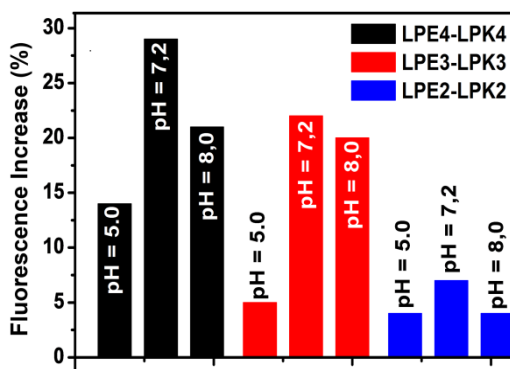


Figure A19: Comparison of lipid mixing of LPE_x-LPK_x modified liposomes as a function of pH.

Reference

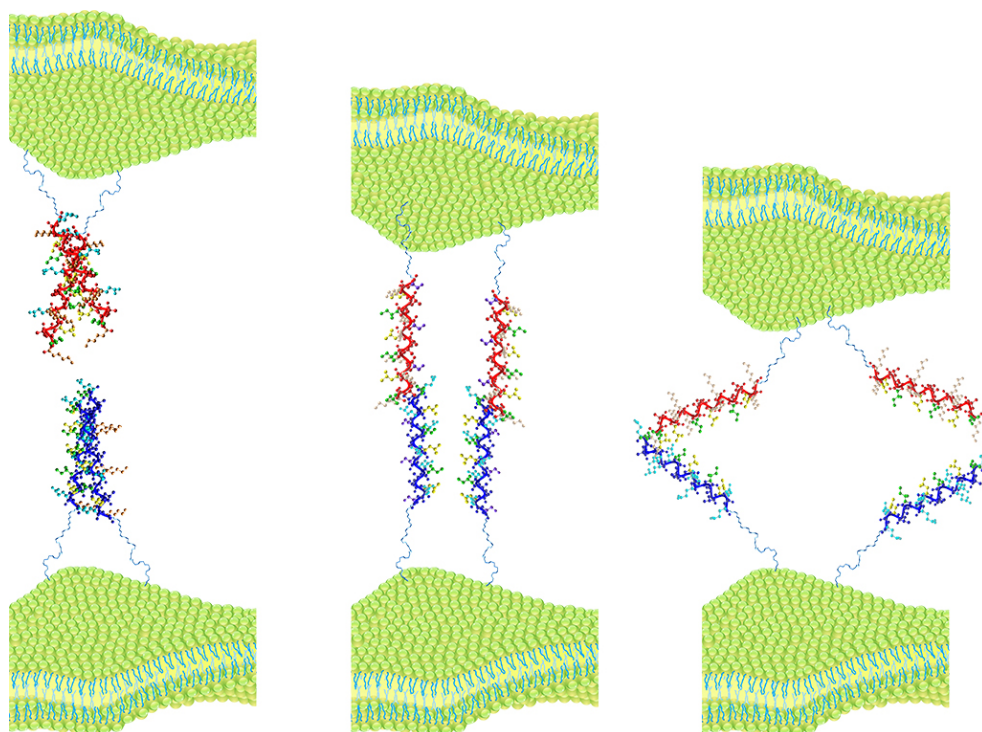
1. J. M. Lehn, *Angewandte Chemie-International Edition in English*, 1990, **29**, 1304-1319.
2. J. H. van Esch and B. L. Feringa, *Angewandte Chemie-International Edition*, 2000, **39**, 2263-2266.
3. Z. Liu, X. Sun, N. Nakayama-Ratchford and H. Dai, *Acs Nano*, 2007, **1**, 50-56.
4. T. Kato, N. Mizoshita and K. Kishimoto, *Angewandte Chemie-International Edition*, 2006, **45**, 38-68.
5. J. Elemans, A. E. Rowan and R. J. M. Nolte, *Journal of Materials Chemistry*, 2003, **13**, 2661-2670.
6. A. R. Hirst, B. Escuder, J. F. Miravet and D. K. Smith, *Angewandte Chemie-International Edition*, 2008, **47**, 8002-8018.
7. L. He, Y. Jiang, C. Tu, G. Li, B. Zhu, C. Jin, Q. Zhu, D. Yan and X. Zhu, *Chemical Communications*, 2010, **46**, 7569-7571.
8. A. R. Hirst and D. K. Smith, *Chemistry-a European Journal*, 2005, **11**, 5496-5508.
9. J. Voskuhl and B. J. Ravoo, *Chemical Society Reviews*, 2009, **38**, 495-505.
10. J. W. Steed, *Chemical Society Reviews*, 2010, **39**, 3686-3699.
11. S. Chiruvolu, S. Walker, J. Israelachvili, F. J. Schmitt, D. Leckband and J. A. Zasadzinski, *Science*, 1994, **264**, 1753-1756.
12. C. Schmuck and W. Wienand, *Angewandte Chemie-International Edition*, 2001, **40**, 4363-+.
13. F. Versluis, J. Voskuhl, M. C. A. Stuart, J. B. Bultema, S. Kehr, B. J. Ravoo and A. Kros, *Soft Matter*, 2012, **8**, 8770-8777.
14. S. Trier, J. R. Henriksen and T. L. Andresen, *Soft Matter*, 2011, **7**, 9027-9034.
15. R. V. Ulijn and A. M. Smith, *Chemical Society Reviews*, 2008, **37**, 664-675.
16. C. Tomasini and N. Castellucci, *Chemical Society Reviews*, 2013, **42**, 156-172.
17. Y. C. Yu, P. Berndt, M. Tirrell and G. B. Fields, *Journal of the American Chemical Society*, 1996, **118**, 12515-12520.
18. F. Versluis, H. R. Marsden and A. Kros, *Chemical Society Reviews*, 2010, **39**, 3434-3444.
19. D. N. Woolfson and Z. N. Mahmoud, *Chemical Society Reviews*, 2010, **39**, 3464-3479.
20. R. Jahn, T. Lang and T. C. Sudhof, *Cell*, 2003, **112**, 519-533.
21. H. R. Marsden, I. Tomatsu and A. Kros, *Chemical Society Reviews*, 2011, **40**, 1572-1585.
22. J. M. White, *Science*, 1992, **258**, 917-924.
23. B. R. Lentz, *European Biophysics Journal with Biophysics Letters*, 2007, **36**, 315-326.
24. T. Weber, B. V. Zelman, J. A. McNew, B. Westermann, M. Gmachl, F. Parlati, T. H. Sollner and J. E. Rothman, *Cell*, 1998, **92**, 759-772.
25. R. B. Sutton, D. Fasshauer, R. Jahn and A. T. Brunger, *Nature*, 1998, **395**, 347-353.

Controlling the rate of coiled coil driven membrane fusion

26. H. R. Marsden, N. A. Elbers, P. H. H. Bomans, N. A. J. M. Sommerdijk and A. Kros, *Angewandte Chemie-International Edition*, 2009, **48**, 2330-2333.
27. H. R. Marsden and A. Kros, *Angewandte Chemie-International Edition*, 2010, **49**, 2988-3005.
28. A. Kashiwada, M. Tsuboi and K. Matsuda, *Chemical Communications*, 2009, 695-697.
29. A. Kashiwada, M. Tsuboi and K. Matsuda, *Langmuir*, 2011, **27**, 1403-1408.
30. A. Kashiwada, M. Tsuboi, N. Takamura, E. Brandenburg, K. Matsuda and B. Kocsch, *Chemistry-a European Journal*, 2011, **17**, 6179-6186.
31. Y.-H. M. Chan, B. van Lengerich and S. G. Boxer, *Proceedings of the National Academy of Sciences of the United States of America*, 2009, **106**, 979-984.
32. G. Stengel, R. Zahn and F. Hook, *Journal of the American Chemical Society*, 2007, **129**, 9584-+.
33. G. Stengel, L. Simonsson, R. A. Campbell and F. Hook, *Journal of Physical Chemistry B*, 2008, **112**, 8264-8274.
34. Y. Gong, M. Ma, Y. Luo and D. Bong, *Journal of the American Chemical Society*, 2008, **130**, 6196-6205.
35. I. Tomatsu, H. R. Marsden, M. Rabe, F. Versluis, T. Zheng, H. Zope and A. Kros, *Journal of Materials Chemistry*, 2011, **21**, 18927-18933.
36. J. R. Litowski and R. S. Hodges, *Journal of Biological Chemistry*, 2002, **277**, 37272-37279.
37. N. Duzgunes, T. M. Allen, J. Fedor and D. Papahadjopoulos, *Biochemistry*, 1987, **26**, 8435-8442.
38. D. Hoekstra and N. Duzgunes, *Methods in Enzymology*, 1993, **220**, 15-32.
39. D. K. Struck, D. Hoekstra and R. E. Pagano, *Biochemistry*, 1981, **20**, 4093-4099.
40. Y. H. Chen, J. T. Yang and K. H. Chau, *Biochemistry*, 1974, **13**, 3350-3359.
41. S. Y. M. Lau, A. K. Taneja and R. S. Hodges, *Journal of Biological Chemistry*, 1984, **259**, 3253-3261.

Chapter 6

Increasing the membrane fusion efficiency by reducing undesired peptide-peptide interactions



Zheng, T. T.; Boyle, A.; Marsden, H. R.; Kros, A., Raising membrane fusion efficiency by reducing fusogen homo interaction. Manuscript in preparation.

Increasing the membrane fusion efficiency by reducing undesired peptide-peptide interactions

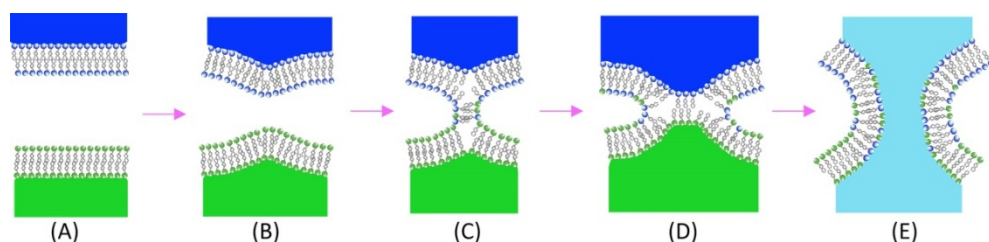
Abstract

The effect of Coil-K peptide homo interaction on coiled coil CC-K/E mediated liposome fusion efficiency was investigated. Coil-K clustering on liposome membranes was tuned by changing the electrostatic interaction between peptides. For this, the original amino acid sequence of Coil-K was varied at the f-position. The glutamate residue ('E') was replaced with either a serine ('S', no charge) or a lysine ('K', positive charge) residue, yielding Coil-K_S and Coil-K_K. Circular dichroism (CD) and fluorescence spectroscopy confirmed that the peptide modifications did not influence the coiled coil formation with the complementary peptide Coil-E. CD studies of lipidated Coil-K_S and Coil-K_K incorporated in liposomal membranes revealed that more electrostatic repulsion between the peptides increased the fusogenicity. Lipid and content mixing assays showed more efficient liposome-liposome fusion using Coil-K_K and Coil-K_S in conjunction with coil-E. A probable cause for this effect might be that repulsion between the peptides in the pre-fusion state results in a more homogeneous peptide distribution on the liposomal membrane.

Introduction

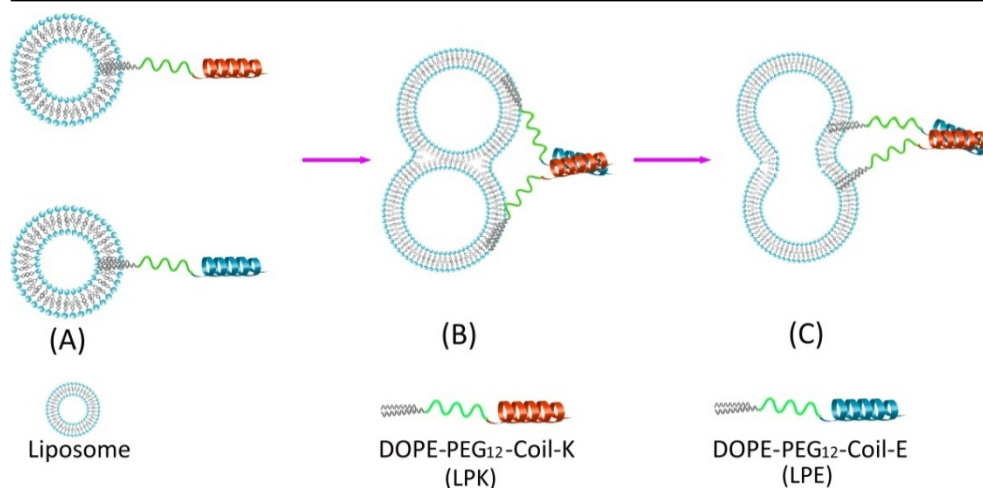
The 2013 Nobel Prize in Physiology or Medicine was awarded to James Rothman, Randy Schekman and Thomas Südhof for their seminal contributions in understanding vesicular transport mechanisms in cells.¹ One of the important actors in membrane trafficking, so called SNARE proteins (soluble N-ethyl maleimide sensitive factor attachment protein receptors), mediate membrane fusion and are widely studied.²⁻⁴ In nature, the distance between biological membranes is typically around 10- 20 nm, due to the electrostatic repulsion between the charged bilayers and the steric interaction of membrane bound proteins and other biomolecules.⁵ Thus the first step of a fusion event is to bring the opposing membrane lipid bilayers into close proximity. Next, local disruption of the bilayer structure results in the formation of a stalk-like structure (Scheme 1). In the stalk intermediate the outer membranes of the approaching lipid bilayers have merged, but not the inner leaflets. It is believed that the stalk which expands into a hemifusion stalk or diaphragm, subsequently enlarges such a pore is being formed. As a result, the contents of the compartments mix, and the fusion process is completed.^{6, 7}

Increasing the membrane fusion efficiency by reducing undesired peptide-peptide interactions



Scheme 1. (A) Two opposing membranes in the pre-fusion state. (B) A point-like membrane protrusion minimizes the energy of the hydration repulsion between the proximal leaflets of the membranes coming into immediate contact. (C) A hemifusion stalk with proximal leaflets fused and distal leaflets unfused. (D) Stalk expansion yields the hemifusion diaphragm. (E) A fusion pore forms either in the hemifusion diaphragm bilayer or directly from the stalk (take from reference 5).⁸

The lipid rearrangements of membrane fusion during intracellular transport are mediated by SNARE proteins.⁴ However, the molecular mechanism is still debated. To induce membrane fusion, a four-helix coiled-coil bundle forms between two membrane-bound SNARE protein subunits and a cytoplasmic SNARE protein subunits forcing the two membranes within a distance of 2-3 nm from one another, resulting in docking of the two opposing membranes followed by lipid and content mixing.^{5,9} Inspired by this natural and highly controlled transport mechanism, supramolecular and biomaterials chemists designed synthetic targeted membrane fusion systems to study the mechanism of membrane fusion at a fundamental level, or to explore future applications in drug delivery or in the design of nanoreactors. Our previously published synthetic membrane fusion system has shown to be very effective in inducing liposome-liposome fusion (Scheme 2).¹⁰⁻¹² There are three key components in the design of our fusion model. First there is the molecular recognition part, which drives the membrane of two liposomes into close proximity. For this we use the complementary peptides Coil-K and Coil-E, which were designed to form a heterodimeric coiled coil complex.^{10, 13} Flexibility and rotational freedom of the peptides is ensured by conjugation of a poly(ethylene glycol) spacer (PEG₁₂) at the N-terminus of the peptides. The third component in our design is the lipid anchor 1,2-dioleoyl-*sn*-glycero-3-phosphoethanolamine (DOPE), which is conjugated to the PEG spacer. This guarantees that the peptides will anchor into a lipid bilayer (Scheme 2).



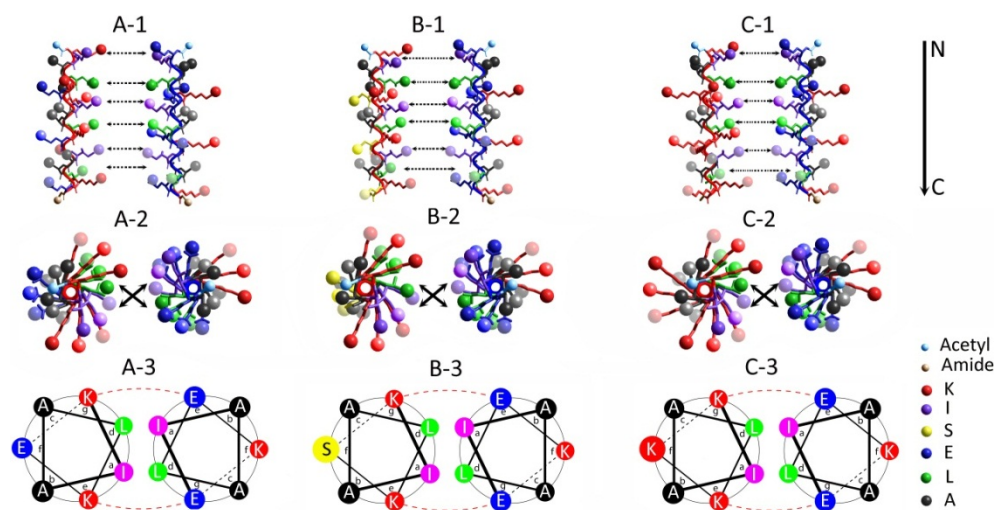
Scheme 2. Illustration of liposome fusion mediated by lipopeptides, as well as an overview of the lipopeptides used in this study. Liposomes are decorated with LPK (red) or LPE (blue) and upon mixing coiled-coil formation brings the opposite liposomes in close proximity, and ultimately leads to fusion.

From previous experiments, we realized that peptide homo-aggregation on the liposomal membrane before fusion reduces its fusion efficiency with the complementary fusion partner.¹¹ It seems that there is an optimal peptide to lipid ratio of ~ 0.75 mol%. Higher ratios did not result in faster fusion. Circular dichroism (CD) spectroscopy showed that at high fusogen concentrations on the membrane, self-aggregation due to homocoiling and increased peptide-membrane interactions seem to occur resulting in a heterogeneous distribution of the peptides on the liposome surface.

A driving force for the observed peptide aggregation might be electrostatic interactions. In the original coiled coil (CC) K/E design, position ‘a’ and ‘d’ in the helical wheel diagram are taken by the amino acid residues isoleucine (I) and leucine (L) respectively, forming the hydrophobic core (Scheme 3). Position ‘b’ and ‘c’ are occupied by alanine (A), which increases the propensity of the peptide to adopt an α -helical configuration.¹⁴ Heterodimerization was programmed by incorporating charged residues at position ‘e’ and ‘g’, adjacent to the hydrophobic core, being lysine (K) residues in peptide Coil-K and glutamate residues (E) in the Coil-E peptide. This coiled coil was designed to function at neutral pH, where the side chains of all lysine residues are protonated, and hence positive charged, while the side chains of all glutamate residue residues are deprotonated and hence negatively charged. The final position in the heptad repeat, position ‘f’, was occupied by an

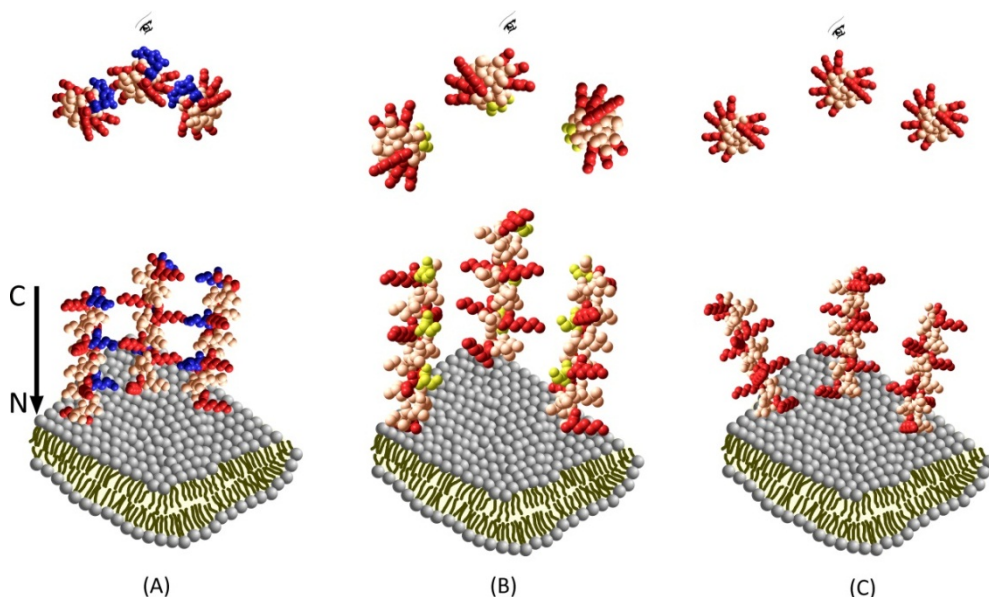
Increasing the membrane fusion efficiency by reducing undesired peptide-peptide interactions

opposite charge relative to positions 'e' and 'g', in order to decrease the overall net charge of the single peptide. Due to the existence of opposite charges residues within one single peptide, electrostatic attraction could cause undesired peptide-peptide interactions at the membrane of the liposomes. This in turn lowers the effective monomeric peptide concentration at the membrane, resulting in the observed lower fusogenicity at higher peptide concentrations. Circular dichroism and dynamic light scattering data shows that the acetylated peptides (i.e. no lipid anchor) uniformly disperse in PBS buffer (pH=7.4), with no noticeable homo-interaction being observed. However, the situation changes when the peptides are confined on a liposome surface. When the peptides are fixed to a liposomal surface through the phospholipid anchor, Coil-K peptide shows significantly homo-interaction and peptide-membrane interactions, as observed in CD measurements.¹¹ However, it is important to note that this does not result in fusion. By decreasing the Coil-K density on liposome surface to 0.75 mol%, the peptide self-interaction significantly decreased and coincidentally, the liposome fusion lipid mixing rate increased.



Scheme 3. Parallel heterodimeric peptide used in this study. (A) column shows Coil-K (left) with Coil-E (right), (B) column shows Coil-K_S (left) with Coil-E (right), and (C) column shows Coil-K_K (left) with Coil-E (right). (A-1) presents lateral view of CC-K/E, (A-2) presents top view of CC-K/E (from N to C-terminus), (A-3) presents simplified top view (from N to C-terminus), so-called helical wheel of CC-K/E (same with column (B) and (C)). Amino acid were expressed by signal letter (K= lysine, I= isoleucine, S= serine, E =glutamate, L= leucine, A= alanine). Black arrows indicate hydrogen bonding, while red imaginary lines indicate helical interface electrostatic attraction.

To investigate whether electrostatic interactions have an effect on Coil-K homo-interaction, the influence of a charge at position 'f' in peptide coil-K on the rate of membrane fusion was studied. Thus, the liposome fusion efficiency was investigated as a function of peptide aggregation by tuning the electrostatic interaction between the peptides on the liposomal surface (Scheme 4). Besides the original Coil-K with a glutamate residue at position 'f', two new sequences were synthesized with either the noncharged serine (S) or the positive charged lysine on position 'f', denoted Coil-K_S and Coil-K_K respectively. The aim here is to increase the electrostatic repulsion between the peptides, and thereby increasing the effective peptide concentration able to form a coiled coil motif with peptide Coil-E yielding a higher fusion efficiency.



Scheme 4. Proposed peptide electrostatic interactions on liposome membrane surfaces (lower) and vertical view of peptides from C to N terminus (upper). (A) indicates interactions among Coil-K peptides when they are anchored on the membrane with crowded surface density. Identically, (B) indicates Coil-K_S interactions, while (C) indicates Coil-K_K interactions. Peptides were modeled by Hyperchem release 8.0 as classical L-alpha helix, with three dihedral angles: $\phi = -58^\circ$, $\psi = -47^\circ$, $\omega = 180^\circ$. Amino acid residues were illustrated by using balls atom rendering. Positive charged lysine residues are in red, negative charged glutamate in blue and '0' net charged serine in yellow, meanwhile other zero net charged residues are in orange. Uniformly, gray bilayers indicates liposome membrane surfaces, PEG₁₂ linker and DOPE anchor are omitted for clarity.

Increasing the membrane fusion efficiency by reducing undesired peptide-peptide interactions

Circular Dichroism (CD) spectroscopy showed that replacing the glutamate residues at position 'f' with serine or lysine reduces their tendency to aggregate. Fluorescence resonance energy transfer (FRET) measurements revealed that less peptide aggregation on liposomal membranes resulted in an increased lipid mixing rate in membrane fusion studies. More importantly, content mixing assays based on fluorescence dequenching of rhodamine B showed a significant increase in fusion efficiency for the least aggregated peptide Coil-K_K. These findings indicate that an increase in electrostatic repulsion yields less interacting Coil-K_K in the pre-fusion state. Upon the addition of liposomes bearing the complementary peptide Coil-E, efficient fusion was observed for the least aggregated peptides. Thus, we successfully optimized our fusion model system resulting in a more efficient rate of content mixing.

Results and discussion

Peptide interaction study

Peptide design

In this study, the charged amino acid residue at 'f' position has been varied, yielding new coil-K peptide mutants, as shown in Table 1.^{11, 15}

Table 1. peptide primary structure

Name	Sequence and residue charge	Molecular Weight (theoretical) (g·mol ⁻¹)	Molecular Weight (experimental) (g·mol ⁻¹)
Coil-K	Ac-(KIAALKE) ₃ -CONH ₂ + + -	2320.89	2320.40
Coil-K _S	Ac-(KIAALKS) ₃ -CONH ₂ + +	2194.78	2194.41
Coil-K _K	Ac-(KIAALKK) ₃ -CONH ₂ + + +	2318.07	2317.59
Coil-E	Ac-(EIAALEK) ₃ -CONH ₂ - - +	2323.71	2323.34

'+' stands for positive charge, '-' stands for negative charge. Yellow column indicates the 'f' position. Sequence presents from N terminus to C terminus. All peptides were acetylated.

Instead of the negatively charged glutamate residue, we introduced either the non-charged serine (S) or the positively charged lysine (K), yielding two new peptides Coil-K_S and Coil-K_K respectively (Scheme 3). Furthermore, Coil-K (and its derivatives) and Coil-E were conjugated to DOPE via the flexible spacer PEG₁₂ at the N-terminus for the fusion studies. This design ensures the binding of these lipidated peptides in the membranes of liposomes (*vide infra*).

Circular Dichroism Spectroscopy.

CD measurements showed that all the peptides adopt to some degree an α -helical structure in PBS buffer with the molar ellipticity ratio $[\theta]_{222}/[\theta]_{208} < 1$. However Coil-K_S revealed a relatively low α -helicity (24 %) compared to coil-K and coil-K_K due to serine's poor propensity to adopt an α -helical conformation (Figure 1A and Table 2).¹⁶ Next, the molar ellipticity of acetylated peptides was measured in a 1:1 (v/v%) mixture of trifluoroethanol (TFE) and PBS. TFE is known to enhance intramolecular α -helicity while disrupting intermolecular interactions.¹⁷ The molar ellipticity, as measured at 222 nm, revealed an increase for all acetylated peptides in the presence of 50 % TFE, verifying their propensity to adopt an α -helical secondary structure and that no peptide aggregation was present in PBS.

When mixing equimolar amounts of Coil-K (or its derivatives: Coil-K_S, Coil-K_K) with Coil-E, the molar ellipticity intensity at 222 nm increased significantly (Figure 1C).¹⁴ For all the peptide pairs, the ellipticity ratio $[\theta]_{222}/[\theta]_{208}$, increased to > 1 (Table 2), which indicated the formation of coiled coils.¹⁸ The peptide interactions were further studied by recording CD spectra in a 1:1 (v/v%) mixture of trifluoroethanol (TFE) and PBS. In this solvent mixture, the observed decrease in molar ellipticity and $[\theta]_{222}/[\theta]_{208}$ ratios strongly suggest the presence of coiled coils, which are destabilized in the presence of TFE (Figure 1D). These initial results confirm that individual Coil-K (and its derivatives) and Coil-E peptides adopt a random coil to α -helical structure in PBS buffer. However, when Coil-K (Coil-K_S or Coil-K_K) are mixed with equimolar amounts of Coil-E, coiled coils are formed immediately. More importantly, this study showed that the charge at the 'f' position of coil-K peptides can be varied without compromising their ability to form coiled coils with coil-E.

Increasing the membrane fusion efficiency by reducing undesired peptide-peptide interactions

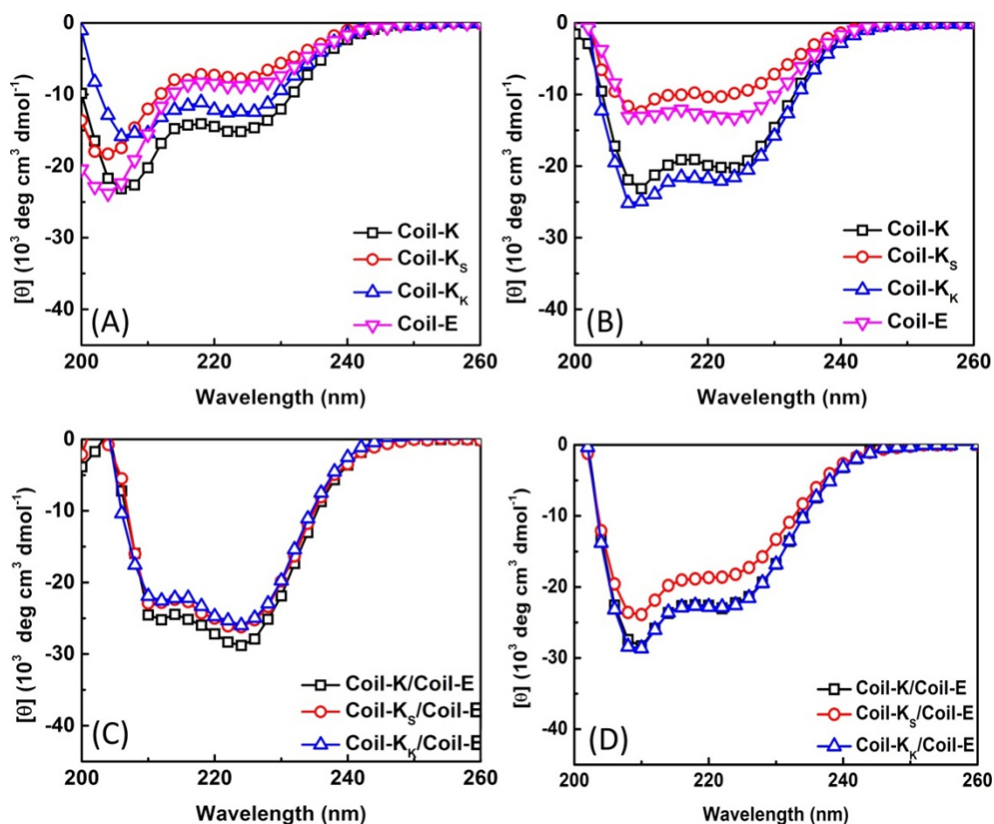


Figure 1. (A) CD spectra of the peptides in PBS buffer and (B) in 1:1 (v/v) PBS: TFE. (C) CD spectra of an equimolar mixture of the Coil-K variants and Coil-E in PBS buffer and (D) in 1:1 (v/v) PBS: TFE. [Total peptide]= 100 μ M, pH 7.4, 25 $^{\circ}$ C.

Table 2. CD spectroscopic data of the acetylated peptides.

Name	$[\theta]_{222}$		$[\theta]_{208}$		$[\theta]_{222}/[\theta]_{208}$		% α -helix ^a	
	PBS	50%-TFE	PBS	50%-TFE	PBS	50%-TFE	PBS	50%-TFE
Coil-K	-15172	-20201	-22647	-21909	0.67	0.92	49	65
Coil-K _S	-7583	-10286	-14656	-11640	0.52	0.88	24	33
Coil-K _K	-12526	-22070	-15375	-25174	0.81	0.88	40	70
Coil-E	-8824	-13147	-19146	-13090	0.46	1.00	28	42

^a The percentage α -helicity is the ratio of the observed $[\theta]_{222}$ to the predicted $[\theta]_{222}$ for an α -helical peptide of n residues times 100. The predicted α -helicity is calculated from $[\theta]_{222} = -40000 * (1 - 4.6/n)$.¹⁸ (PBS buffer pH=7.4)

Table 3. CD spectroscopic data of the peptide complexes.

Complex ^a	[θ] ₂₂₂ ^c		[θ] ₂₀₈ ^c		[θ] ₂₂₂ /[θ] ₂₀₈ ^c		% α -helix ^c		Coiled-coil ^b
	PBS	50% TFE	PBS	50% TFE	PBS	50% TFE	PBS	50% TFE	
CC-K/E	-28323	-23016	-15946	-27449	1.14	0.84	91	74	+
CC-K _S /E	-26106	-18619	-16001	-23583	1.14	0.79	84	60	+
CC-K _K /E	-25314	-22833	-17551	-28388	1.15	0.84	81	73	+

^a A/B refers to mixtures of the stated compounds with equimolar concentrations. ^b The + sign signifies a significant decrease in the [θ]₂₂₂/[θ]₂₀₈ ratio from benign to 50% TFE in PBS, indicative of the folded coiled-coil structure in PBS.

Next, the binding properties were determined of the coiled coil complexes (CC-K/E, CC-K_S/E, CC-K_K/E) by CD spectroscopy. A job-plot showing the [θ]₂₂₂ as a function of the mol fraction of Coil-E peptide yields information on the binding stoichiometry of the coiled coils.^{19, 20} The job-plot of Coil-K (and its derivatives) and Coil-E mixtures were measured with a total peptide concentration of 200 μ M and with variable mol fractions of the two peptides. For all CC-K/E (including derivatives) coiled coil complexes studied, a minimum of [θ]₂₂₂ was always observed at an equimolar ratio of peptide Coil-K (and derivatives) and Coil-E, revealing the formation of a coiled coil complex with a 1:1 stoichiometry (Figure 2A).

As the molar ellipticity at 222 nm is directly proportional to the amount of helical structure and therefore thermal denaturation curves provide information of their folding stabilities.^{18, 21} Thus the thermodynamic stability of the CC-K/E pairs was determined by measuring the molar ellipticity at 222 nm wavelength as a function of temperature.^{13, 22} All coiled coil pairs showed a smooth cooperative transition from a α -helical coiled coil structure to a random coil conformation (Figure 2B). All transitions showed to be fully reversible by lowering the temperature (See Appendix Figure A4). Temperature-dependent CD measurements showed that all the peptide complexes used in this study have an identical two-state transition denaturation process, dissociating from a coiled coil to random coils.

Increasing the membrane fusion efficiency by reducing undesired peptide-peptide interactions

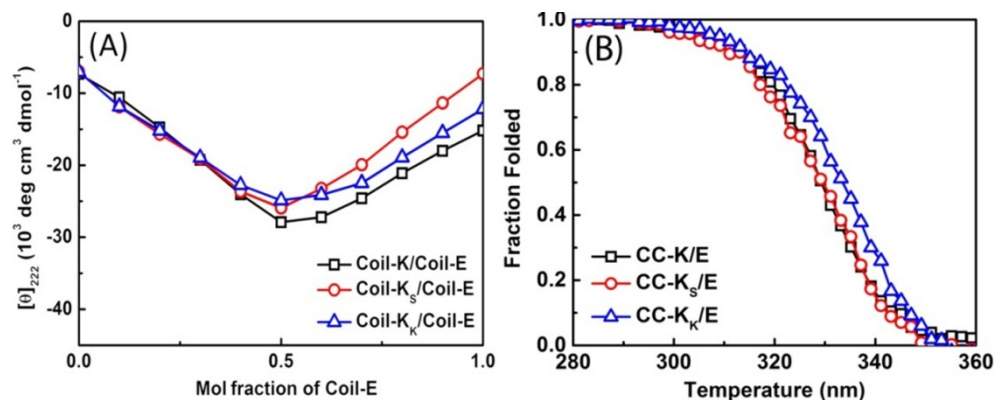


Figure 2. (A) Mean residue molar ellipticities at 222nm wavelength for mixtures of the Coil-K (or its derivants) and Coil-E peptides as a function of the mol fraction of the Coil-E peptide. [Total peptide]=100 μM , 25 $^\circ\text{C}$, 2 mm quartz cuvette. (B) Thermal unfolding curves of coiled coils in PBS buffer (pH=7.4) with increasing temperature. A 1cm quartz cuvette with stirring bar at 900 rpm was used. [Total peptide]=40 μM , PBS, pH=7.4.

The binding parameters of the studied coiled coil heterodimers are summarized in Table 4. Either the similarity in binding stoichiometry or the resemblance in dissociation constant of all coiled coils show that replacing a glutamate (charge ‘-’) with a serine (charge ‘0’) or a lysine (charge ‘+’) residue on the ‘f’ position in peptide Coil-K did not influence the ability to form coiled coils, while the changes in ΔG were minor.

Table 4. Binding constants of coiled coils from CD spectroscopy.

Peptide pair ^a	T_m ($^\circ\text{C}$) ^b	Stoichiometry	ΔG_u ($\text{kcal} \cdot \text{mol}^{-1}$) ^c	K_d ($\cdot 10^{-8} \text{ M}$) ^d
CC-K/E ^a	56 _o	1:1 _o	10 _o	6.7 _o
CC-K _S /E _o	56 _o	1:1 _o	9.5 _o	7.4 _o
CC-K _K /E _o	60 _o	1:1 _o	9.9 _o	5.4 _o

^a CC indicates coiled coil. ^b T_m =melting temperature, at which half of the peptide is in the unfolded form. ^c ΔG_u = Gibbs free energy of unfolding at 25 $^\circ\text{C}$. ^d K_d =dissociation constant at 25 $^\circ\text{C}$.

Fluorescence spectroscopy

The relative peptide orientation within a coiled coil motif (i.e. parallel vs antiparallel) was investigated by fluorescence spectroscopy. For this, Coil-K (Coil-K_S and Coil-K_K) were labeled with a tryptophan (W) at the C-terminus, yielding Coil-K’ (Coil-K_S’ or Coil-K_K’),

see Table 5). In addition, Tyrosine (Y) was added to the C-terminus of Coil-E, giving Coil-E'. As mentioned in Chapter 3 and Chapter 4, glycine (G) was added in between aromatic amino acid (W and Y) and original peptide sequence to avoid significant structure alteration. The relative orientation of the two peptides within a coiled coil complex was confirmed by a fluorescence resonance energy transfer (FRET) between the donor Y on Coil-E', and the acceptor W on Coil-K' (including its derivatives). Both fluorophores are at the C-termini of the peptides, and the Förster distance ($R_0 \approx 1$ nm) is shorter than the length of the peptides in a α -helical fashion (~ 3 -4 nm) (see Appendix, Figure A4), which stringently ensures that FRET can only occur when the peptides are assembled with a parallel orientation, not when an antiparallel orientation is adopted.²³

Table 5. Fluorescent labeled peptide primary structure

Name ^c	Sequence and residue charge ^a	Mw (g mol ⁻¹) ^b (theoretical)	Mw (g mol ⁻¹) (experimental)
Coil-K'	Ac-(KIAALKE) ₃ -GW-CONH ₂	2563.6	2564.15
Coil-K _S '	Ac-(KIAALKS) ₃ -GW-CONH ₂	2437.59	2438.04
Coil-K _K '	Ac-(KIAALKK) ₃ -GW-CONH ₂	2560.59	2561.33
Coil-E'	Ac-(EIAALEK) ₃ -GY-CONH ₂	2543.61	2543.94

^a All the peptides primary structures present from N to C terminus. ^b Mw= molecular weight.

Figure 3 shows the emission spectra (excitation at 275 nm) of peptides Coil-K' (and its derivatives) and Coil-E', CC-K'/E' (including its derivatives) in PBS and in 1:1 PBS: TFE solution. An equimolar mixture of Coil-K' and Coil-E' results in an increased fluorescence signal of acceptor W and a decreased fluorescence signal of donor Y due to fluorescence resonance energy transfer (FRET), thus indicating a parallel coiled coil orientation for CC-K'/E' (Figure 3A). In the presence of 50% TFE, the energy transfer is lost due to the dissociation of coiled coil complex. Consistently, CC-K_S'/E and CC-K_K'/E also showed a parallel coiled coil orientation (Figure 3B, C).

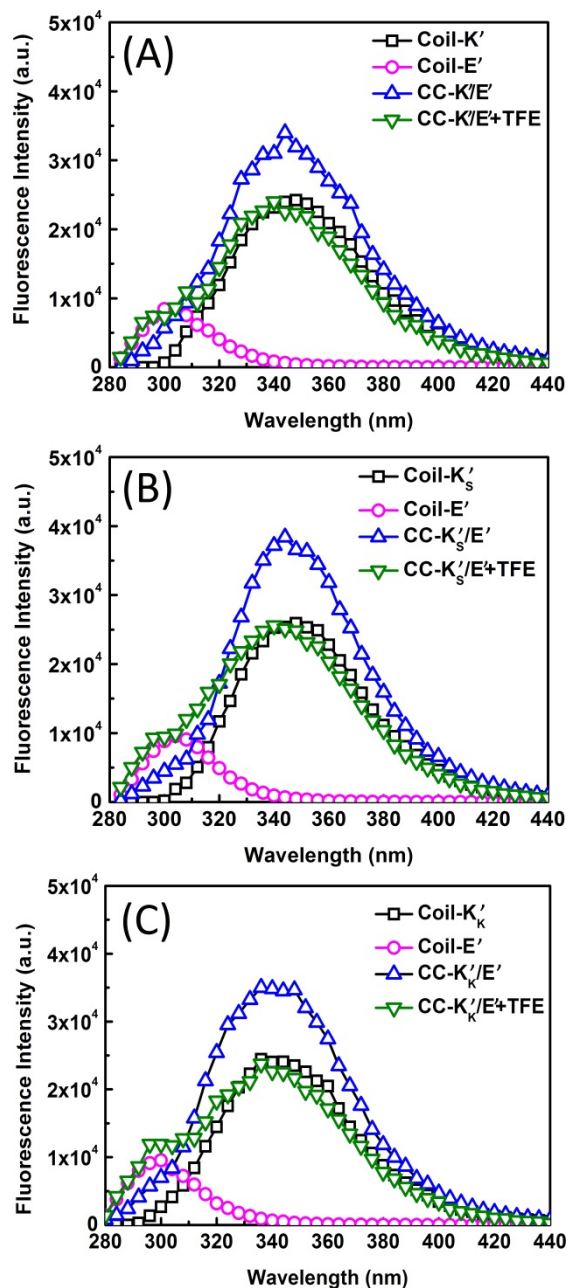


Figure 3. Fluorescence emission spectra (extension at 275 nm) of fluorescent labeled peptides 50 μ M in either pH=7.4 PBS buffer or 1:1 TFE/PBS solution on 25 $^{\circ}$ C. (A) Coil-K' $'$ =Ac-(KIAALKE) $_3$ -GW-CONH $_2$, Coil-E' $'$ =Ac-(EIAALEK) $_3$ -GY-CONH $_2$. (B) Coil-

$K_S^* = \text{Ac}-(\text{KIAALKS})_3\text{-CONH}_2$. (C) Coil- $K_K^* = \text{Ac}-(\text{KIAALKK})_3\text{-CONH}_2$. W is tryptophan, while Y is tyrosine.

Both CD and fluorescence measurements showed that replacing the negatively charged glutamate residue at the 'f' position with either the positively charged lysine or non-charged serine on position 'f' in Coil-K did not significantly alter the peptide ability to form a coiled coil. Hence, we consider the electrostatic interaction as the only difference in the following liposome fusion studies.

Lipopeptide mediated liposome fusion study

Lipopeptide synthesis

The lipopeptides were synthesized as previously mentioned in Chapter 5. However, the lipopeptides cleavage from the resin was optimized by using a cocktail of TFA, DCM, phenol and TIS (70:22.5:5:2.5% v/v) for peptide precipitation. The purification of the crude lipopeptides was performed as described in Chapter 5 and the resulting products are presented in Table 6.

Table 6. Lipopeptides used in this study

Name ^a	Mw (g mol ⁻¹) ^a (theoretical)	Mw (g mol ⁻¹) (experimental)	Yield ^b	Purity ^c
LPK ^a	3704.10	3704.01	60 %	>95 %
LPK _S ^a	3577.88	3577.80	65 %	>95 %
LPK _K ^a	3701.00	3701.19	50 %	>95 %
LPE ^a	3706.82	3706.54	63 %	>95 %

a Mw is molecular weight. b and c were calculated after HPLC purification.

CD spectroscopy

The peptides were incorporated into the surface of liposomal membranes at a concentration of 1 mol%. Compared with the acetylated peptides in PBS, the membrane bound lipopeptides showed a red shift in the minimum (from 222 nm to 225 nm) in the CD

Increasing the membrane fusion efficiency by reducing undesired peptide-peptide interactions

spectra (Figure 4). This is due to different dielectric of the membrane environment relative to that of single peptides in aqueous buffered solutions.²⁴⁻²⁶

CD measurements of lipopeptide LPK in liposomes revealed a $[\theta]_{225}/[\theta]_{208}$ ratio larger than 1, indicating that it has a tendency to either homocoil or interact with the lipid membrane (Figure 4A). In contrast, the other individual lipopeptides (LPK_S, LPK_K and LPE) all showed a $[\theta]_{225}/[\theta]_{208}$ ratio <1 , implying that homocoiling occurring at the membrane was significantly suppressed.^{22, 27} Upon equimolar mixing of LPE-modified liposomes with LPK-modified liposome, immediate coiled coiling of the peptides was observed as well as peptide aggregation since the ellipticity ratio increased significantly to larger than 1 (Figure 4B).²⁸ This ellipticity ratio increase was less pronounced for mixtures of LPK_S (or LPK_K) liposomes interacting with LPE liposomes. This circular dichroism study indicates that changes of the charge at the 'f' position in coil-K influences the peptide behavior at the liposomal membrane, most likely by decreasing the tendency to self-aggregate in the pre-fusion state.

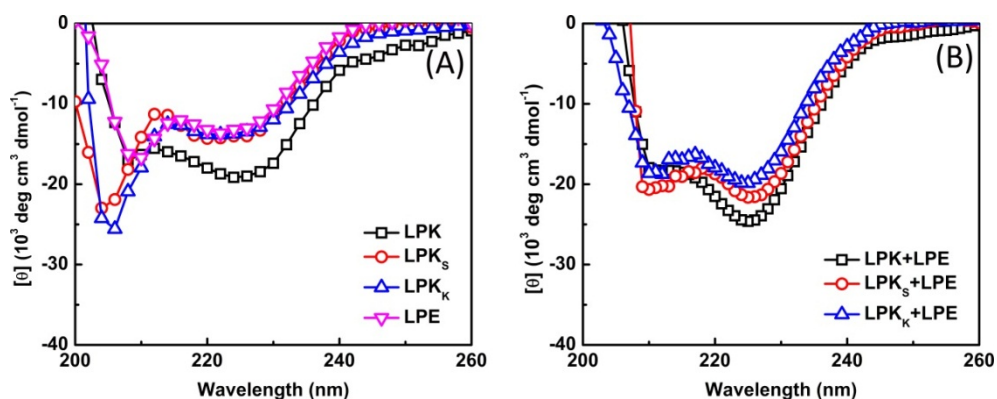


Figure 4. (A) Circular dichroism spectra of 1 mol% lipopeptide on liposomal membranes. (B) Equimolar mixture of LPK (and its derivatives) and LPE on liposomes. [Lipids]=0.5 mM, PBS buffer, pH=7.4, 25 °C.

Liposome fusion studies

The effect of charge at the 'f' position of coil-K on the rate of membrane fusion was studied with lipid and content mixing assays as well as dynamic light scattering (DLS). In general, the process of liposome fusion is initiated by docking of two opposing liposome membranes in close proximity, followed by the formation of a so-called the stalk

intermediate and merging of two liposomes outer lipid leaflets (Scheme 1). Finally, a membrane pore is formed resulting in content mixing between the two liposomes. Coiled coil formation between the two complementary peptides on the opposing membranes is the driving force inducing liposome docking followed by fusion. Peptide aggregation at the surface of liposomes in the pre-fusion state might lead to steric hindrance at the membrane and/or lowering the effective peptide concentration. As a result, fewer peptides are available to form coiled coils which lowers the liposome fusion rate and efficiency.^{11, 28}

First, the rate of lipid mixing was determined by a standard FRET assay. Coil-K modified liposomes (shortname K-L_F), contained both the donor dye nitrobenzofuran (NBD) and the acceptor dye lissamine rhodamine (LR) attached to the membrane, while Coil-E modified liposomes (shortname E-L) were not decorated with fluorescent dyes. These liposomes were stable with time and did not show any self-aggregation or fusion for at least 24h (See Appendix Figure A6). Upon equimolar mixing of K-L_F liposomes with E-L liposomes, an immediate increase in the NBD emission was observed as a result of a decreased FRET efficiency due to the increase in the average distance between NBD and LR. This is due to lipid mixing between K-L_F and E-L liposomes. Figure 5A shows that in all three experiments full lipid mixing (i.e. 100%) was achieved within 60 min. However, fusion between K_K-L_F and E-L liposomes showed the highest initial lipid mixing rate. Also fusion between K_S-L_F with E-L liposomes resulted in a higher lipid mixing rate as compared to the fusion induced by the original coil-K and coil-E peptides. Thus, varying the charge in coil-K at the 'f' position resulted in differences in the initial lipid mixing rate, albeit these became smaller at longer time scales.

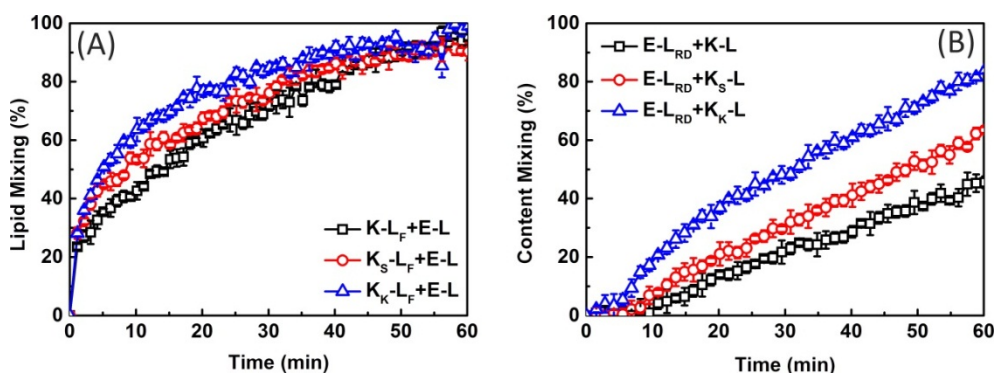


Figure 5. (A) Fluorescence traces showing lipid mixing between fluorescence (NBD/LR) labeled LPK (and derivatives) liposomes with non-fluorescence labeled LPE liposomes. (B)

Increasing the membrane fusion efficiency by reducing undesired peptide-peptide interactions

Content mixing between non-fluorescent LPK liposomes with sulforhodamine labelled (20 mM) LPE liposomes. Liposome concentration is 0.1 mM with 1% peptide decoration. The bars show the standard deviations (σ). See Figure A6/A7 for the lipid mixing and content mixing fluorescence spectra. All the measurements were performed in PBS, pH 7.4, at 25 °C.

Next, a liposome fusion content mixing assay was performed, which revealed a more pronounced difference between the three pairs of lipidated peptides (i.e. CC-K/E, CC-K_s/E, CC-K_k/E). In this experiment, Coil-E modified liposomes were loaded with sulphorhodamine B at a self-quenching concentration of 20 mM, yielding E-L_{RD} liposomes, while Coil-K (including its derivatives) modified liposome did not contain dyes in the aqueous interior, yielding K-L liposomes. Upon mixing of the liposomes, fusion resulted in the transfer of content transfer with a concomitant dilution of the rhodamine dye, thereby alleviating the self-quenching and a subsequent increase in fluorescence intensity (Figure 5B).

Here, significant differences in content mixing were observed as a function of the peptides used. Within 60 min, fusion between E-L_{RD} liposomes and K_k-L liposomes yielded 85% of content mixing, which is significantly higher as compared to the original peptide design (i.e. coil-K/coil-E modified liposomes) Using coil-K_s/coil-E modified liposomes with a neutral charge at the 'f' position also gave an increased fusion efficiency, but less pronounced when compared to the coil-K_k/coil-E liposomes.

Dynamic light scattering

To study the size increase due to aggregation and fusion events upon mixing of the liposomes, we used dynamic light scattering (DLS) measurements in order to determine whether the average liposome size increase correlated with the lipid and content mixing results. The results revealed similar initial docking rate and size increasing due to the limited instrumental sensitivity. It is important to note that dynamic light scattering cannot distinguish between liposome-liposome docking and liposome-liposome fusion events. Therefore it can be concluded that all studied coiled coil pairs were able to at least induce docking between opposing liposomes with comparable efficiency. After 30 minutes the increase in the hydrodynamic diameter deviates. However, at these diameters DLS becomes less reliable and therefore it is difficult to draw any conclusions on the size increase in this time range.

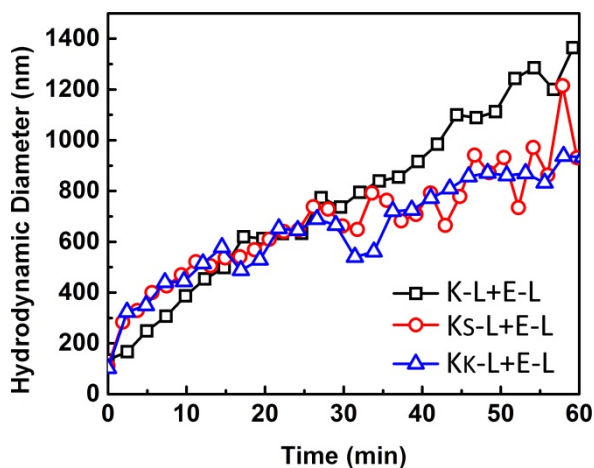


Figure 6. Hydrodynamic diameter increase of the liposomes as a function of time, determined by dynamic light scattering of liposome fusion size increasing. Liposome concentration is 0.1 mM with 1% peptide decoration. See Figure A8 for size increase in the control samples. All the measurements were performed in PBS, pH 7.4, at 25 °C.

Conclusion

In this study the effect of charge at the f- position of one of the peptides in a heterodimeric coiled coil pair on the rate of liposome fusion was investigated. Studies with the acetylated peptides showed that varying the charge at the ‘f’ position of coil-K did not alter the ability to form coiled coils. In contrast, when lipidated versions of these peptides were incorporated in liposome membranes, a significant difference in fusion efficiency was observed. Remarkably, the content mixing rate is strongly dependent on mutations of the f-position. By replacing the original negative charge with either no charge or a positively charged side group, the rate of fusion increased as was shown by a content mixing assay. This might be due to lowering the amount of homocoiling in the pre-fusion state resulting in a higher effective peptide concentration. However, more research is needed to confirm this hypothesis.

Experimental section

Materials

Peptides and lipopeptides were synthesized and purified as described previously.²⁹ DOPE was purchased from Lipoid AG, and cholesterol was obtained from Fluka. DOPE-NBD and DOPE-LR were obtained from Avanti Polar Lipids. All other reagents and solvents were obtained at the highest purity available from Sigma-Aldrich or BioSolve Ltd. and used without further purification. Milli-Q water with a resistance of more than 18.2 M Ω /cm was provided by a Millipore Milli-Q filtering system with filtration through a 0.22 μ m Millipak filter.

Liposome Preparation

Liposome for lipid mixing and DLS measurement

Liposomes were composed of DOPC/DOPE/CH (50:25:25 mol%). Fluorescent labeled liposomes also contained 0.5 mol% LR-DOPE and NBD-DOPE. Lipid stock solutions (1 mM) were prepared in chloroform. Lipopeptide stock solutions (10 μ M) were prepared in 1:1 (v/v) chloroform:methanol. Liposomes were prepared by drying appropriate volumes of the lipid and lipopeptide stock solutions in a 20 mL bottle under reduced pressure, addition of PBS buffer (pH 7.4) and sonication for ~5 minutes in a bath sonicator with the water bath at 55°C. liposome samples for DLS measurement follow the same procedure as above, but without fluorescent dyes.

Liposome for content mixing

For this assay, 1 mM 1 mol % Coil-E decorated liposome was prepared, encapsulating 20 mM sulforhodamine B in pH=7.4 PBS buffer (shortname E-L_{RD}). E-L_{RD} was further purified by sephadex G-100 column manually (column length= 400 mm, diameter= 30 mm, flow rate= 1 drop s⁻¹), yielding 0.1 mM with 1 mol% Coil-E decoration E_{RD}-L. Meanwhile, 0.1 mM 1 mol % Coil-K decorated liposome was prepared as the way mentioned above (shortname K-L).

Experimental Methods

Experimental diffusion coefficients, D , were measured at 25 °C by dynamic light scattering using a Malvern Zetasizer Nano ZS ZEN3500 equipped with a peltier-controlled thermostatic cell holder. The laser wavelength was 633 nm and the scattering angle was 173°. The Stokes-Einstein relationship $D = k_B T / 3\pi\eta D_h$ was used to estimate the hydrodynamic radius, D_h . Here k_B is the Boltzman constant, and η is the solvent viscosity. The results are expressed as the hydrodynamic diameter with units of nm. For individual liposome batches the sample was allowed to equilibrate for 2 minutes. For DLS time series the solutions were mixed in the cuvette (1000 rpm for 30 seconds). Measurements were started immediately after mixing.

FRET-based lipid mixing experiments were conducted on a Tecan X fluorometer using a 96 well plate. The z-position was 12500 μm , and the gain was optimized according to the amount of fluorophore in the sample. Excitation and emission slits were set at 10 nm. The excitation wavelength was 460 nm, and NBD emission was monitored 535 nm. The measurements were done in room temperature. 100 μL of fluorescent and non-fluorescent liposomes were combined, and for consistent mixing the plate was shaken inside the fluorometer for 30 seconds (2mm linearly, 70 x per minute). Data was collected every 20 seconds for at least 1 hour. Using 0.5 mol% of each fluorophore in the fluorescent liposomes and mixing fluorescent and non-fluorescent liposomes in a 1:1 molar ratio the increase in NBD fluorescence is proportional to lipid mixing. The data was calibrated to show the percentage of liposomes that have undergone lipid mixing by $\text{LM} (\%) = (I_t - I_0) / (I_{100} - I_0) \times 100$, where I_0 is the NBD intensity of 1:1 (v/v) fluorescent liposomes:PBS, and I_{100} is the NBD intensity of liposomes of the same concentration prepared using an equimolar mixture of fluorescent and non-fluorescent stock solutions. I_0 and I_{100} were monitored with time as they are temperature sensitive. This assay only detects fusion between the original liposomes. e.g. if two pre-fused liposomes fuse the distance between the fluorophores does not change so the event is not detected.

For content mixing assay, the fluorescence signal of the sulforhodamine ($\lambda_{em} = 580 \text{ nm}$) was detected once upon 1:1 mixing E_{RD-L} (100ul) with K-L (100 ul). The increase of sulforhodamine B fluorescence is due to a relief of self-quenching following by content mixing, named Ft. The F0 is 100 uL ERD-L with 100 ul PBS, and the F100 is the fluorescence signal intensity after addition of 1% (w/v) Triton X-100 in PBS into the E_{RD-L}

Increasing the membrane fusion efficiency by reducing undesired peptide-peptide interactions

L+K-L well. And the content mixing is calculated by $CM (\%) = (F_t - F_0)/(F_{100} - I_0) \times 100$. All the data are calculated from 3 times measurements.

For either lipid mixing or content mixing, the standard deviations (σ) are calculated by formula: $\sigma = \sqrt{\frac{1}{N} \sum_{i=1}^N (x_i - \mu)^2}$, where $\mu = \frac{1}{N} \sum_{i=1}^N x_i$ (x_i is the fluorescence intensity from measurement, N is the number of measurement. In this study, N=3).

Circular dichroism spectra were obtained using a Jasco J-815 spectropolarimeter equipped with a peltier-controlled thermostatic cell holder (Jasco PTC-423S). Spectra were recorded from 260 nm to 200 nm in a quartz cuvette with 5.0 mm pathlength at 25 °C. Data were collected at 1.0 nm intervals with a 1 nm bandwidth and 1 s readings. Each spectrum was the average of 5 scans. The spectra had a baseline of plain liposomes in TES buffer subtracted. The ellipticity is given as the mean residue molar ellipticity, $[\theta]$ ($10^3 \text{ deg cm}^2 \text{ dmol}^{-1}$), calculated from $[\theta] = (\theta_{\text{obs}} \times \text{MRW}) / (10 \times l \times c)$, where θ_{obs} is the observed ellipticity in millidegrees, MRW is the mean residue molecular weight (i.e. the molecular weight of the peptide divided by the number of amino acid residues), l is the path length of the cuvette in cm and c is the peptide concentration in mg mL^{-1} .

A 1.0 mm quartz cuvette and a final concentration of 200 μM peptide in PBS (pH=7.4). Spectra were recorded from 250 nm to 200 nm at 25 °C. Unless stated otherwise data points were collected with a 0.5 nm interval with a 1 nm bandwidth and scan speed of 1 nm per second. Each spectrum was an average of 5 scans. For analysis each spectrum had the appropriate background spectrum (buffer or 50% TFE) subtracted.

For determination of the coiled coil thermal dissociation constant, temperature dependent CD spectra were obtained using an external temperature sensor immersed in the sample.^{30, 31} The temperature was controlled with the internal sensor and measured with the external sensor. A 10 mm quartz cuvette was used, and the solutions were stirred at 900 rpm. Spectra were recorded from 250 nm to 200 nm, with data collected at 0.5 nm intervals with a 1 nm bandwidth and a scan speed of 1 nm per second. The temperature range was 6 °C to 96 °C with a temperature gradient of 2.0 °C/minute and a 60 s delay after reaching the set temperature. The spectrum of PBS at 6 °C (average of 5 scans) was subtracted from each spectrum. All the thermal unfolding curves were analyzed using a two-state conformation transition model.^{32, 33}

The data were analyzed using a two-state unfolding model to determine the fraction folded using Eqn. (2),

$$F_f = ([\theta] - [\theta]_U) / ([\theta]_F - [\theta]_U) \quad (2)$$

Where $[\theta]$ is the observed molar ellipticity, $[\theta]_U$ is the ellipticity at 222 nm of the denatured state, as determined from the plateau of the ellipticity vs. temperature curve, and $[\theta]_F$ is the ellipticity at 222 nm of the folded state at that temperature as determined from a linear fit of the initial stages of the ellipticity vs. temperature curve.

The fraction unfolded, F_U , was calculated by Eqn. (3),

$$F_U = 1 - F_f \quad (3)$$

The dimer dissociation constant in the transition zone was calculated using Eqn. (4),

$$K_U = 2P_t F_U^2 / F_f \quad (4)$$

P_t is the total peptide concentration. By taking the derivative of the $\ln(K_U)$ vs. temperature and using this in the van't Hoff equation, Eqn. (5), the change in enthalpy associated with unfolding with temperature can be plotted:

$$\Delta H_U = RT^2 \times \frac{d \ln(K_U)}{dT} \quad (5)$$

The gradient of enthalpy vs. temperature plot ΔC_p , is the difference in heat capacity between the folded and unfolded forms, and can be used in the Gibbs-Helmholtz equation adapted to monomer-dimer equilibrium, Eqn. (6), to obtain the Gibbs free energy of unfolding as a function of temperature by least-squares fitting,

$$\Delta G_U = \Delta H_m(1 - T/T_m) + \Delta C_p[T - T_m - T \ln(T/T_m)] - RT \ln[P_t] \quad (6)$$

T_m and H_m are the temperature and enthalpy at the midpoint of the transition at which the fraction of monomeric peptide is 0.5.¹²

Appendix

1. Liquid chromatography mass spectroscopy

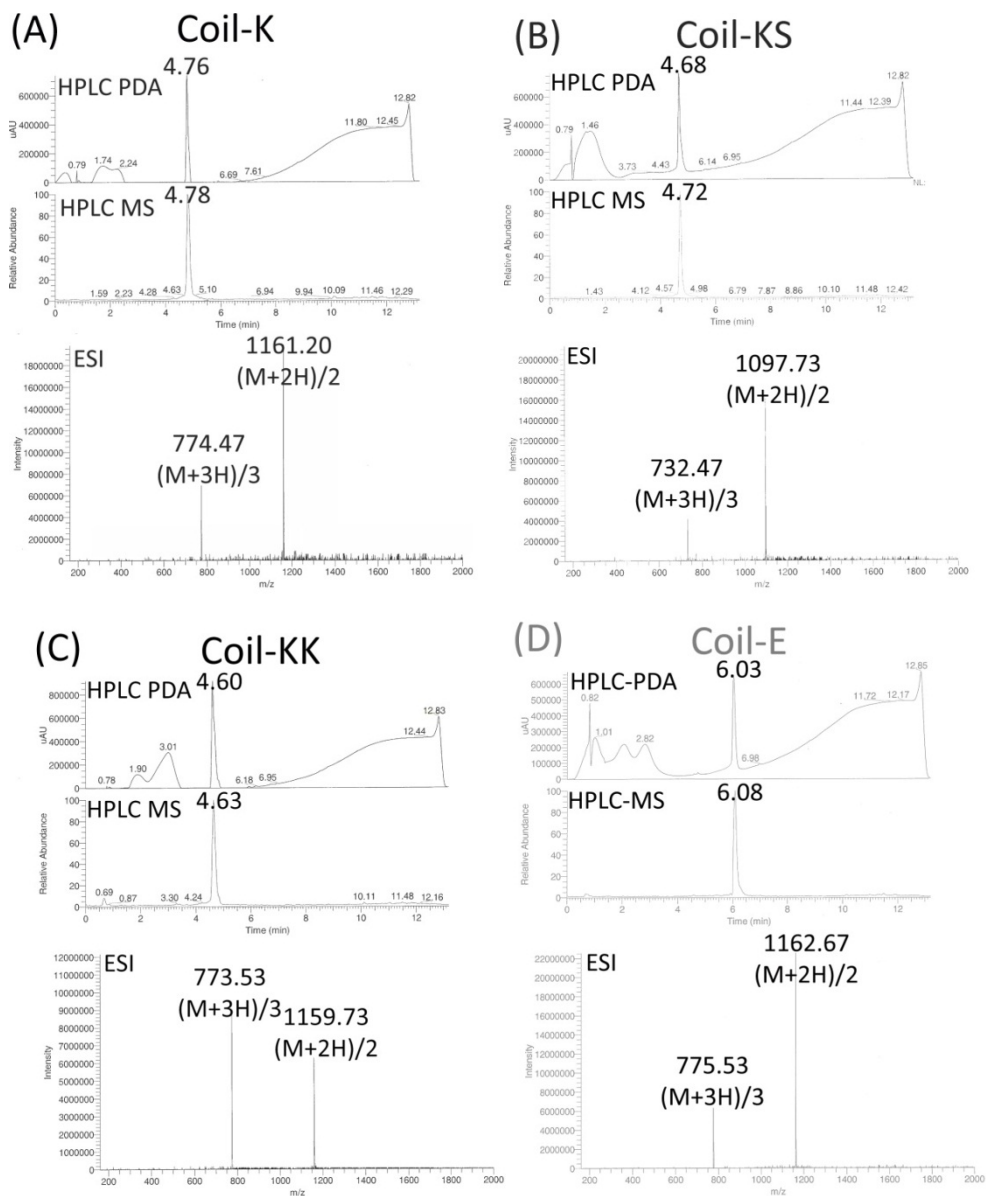


Figure A1. LC-MS spectra of peptide (A) Coil-K, (B) Coil-K_S, (C) Coil-K_K, (D) Coil-E. From top to bottom: UV (ultraviolet-visible) detection wavelength at 214 nm, and ESI (electrospray ionization) mass spectrum.

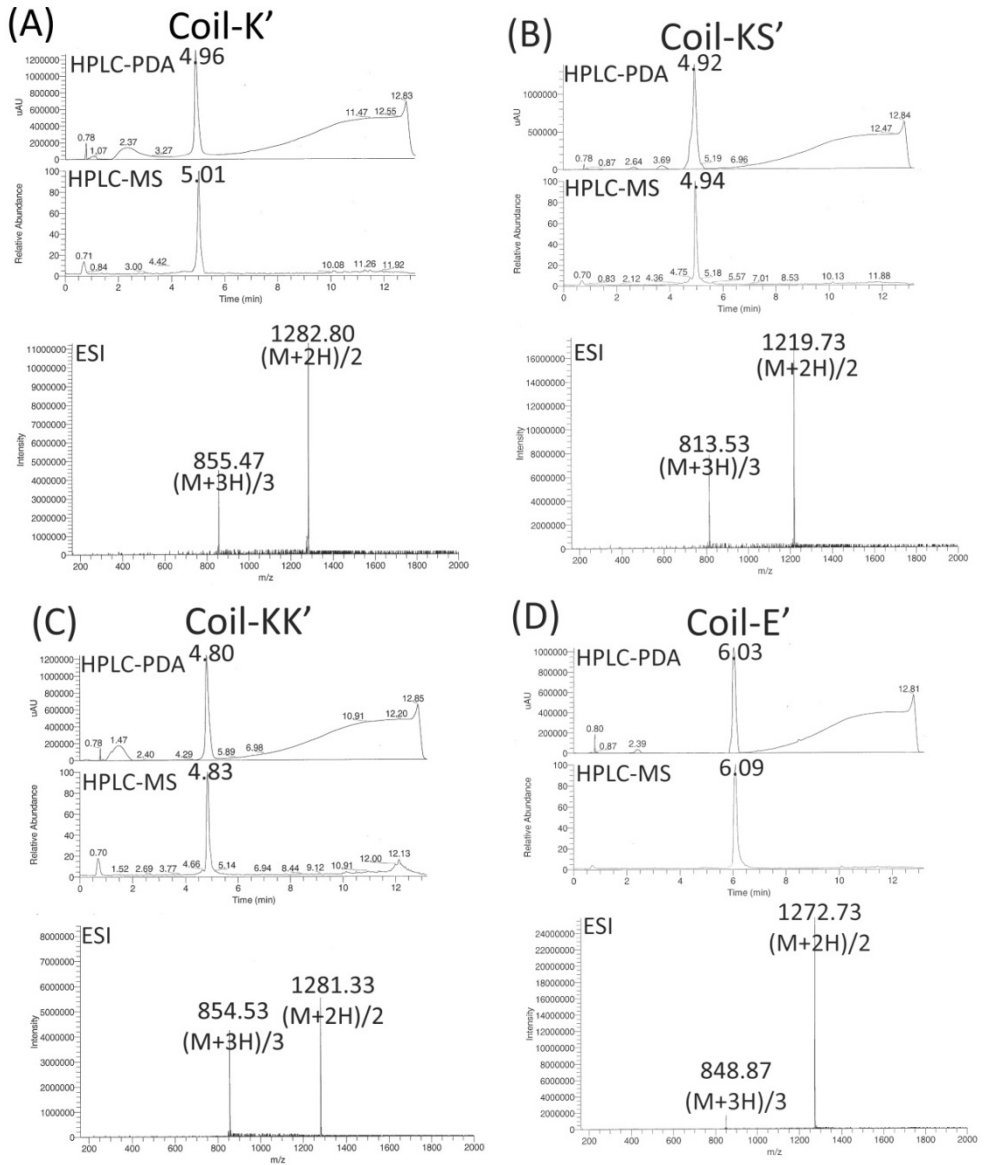


Figure A2. LC-MS spectra of fluorescent labeled peptide (A) Coil-K' (Ac-(KIAALKE)₃-GW-CONH₂), (B) Coil-K_S' (Ac-(KIAALKS)₃-GW-CONH₂), (C) Coil-K_K' (Ac-(KIAALKK)₃-GW-CONH₂), (D) Coil-E' (Ac-(EIAALEK)₃-GW-CONH₂). From top to bottom: UV (ultraviolet-visible) detection wavelength at 214 nm, and ESI (electrospray ionization) mass spectrum.

Increasing the membrane fusion efficiency by reducing undesired peptide-peptide interactions

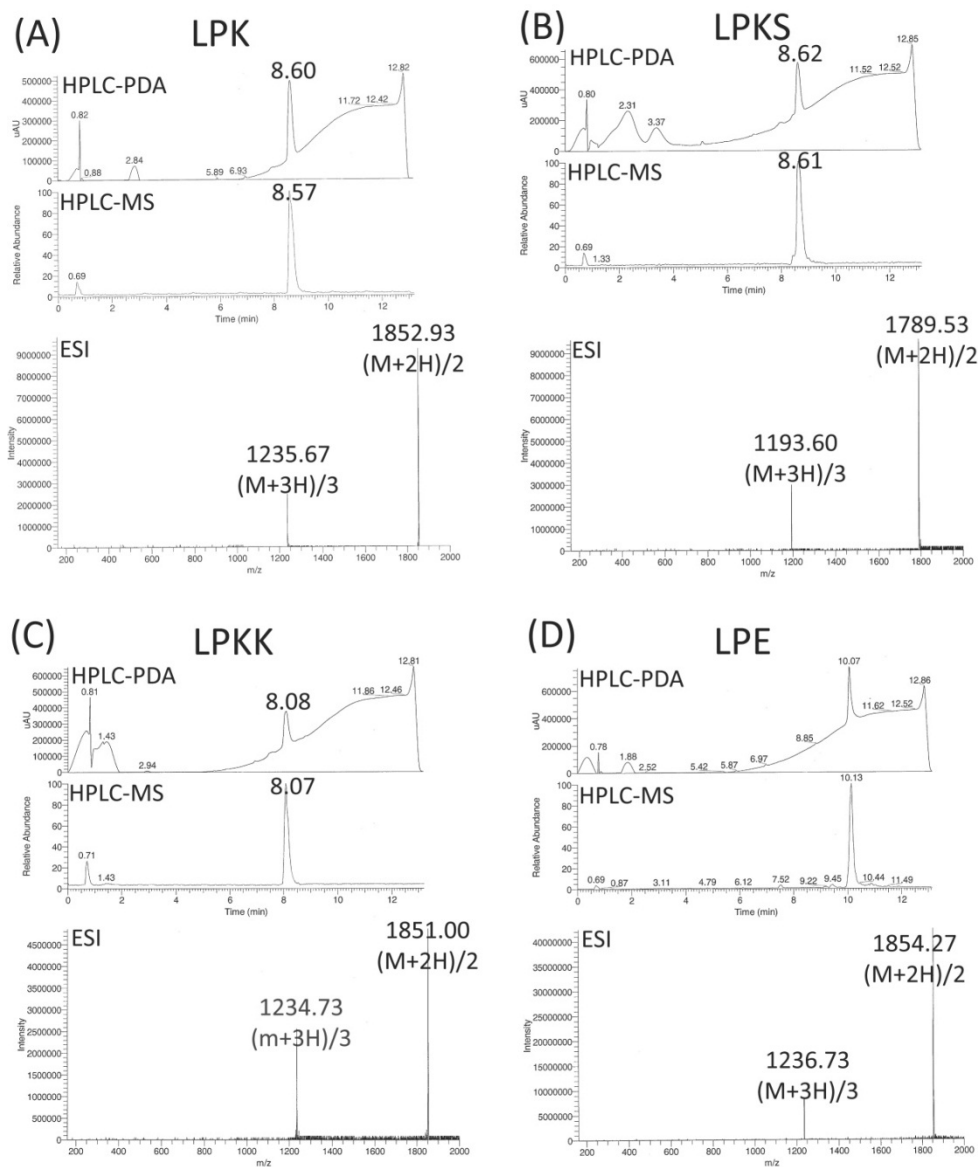


Figure A3. LC-MS spectra of fluorescent labeled peptide (A) LPK, (B) LPK_s, (C) LPK_k, (D) LPE. From top to bottom: UV (ultraviolet-visible) detection wavelength at 214 nm, and ESI (electrospray ionization) mass spectrum.

2. Hyperchem simulation

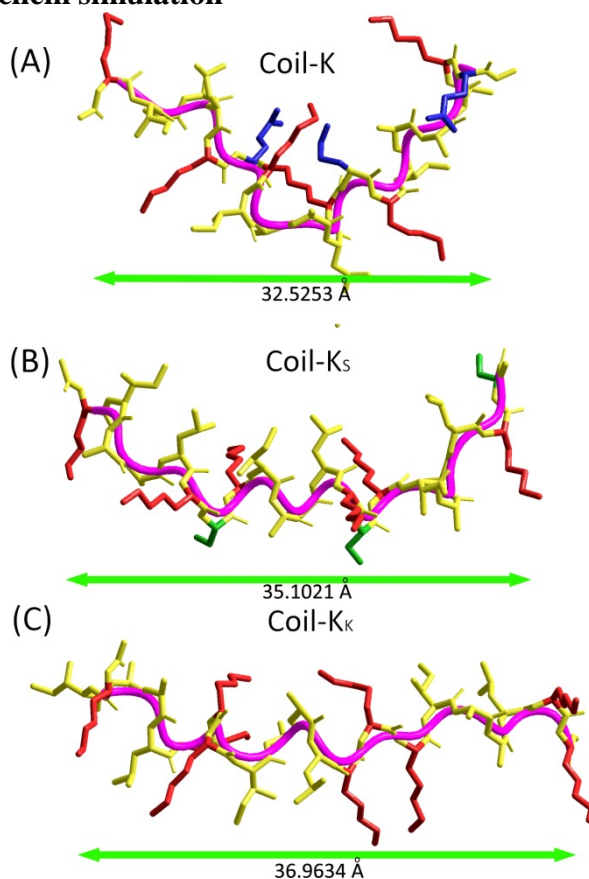


Figure A4. Hyperchem simulation structures of peptides Coil-K, Coil-KS and Coil-KK. The detail simulation method is the same as description in Chapter 3. Green bar indicates peptide length.

3. CD thermal dynamic curves

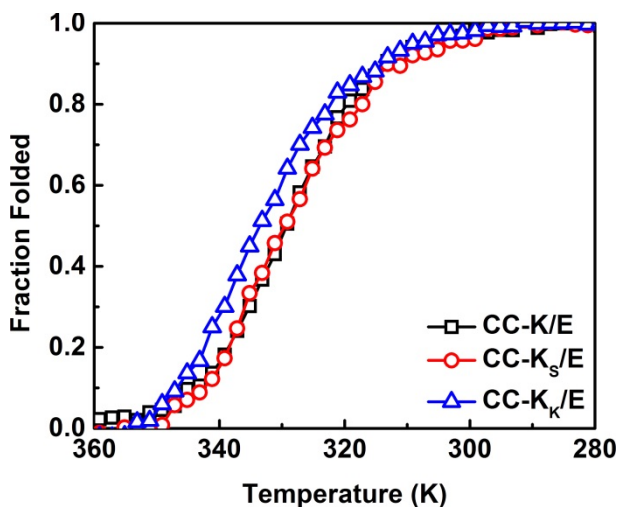


Figure A5. Thermal folding curve based on changes in $[\theta]_{222}$ as followed by CD by decreasing the temperature from 360 to 280 K. [Total peptide]= 40 μ M, PBS pH=7.4, 25 $^{\circ}$ C, 1 cm quartz cuvette.

4. Liposome fusion control data

4.1 Lipid mixing control

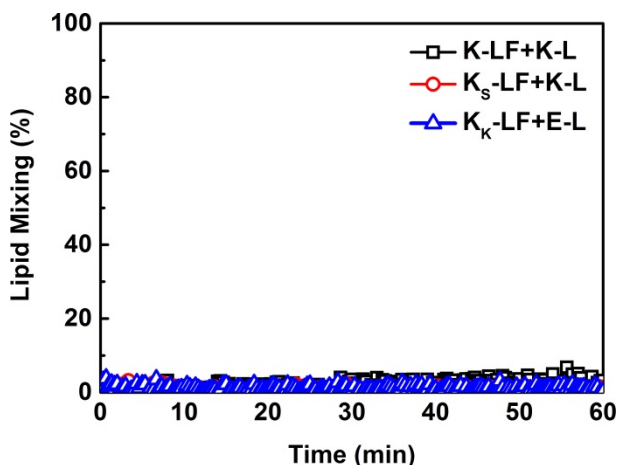


Figure A6. Lipid mixing control as monitored by fluorescence spectroscopy between fluorescent labeled K-LF (and its derivatives) and non-fluorescent K-L (and its derivatives). Fusogen proportion= 1 mol%, [lipids]=0.1 mM, PBS buffer, pH=7.4, 25 $^{\circ}$ C.

4.2 Content mixing control

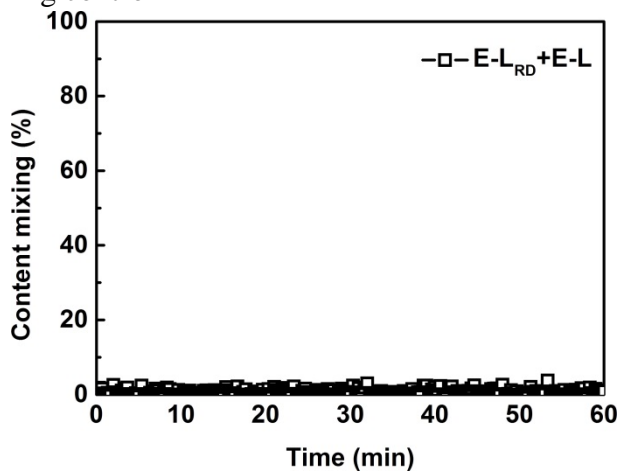


Figure A7. Content mixing control as monitored by fluorescence spectroscopy between sulphorhodamine B loaded E-LRD and non-loaded E-L. Fusogen proportion =1 mol%, [lipids]=0.1 mM, PBS buffer, pH=7.4, 25 °C.

4.3 DLS size increasing control

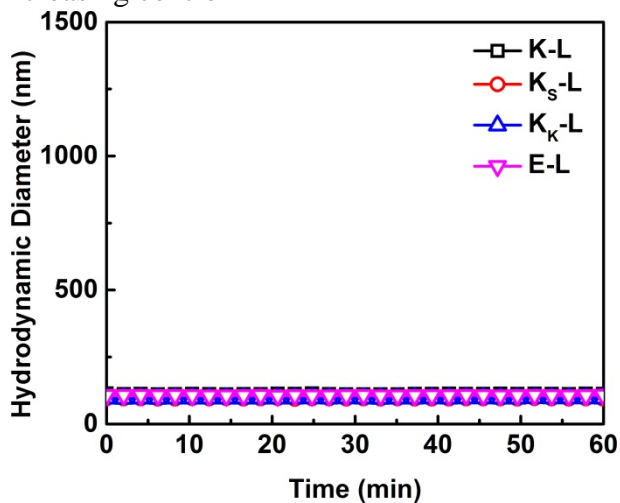


Figure A8. DLS size increasing control as monitored by dynamic light scattering. Fusogen proportion =1 mol%, [lipids]=0.1 mM, PBS buffer, pH=7.4, 25 °C.

Reference

1. I. Mellman and S. D. Emr, *Journal of Cell Biology*, 2013, **203**, 559-561.
2. T. C. Sudhof and J. E. Rothman, *Science*, 2009, **323**, 474-477.
3. W. Wickner and R. Schekman, *Nature Structural & Molecular Biology*, 2008, **15**, 658-664.
4. W. Antonin, D. Fasshauer, S. Becker, R. Jahn and T. R. Schneider, *Nature Structural Biology*, 2002, **9**, 107-111.
5. H. R. Marsden, I. Tomatsu and A. Kros, *Chemical Society Reviews*, 2011, **40**, 1572-1585.
6. R. Jahn, T. Lang and T. C. Sudhof, *Cell*, 2003, **112**, 519-533.
7. R. Blumenthal, M. J. Clague, S. R. Durell and R. M. Epanand, *Chemical Reviews*, 2003, **103**, 53-69.
8. L. V. Chernomordik and M. M. Kozlov, *Nature Structural & Molecular Biology*, 2008, **15**, 675-683.
9. X. C. Chen, D. Arac, T. M. Wang, C. J. Gilpin, J. Zimmerberg and J. Rizo, *Biophysical Journal*, 2006, **90**, 2062-2074.
10. H. R. Marsden, N. A. Elbers, P. H. H. Bomans, N. Sommerdijk and A. Kros, *Angewandte Chemie-International Edition*, 2009, **48**, 2330-2333.
11. H. R. Marsden, A. V. Korobko, T. T. Zheng, J. Voskuhl and A. Kros, *Biomaterials Science*, 2013, **1**, 1046-1054.
12. T. Zheng, J. Voskuhl, F. Versluis, H. R. Zope, I. Tomatsu, H. R. Marsden and A. Kros, *Chemical Communications*, 2013, **49**, 3649-3651.
13. J. R. Litowski and R. S. Hodges, *Journal of Peptide Research*, 2001, **58**, 477-492.
14. P. C. Lyu, M. I. Liff, L. A. Marky and N. R. Kallenbach, *Science*, 1990, **250**, 669-673.
15. H. R. Marsden, T. T. Zheng and A. Kros, *Abstracts of Papers of the American Chemical Society*, 2013, **245**.
16. C. N. Pace and J. M. Scholtz, *Biophysical Journal*, 1998, **75**, 422-427.
17. B. Apostolovic and H. A. Klok, *Biomacromolecules*, 2008, **9**, 3173-3180.
18. Y. H. Chen, J. T. Yang and K. H. Chau, *Biochemistry*, 1974, **13**, 3350-3359.
19. C. Y. Huang, *Methods in Enzymology*, 1982, **87**, 509-525.
20. Z. D. Hill and P. Maccarthy, *Journal of Chemical Education*, 1986, **63**, 162-167.
21. J. A. Boice, G. R. Dieckmann, W. F. DeGrado and R. Fairman, *Biochemistry*, 1996, **35**, 14480-14485.
22. J. R. Litowski and R. S. Hodges, *Journal of Biological Chemistry*, 2002, **277**, 37272-37279.
23. J. Eisinger, B. Feuer and A. A. Lamola, *Biochemistry*, 1969, **8**, 3908-&.
24. K. Park, A. Perczel and G. D. Fasman, *Protein Science*, 1992, **1**, 1032-1049.
25. M. Cascio and B. A. Wallace, *PROTEIN PEPT. LETT.*, 1994, **1**, 136-140.
26. B. A. Wallace, J. G. Lees, A. J. W. Orry, A. Lobley and R. W. Janes, *Protein Science*, 2003, **12**, 875-884.
27. N. E. Zhou, C. M. Kay and R. S. Hodges, *Biochemistry*, 1992, **31**, 5739-5746.

- 28.I. Tomatsu, H. R. Marsden, M. Rabe, F. Versluis, T. Zheng, H. Zope and A. Kros, *Journal of Materials Chemistry*, 2011, **21**, 18927-18933.
- 29.H. Robson Marsden, N. A. Elbers, P. H. H. Bomans, N. A. J. M. Sommerdijk and A. Kros, *Angewandte Chemie International Edition*, 2009, **48**, 2330-2333.
- 30.S. M. Kelly and N. C. Price, *Biochimica Et Biophysica Acta-Protein Structure and Molecular Enzymology*, 1997, **1338**, 161-185.
- 31.S. M. Kelly, T. J. Jess and N. C. Price, *Biochimica Et Biophysica Acta-Proteins and Proteomics*, 2005, **1751**, 119-139.
- 32.P. Lavigne, M. P. Crump, S. M. Gagne, R. S. Hodges, C. M. Kay and B. D. Sykes, *Journal of Molecular Biology*, 1998, **281**, 165-181.
- 33.P. Lavigne, L. H. Kondejewski, M. E. Houston, F. D. Sonnichsen, B. Lix, B. D. Sykes, R. S. Hodges and C. M. Kay, *Journal of Molecular Biology*, 1995, **254**, 505-520.

Chapter 7

Summary



Fusion of lipid bilayers in cells facilitates the active transport of chemicals. Non-viral membrane fusion is regulated by a cascade of proteins as the process is highly regulated both in space and time. In eukaryotic cells, the so-called SNARE protein complex is at the heart of fusion. However, little is known about the actual mechanism at the molecular level. Inspired by the SNARE protein complex, our group previously developed a model system composed of a pair of lipidated complementary coiled coil peptides enabling targeted liposome-liposome fusion. This model system possesses all the key characteristics of membrane fusion similar to SNARE mediated fusion. The tetrameric coiled-coil of SNAREs is mimicked by a complementary pair of coiled coil forming peptides composed of three heptad repeat units (denoted “coil-E” and “coil-K”). A flexible poly(ethylene glycol) spacer is conjugated to the N-terminus ensuring rotational freedom of the peptides. Lipidation warrants the anchoring of the peptides in the membrane by means of a phospholipid anchor (DOPE), mimicking the transmembrane domain of SNAREs.

In order to develop future applications of this model system, the mechanism of membrane fusion needs to be studied in more detail and this has been the goal of this thesis. The first part of this thesis (Chapter 2 and 3) studies the peptide self-assembly, while in the second part (Chapter 4,5 and 6) liposomal fusion studies are described and the effect of the peptide design on the rate of fusion.

Chapter 2 shows a new method to determine the oligomeric state and orientation of coiled-coil peptide motifs is described. Peptides K and E, which are designed to form a parallel heterodimeric complex in aqueous solution, were labeled with the aromatic amino acids tryptophan and tyrosine on the C-terminus respectively as ‘fingerprint’ residues. One of the peptides was also labeled with the paramagnetic probe MTSL. One dimensional proton NMR spectroscopy was used to study the peptide quaternary structure by monitoring the signal suppression of the aromatic labels due to proximity of the nitroxyl radical. 1D-NMR confirmed that the peptides K and E form a heterodimeric coiled coil with a parallel orientation. In addition, fluorescence emission quenching of the aromatic labels due to electron exchange with a nitroxyl radical confirmed the parallel coiled coil orientation. Thus, paramagnetic nitroxide and aromatic fluorophore labeling of peptides yields valuable information regarding the quaternary structure from 1D-NMR and steady-state fluorescence measurements. This convenient method is useful not only to investigate coiled coil assembly, but can also be applied to any defined supramolecular assembly.

Summary

In **Chapter 3**, the reversed sequence of coil-E was synthesized and its self-assembly behavior with coil-K was studied using the method described in **Chapter 2**. These studies were combined with modeling data, showing that Coil-E_r and Coil-K assemble into an antiparallel tetrameric coiled coil motif (CC-K/E_r). Interestingly, the stability of this complex was comparable to the original heterodimeric CC-K/E. Next, the CC-K/E_r triggered liposome fusion was determined and compared with CC-K/E triggered fusion. Surprisingly, the results show that both the fusion rate and efficiency are similar. This indicates that in our peptide mediated membrane fusion system, the peptide orientation or oligomer state is not a critical factor.

In **Chapter 4**, the effect of lipopeptide and lipid concentration on liposome fusion were investigated. The lipid mixing efficiency was obtained when the liposomes were decorated with 0.75 mol% lipopeptide. Dynamic light scattering and optical microscopy studies revealed that by tuning the lipid and peptide concentrations, two fusion regimes are possible: in the first regime multiple rounds of fusion results in the formation of giant liposomes, while in the second regime fusion can be limited to a single liposome-liposome fusion event. The mapping of the rate and route of liposome fusion under different conditions gave a detailed understanding of the capacity of the SNARE mimicking model system. This understanding paves the way for future applications of the fusion model system such as utilizing liposomes as nanoreactors and as a drug delivery tool.

In **Chapter 5**, the rate of peptide mediated liposome fusion was controlled by varying the coiled coil binding energy. In the original model system, both coil-E and coil-K were composed of 3 heptad repeat units. In this study the length of the peptides was decreased to 2 heptad repeats (coil-E₂, coil-K₂) or increased to 4 repeat units (coil-E₄, coil-K₄). Next, the thermal stability of the coiled coils was studied in order to determine the binding energy of the peptide complexes. As expected, the binding energy was the highest for the longest peptides. Next the rate of fusion was studied using dynamic light scattering studies as well as lipid mixing and content mixing assays. The strongest-binding coiled coil E₄/K₄ motif induced membrane fusion most efficiently. In addition, this coiled coil is also able to induce liposomal membrane fusion in a wide range of either temperature or pH. This study expands the possible scope of future applications of this fusion model system.

In **Chapter 6**, the influence of electrostatic interactions on the rate of liposome fusion was investigated. In order to design new derivatives of CC-K/E with a similar binding energy,

coil-K mutants were synthesized in which the charge at the 'f' position was modified. The fusogenicity of the new derivatives Coil-K_S (no charge on 'f') and Coil-K_K (positive charge on 'f') in combination with coil-E was investigated. Remarkably, the rate of content mixing and efficiency was strongly dependent on these mutations at the 'f' position of Coil-K. By replacing the original negative charge (Coil-K) with either no charge (Coil-K_S) or a positively charged (Coil-K_K) side group, the rate of lipid and content mixing increased significantly. This might be due to lowering the amount of homocoiling in the pre-fusion state resulting in a higher effective peptide concentration. However, more studies are required to support this hypothesis. This thesis focuses on de novo designing coiled coil forming peptides and optimizing coiled coil mediated liposome fusion. There is still room for improvement. In Chapter 3, the sequence of Coil-E was reversed. However, it will be of interest to reverse in future studies the sequence of coil-K, as recent studies have shown that this peptide interacts with liposomal membranes via a so-called snorkeling mechanism. This in turn might destabilize the lipid packing resulting in the observed efficient membrane fusion in this model system. By reversing the sequence of Coil-K this hypothesis might be validated. Chapters 4, 5 and 6 present data showing that this model system can be improved in terms of lipid- and content mixing, which will pave the way for using this model system in an *in vivo* environment. If this can be achieved, this model system would be a true mimic of the natural occurring SNARE proteins.

Samenvatting



Eén van de manieren waarop chemicaliën getransporteerd worden binnen de cel is door fusie van lipide bilagen. Membraanfusie wordt gereguleerd door een verzameling eiwitten, zodat er controle is over waar en wanneer er fusie plaatsvindt. In eukariotische cellen zijn het SNARE eiwitten die aan de basis staan van fusie. Echter, er is nog weinig bekend over het mechanisme waardoor fusie plaatsvindt op het moleculaire niveau. Onze groep heeft een modelsysteem voor membraanfusie ontwikkeld, dat geïnspireerd is door het natuurlijke SNARE eiwit complex. Dit modelsysteem bestaat uit twee complementaire, gelipideerde, coiled coil vormende peptiden die de gerichte fusie tussen liposomen mogelijk maken. In dit modelsysteem worden alle essentiële eigenschappen van SNARE-gedreven fusie nagebootst. Het tetramerische coiled coil complex wordt nagebootst door een complementair paar van coiled coil vormende peptiden, die elk bestaan uit 3 repeterende eenheden van 7 aminozuren (genaamd “coil-E” en “coil-K”). Aan de N-terminus van deze peptiden werd een flexibele poly(ethyleenglycol) keten gekoppeld, die ervoor zorgt dat de peptiden vrijelijk kunnen bewegen op het oppervlak van liposomen. Vervolgens werd er een lipide gekoppeld, zodat we zeker konden zijn dat het peptide zich zou verankeren in lipide membranen.

Om toepassingen te kunnen ontwikkelen voor dit modelsysteem, moet het mechanisme waardoor fusie plaatsvindt in meer detail bestudeerd worden. Dit is dan ook het doel van dit proefschrift. Het eerste deel van dit proefschrift (hoofdstuk 2 en 3) bestudeert de zelfassemblage van de peptiden terwijl het tweede deel (hoofdstuk 4, 5 en 6) zich richt op fusie tussen liposomen, waarin het effect van variaties in de structuur van de peptiden op de mate van membraanfusie wordt beschreven.

Hoofdstuk 2 beschrijft een nieuwe methode om de oligomere toestand en oriëntatie van coiled coil peptiden te bepalen. Peptiden K en E zijn ontworpen om parallelle, heterodimerische coiled coils te vormen (CC-K/E) en deze peptiden werden gelabeld met de aromatische aminozuren tryptofaan en tyrosine aan hun C-termini. Vervolgens werd één van de peptiden gelabeld met een paramagnetische groep, MTSL genaamd. Proton NMR metingen werden vervolgens gebruikt om te bepalen in welke mate het signaal van de aromatische protonen onderdrukt werd door het nitroxyl radicaal. Hiermee kon de quaternaire structuur van de peptiden bepaald worden en werden de parallelle oriëntatie en de heterodimerische zelfassemblage van peptiden E en K bevestigd. Bovendien onderdrukken de MTSL labels ook de fluorescentie van de aromatische aminozuren en fluorescentie metingen bevestigde de NMR data. Dit alles laat zien dat het labelen van

Samenvatting

peptiden met nitroxyl radicalen en aromatische, fluorescente groepen zeer waardevolle informatie kan geven over de quaternaire structuur van de peptiden. Deze handige methode kan bovendien toegepast worden op alle supramoleculaire systemen die een goed gedefinieerde structuur hebben.

In **hoofdstuk 3** werd de aminozuur sequentie van coil-E omgedraaid en de zelfassemblage met peptide K bestudeerd, gebruik makend van dezelfde methode als in **hoofdstuk 2**. Deze studies werden aangevuld met data uit computersimulaties en laten zien dat coil-E_r en coil-K assembleren in een anti-parallel, tetramerisch coiled-coil motief (CC-K/E_r). Verassend genoeg bleek de stabiliteit van dit complex vergelijkbaar met de originele heterodimerische coiled coil CC-K/E. Vervolgens werd de mate waarin CC-K/E_r membraanfusie kon veroorzaken bepaald en vergeleken met CC-K/E. Beide coiled coils laten vergelijkbare fusie efficiënties en snelheden zien, wat demonstreert dat in ons modelsysteem voor membraanfusie zowel de oriëntatie en oligomere toestand van de coiled coil geen cruciale rol spelen.

In **hoofdstuk 4** wordt de invloed van de concentratie van lipiden en gelipideerde peptide op de fusie van liposomen besproken. Het mengen van de lipiden van liposomen was optimaal wanneer 0.75 mol% gelipideerde peptiden werden gebruikt. Dynamische lichtverstrooiing (DLS) en microscopie studies laten zien dat het variëren van de lipide en peptide concentraties toegang geven tot twee fusie regimes: in het eerste regime resulteren meerdere fusies van liposomen tot de vorming van zeer grote liposomen, terwijl in het tweede regime fusie beperkt blijft tot gemiddeld twee liposomen die met elkaar fuseren. Door fusie experimenten uit te voeren onder verschillende condities was het mogelijk om de potentie van ons model systeem voor membraan fusie gedetailleerd in kaart te brengen. De resultaten maken de weg vrij voor toekomstige toepassingen zoals bijvoorbeeld nanoreactoren en drug delivery.

In **hoofdstuk 5** werd de mate waarin fusie plaatsvond gecontroleerd door de bindingsenergie van de coiled coils te variëren. In het oorspronkelijke modelsysteem bestonden zowel coil-E als coil-K uit drie repeterende eenheden van 7 aminozuren. In dit hoofdstuk werd de lengte van de peptiden gevarieerd tussen respectievelijk twee (coil-E₂, coil-K₂) en vier (coil-E₄, coil-K₄) repeterende eenheden. Eerst werden de bindingsenergieën bepaald van de peptiden en zoals verwacht bleek de stabiliteit van de langste peptiden het hoogst. De mate waarin deze peptiden fusie konden induceren werd

vervolgens bepaald door DLS metingen en door de menging van de lipiden en inhoud van de liposomen te kwantificeren. Het langste coiled coil paar (K_4/E_4) induceerde fusie op de meest efficiënte manier en bovendien bleek deze coiled coil resistent tegen hoge temperaturen en ongevoelig voor variaties in de pH. Dit onderzoek breidt de potentiële toepassingen van het modelsysteem verder uit.

In **hoofdstuk 6** werd de invloed van elektrostatistische interacties op de mate van fusie onderzocht. Om ervoor te zorgen dat de bindingsenergie van afgeleiden van CC-K/E niet verschillend waren van de oorspronkelijke coiled coil, werden er coil-K peptiden gesynthetiseerd die een andere lading hadden op de 'f' positie. De mate waarin de nieuwe coil-K derivaten (coil- K_S (geen lading op 'f') en coil- K_K (positieve lading op 'f') in staat waren om, in combinatie met coil-E, fusie te induceren werd onderzocht. Opmerkelijk was dat de invloed van de lading op de 'f' positie zeer groot was, wat bleek uit experimenten waarin het mengen van lipiden en inhoud van de liposomen werd gemeten. Door de oorspronkelijke negatieve lading (coil-K) te vervangen door geen lading (coil- K_S) en een positieve lading (coil- K_K) werd de fusie significant versterkt. Mogelijk komt dit doordat er minder KK coiled coils zijn voordat fusie plaatsvindt. Er is echter meer onderzoek nodig om deze hypothese te bevestigen.

Dit proefschrift richt zich op het ontwerpen van nieuwe coiled coil peptiden en het optimaliseren van coiled coil gedreven membraanfusie. Er is nog ruimte voor vervolgstudies, bijvoorbeeld in hoofdstuk 3, waarin de aminozuur sequentie van coil-E werd omgedraaid. Het zou bijvoorbeeld interessant kunnen zijn om de sequentie van coil-K om te draaien omdat recent onderzoek heeft laten zien dat coil-K interacteert met membranen. Deze interacties zorgen er wellicht voor dat de membranen verstoord worden waardoor de fusie zo efficiënt mogelijk verloopt. Door de sequentie van coil-K om te draaien zou deze hypothese bevestigd kunnen worden. Hoofdstukken 4, 5 en 6 laten zien dat het modelsysteem nog sneller en efficiënter fusie kan induceren, wat een belangrijke stap is voor het in-vivo gebruik van dit model systeem. Als dat gerealiseerd kan worden is het modelsysteem werkelijk in staat de natuurlijke, SNARE gedreven, membraanfusie na te bootsen.

Abbreviations

A	Alanine
Ac	Acetyl
ACH	α -cyano-4-hydroxycinnamic acid
AcN	Acetonitrile
AUC	Analytical ultracentrifugation
BOC	Tertiary-butoxycarbonyl
C	Cysteine
CC	Coiled coil
CD	Circular dichroism
CH/CHOL	Cholesterol
Coil-E=E₃	(EIAALEK) ₃
Coil-K=K₃	(KIAALKE) ₃
D	Aspartic acid
D	Dimensional
D₂O	Deuterated water
DCM	Dichloromethane
D_h	Hydrodynamic diameter
DIC	N,N'-Diisopropylcarbodiimide
DIPEA	N,N-diisopropylethylamine
DLS	Dynamic light scattering
DMF	N,N-dimethylformamide
DNA	Deoxyribonucleic acid
DOPC	1,2-dioleoyl-sn-glycero-3-phosphatidylcholine
DOPE	1,2-dioleoyl-sn-glycero-3-phosphatidylethanolamine
DOPE-LR	1,2-dioleoyl-sn-glycero-3-phosphatidylethanolamine-lissamine-rhodamine B
DOPE-NBD	1,2-dioleoyl-sn-glycero-3-phosphoethanolamien-N-(7-nitro-2-1,3-benzoxadiazol-4-yl) (ammonium salt)
E	Glutamic acid
E₂	(EIAALEK) ₂
E₄	(EIAALEK) ₄
EPR	Electron paramagnetic resonance
ESI	Electrospray ionization
Epn	Equation
Fmoc	Fluorenylmethoxycarbonyl
FRET	Fluorescence resonance energy transfer
G	Glycine
ΔG_u	Gibbs free energy of unfolding
HCTU	1H-benzotriazolium 1-[bis(dimethylamino)methylene]-5-chloro-hexafluorophosphate (1-),3-oxide
HOBT	1-Hydroxybenzotriazole hydrate
HPLC	<i>High-performance liquid chromatography</i>
ΔH_u	Enthalpy of unfolding
I	Isoleucine
K	Lysine
K/E	Complex of peptide K and E
K₂	(KIAALKE) ₂
K₄	(KIAALKE) ₄
K_u	Dimer dissociation constant
L	Leucine

Abbreviations

LC-MS	Liquid chromatography-mass spectrometry
LPK	Lipopeptide-K (DOPE-Peg12-peptide K)
LPE	Lipopeptide-E (DOPE-Peg12-peptide E)
MALDI-TOF	Matrix-assisted laser desorption-ionization time-of-flight
MTSL/*	S-(2,2,5,5-tetramethyl-2,5-dihydro-1H-pyrrol-3-yl)methyl methanesulfonylthioate
MD	Molecular dynamics
NBD	Nitrobenzofuran
NMP	N-methyl-2-pyrrolidone
NMR	Nuclear Magnetic Resonance
NSF	N-ethylmaleimide sensitive fusion protein
PBS	Phosphate buffered saline
PDA	Photo Diode Array
PDI	Polydispersity index
PEG	Poly (ethylene glycol)
PRE	Paramagnetic relaxation enhancement
R	Arginine
RNA	Ribonucleic acid
RP-HPLC	Reverse-phase high-pressure liquid chromatography
RT	Retention Time
S	Serine
SDSL	Site-directed spin label
SNARE	Soluble NSF attachment protein receptor
SPPS	Solid-phase peptide synthesis
TBS	Tris-buffered saline
TEA	triethanolamine
TFA	Trifluoroacetic acid
TFE	Trifluoroethanol
TFE-D₃	Deuterium oxide of TFE
Tris	Tris(hydroxymethyl)aminomethane
tBu	Tertiary butyl
T_m	Melting temperature
THF	Tetrahydrofuran
TIS	Triisopropylsilane
Trt	Trityl
UV	Ultraviolet
V_{dw}	Van der Waals
W	Tryptophan
Y	Tyrosine

Curriculum Vitae

Tingting Zheng was born on 30th November 1982 in Fuzhou City, Fujian Province, China. She entered College of Chemistry, Beijing Normal University as top one of her senior high school in 2002. She obtained teacher qualification certification in 2006. In the same year, she accomplished her research in ‘Chemistry education in middle school’, and received her BSc degree under supervision of Prof. Dr. Lei Wang. She continued her study at the Key Laboratory of Radiopharmaceuticals, Ministry of Education, College of Chemistry, Beijing Normal University, under supervising of Prof. Bo-Li Liu and Dr. Hongmei Jia. Her research focused on overcoming the blood brain barrier for in vivo drug delivery. She received her MSc degree in 2009 with and the thesis was entitled ‘Improved brain uptake of 99m Technetium labeled radiopharmaceutical for SPECT imaging’. In the same year, she was awarded a research scholarship from the ‘Chinese Scholarship Council’. With this scholarship, she joined the Soft Matter Chemistry group at the Leiden institute of Chemistry, Leiden University, under supervision of Dr. Alexander Kros as a Ph.D candidate. Her research is described in this thesis. Since 1st January 2014, she is a postdoc in the Physical Chemistry and Colloid Science group at Wageningen University, under the supervision of Dr. Joris Sprakel and Dr. Renko de Vries.

List of Publications

In this thesis:

- ❖ **Zheng, T. T.**; Voskuhl, J.; Versluis, F.; Zope, H. R.; Tomatsu, I.; Marsden, H. R.; Kros, A., Controlling the rate of coiled coil driven membrane fusion. *Chemical Communications* **2013**, 49 (35), 3649-3651.
- ❖ Marsden, H. R.; **Zheng, T. T.**; Voskuhl, J.; Kros, A., Controlled liposome fusion mediated by SNARE protein mimics. *Biomaterials Science* **2013**, 1 (10), 1046-1054.
- ❖ **Zheng, T. T.**; Boyle A.; Marsden, H. R.; Raap, J.; Valdink, D.; Martelli, G.; Kros, A., Probing coiled-coil assembly by paramagnetic NMR spectroscopy. *Organic & biomolecular chemistry*. **2014**, Accepted.
- ❖ **Zheng, T. T.**; Bulacu, M.; Boyle, A.; Versluis, F.; Marsden, H. R.; Valdink, D.; Martelli, G.; Raap, J.; Sevink, A.; Kros, A., An antiparallel tetrameric coiled coil. Manuscript in preparation.
- ❖ **Zheng, T. T.**; Boyle, A.; Marsden, H. R.; Kros, A., Increasing the membrane fusion efficiency by reducing undesired peptide-peptide interactions. Manuscript in preparation.

Other publications:

- ❖ Tomatsu, I.; Marsden, H. R.; Rabe, M.; Versluis, F.; **Zheng, T. T.**; Zope, H.; Kros, A., Influence of pegylation on peptide-mediated liposome fusion. *Journal of Materials Chemistry* **2011**, 21 (47), 18927-18933.
- ❖ van Son, M.; **Zheng, T. T.**; Kumar, P.; Valdink, D.; Raap, J.; Kros, A.; Huber, M., Towards Artificial Membrane Fusion: Ek-Peptides, the Coiled-Coil Zipper. *Biophysical Journal* **2014**, 106 (2), 506A-506A.
- ❖ Marsden, H. R.; **Zheng, T. T.**; Kros, A., Controlled liposome fusion mediated by SNARE protein mimics. *Abstracts of Papers of the American Chemical Society* **2013**, 245.
- ❖ **Zheng, T.**; Zhou, H.; Chen, R.; Li, Z.; Xie, Y.; Jia, H., Improved brain uptake of ^{99m}TcN-NOET loaded by targeted sterically stabilized liposomes in ICR mice. *Journal of Labelled Compounds & Radiopharmaceuticals* **2009**, 52, S80-S80.

Patent:

- ❖ **Zheng, T.**; Jia, H.; Xie, Y.; Zhou, H.; a novel ^{99m}Tc-labeled radiopharmaceutical for SPECT brain tumor imaging. *State intellectual property office of P.R.C.*, **2009**, No. 200910141973.6.

